Preparation of Heterobimetallic Catalysts

Navpreet Kaur Sethi

A thesis for the degree of
Doctor of Philosophy in Chemistry

The University of York

Department of Chemistry

September 2012

Abstract

In an attempt to synthesise mesoporous silicas doped with truly heterobimetallic nanoparticles, the use of single-source precursors has been proposed. The method of preparation of the silicas has employed true liquid crystal templating (TLCT), a methodology used to synthesise mesoporous silicas, previously employed in one-pot syntheses to prepare silicas containing heterobimetallic nanoparticles from separate metal precursors. Using single source precursors was expected to lead to bimetallic nanoparticles of uniform composition dispersed throughout the silica framework.

In this work several attempts were made to prepare heterobimetallic complexes that possessed an equivalent metallic ratio (1 : 1), which were to be used as precursors in the one-pot synthesis mentioned above. However, none of them produced complexes of the desired stoichiometry. In these attempts, two different approaches were used namely a polydentate ligand (TTHA, Triethylene tetraaminehexaacetic acid) and usage of halogeno bridges. From these methods of preparation only one stoichiometrically precise TTHA complex was isolated, that of Rh-Zn (1 : 1) obtained as a single crystal. Apart from that two more heterobimetallic complexes *e.g.* Cr-Rh (3 : 1) TTHA complex and one halobridged Pd-Pt (3 : 1) complex, were isolated.

Despite the imperfect stoichiometry of the TTHA complexes, some (Rh-Ni, Cr-Pd, Rh-Pd) were nonetheless used in the preparation of mesoporous silicas. The combinations Cr/Pd and Rh/Pd evidently led to deposition of nanoparticles of the different metals, although there was some evidence for the formation of heterobimetallic nanoparticles with Rh/Ni.

In investigating the possible preparation of heterobimetallic complexes between gold and platinum or palladium, the oxidation of the Group 10 metal by gold was

observed and studied. One unexpected outcome of the reaction between Pt^{II} and Au^{III} as their NBu_4^+ salts was the observation of the bimetallic complex $[NBu_4]_2[Cl_3Pt\{\mu\text{-}(\eta^2{:}\eta^2\text{–}trans\text{-butadiene})\}PtCl_3]$ and possible mechanisms of formation are discussed.

Contents

List of Figures

Chapter 1 Introduction

Chapter 2 Halo-bridged Complexes

Chapter 3 TTHA Metal Complexes

Chapter 4 Mixed-Metal Silicas

List of Tables

Chapter 1 Introduction

Chapter 2 Halo-bridged Complexes

Chapter 3 TTHA Metal Complexes

Chapter 4 Mixed-Metal Silicas

List of Schemes

Chapter 2 Halo-bridged Complexes

Chapter 3 TTHA Metal Complexes

Abbreviations

AA	Atomic Absorption
AAS	Atomic Absorption Spectroscopy
AcOH	Acetic acid
adp	Anisotropic displacement parameters
bcc	Body centred cubic
BET	Brunauer, Emmett, and Teller
BJH	Barret-Joyner-Halenda
CCD	Charge-coupled device
CCDC	Cambridge Crystallographic Data Centre
cmc	Critical micelle concentration
$C_{12}EO_{10}$	dodecaethyleneglycolmonodecylether
$C_{12}EO_8$	dodecaethyleneglycoloctaethlylether
CFSE	Crystal Field Stabilisation Energy
conc.	concentrated
CP	Chemically pure
[18-crown-6]	1,4,7,10,13,16-hexaoxacyclooctadecane
3D	Three dimensional
δ	Delta
d	Doublet
dil.	Dilute
DTGS	deuterated triglycine sulfate
DTPA	diethylenetriamine-N, N′, N″-pentaacetic acid
DMF	dimethylformamide
DMSO	dimethylsulfoxide
D_2O	deuterium oxide
DOPA	L-3,4-dihydroxyphenylalanine
dppm	bis(diphenylphosphino)methane

en	ethylenediamine
EDTA	ethylenediamminetetraacetic acid
ESI	Electronspray Ionisation
ESR	Electron Spin Resonance
EDX	Energy-dispersive X-ray diffraction
Et_2O	diethylether
EtOH	ethanol
fcc	Face centered cubic
FSM	Folded Sheet mesoporous Materials
FTIR	Fourier transform infrared spectroscopy
FWHM	Full width at half max
$\Delta G°$	Change in free energy
h	Hours
$\Delta H°$	Change in enthalpy
H	Hexagonal phase
H_1	Normal hexagonal phase
H_1	Normal hexagonal phase
HPLC	High-performance liquid chromatography
HSAB	Hard and soft (Lewis) acids and bases
Hz	Hertz
I	Micellar isotropic
I_1	Normal micelles
I_2	Inverse micelles
IR	Infra-red
L	Isotropic micellar solution
L_α	Lamellar phase
LC	Liquid-Crystalline
LCT	Liquid Crystal Templating
LCQ	Liquid Chromatography Quadrupole

MCM	Mobil Composition of Matter
MHz	Megahertz
MeOH	methanol
MRI	Magnetic Resonance Imaging
MS	Mass spectrometry
m/z	Mass to charge ratio
NMR	Nuclear magnetic resonance
O1P	Transmitter Frequency
PEG	polyethylene glycol
POM	Polarised Optical Microscopy
PPO	polypropylene oxide
PPG	polypropylene glycol
ppm	Parts per million
s	Singlet
$\Delta S°$	Change in entropy
salen	2,2'-ethylenebis(nitrilomethylidene)diphenol
SBA-15	Santa Barbara No. 15
SEM	Scanning Electron Microscopy
t	Triplet
TEM	Transmission Electron Microscopy
TEOS	tetraethoxysilane
THF	tetrahydrofuran
TLCT	True Liquid Crystal Templating
TTHA	triethylenetetraamine-N, N′, N″, N‴-hexaacetic acid
TMOS	tetramethoxysilane
V	Bicontinuous cubic
XRD	X-ray diffraction

Acknowledgements

I would like to express my heartfelt gratitude to my supervisor Professor Duncan Bruce without whom it was nearly impossible to carry on with this project and to complete this PhD thesis. His suggestions, understanding nature, guidance, generosity and constantly encouraging attitude along with vast knowledge in different areas has added gradually to my research experience.

I greatly acknowledge my IPMs Dr. Karen Wilson and Dr. Anne Duhme-Klair for their guidance and useful suggestions in the Thesis Advisory Panel meetings.

I am grateful to Professor Wuzong Zhou at the University of St. Andrews for carrying out significant TEM analysis. A very special thanks goes out to Dr. Nigel Young at University of Hull for his assistance in carrying out IR measurements.

I am immensely thankful to all the people of the Department of Chemistry at The University of York who have helped me during the crucial time of my research, especially Heather Fish for her great assistance with NMR experiments, Dr. Adrian Whitwood for his extraordinary help with the X-ray Crystallography and the X-ray Diffractometer, Dr. Trevor Dransfeld, Ben Hodgson, and Karl Heaton for their assistance with mass spectrometery, Dr. Phil Helliwell for CHNs as well as Atomic Absorption spectroscopy, and Dr. Graeme McAllister for carrying out prompt CHNs in the last year. I am extremely thankful to Helen and Alice in the Chemistry Graduate Office for helping me all the way through assistance with different matters. Thanks go to Nasir and Imam for support and assistance of all sorts.

I would also like to thank all the members of the group, former as well as new, who have played a special role in helping me carrying out my lab work with a great ease.

I really appreciate our lunch and coffee time conversations and our precious timeouts with my friends in the group. It is difficult to mention every name but I am glad that you all were there, thanks a ton!

I am grateful to the Department's Wild Fund without which it would not have been possible to continue this research.

Finally, I would like to express my sincere gratitude and appreciation to Dr. Avtar Matharu, University of York and Mrs. Sukhwinder Matharu for their backup support and in making me feel like home. Above all, huge thank you to my parents, and my brother Ruble for their patience, love, support and understanding which constantly motivated me to carry on.

Not to forget my friends in the Department of Chemistry, in and around York, back home, and around different parts of the world for their kindness, encouragement and support which helped me out to have an optimistic attitude most of the times.

Lord I am grateful to what I am today although there is much more to say but words are enough.

Declaration

This thesis is available to the Library use on the understanding that is copyright material and no quotation from this may be published without proper acknowledgement. I certify that all the material in this thesis which is not my own work has been identified and that no material has previously submitted and approved for the award of a degree by this or any other university.

Chapter 1
Introduction

This chapter will introduce the various terminologies, methodologies, applications and other information covering historic as well as recent developments in the field of mesoporous solids and heterobimetallics. The chapter will begin from the basic understanding of the surfactants and micelles and then discuss the synthesis of well-known mesoporous silicas through different methodologies. Finally, applications of the mesoporous network to produce heterobimetallic catalysts *via* various different routes will be discussed.

1.1 Micelles

Surfactants

The term surfactant originated from the term surface-active agent[1] *i.e.* from their tendency to act upon the surface that is by reducing its surface tension by being adsorbed onto the surface of water. Each surfactant molecule, or monomer, is composed of two parts: polar head and non-polar tail regions, which are hydrophilic and hydrophobic, respectively (**Fig. 1.1**).

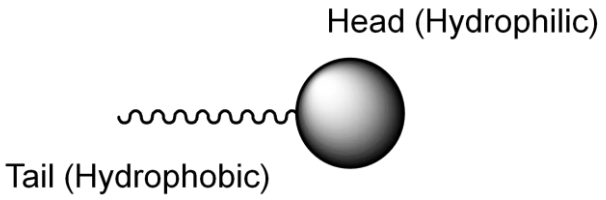

Fig. 1.1 Schematic representation of a surfactant monomer.

The hydrophobic tail is usually hydrocarbon in nature however; the hydrophilic head group can be cationic, anionic, zwitterionic or neutral, as shown in **Fig. 1.2**.

Cationic

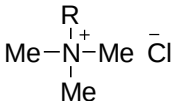

Anionic

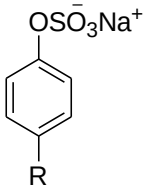

Zwitterionic

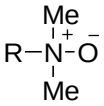

Neutral

$R(OC_2H_4)_mOH$

Fig. 1.2 Types of surfactant head groups.

To understand the concept of surface tension, it is important to consider the role and properties of solvent molecules. In water, the molecules interact with each other due to hydrogen bonding between the molecules. On average these interactions are experienced equally by all molecules in all directions except at the interface. At the air-water interface, water molecules experience an imbalance of attractive forces due to non-formation of hydrogen bonds in all directions (**Fig. 1.3**). This results in an inward pull at the interface due to which a contracting force acts at the surface and is known as *surface tension*. The surface tension of the pure water at 295 K is 72.4 mN m^{-1}, irrespective of the size of the container.[2]

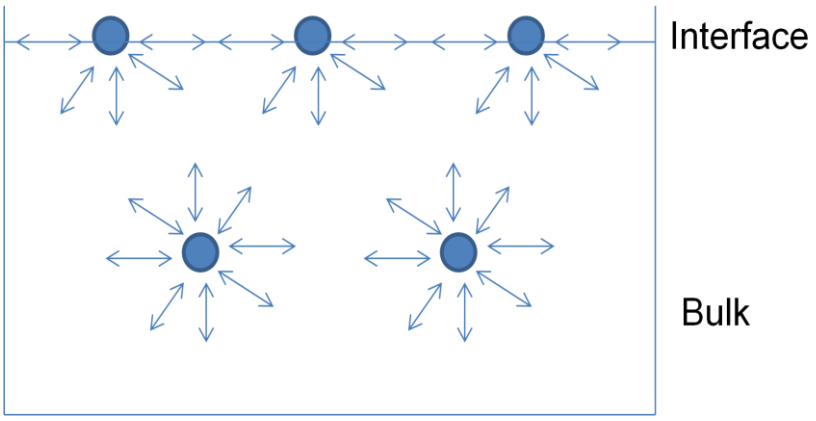

Fig. 1.3 Diagrammatic representation of surface tension.

When the surfactant molecules are added to the water, they adsorb at the surface with the polar head groups interacting with the water molecules at the surface and, the non-polar chains pointing to the air. This results in a decrease in surface tension, which thereby reduces the free energy of water. In addition, isolated surfactant molecules present inside the water disrupt the three-dimensional network formed by intermolecular hydrogen bonds, due to the introduction of the hydrophobic chains. More significantly, these hydrophobic chains are, in effect, frozen in the water as they cannot interact with the water molecules, which in fact form an ordered 'skin' around them. All of these effects act to increase the free energy of the system.

As the amount of surfactant increases, so does the free energy until the increase in free energy is great enough to lead to another event, the formation of micelles (**Fig. 1.4**). The concentration at which this event takes place is known as the *critical micelle concentration* (cmc). However, micelles represent a more ordered arrangement (decrease in entropy) so what is the driving force for their formation? Consider the normal micelle in **Fig. 1.4** where the headgroup is charged. Clearly the repulsion of like charges

represents an increase in the enthalpy of the system, which on its own would disfavour micelle formation. However, the interior of the micelle is a very hydrophobic environment – so much so that the hydrophobic chains are now free to move around (increase in entropy). Furthermore, in forming this hydrophobic pocket, the ordered 'sheath' of water from around the chains is released resulting in disordered, free-moving water (another increase in entropy).[3] In fact, the increase in entropy from these two effects is substantial and, while there are other effects both enthalpic and entropic at play, they are less significant and tend to cancel out, so that the positive change in ΔS overcomes the enthalpic repulsion between the headgroups, driving the formation of the micelle. The combination of these factors is known as the *Hydrophobic Effect*.

A brief evaluation of the key factors then readily reveals that the cmc will be lower for neutral surfactants (very much lower headgroup repulsion) and that it will decrease as the length of the hydrophobic chain increases (great entropic contribution).

The value of cmc for non-ionic surfactants lies within the range of 10^{-5}-10^{-6} M at room temperature.[3] The state of a micelle is never constant as there is an equilibrium established between monomers and the aggregated monomers or micelles. Hence, a continuous movement of monomers or surfactant molecules from and into the micelles occurs.

Micellar size and shape are dependent on the nature of the surfactant, the medium surrounding the surfactant, and the temperature as well as concentration. The lowest temperature at which micelles are formed is known

as *Krafft temperature*,[4] which is dependent on the solubility of the surfactant as below this temperature the surfactant can crystallise. The presence of electrolyte influences greatly the cmc of ionic surfactants but has little effect on the cmc of non-ionic surfactants.

Micelles can be categorised as "normal" or "inverse". Normal micelles consist of a hydrophobic interior and hydrophilic exterior *i.e.* the head group or polar part is on the outer side and the chain length is on the inner side (**Fig. 1.4 A**). However, inverse micelles have a hydrophobic exterior and hydrophilic interior *i.e.* the tail part is on the outer side while the head part is at the inner side (**Fig. 1.4 B**).

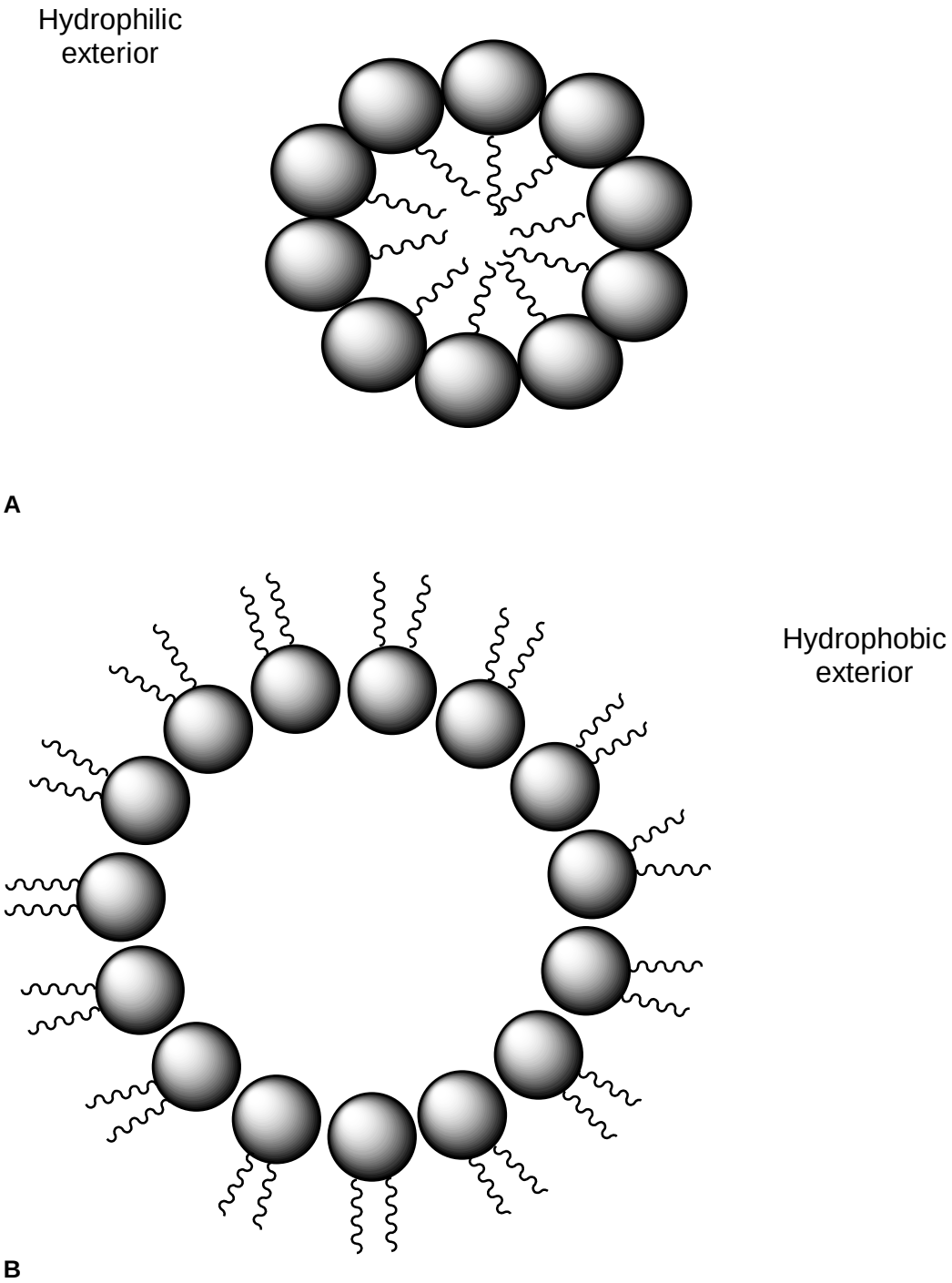

Fig. 1.4 Shapes of micelles. **A** is a normal micelle and, **B** is an inverse micelle.

Micelles can form different shapes *e.g.* spheres, discs, and cylindrical rods (**Fig. 1.5**).

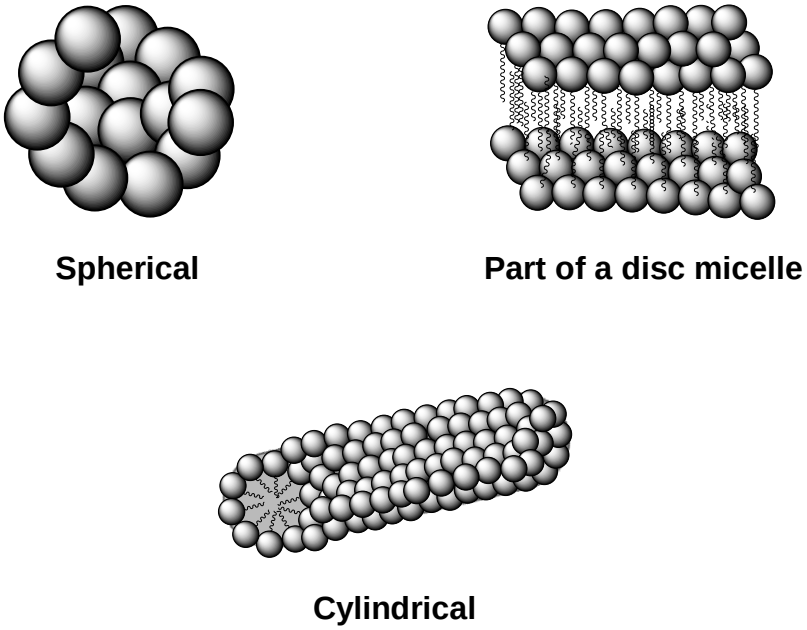

Fig. 1.5 Different shapes of micelles.

The shape of a micelle is influenced by the properties of the surfactants namely, chain volume (*v*), area of the head group (*a*), and chain length (*l*).[5] Israelachvilli[6] developed a method to interpret the shape of the micelle formed in the medium, from the above parameters. According to his model, the surfactant of a micelle acts like an ice cream cone inside the polar medium (**Fig. 1.6**).[7] The approach involves calculation of the shape factor or packing parameter (η) of the micelle by using following equation,

$$\eta = \frac{v}{al} \qquad (1)$$

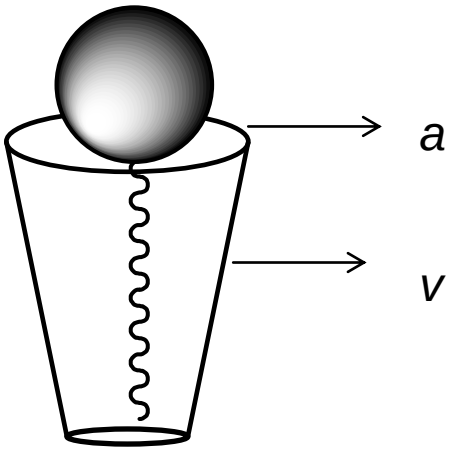

Fig. 1.6 Schematic representation of surfactant molecule as an ice cream cone.[7]

The packing parameter is considered as a true variable, which determines the shape of micelle formed and so normally predicts well the nature of the first-formed liquid crystal phase (see below). It is known that the hydrophobic chain length (l) is always shorter than that of a fully extended surfactant (l_t). Therefore, considering the chain length factor ($l < l_t$), and by using the above equation, the shape factor can be calculated for spherical, cylindrical and bilayer shapes hence the estimation of the geometry of the micelles is possible (**Table I.I**). From the values of a and v the number of molecules in a micelle is easily calculated.

Table I.I Shape factor observed for different micellar shapes.[8]

Micelle Shape	Shape factor (η)
Spherical	$\eta \leq 1/3$
Cylindrical rod	$1/3 \leq \eta \leq 1/2$
Disc	$1/2 < \eta \leq 1$.

1.2 Liquid-crystalline Phases

Pure organic substances, either on their own or in an aqueous solution which can self organise in such a way that they exhibit properties intermediate between a solid and liquid state, are known as *liquid crystalline*. A liquid-crystalline substance can form different phases, which are governed by their tendency to self-organise: such organised phases are termed *mesophases*. Depending upon factors that are responsible for the mesophase formation of a liquid-crystalline substance, they are divided into two categories, namely *Thermotropic* and *Lyotropic*. Thermotropic liquid-crystalline materials are formed due to variation in temperature only and are not discussed further here.[9] However, the formation of lyotropic liquid-crystalline materials is governed by concentration (and temperature).

At the cmc, the organisation of amphiphilic molecules begins and such monomers, when associating in this way they are known as *association colloids*. Such a micellar solution does not show any liquid-crystalline behaviour and is, therefore, isotropic. If the amphiphile concentration increases then all additional amphiphile goes into the formation of micelles and so the micelle concentration increases until the micelles eventually order to form a liquid crystal phase and the solution becomes anisotropic and more viscous than the isotropic phase. No surfactant can show the formation of all the possible liquid-crystalline phases as shown in **Fig. 1.7.**

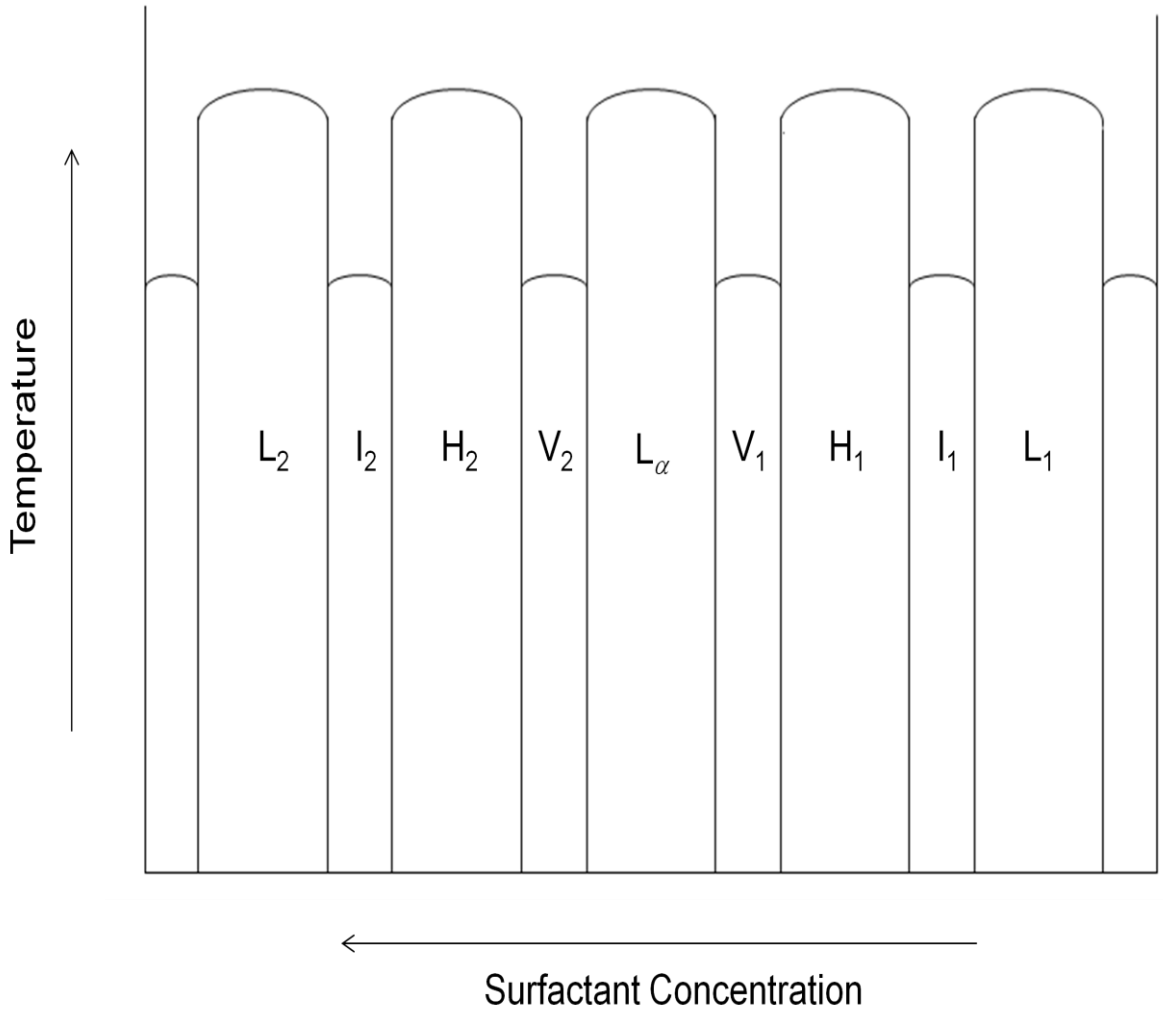

Fig. 1.7 Phase diagram (hypothetical) of surfactant in water showing different possible liquid-crystalline phases. Here H, V, I, and L_α are hexagonal, bicontinuous cubic, micellar isotropic, and lamellar, respectively. L represents isotropic micellar solution and 1 and 2 stand for normal and inverse types.

The binary phase diagram for a non-ionic surfactant, *e.g.* $C_{12}EO_{10}$ (dodecaethylene monodecylether) showing different liquid-crystalline phases, is given in **Fig. 1.8.**

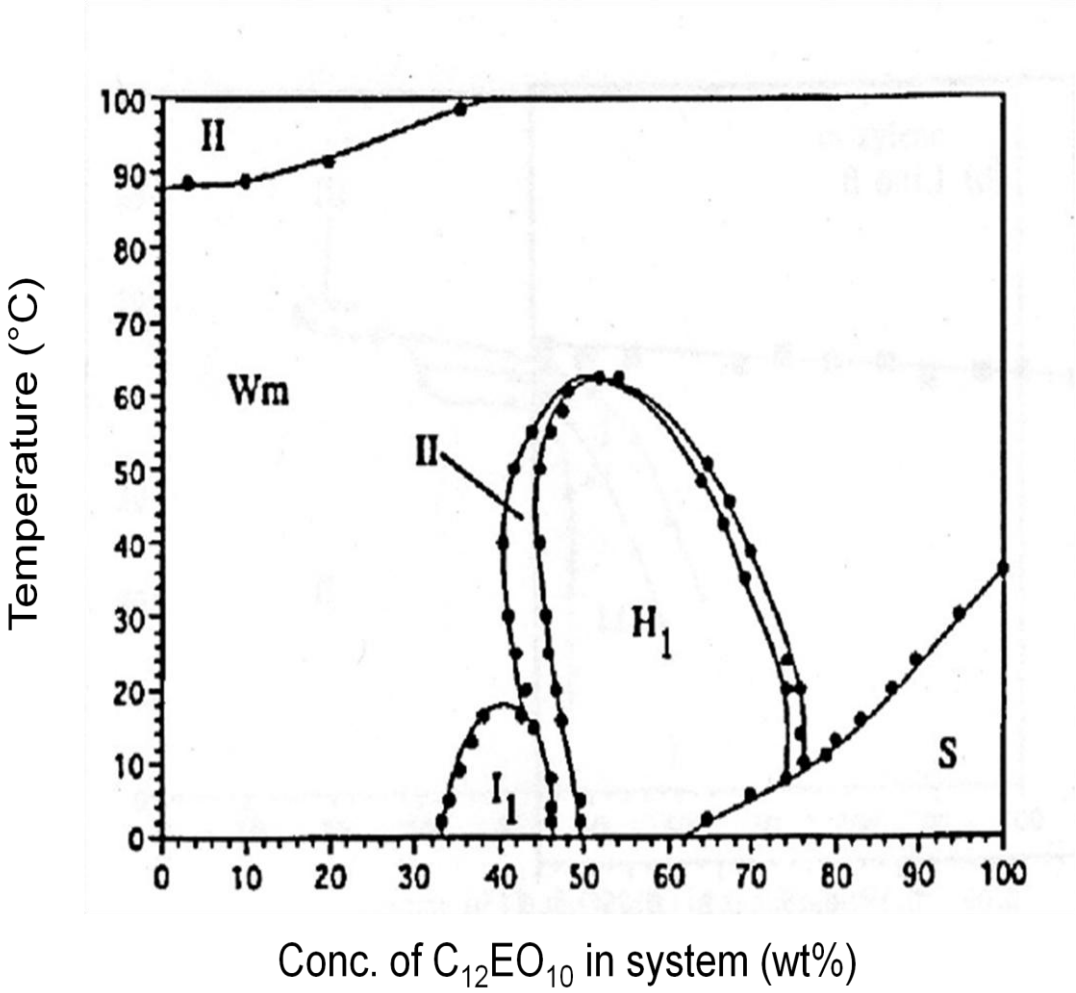

Fig. 1.8 Phase diagram of water/$C_{12}EO_{10}$ system as a function of surfactant concentration and temperature.[10] W_m is an aqueous micellar solution phase; H_1 and I_1 stands for hexagonal and cubic liquid-crystalline phases, respectively; S is solid phase, II indicates a two-phase region.

The hexagonal phase exists both in the normal (H_1), **Fig. 1.9. (A)**, as well as in the reverse (H_2) structures. In a hexagonal phase, the micelles are assembled in the form of rods packed together forming a hexagonal structure, the viscosity of the hexagonal phase is higher than that of a lamellar phase and is anisotropic. The rods in the H_1 phase usually possess a diameter within range

of 1.3 to 2.0 nm, while the separation of the two rods in the H_1 phase may vary from 0.8 to 5 nm.[11]

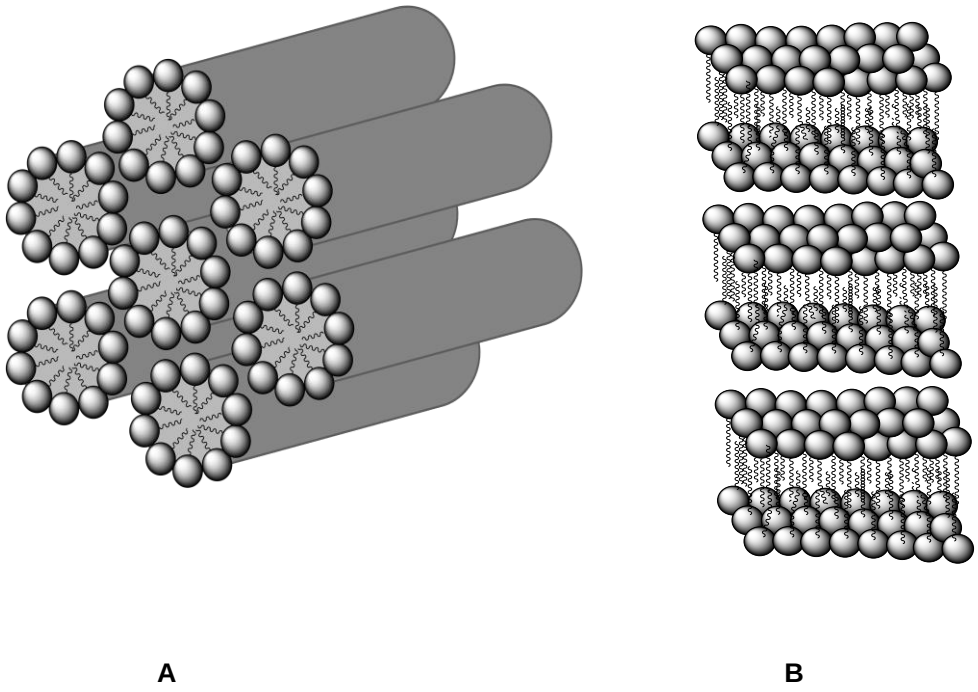

Fig. 1.9 Normal hexagonal H_1 phase (**A**) and lamellar L_α phases (**B**).

The lamellar phase is considered as one of the most common of all the lyotropic phases. Like any other mesophase (except the cubic phase), it is anisotropic and can exist in the form of double layers commonly known as bilayers (**Fig. 1.9 B**).[12] The ordered bilayer structure is organised in such a way that the polar head groups can interact with water or are water facing, while the non-polar chains are in contact with one another so as to avoid any contact with water.[11] The structure is shown in **Fig. 1.9 (B)** depicting the bilayer, that repeats to give a lamellar phase. The separation between bilayer is an area where water is found. (**Fig. 1.9 B**). Bilayers can easily slip over one another hence making the phase less viscous. The width of a double layer is

approximately 3.0 to 4.0 nm. The width of the layer may vary depending upon the chain folding, the tilting tendency of the bilayers and the water content.

The existence of cubic phases was first confirmed from X-ray diffraction (XRD) by Luzzati and Husson,[13] and by Luzzati *et al.*[14] In so-called *discrete cubic mesophases*, the micelles are organised in a three-dimensional lattice in the phase, which is characterised by its viscous and isotropic nature, possessing no optical texture and being highly viscous. The discrete cubic mesophases are formed either from either normal (I_1) or inverse (I_2) micelles, and two common forms are the body-centred cubic (bcc, $Im\bar{3}m$), face-centered cubic (fcc, $Fm\bar{3}m$) modifications. *Bicontinuous cubic phases* (V_1 and V_2) (**Fig. 1.10**) are different and have a more complex structure that has been described in a rod model[15] and in a model using infinite minimal periodic surfaces.[16] In common with the micellar cubic (I) phases, these are also optically isotropic and viscous.

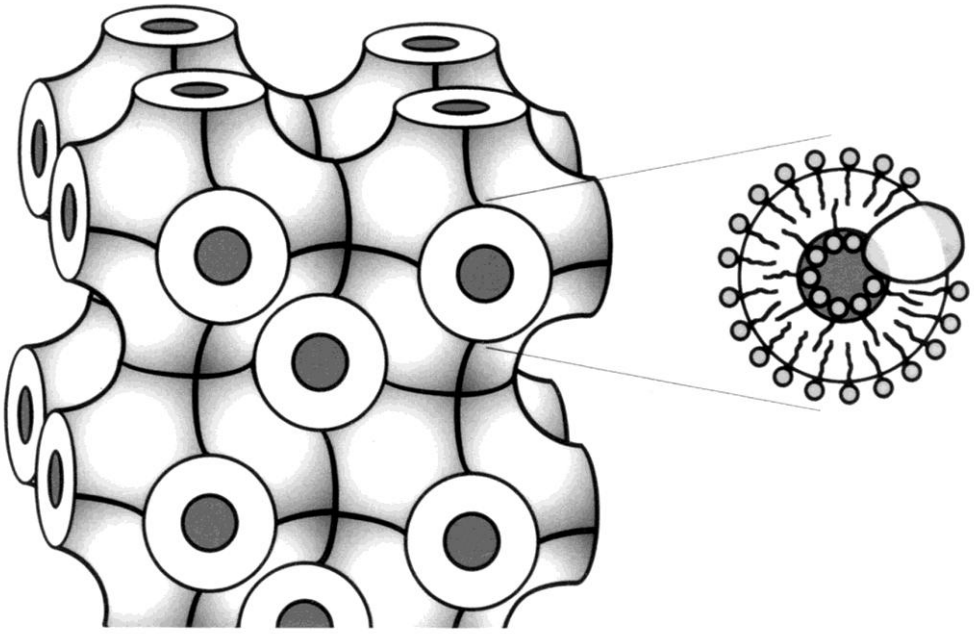

Fig. 1.10 Schematic model of a bicontinuous cubic phase.[17]

1.3 Mesophases as Templates[8]

As discussed above, the concentration of a surfactant in a solvent far above the cmc is known to be responsible for formation of a particular mesophase such as hexagonal, cubic, and lamellar. This information is obtained from a phase diagram of a particular surfactant. The mesophases formed then can be used as templates for the preparation of a mesoporous network irrespective of the nature of surfactant being used. Mesophases can be prepared from cationic and non-ionic surfactants such as alkyltrimethylammonium and polyethylene glycol (PEG), polypropylene oxide (PPO) or mixture of both, respectively. Non-ionic surfactants are the most common. This is due to their low cost and commercial availability.

By using the phase diagram, a particular wt% of the template with respect to solvent is employed in different methods of preparations of which some of them are discussed below in details.

1.4 Ordered Porous Solids

History

Mesoporous materials were well-known before the discovery of ordered mesoporous materials.[18] The term *ordered porous materials/solids* is used for those materials (*e.g.* micro-, meso- or macro- porous) in which the atoms are linked together by chemical bonds and the voids between the linked atoms are arranged in an organised manner.[19] They are named as micro-, meso-, or macro- porous materials according to their pore size. The materials which

possess pores of diameter less than 2 nm are categorised as *microporous* materials *e.g.* zeolites[20,21] (general formula $M_{x/m}[Al_xSi_{1-x}O_2]\cdot nH_2O$, where M is a cation and *m* is its valency). They possess application mainly in separation technology, primarily for adsorption of harmful gases (*e.g.* in masks) as well as in providing a sterilised environment (*e.g.* bandages). Other important roles are in industrial and catalytic applications.[22,23] The materials with diameters higher than 50 nm lie in the category of macroporous materials *e.g.* biological molecules, polymers of titania and zirconia.[24] The applications of macroporous materials mostly similar to mesoporous solids described below. Materials which contains pore diameters in the range of 2-50 nm (IUPAC recommendation)[25] are recognised as *mesoporous* materials.

The first ordered mesoporous materials were discovered in late 1980s by Mobil Oil Company, who reported MCM-41.[26,27] MCM-41 is silica with characteristic hexagonal array of channels (honeycomb-like lattice, (**Fig. 1.11**)),[26,27] with well-organised pores of varying diameter from 2.0 up to 100 nm.[28]

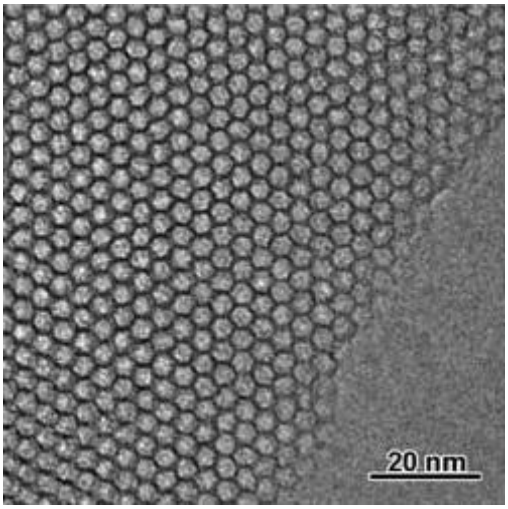

Fig. 1.11 TEM image of ordered MCM-41 silica showing honeycomb-like structure.[29]

Mesoporous materials are categorised into different type known as pillared clays and others including amorphous silicas. MCM-41 belongs to the family of molecular sieves known as M41S.[30,27,31] MCM is also known in the literature with a non-hexagonal pore structure under the name of MCM-48[32] or MCM-50[33] based on templating on the cubic and lamellar phase, respectively. Another type of ordered mesoporous silicate, Kanemite,[34,35] ($NaHSi_2O_5.H_2O$) was discovered during the same time as that of MCM-41 but was commonly known as a *layered silica*.[36,37] (**Fig. 1.12**).

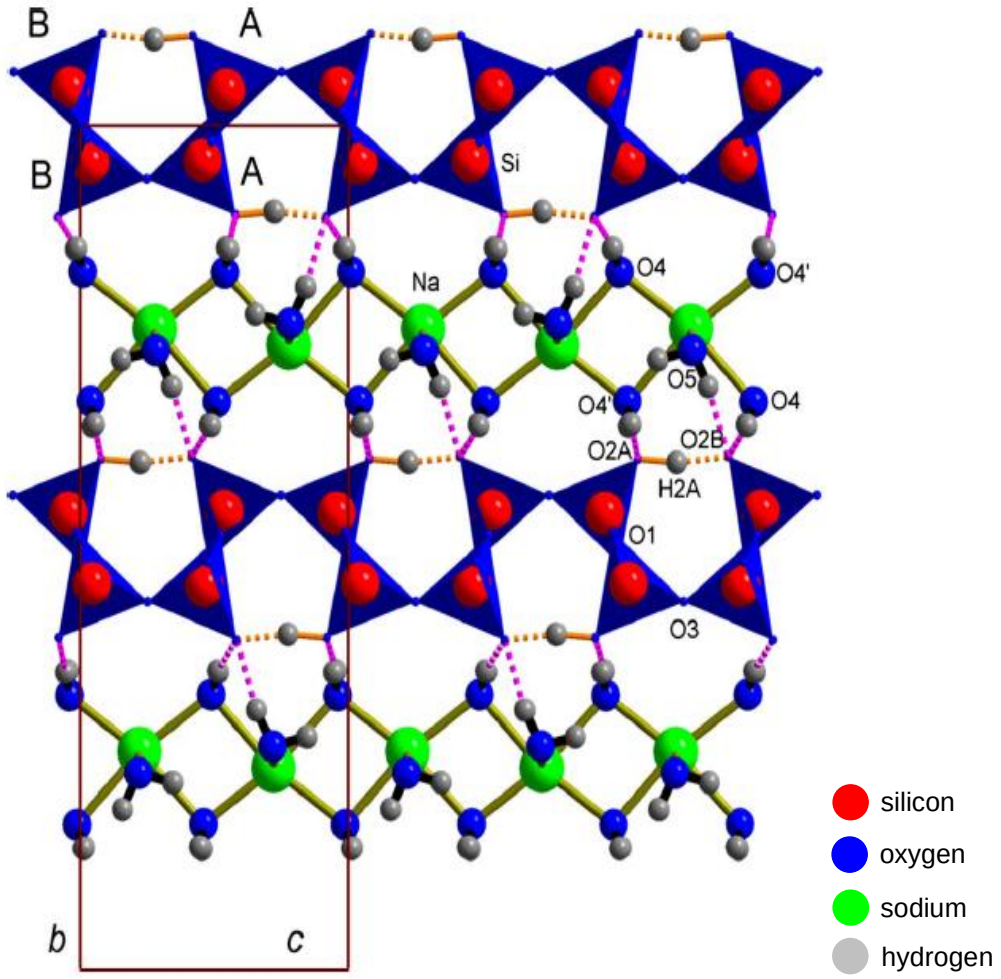

Fig. 1.12 Structure of Kanemite as observed at low temperature showing *bc* plane.[38]

The discovery of Kanemite provided an alternative pathway to synthesise ordered mesoporous silicas (**Fig. 1.13**). However, this approach was less versatile when compared to MCM-41 as it involved the intercalation of surfactant molecules and optimisation of the reaction conditions somewhat similar to the *pillaring method* (see section **1.5.1**) as used for zeolites. Using the same alternative approach materials that were obtained were known as FSM-*n* (*Folded Sheet mesoporous Materials-n*), where *n* is the number of carbon atoms in the surfactant (alkyl) chain length used as intercalate in the synthesis. FSM-*n* materials were known to form both ordered mesoporous silicas and aluminosilicates.[39,40]

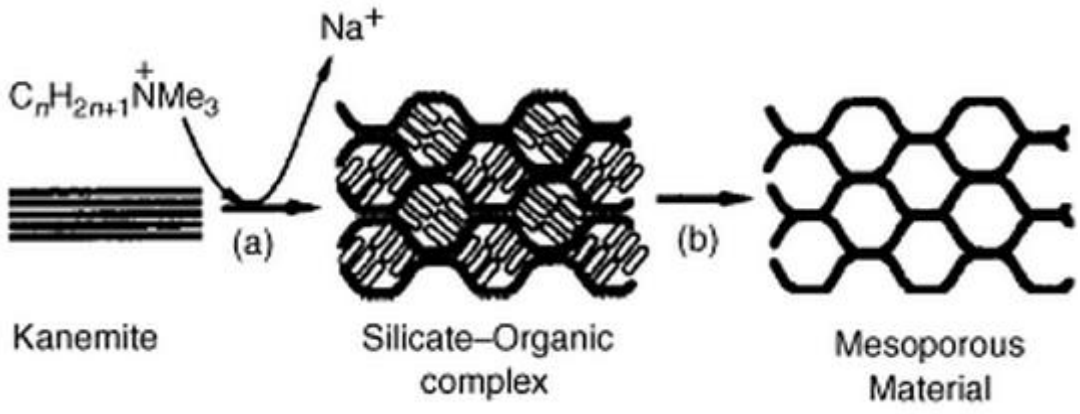

Fig. 1.13 Folded silica sheets around intercalated surfactant molecules, a) ion exchange, b) calcination.[39]

In the category of ordered mesoporous materials, one more type has been included, namely SBA-15 (*Santa Barbara No. 15*). This was prepared using mesophases formed from triblock copolymers as template (general formula $(PEO)_x$-$(PPO)_y$-$(PEO)_x$, where PEO (polyethylene oxide) and PPO is (polypropylene oxide). Triblock copolymers are also known by the trade name Pluronics.[39] The method of preparation was different than that used for FSM, and MCM-41, and is discussed below. The resulting mesoporous materials

showed a two-dimensional hexagonal morphology and differed from MCM-41 and Kanemite by having greater hydrothermal stability, wall thickness and pore size. SBA-15[41] has the distinguishable feature of also having micropores not present in other ordered mesoporous materials.

In order to describe the methodologies involved in the preparation of such mesoporous materials (*i.e.* MCM-41 and SBA-15), it is necessary to consider their mechanism of formation. These mechanisms are not very well established and are known in the literature under the headings: Silicate Layer Puckering,[42] Charge Density Matching,[42] Folding Sheets,[43,39] Silicatropic Liquid Crystals,[44] and Silicate Rod Clusters.[45] These mechanisms are not discussed in this chapter but other well-known methodologies are described in details in the section **1.5** of the Introduction.

Mesoporous materials, due to their specific pore size between micro- and macro-porous materials, have attracted most attention in the past years and possess numerous potential applications that are developing constantly.[46,47] The reason for this is their structural specificity (morphology), physical properties and chemical composition. The pores in mesoporous materials show long-range order and are distributed uniformly throughout the material. They have extremely high surface areas (100 to 1500 m^2 g^{-1}), which are a unique characteristic and make them useful as a catalyst support. The mesopores are uniform in diameter and can be easily tuned within the range (2-50 nm) with high chemical and thermal stability along with a tendency to be functionalised easily. All these characteristics make them ideal materials to be used as supports in adsorption, biotechnological devices and in catalysis.[48] They have

many other applications[36] for example, electrochemistry,[49] adsorption, separation technology,[50] molecular engineering,[51] drug delivery,[52] bioadsorption and biocatalysis[53] as well as in medicinal chemistry.[52]

1.5 Methodologies Involved in the Preparation of Mesoporous Solids

1.5.1 Pillared Clays[34]

The preparation, of pillared clays, is shown diagrammatically in **Fig. 1.14**. The methodology requires guest species that are intercalated in the system to generate a porous network. Thereafter, the pillars are introduced to the framework to maintain the spacing laterally as well as throughout the system (*i.e.* mesoporous network) as the pores collapse without them. The size and regularity of the pores is maintained by the type of pillar being used. Most of the examples of such systems include smectic clays.[54]

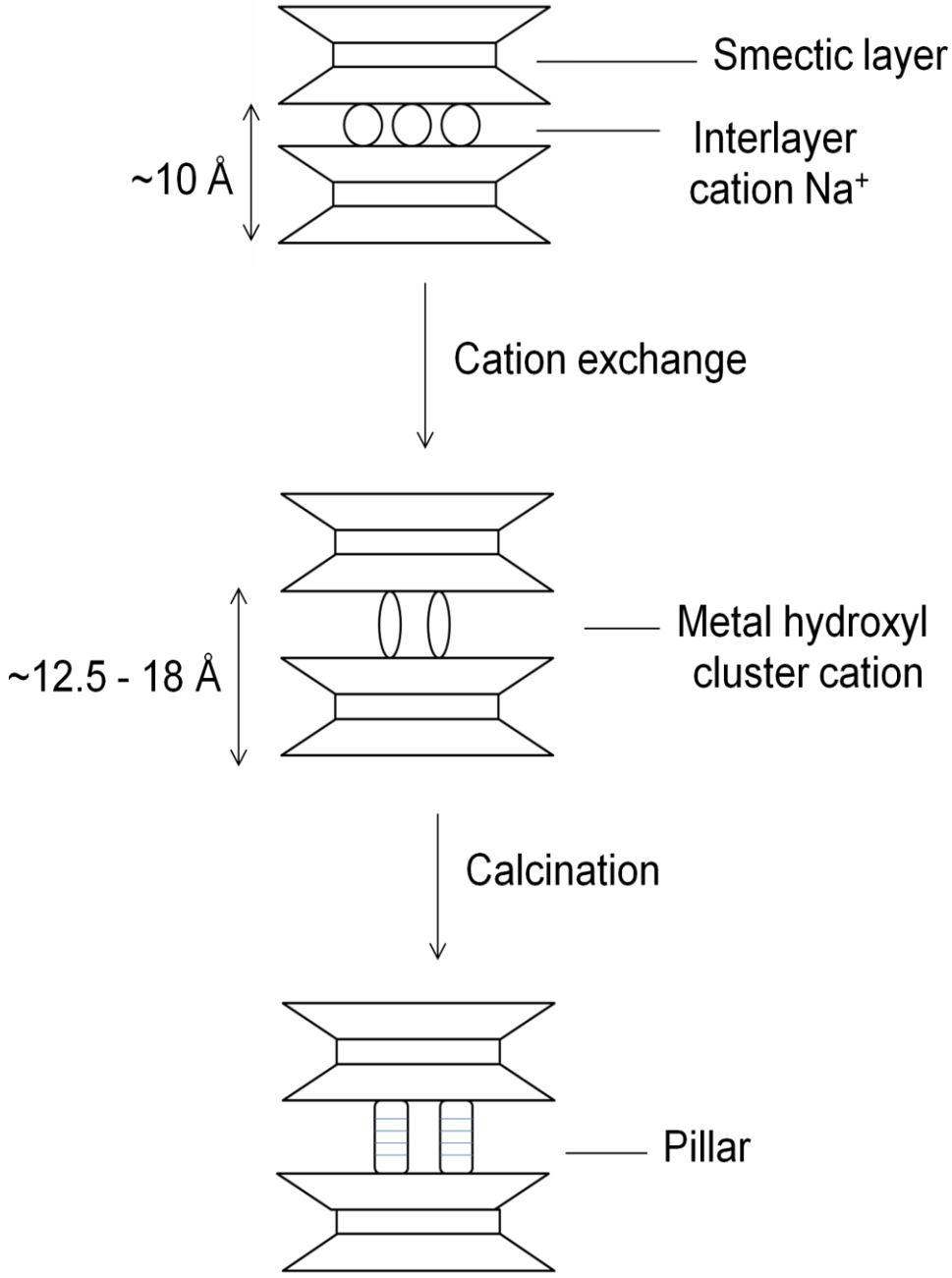

Fig. 1.14 Schematic diagram of prepared pillared clay minerals (adapted from Moore and Reynolds).[55]

The moieties that have been used as pillars to keep the smectic clays from collapsing at high temperatures (>200 ˚C) include tetraalkylammonium ions, bicyclic amine cations, metal chelate complexes and polynuclear hydroxy metal complexes.[56,57] The polynuclear hydroxy metal complexes are much more stable at high temperatures (*i.e.* > 200 ˚C) than the others.[56,57] Thermally stable clays have surface areas ranging from 200 to 500 m^2 g^{-1}. Charge stability has always been a problem in the concept, because the number of cationic precursors used and the number of pillars introduced is dependent on the cation-exchange capacity of the clay as well as the charge of the precursor used.[58] So, depending on both these factors, a greater number of pillars supporting the pores are employed, which is observed as an irregularity due to the presence of the uneven number of pillars per layer. This non-uniformity, present throughout the smectic layers, is overcome by the insertion of polynuclear hydroxy metal pillars, where the ions filled in each interlayer were of same population density. That is why a stable equivalent pore structure can be obtained. Therefore, the method has been applied limitedly to certain processes such as diesel production and cracking in petroleum production.[59] However, with the refinement of the above method then they have been employed in other applications such as adsorption and catalysis.[60,61]

1.5.2 Liquid Crystal Templating (LCT)

This method came into being with the preparation of MCM-41.[62,64] The LCT method involves the synthesis of mesoporous materials by the interaction of a silica precursor with an appropriate quaternary ammonium surfactant. Thereafter, the template was subjected to calcination for specific period of time resulting in the formation of a uniform array of channels (pores).

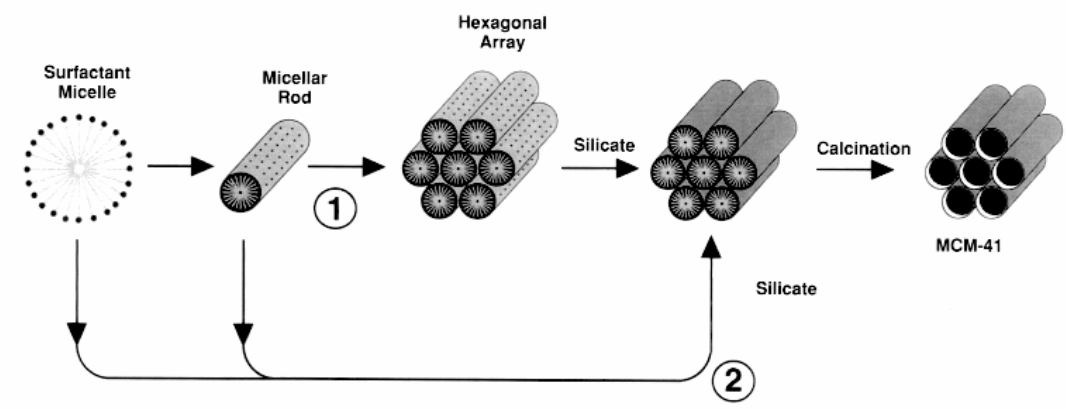

Fig. 1.15 Possible mechanistic pathways of formation of MCM-41: (1) liquid crystal phase initiated, (2) silicate anion initiated.[31]

As shown in **Fig. 1.15**, two possible mechanisms have been proposed for the formation of these mesoporous silicas. In the first mechanism (**Fig. 1.15** (1)), the formation of the liquid crystal phase is initiated by the formation of the micellar rod. On addition of a silicon source, the liquid crystal phase results in the arrangement of those micellar rods entrapped by silica. However, the second mechanism (**Fig. 1.15** (2)) provides a different explanation according to which the silicate anion on addition to the solvent surfactant mixture, acts as a phase initiator. Then, that phase results in the encapsulation of micellar

rods with silica *via* sol-gel condensation,[63] so that the surfactant organises itself as a micellar rod and the anion forms a layer around it. The resulting structure (*i.e.* micellar rod enclosed with the anionic layer) initiates the formation of hexagonal array of pores throughout. The size of the pores was influenced by two factors, the surfactant alkyl chain length and the use of an organic auxiliary[65] (*e.g.* 1,3,5-trimethylbenzene)[66] as shown in **Fig. 1.16**. On addition of 1,3,5-trimethylbenzene (mesitylene) to the synthetic mixture, the pore diameter widens and the increase in pore size can be observed in the range of 3.0 nm to 10.0 nm. Apart from organic auxillaries (as mentioned before), there are other additives known in the literature which can also be used to manipulate the pore size and to keep it constant throughout the mesoporous solids. The examples include PEG (polyethylene glycol),[67] PPO (polypropylene oxide),[68] liquid paraffin[69] and PPG (polypropylene glycol).[70] The organic auxiliaries or additives used for the modification of the pore size are generally categorised as *swelling agents*.

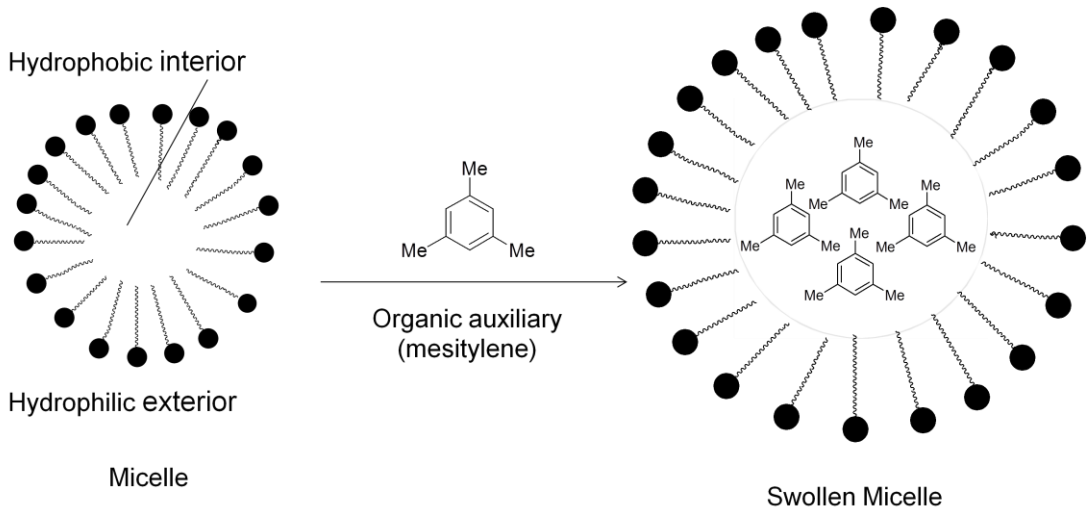

Fig.1.16 Pore size enhancement due to addition of organic auxiliary (mesitylene).

1.5.3 True Liquid Crystal Templating (TLCT)

This methodology was introduced by Attard *et al.*,[65] and involves the initial preparation of the liquid-crystalline phase (confirmed by OPM) followed by the addition of a silica precursor (TMOS, tetramethoxysilane) and a sol-gel condensation. The liquid-crystalline phase was prepared by the addition of an equimolar ratio (*i.e.* 1 : 1) of water (acidified to pH 2) and surfactant (*e.g.* $C_{12}EO_{10}$, $C_{12}H_{25}(OCH_2CH_3)_{10}OH$). The acid used for the adjustment of the pH has no effect on the methodology and is used only to achieve the isoelectric point of silica. On addition of the silica precursor (TMOS, 0.25 mol equivalent), MeOH (by-product) was released which was removed instantaneously (under gentle, dynamic vacuum) to protect the hexagonal phase (H_1) from being disrupted. Thereafter, the mixture was condensed (for 12 h) followed by calcination so as to achieve the solid with aligned pores.

1.5.4 LCT and TLCT

With TLCT, no precursor inorganic framework is required as used in LCT which has to initiate liquid crystal phase formation, rather, a pre-formed liquid-crystalline phase is used. The phase formation is directly under the influence of concentration at a particular temperature and pH.

Due to initial phase formation, the interaction between the silica and surfactant ensure the encasing of the precursor without phase separation. The interactions between the surfactant and the precursor may vary depending upon the nature of surfactants being used.

Unlike LCT, in TLCT a preformed liquid-crystalline phase was used with which there was always a confirmation of the existence of phase.

Although, both LCT and TLCT can use ionic or neutral surfactants, the silica source differs. There are certain differences which have marked effect in both the processes. In TLCT an alcohol is formed as a by-product, which is difficult to remove. However, the by-product in LCT is removed during the working up of the porous solid formed. This difference is due to the different silica precursors used. The by-product removal is a crucial step in TLCT, whereas interaction between surfactant and silica is the most crucial step in LCT. The concentration of surfactant in LCT is just above cmc but is far less than required for liquid-crystalline phase formation. Hence, the certainty of equivalent pore formation in LCT is difficult to achieve however, the reverse is true for the TLCT due to the preformed LC phase, which confirms that the pores formed will be uniform in nature. Due to this, the pores observed in M41S are in the range of micro- and meso- porous materials with pore size range of 1.7 to 2.5 nm. In TLCT, the surface area (> 1500 m^2 g^{-1}) obtained is much higher than that of LCT and or any other method.[30] the calcination process of the templates (prepared by TLCT), the pore morphology is influenced by temperature and atmospheric conditions of the furnace (*i.e.* needs control)[65] but it is not so for LCT. The latter, shows some mechanistic resemblance with methods involved in zeolite preparations.[71]

The two methodologies discussed have created a clear image of templating. However, the mechanistic models that have been suggested in different literature reviews have been discussed separately here. The mechanism is

dependent upon the nature of the surfactant. The interactions between silica and the surfactant are electrostatic.[72] Zwitterionic and non-ionic surfactants (such as Pluronics) have also been utilised for condensation but with no explanation to the charged interactions rather relative rates of assembly of the process is said to be as governing the phase formation.[73,74] However, Tanev and Pinnavaia[75] proposed a new perspective in order to give an explanation for the interactions involved in the non-ionic surfactants by making use of some functional groups on the surfactant and the silicon source. Their concept involved the formation of hydrogen bonding between the two (*i.e.* non-ionic surfactant and the silicon source (*e.g.* TEOS)), which leads to formation of mesoporous network. Although, the resulting materials was devoid of long-range order of pores but the mesoporous material had thick walls that possess high thermal stability. Huo *et al.*,[72] presented a mechanism similar to Tanev and Pinnavaia[75] which presented a general point of view of the interactions existing between the inorganic precursor and the surfactant head group. However, they also proposed reaction pathways for differently charged surfactant head groups and inorganic precursors. For instance, the oppositely charged surfactant will be interacting by S^+I^- *or* S^-I^+ *pathway* also known as *direct condensation*. They also proposed mechanistic pathways for the same charged surfactant head group and inorganic precursor. According to which, if both the surfactant and silica are cationic, then the reaction is mediated by counterions such as halides (X^- = Cl^-, Br^-) for condensation ($S^+X^-I^+$) also known as $S^+X^-I^+$ *pathway*. If the surfactant as well as silicon source are anionic, then the reaction is mediated by Group 1 metal ions (M^+ = Na^+, K^+) and forms ($S^-M^+I^-$), known as $S^-M^+I^-$ *pathway*. For neutral surfactants and

silica precursor, hydrogen bonding between surfactant head group and silica precursor is involved. The interactions within the surfactant and silica are shown with the examples in the table given below.

Table I.II The interactions involved in the condensation of surfactant and silicate with examples.[72]

(S) Surfactant	(I) Silica	Mediator	Condensation complex	Examples
(S^+) Cationic	(I^-) Anionic	_	S^+I^-	MCM-48, MCM-41S
(S^-) Anionic	(I^+) Cationic	_	S^-I^+	Iron oxide, lead oxide
(S^+) Cationic	(I^+) Cationic	X^- Halide	$S^+X^-I^+$	Silica (pH < 2)
(S^-) Anionic	(I^-) Anionic	M^+ Metal	$S^-M^+I^-$	Zinc oxide (pH>12.5)
(S^0) neutral	(I^0) neutral	_	$S^0 \cdots\cdots I^0$ *hydrogen bonding*	Alkyl amine & hydroxylated TEOS

1.6 Heterogeneous Catalysis and Heterobimetallic Nanoparticles

Catalyst technology plays a major role in almost every industry from polymers, fuels and fertilisers to pharmaceuticals.[76] Indeed industrial production, which is approximately 20 to 30% of global economy is dependent on catalysis.[77] Catalysis is a vast and emerging field and has brought changes with time in different forms, for instance from single-crystal catalysts, to activated catalysts, and then to homo- and hetero-geneous catalysts (**Fig. 1.17**). The target has always been to increase industrial efficiency which relies on a catalyst's recyclability, activity and selectivity.

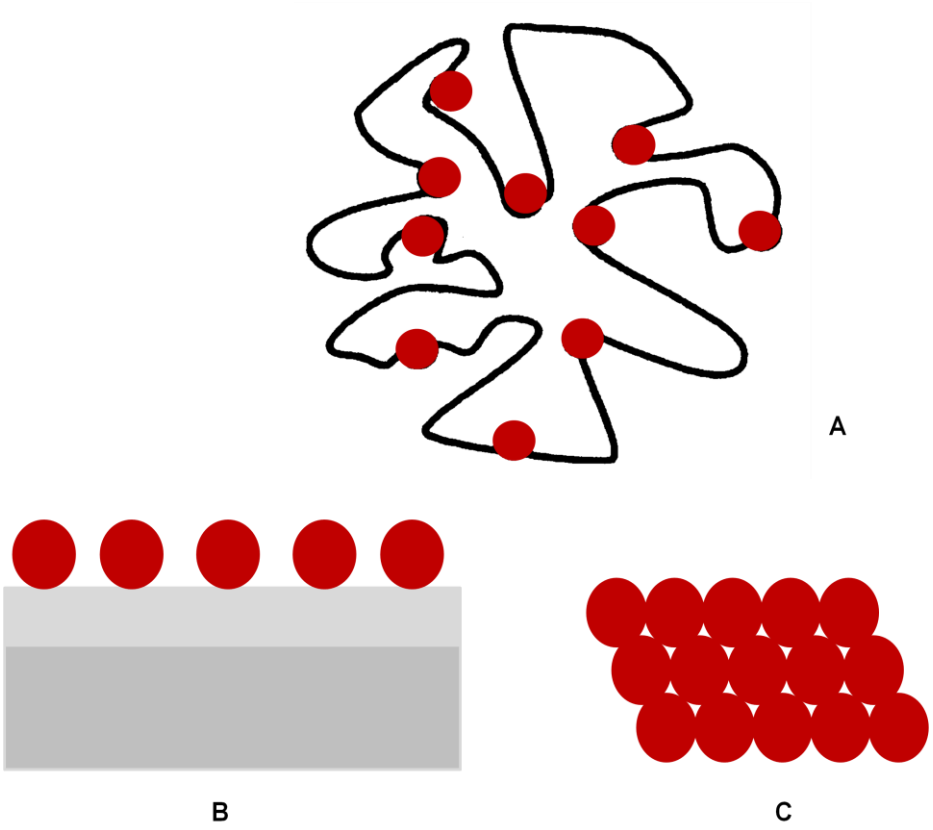

Fig. 1.17 Schematic drawings of: **A** a conventional porous catalyst; **B** a model of supported catalyst with activated phase as thin layer of support like material, and **C**, a single crystal model of supported phase.[78]

Porous solids have a great impact in the field of heterogeneous catalysis. The discovery of MCM-41, an ordered mesoporous solid, brought a revolution in the field of catalysis. It is known that catalytic performance is greatly influenced by reduced particle size due to the greater surface area and charge influencing electronic properties thus, influencing the activity of the catalyst. Therefore, with a deeper understanding of structure-activity relationships, mesoporous solids have been used as catalyst supports to enhance the activity as well as the selectivity of a catalyst. Due to their unique pore morphology, higher surface area (up to 1500 m^2 g^{-1}) and long-range order, mesoporous solids are well suited to use as catalytic support materials. The wide and

tuneable pores of mesoporous solids provide an advantage enabling them to entrap the catalysts without becoming blocked completely and a significant effort has been observed in the synthesis of such catalytic supports and resulting catalysts.

The synthesis of the catalyst is usually carried out in two steps:

Step 1: Introduction of the metal precursor or complex to the porous solid or solid support.

Step 2: Drying and calcination or reduction of the precatalytic precursor/ porous solid to remove organic matter and to obtain pores.

The step that involves introduction of metal particles or complexes into the pores of silica, is carried out by involvement of different strategies, commonly known as *direct synthesis* or *post-synthetic modification*. Some of the most common methods used in such syntheses to prepare bimetallic nanoparticles are now described.

Thomas, Johnson and co-workers have carried out work in the field of mixed-metal clusters as well as in the preparation of bimetallic nanoparticles on mesoporous supports *i.e.* MCM-41. They have also studied the catalytic activity of the bimetallic nanoparticles prepared by this method. They successfully synthesised bimetallic carbonyl clusters that included Ag_3Ru_{10},[79] Cu_4Ru_{12},[80] Pd-Ru,[82] Ru_6Sn[81] units. The method of preparation and encapsulation within the mesopores of silica was identical for the four of them, which involved postsynthetic introduction of metal carbonyl precursors to separately prepared MCM-41 support followed by thermal decarbonylation

and then removal of organic content to give bimetallic nanoparticles. For example, the preparation of bimetallic Pd-Ru nanoparticles involved use of $[NEt_4]^+[Pd_6Ru_6(CO)_{24}]$ through insertion of the mixed metal cluster onto MCM-41 support *via* adsorption, which on decarbonylation at high temperature (170 °C) resulted an active hydrogenation catalyst. The TEM analysis showed uniform particle distribution of discrete nanoparticles (*ca.*17 Å diameter) and the particles formed were confined within pores of silica (*ca.*30 Å diameter). The activity of the Pd-Ru catalyst was tested for hydrogenation of linear alkenes as well as aromatic hydrocarbons and it was found that in comparison to previously prepared catalysts (*i.e.* Ag_3Ru_{10} and Cu_4Ru_{12}) it was highly active.[82] In addition, it was easily recyclable by simple filtration and it did not influence its activity or any segregation of the two metals as components of the bimetallic catalyst.

Panpranot and co-workers[83] demonstrated synthesis of bimetallic Ru-Co catalysts through the wetness impregnation technique. The catalysts were prepared using solutions of cobalt nitrate and ruthenium nitrosyl nitrate of different concentrations impregnated into MCM-41 of different pore sizes (3 and 7 nm) and onto amorphous silica for comparison. The Co : Ru ratio was varied *i.e.* $Co_2Ru_{0.5}$/S, $Co_5Ru_{0.5}$/S, $Co_8Ru_{0.5}$/S, and $Co_{14}Ru_{0.5}$/S (where S is catalytic support used and the subscripted numbers refer to the wt% of each metal). Due to higher loadings of Co *i.e.* > 5 wt%, the XRD pattern for the bimetallic particles disappeared, probably due to blocked pores on account of the presence of high metal loadings. The reason for this was that the excess of metal present caused pore blockage. Further, to support this, the metal was completely removed from the silica framework which produced well-defined

silica pores. The reason for the pore blockage was considered as agglomerated metal particles. The wide-angle XRD results showed presence of oxides of the metals (Co_3O_4, RuO_2) and not reduced cobalt and ruthenium. Therefore, a temperature-controlled reduction was carried out to obtain reduced metal either in a single step or in two steps for SiO_2 support and MCM-41 supports, respectively. The reduction of the resulting catalyst was done under controlled temperature conditions in order to avoid any demetallation. The low-angle XRD results of the doped silicas did not show sharp peaks corresponding to well-defined pore-structure. Therefore, no TEM was performed but SEM was carried out instead. The EDX of the SEM images showed the presence of exactly the same concentrations of metals in MCM-41 (7 nm) as used in the preparation. Although the EDX results illustrated the formation of bimetallic nanoparticles of varying concentration, without TEM analysis it was not certain that they were present on the surface of the support or were embedded into the pore walls. The bimetallic catalysts prepared with MCM-41 showed high surface area even at higher loadings of Co. The results obtained showed that the Co-Ru/MCM-41 appeared to be a better catalyst than Co-Ru/SiO_2. Therefore, for catalytic activity analysis they were tested for Fischer-Tropsch synthesis as well as for CO hydrogenation[84] and the results obtained were found to complement the previous results.

The above methods of synthesis involved step-wise introduction of transition metals to the support which does not necessarily result in metal particles incorporated within the pores of silica. Therefore, another approach, called a ‘one-pot’ synthesis, was discovered, which showed the possibility of direct

incorporation of transition metal precursor to the preformed liquid-crystalline phase[85] *i.e.* before sol-gel condensation.

Dag and co-workers developed a method to produce liquid-crystalline phases with aqueous solutions of transition metals and non-ionic surfactants. Later, following this approach, they demonstrated the possibility of introducing noble metal particles though chlorometallic acids of Pt^{II}[86] and Au^{III}[86] to produce nanoparticle-doped mesoporous silicas though TLCT. Although, some success was achieved in doping the metal nanoparticles onto the silica framework, the inorganic framework produced had certain limitations such as low mechanical stability, weak pore structure and absence of long-range order of the pores.

Bruce and co-workers used metallosurfactants in a one-pot synthesis to produce metal nanoparticles, employing surfactants bipyridine complexes of Ru^{II}[87,88] (**Fig. 1.18**).

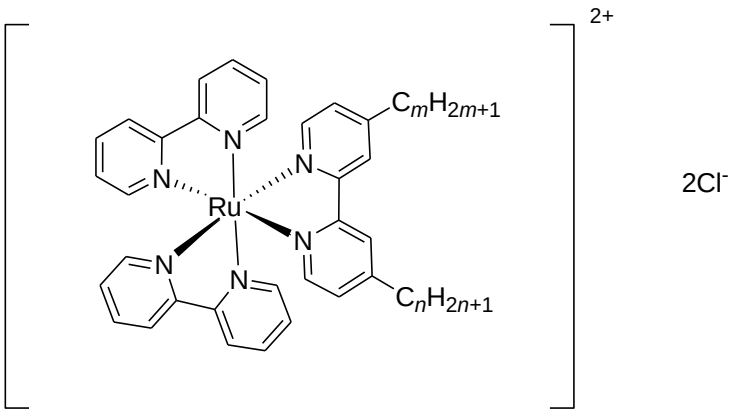

Fig. 1.18 Surfactant Ru^{II} complexes investigated by Bruce (where, n, $m \geq 12$ give hexagonal phases, and $n = m = 12$ give cubic phases).

In their work, they used an amphiphile derived from *tris*-(2,2′-bipyridine)ruthenium(II) in its hexagonal liquid-crystalline phase as a template for a TLCT synthesis to prepare mesoporous silica with hexagonal pores. On condensation of the metallosurfactant and the TMOS, a bright-orange coloured monolith resulted with the retention of the texture of the hexagonal phase. The glassy solid was then subjected to calcination, resulting in a black solid with well-dispersed RuO_2 nanoparticles (2.4 nm diameter, Ru 6 wt%) present within the mesoporous silica network. The doped silica so prepared was observed to possess high activity when analysed for hydrogenation[89] and oxidation[90] reactions.

The same research group used TLCT in a different way to demonstrate a 'one-pot' synthesis of mono-[91] as well as bi-[92] metallic nanoparticles on a mesoporous silica support. For monometallic nanoparticles, Group 1 metal salts of the halometallate anions of Pt^{II}, Pd^{II} and Au^{III}, were used. However, for mixed-metal silicas, an EDTA complex (as the sodium salt) of some first-row transition metals (Co^{II}, Fe^{II}, Cr^{III}) was employed to get round the kinetic lability of their chlorometallate anions in water. The methodology involved using aqueous solutions of the EDTA complexes in water to produce the mesophase before addition of silica precursor. The homogenisation of the mixture was the key in producing uniformly distributed mono- or bi- metallic nanoparticles. The nanoparticles produced from single metal salt showed results very similar to those observed previously for $[Ru(bipy)_2(bipy')]^{2+}$ surfactants with respect to the silica framework such as wall thickness, pore dimensions *etc.* except that the particles were sometimes observed to be present outside the pores. Hence, efforts were made in the direction of

synthesis of metal nanoparticles incorporated into the silica framework by employment of different noble metals using readily available simple metal salts as off-the shelf reagents. For bimetallic nanoparticles, two different metal precursors were employed, for instance Pt-Co, $K_2[PtCl_4]$, and $Na_2[Co(EDTA)]$; Pd-Au, $K_2[PdCl_4]$, and $K[AuCl_4]$; Pd-Ru, $K_2[PdCl_4]$, and $Na_3[Ru(EDTA)]$.

The coloured translucent monoliths formed after sol-gel condensation resulted in a dark-coloured, porous solid after calcination and the method successfully produced bimetallic nanoparticles. Low-angle XRD analysis showed the presence of a well-defined hexagonal pattern of the porous solid. TEM and EDX analysis showed that the nanoparticles were present within the pores but were not always confined to a single pore (Pt-Co, Pd-Au). Also, the particles formed were not truly bimetallic as a wide variation in the atomic ratio of a set of bimetallic nanoparticles *i.e.* from 44 : 56 to 97 : 3 for Co : Pt were observed even though the overall loading was 50 : 50. This variation was rationalised as being due to incomplete mixing of the metal mixture at the beginning of sol-gel condensation.

Origin of current project

Given that the routes to heterobimetallic particles described above did not lead to particles with uniform composition, it was of interest to determine whether better results could be obtained if single-phase, hetero-binuclear metal complexes were used as the origin of the metals. The work described in this thesis details efforts in this direction.

1.7 Ditopic Ligands

The term ditopic ligands originated from the term 'doubly connecting ligands' with the same or different functional groups. In other words, a ditopic ligand is a receptor which possesses two coordinating regions irrespective of the number of coordination sites or atoms available for binding with the metal ion.[93]

The common donor atoms found in ditopic ligands are N, P, O and S, present along with the organic part that is often a heterocyclic ring (**Fig. 1.19 A**, **B**), salen (**Fig. 1.19 C**), a Schiff's base (**Fig. 1.19 D**), a macrocycle (**Fig. 1.19 E**, **F**), *etc.* However, other examples include miscellaneous mixed systems which are formed as a result of joining of cryptands or crown ethers (**Fig. 1.19 G**, **H**) with different heterocyclic rings and other ligands.

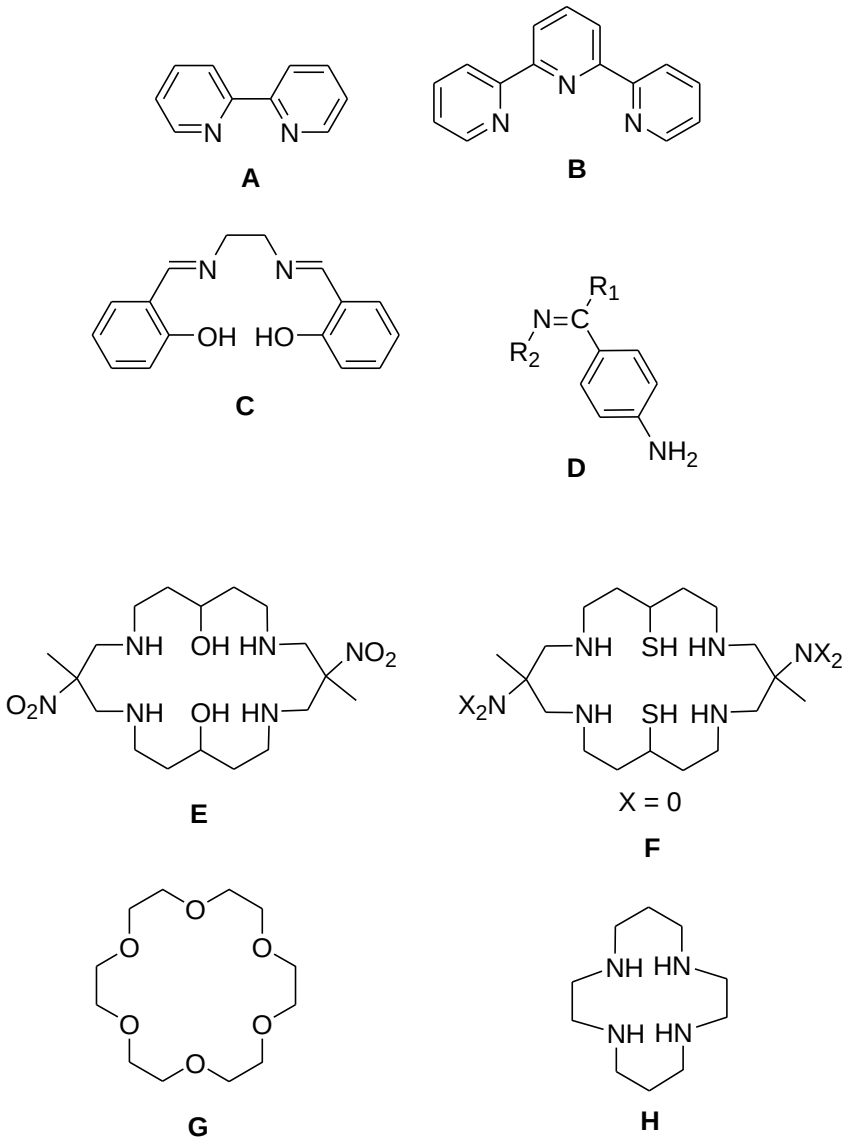

Fig. 1.19 Structures of different ligands, heterocyclic rings **A** 2,2′-bipyridine, **B** Terpyridine, **C** Salen, **D** Schiff's base with aniline, where R_1 and R_2 organic moieties, **E** and **F** Macrocycles with *N*, *O* donor and *N*, *S* donor atoms, **G** and **H** are crown ether and aza crown, respectively.

In addition to these examples, there are other examples of the ligands that have been recently introduced and are reported to be new generation ditopics.[94,95,96] **Fig 1.20**. Nevertheless, the examples of the recently discovered ligands or the new generation ligands (**Fig. 1.20 A** and **B**) and their applicability in the formation of heterobimetallic complexes is yet to be detected or found.

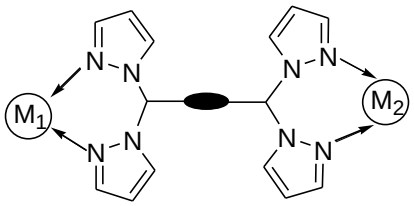

A

spacer,= *o*-phenylene; M_1, M_2 possible metals of coordination

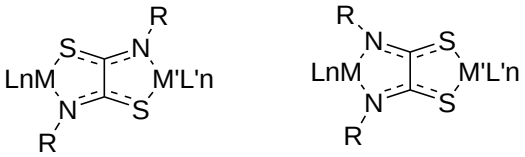

B

where M, M′ = Pd, L = η^3-allyl, R = ethyl, isopropyl, benzyl, isoamyl or 1-(S)-(1-phenyl)ethyl and/or (R)-(1-phenyl)ethyl

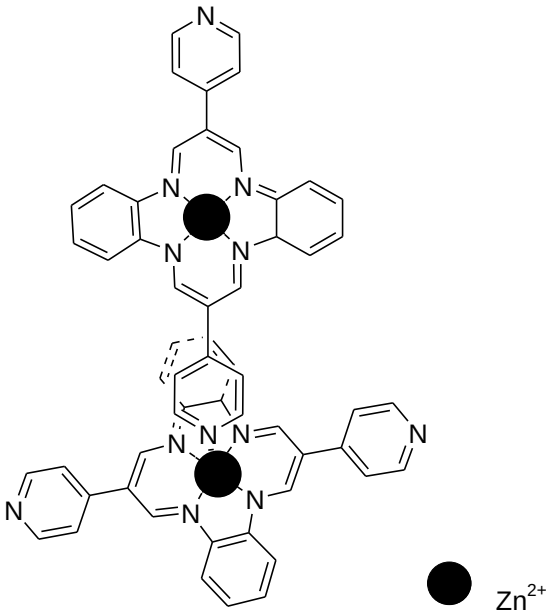

C[96]

Fig. 1.20 Showing examples of new generation ditopic ligands.

Examples illustrating the use of ditopic ligands in heterodinuclear coordination have been reported in the literature and are discussed below.

Ditopic ligands have been known since the 1980s, but the concept has evolved with time with the need or requirement for homo-, hetero- or poly-metallic complexes for applications such as involvement in developing coordination chemistry,[93] catalysis,[97] luminescence,[98,99] magnetic materials,[100] as building blocks,[101,102] environmental science[103] and hydrometallurgy[103]. On the basis of the nature of coordination sites which are the same or different, they have been broadly classified as homo-ditopic and hetero-ditopic ligands, respectively. (**Fig. 1.21**).

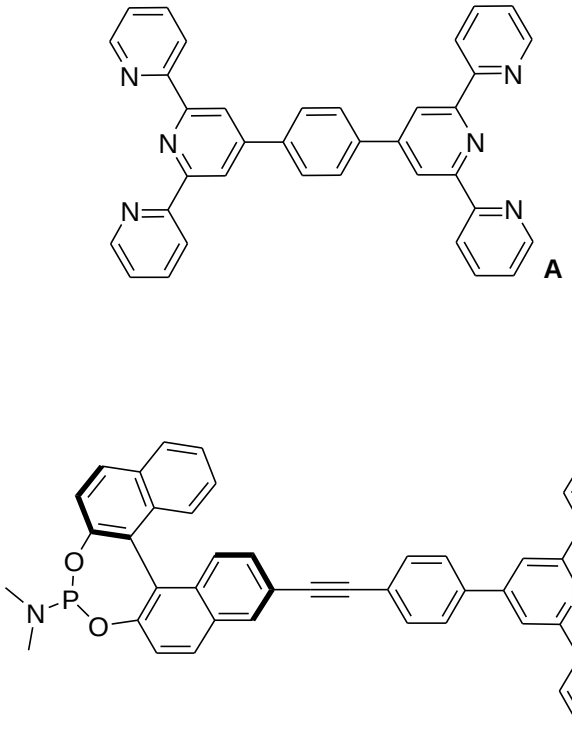

Fig. 1.21 Structures of **A** homo-ditopic ligand with N donor atoms,[104] **B** hetero-ditopic ligand with P and N donor atoms.[97]

The presence of a different number of coordination sites in turn influences the binding affinity of the ligand towards different metal ions when they are

introduced into the system or to the ligand. This is discussed in the examples given later in this section.

An underlying principle of the binding preferences is the HSAB concept[105] according to which, a soft ligand (base) prefers to bind with a soft metal (acid), while a hard ligand (base) prefers binding with a hard metal (acid). The general trend of an increase in the softness of metals (or decrease in the hardness) in the Periodic Table is from left to right across the period and from top to bottom in a group. Typical examples of soft metals include heavier transition metal ions in lower oxidation states (*e.g.* Pt^{II}, Ag^{I}, Au^{I}) as well as low-valence metal ions (*i.e.* M(0)). However, examples of hard metals include smaller metal ions (*e.g.* alkali, alkaline earth metals) as well as the metals with high charge (*e.g.* Fe^{III}, Cr^{III}). Some metals are termed 'intermediate', such as Fe^{II}, Cu^{II} and Zn^{II}. In ligands, the decrease in softness or increase in hardness is observed with an increase in the electronegativity of the donor atom of the ligand as shown in the figure below.[105]

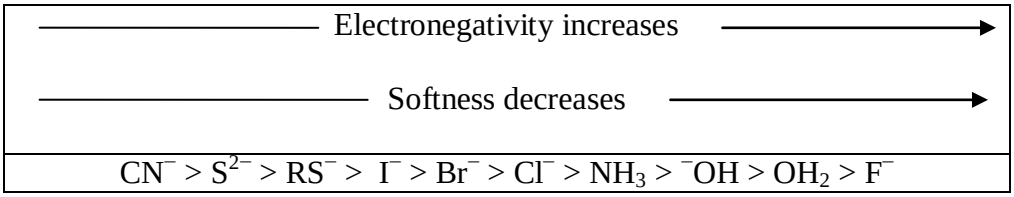

Fig. 1.22 Effect of electronegativity of the ligand on hardness/softness of metals.

In order to meet the criteria of the HSAB principle, the focus has been localised on the synthesis of the bifunctional ligands, in which, the presence of at least two functional groups, which may be same (hard-hard or soft-soft) or different (hard-soft), is essential. However, the number of coordination sites

may vary depending upon the requirement or the nature of metal(s) being targeted. The introduction of metals is usually carried out in a sequential manner for heterobimetallic systems in order to avoid any side reaction or competition between the two coordination sites. (*e.g*. see **Fig. 1.30**) However, if the thermodynamic stability of the complex is greater then both hard as well as soft metal cation can be introduced at the same time (*e.g.* see **Fig. 1.31**), if sufficient reaction time is provided to allow equilibrium to be reached. Nonetheless, an alternative way is to introduce one metal first to both sites *i.e.* M_1 to the ligand, followed by a differential demetallation (*i.e.* removal of one metal out of the homo-dinuclear complex and to obtain a mononuclear complex with vacant coordination sites), shown in **Fig. 1.23**. While considered as rather difficult, this approach has been reported as a good method for *f-f* metal systems used as MRI contrast agents.[106] This approach was employed to show an example where the chelates used in a ligand were thermodynamically indistinguishable *i.e.* DOTA and DTPA (**Fig. 1.23**). Nevertheless, the DTPA site was prone to kinetic dissociation, and due to the difference in complexation rates of the two sets of coordination sites, this method of sequential addition was postulated.

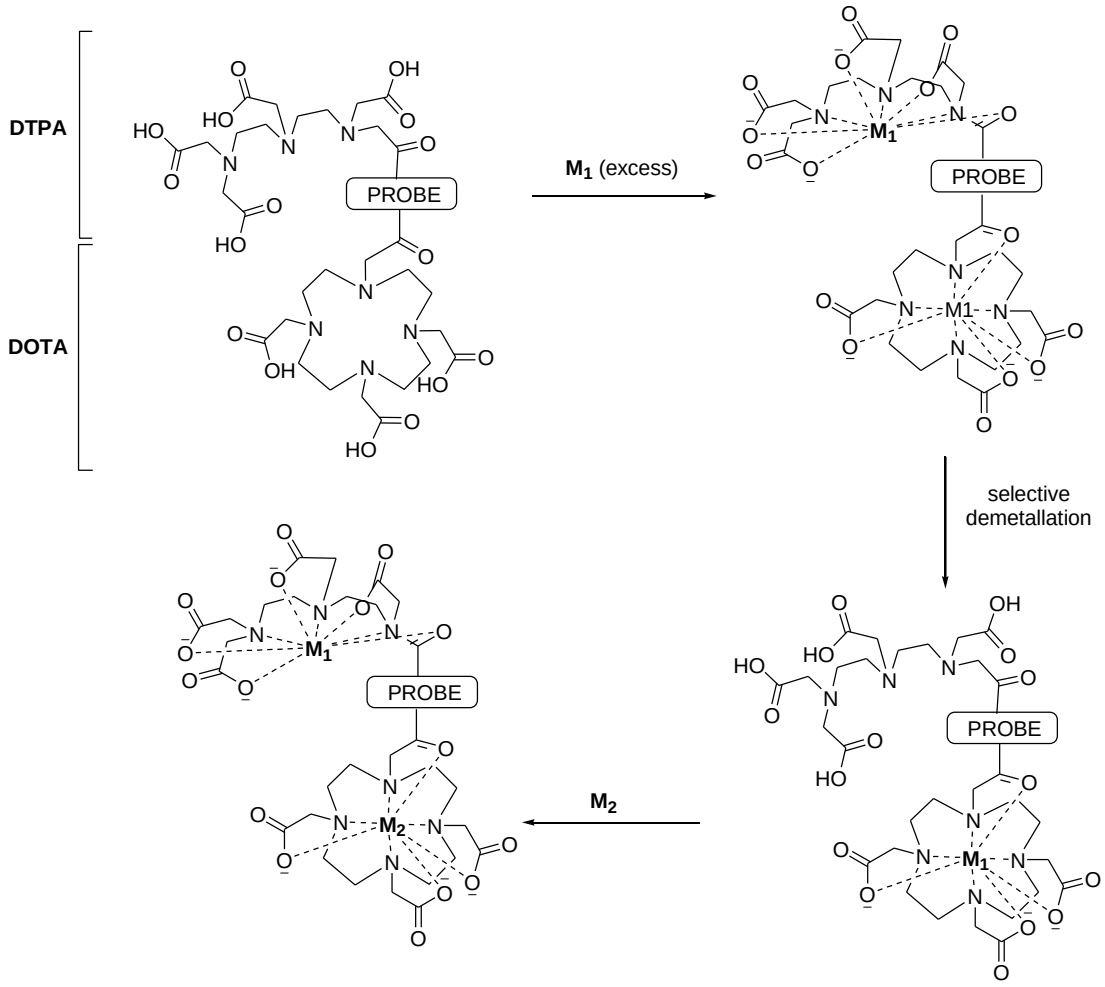

Fig. 1.23 Schematic representation of the sequential, differential metallation of a DOTA/DTPA bis-chelate with two different metal ions M_1 and M_2.[106]

Some examples of homo-ditopic ligands are also included in the discussion, whereas polytopic ligands are excluded as a part of discussion for convenience although, a couple of examples are shown where the heterobimetallic complexes act as building blocks. Also, the bimetallic complex combinations are indicated through the examples of *d-d*, *d-f*, and *f-f* block elements only.

Shaw, Pringle and co-workers showed a pathway to generate homo- as well as hetero-dinuclear transition metal complexes (mainly alkynyl complexes) containing two bridging dppm ligands such as Pt^{II}-Pt^{II},[107,108,109,110] Rh^{I}-Rh^{I},[111] Pd^{II}-Pd^{II},[112] Pt^{II}-Pd^{II},[113,114,115,116] Pt^{II}-Hg^{I},[111,112,117,118,119] Pt^{II}-

Ag^{I},[120,114,107,112,117,118,119] Pt^{II}-Cu^{I},[120] Pt^{II}-Au^{I},[120,114,107,112,119] Rh^{I}-Pt^{II},[107,121,112,118,122] Ir^{I}-Pt^{II},[123,112,122], Pd^{II}-Mo,[112] Pd^{II}-Hg^{I},[112,118] Pd^{II}-Ag^{I},[107,118] Pd^{II}-Ir^{I},[112] Pd^{II}-Rh^{I},[112,118] Rh^{I}-Mo, Pt^{II}-Mo,[112] Ir^{I}-M and Rh^{I}-M (where M = Mo, Co or Cr),[124] Pt^{II}-W[122], Pt-Cd.[119]. The generation of such hetero-dinuclear complexes was to study their luminescent properties and the influence of spacer length of alkynyl groups or the separation between the two metal atoms on the luminescent property of the metal. A few examples are given in **Fig. 1.24**.

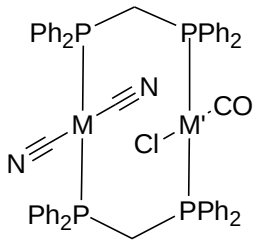

1[112]

M = Pt^{II} or Pd^{II}, M′ = Rh^{I} or Ir^{I}

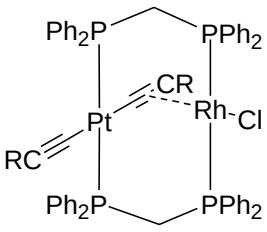

2[121]

R = Ph or p-tolyl

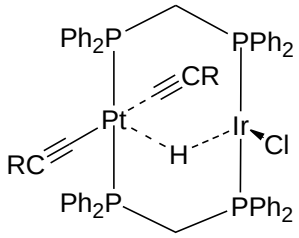

3[123]

R = p-tolyl or phenyl

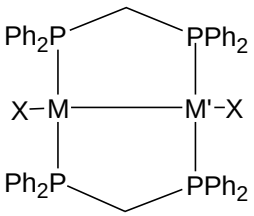

4[113]

M= Pt^{II}, M′= Pd^{II},

X = Cl, Br, I or SCN.[113]

Fig. 1.24 Heterobimetallic dppm bridged complexes.

The ligands used by them were homo-ditopic which involved the use of dppm as a prime bridging ligand. However, in some cases acetylide[125,121,123,116] or hydride[108] is observed acting as a third bridge while in others a metal-metal bond formation[112,122] or interactions have also been reported.

The general methodology used to generate most of the above-mentioned complexes mainly involved the coordination of the two dppm ligands in a monohapto manner to the first metal atom (mononuclear complex, generated *in situ*) followed by the use of the two free phosphorus atoms to coordinate with the second metal atom (**Fig. 1.25**).

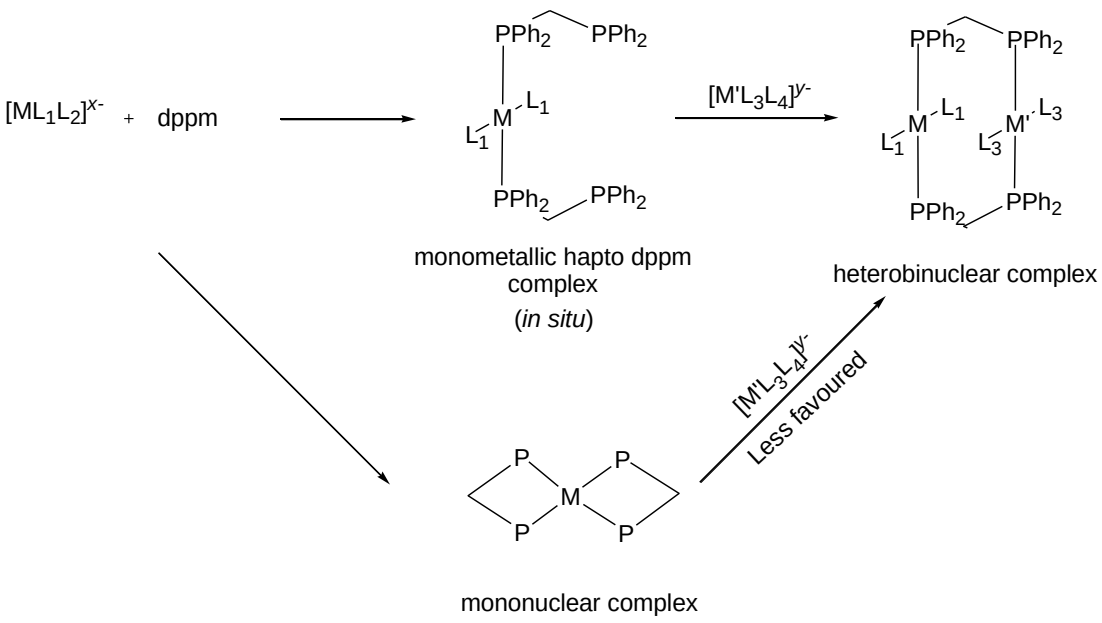

Fig. 1.25 General method of synthesis adopted for the formation dppm bridged complexes. where $L_1=L_2$ or $L_1 \neq L_2$, $L_3=L_4$ or $L_3 \neq L_4$.

In this method of preparation the role of associated ligands (*i.e.* ligands other than dppm) is of considerable importance for charged as well as neutral metal ions. The associated ligands are selected for their strong binding ability to the metal atom, which assists to prevent the cyclisation of metal atom to dppm

which would have resulted into a four-membered chelate ring, (a mononuclear complex). The associated ligands should also be able to provide stability to the monometallic hepto dppm complex formed initially before the coordination of the free phosphorus atoms of dppm to the second metal. Hence, ligands such as halogens were neglected in most of the cases as they can easily be replaced and can promote cyclisation. However, good examples of associated ligands include C≡CR, CNR, CN, aryl, alkyl *etc.*

Yam and co-workers prepared different heterobimetallic alkynyl complexes of Fe^{II}-Re^{I}[126] and Au^{I}-Re^{I},[127] to study the luminescent properties of bimetallic systems. The method of preparation involved the combination of two different mono-metallic organic moieties ([(C_5Me_5)(dppe)Fe(C≡C–R)] and [Re(diimine)$(CO)_3$(C≡C–R)]), or the tethering of two different metal centres through alkynyl and pyridine groups, respectively. This resulted in two active metal centres held together with a coordinated system as shown in **Fig. 1.26**.

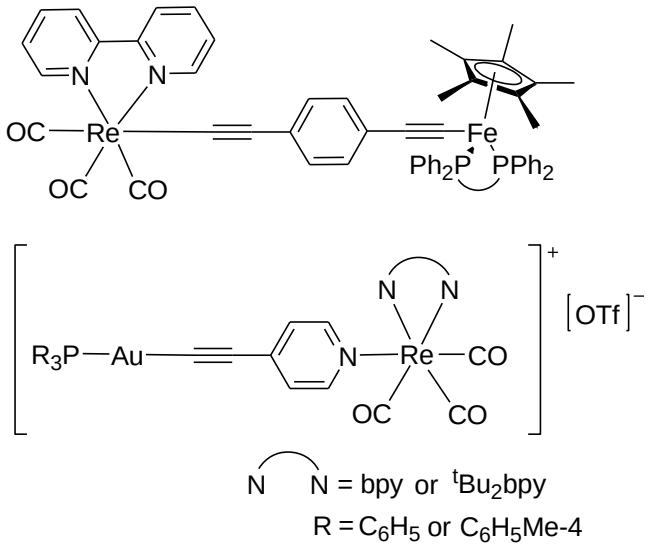

Fig. 1.26 Heterobimetallic alkynyl Fe^{II}-Re^{I}[126] and Au^{I}-Re^{I}[127] complexes.

Apart from the above-listed examples, the use of *N*-rich heterocyclic rings to prepare bimetallic complexes is very common and many examples can be found in which various bipyridine, terpyridine, and azole rings are involved in the coordination of metal ions. Other examples include S- and P-containing rings, thiophene and phosphine. However, O-containing ditopic ligands involve examples of salen complexes. Mixture of all the ligands such as N- with S-, P- and/or O- containing moieties have proved to be far more successful in their ability to coordinate with different metal ions (discussed below). This again relates to the HSAB principle as the ligand containing N and O donor atoms is considered as a hard ligand (due to greater basic strength of the ligand) in comparison to P- and S-containing donor atoms, which are considered as softer donor sites.

The strategies that have been reported to be commonly used in most heterocyclic metal binding systems (*i.e.* bipyridines and terpyridines) are: synthesis of a free ligand with desirable coordination sites, which is done by the selection of coordination sites based on the HSAB principle and other factors *e.g.* flexibility, metal size *etc*. The second, and most commonly used method in the generation of new multinuclear ligands is reaction of electrophilic and nucleophilic components of two or more metals (that may be the same or different), resulting in homo- or hetero-metallic complexes. One of the examples of homo-dinuclear complex formed as a result of the second strategy is shown in **Fig. 1.27**.

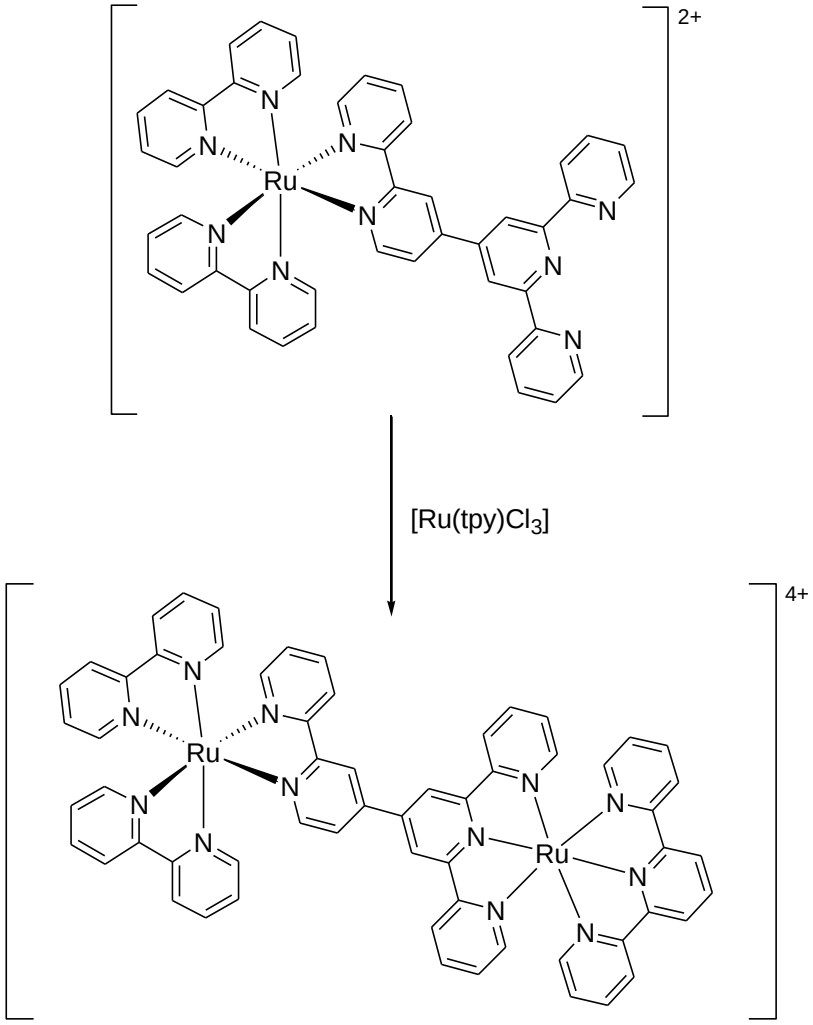

Fig. 1.27 Synthesis of homo-dinuclear Ru complexes containing bipyridine and terpyridine ligands.[128]

1,10-Phenanthroline derivatives have also been reported to be used as ditopic ligands so as to synthesise homo- as well as hetero-bimetallic complexes. The strategy to synthesise such ligands involves functionalisation of the 1,10-phenanthroline nucleus to form respective derivatives by substituting various functional groups or organic moieties with desirable coordination sites at 2,9-position of the phenyl ring. The latter have been reported to be the most favourable positions as many examples of homo-dinuclear complexes with 2,9-substituents of 1,10-phenanthroline derivatives are known in the literature.

Other, less common, functionalised positions are 3,8-, 4,7- and 5,6-. Nevertheless, the examples of functionalised phenanthrolene derivatives that have been reported to be heterobimetallic contains 1,10-phenanthroline derivatives functionalised other than 2,9-position. For instance, the example shown in **Fig. 1.28** of Ru^{II}-Cu^{II} complex has been synthesised by functionalisation of 5,6-phen position of 1,10-phenanthroline nucleus.

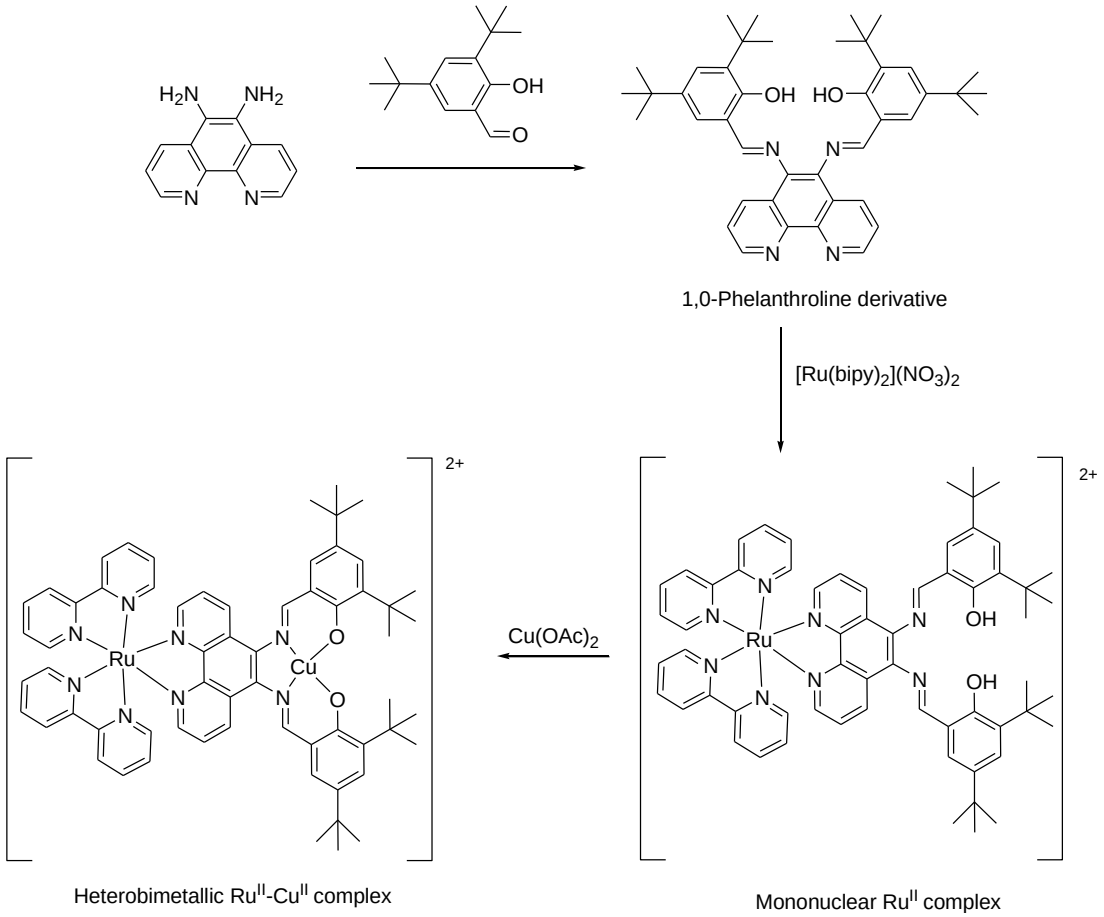

Fig. 1.28 Heterobimetallic Ru^{II}-Cu^{II} complex coordinated by heteroaromatic ring with phenanthroline derivative.[129]

Macrocyclic ligands have also been used over the past few years to form homo- as well as hetero-binuclear metal complexes for a wide range of metals such as *s-f*, *d-d*, *f-f* and *d-f* -block metals. The reason for their versatility is their

flexible cavity in a cage-like structure which can adjust according to the coordinating metal size, hence making the system more stable. Most common examples include Schiff bases (cyclic or acyclic), however others include pendant-arm macrocyclic or acyclic ligands which possess polyaza or polyoxa donor sets.[130,131] (**Fig. 1.29**). Further examples include cyclic lactams, phosphorus macrocycles *etc.*

A[132] **B**[133]

Fig. 1.29 Pendant arm structures of macrocyclic ligands used for heterobimetallic complexes of **A** Gd^{III}-Rh^{I}, **B** Gd^{III}-Fe^{II} or Gd^{III}-Ni^{II}.

The strategy used in the preparation of macrocyclic systems involves self-condensation of keto-, formyl, or primary amine-like precursors, which are initially designed with respect to steric and electronic factors targeting the synthesis of the final product (or desired ligand). The conditions are selected in such a way that the formation of by-product/s (separation difficulties) or side reaction/s (*e.g.* metathesis, exchange reactions) can be minimised.[134] The condensation is usually achieved by a single step reaction for acyclic ligands. However, in others multiple steps may be required. For instance, the generation of the heterobimetallic Cu^{II}-Ni^{II}[135,103] or Ni^{II}-Zn^{II}[136,103]complex (**Fig. 1.30**) was carried out in a step-wise fashion. In this synthesis, a mononuclear complex was generated by a [1+1] condensation of a 4,5-

dialkoxy-1,2-diamine derivative with a substituted monoamine ligand (4,5-dialkoxy-1,2-diamine derivative) in the presence of the first metal *i.e.* M. In the next step, the mononuclear complex was again treated with the same substituted monoamine ligand, along with the presence of second metal salt, M′ (two equivalents) resulting the respective heterobimetallic complex. The percentage yield for each of the hetero-binuclear complexes was 91%.

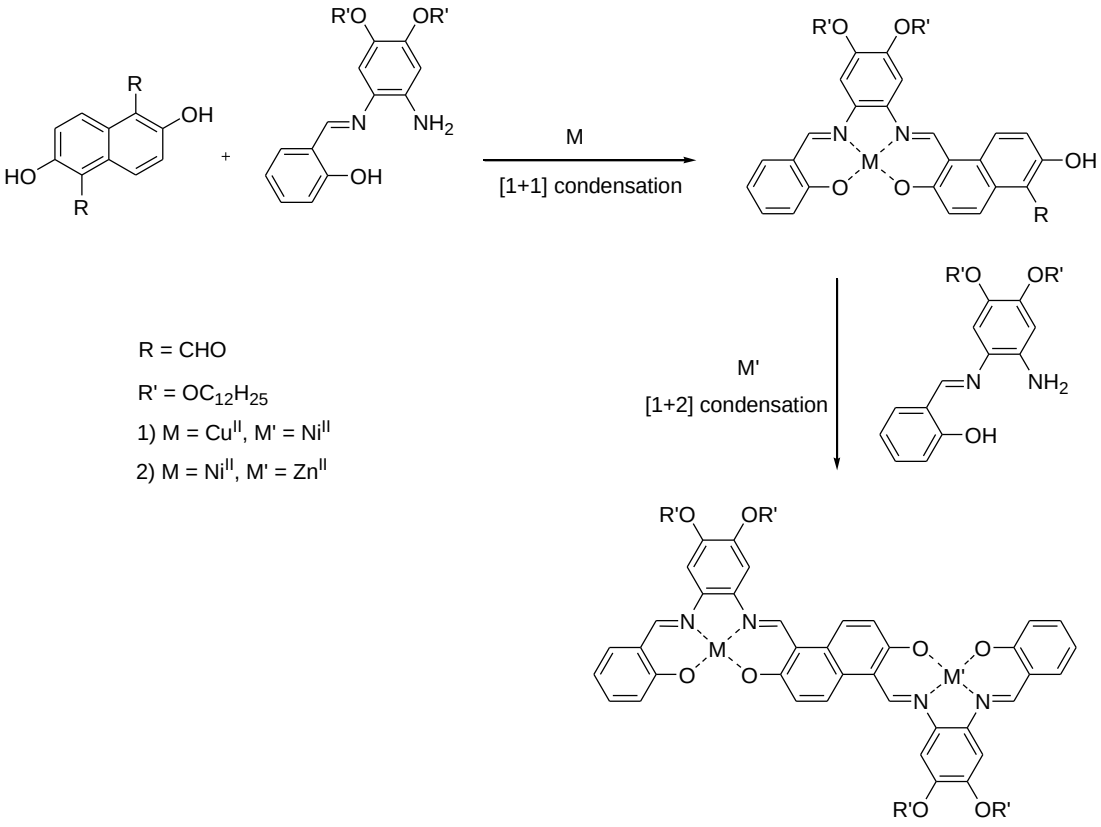

Fig. 1.30 Schematic representation of formation of Cu^{II}-Zn^{II}[135,103] and Ni^{II}-Zn^{II}[136,103] complex.

Another example is of a heterodinuclear Cu^{II}-Zn^{II} complex (**Fig. 1.31**) resulting from the sequential condensation of an aromatic dicarbonyl derivative (*i.e.* 2,6-diformyl-4-methylphenol) with two different primary amines (*i.e.* (2-aminoethyl)bis(2-pyridylmethyl)amine and thiosemicarbazide), followed by reduction. In this case, the preformed ligand formed was exposed to two

different metal salts in equimolar ratios with respect to the ligand resulting in heterodinuclear Cu^{II}-Zn^{II} complex.[137]

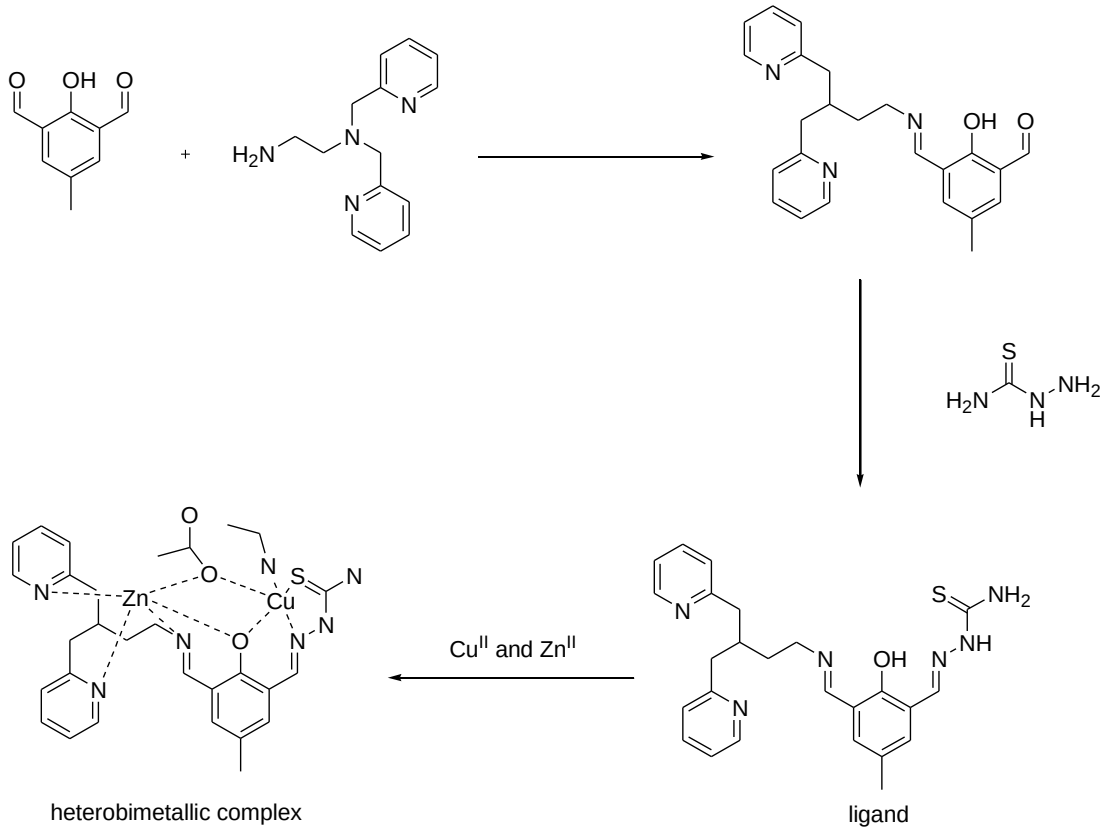

Fig. 1.31 Synthesis of heterobimetallic Cu^{II}-Zn^{II} complex.[137]

Mixed-ligands are also widely used and there are innumerable examples with various coordinating metals. In these systems, two entirely different ligands are combined *e.g.* heterocyclic rings with acyclic ligands (*d-d, d-f, f-f*), polyaminocarboxylates with crown ether (for *s-f* block metals, *d-f* block metals). The applications of such mixed ligands are as building blocks.[138,139] For instance, the trinuclear Gd^{III}-Fe^{II}-Gd^{III} complex shown in **Fig. 1.32** below indicates a recent example of a mixed-ligand heteronuclear complex which is formed as a result of a self-assembly process. In this method, the ligand was

synthesised prior to exposing it to the metal ions, resulting in a coordinated self-assembled trinuclear complex.

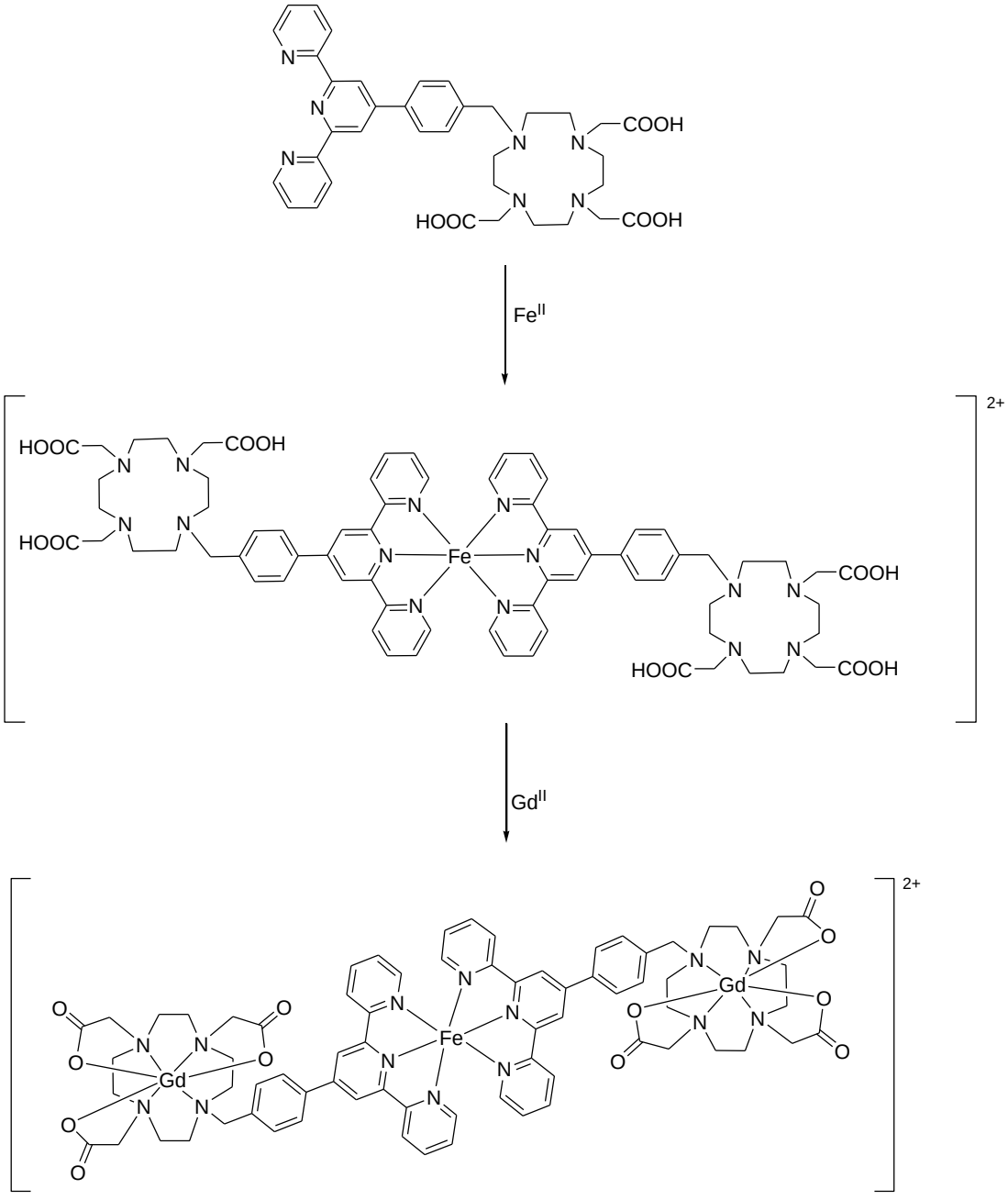

Fig. 1.32 Synthesis of heterotrinuclear metal Gd^{III}-Fe^{II}-Gd^{III} complex with terpyridine substituted aminopolycarboxylate.[140]

Another example, of a mixed ligand forming a heteronuclear Pt_2-Fe_2 complex is shown in **Fig. 1.31**, which also resulted from self-assembly. In this case a

mononuclear metal complex with uncoordinated terpyridine linked through a –CH_2O unit to acetylene (used to bind to Pt^{II}) was exposed to the second metal ion (Fe^{II}), resulting in a heterometallic mixed-ligand complex (**Fig. 1.33**).

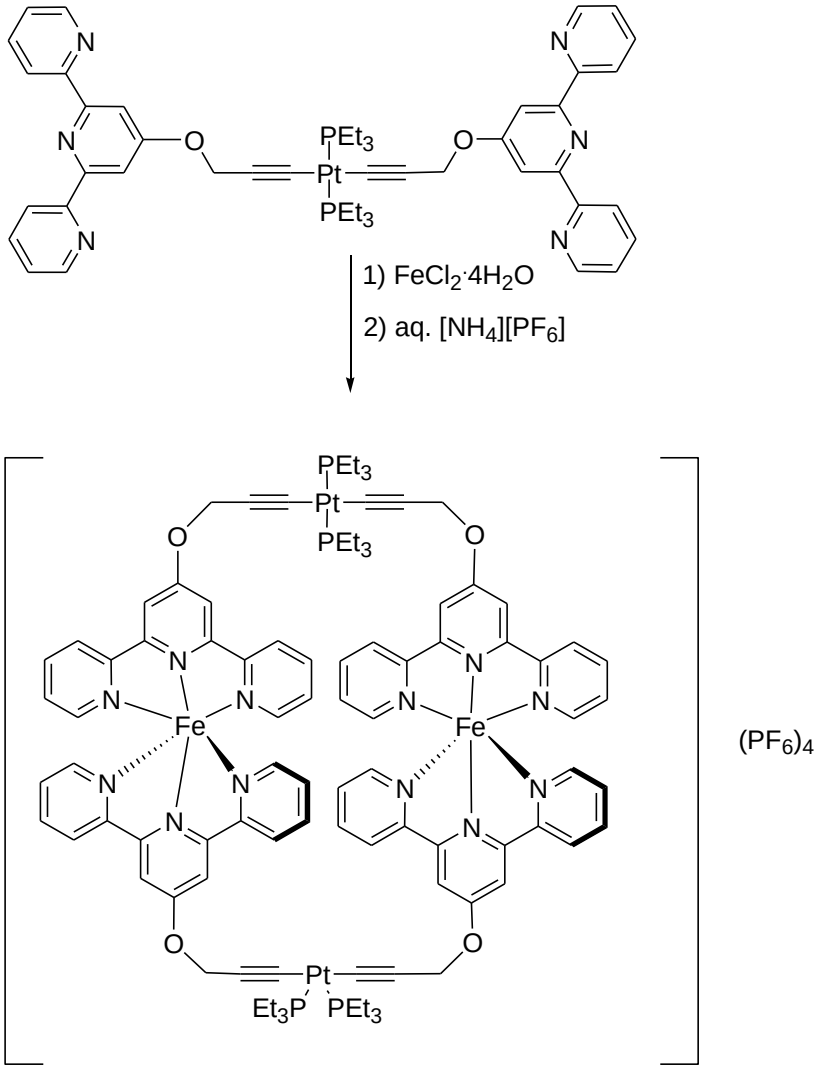

Fig. 1.33 Synthesis of heterometallic Fe^{II}-Pt^{II} complex with terpyridine and alkyne ligands with a short-spacer.[141]

The coordination of the two metal systems can also be carried out by using bifunctional ligands separated by extended spacers. The spacer may or may not be involved in the properties of the two metals but is acting to keep the inter-

metal distances fixed. There are various mixed-metal systems reported to be formed in this way. For example, heterobimetallic Rh-Os[142] and Pd-Pt,[143] complexes are prepared using in which two different ligands acts as spacers *i.e.* an alkyne spacer (*i.e.* a cumulene bridge) and phosphine ligands (*i.e.* diphosphine $Ph_2P–C≡C–PPh_2$), respectively. The spacers participating in both the complexes participate in an electron transfer and luminescence, respectively.

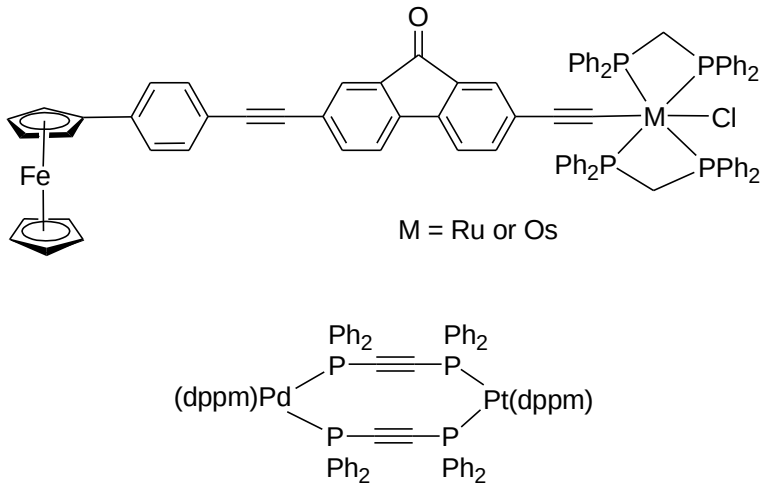

Fig. 1.34 Heterobimetallic complexes formed through conjugated molecules (acting as spacer).[143,144]

There are also examples of some spacer-linked polyaminocarboxylates in the literature where two different binding groups *i.e.* DTPA and DOPA have been joined to form *f-f* block bimetallic complexes.[106] This has already been described in **Fig. 1.23** and is given below in **Fig. 1.35**.

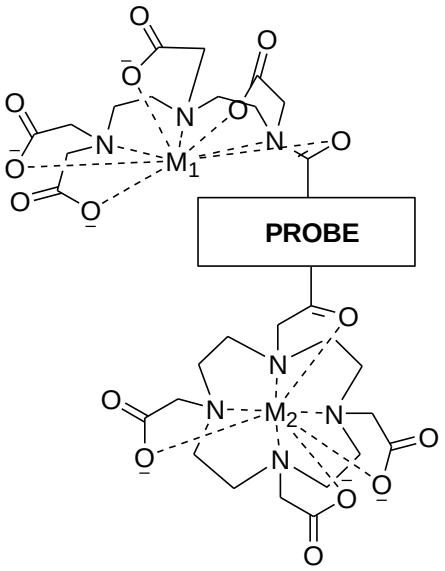

Fig. 1.35. A heterobimetallic lanthanide complex, where M_1 and M_2 are two different metals (lanthanides).

Early-late heterobimetallic complexes are involved in chemical transformations as catalysts in different reactions.[145,146,147,147] The synthetic strategies of early-late heterobimetallic complex preparations involves use of bridges, which are helpful to bring two different metal atoms together. Such methods used to form early-late heterobimetallic complexes have been reported to possess problems when close proximity is desired. Some of the problems include metal-metal bridging interactions *i.e.* communication of two different metals which are of different coordination chemistry.[148] Such metal-metal interactions can affect the reactivity of a bimetallic system when involved in a chemical transformation. In order to avoid this problem, it is important to use a ligand that minimises the possibility of metal-metal interactions or ensures that there are no interactions between the two metals. This can be exemplified with the help of a few heterobimetallic complexes shown below.

For example, the dithiolate bridged heterobimetallic Pt^{II}-Ir^{I} complexes (**Fig. 1.36**)[149] show intermetallic distances that preclude metal-metal interactions.

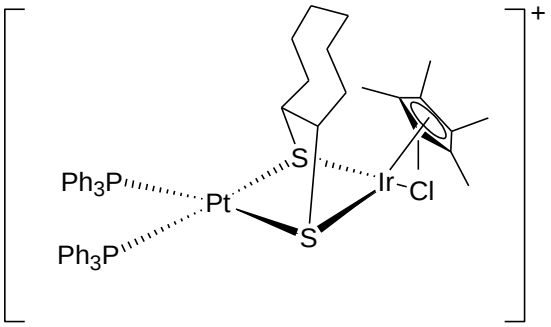

Fig. 1.36 Heterobimetallic Pt^{II}-Ir^{I} dithiolate-bridged complex.[149]

On the other hand, in the Nb-Rh heterobimetallic complex (**Fig. 1.37**) with phosphido- and imide-bridge,[150] then the interaction between the two metal centres is very prominent as the metals are forced to be close by the bridging ligands. The latter showed less reactivity in hydrosilylation reactions when tested for catalytic activity.

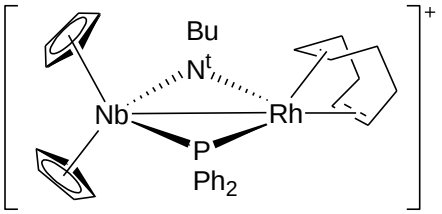

Fig. 1.37 Heterobimetallic Nb-Rh complex showing interactions between the two metal atoms.[150]

In another example, an aminophosphine ligand was used to overcome the intermetallic interactions between Ti and Pt. In this ligand, a rigid spacer *i.e.* aryl group was used which acted effectively to separate the two metals.

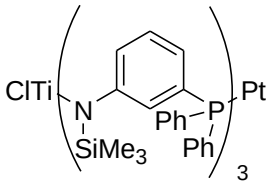

Fig. 1.38 An aminophosphine ligand forming a Pt^{0}-Ti^{IV}, early-late heterobimetallic complex.[151]

The method of preparation of an aminophosphine ligand involves two steps *i.e.* proton abstraction, and lithiation (**Fig. 1.39**). In step 1, a proton is abstracted from the primary aminophosphine ligand which is then followed by lithiation and then it is reacted with addition of first metal complex (*i.e.* $TiCl_4(THF)_2$). The latter results in a mononuclear complex which is then exposed to the second metal salt resulting into the desirable heterobimetallic complex (**Fig. 1.38** and **1.39**).

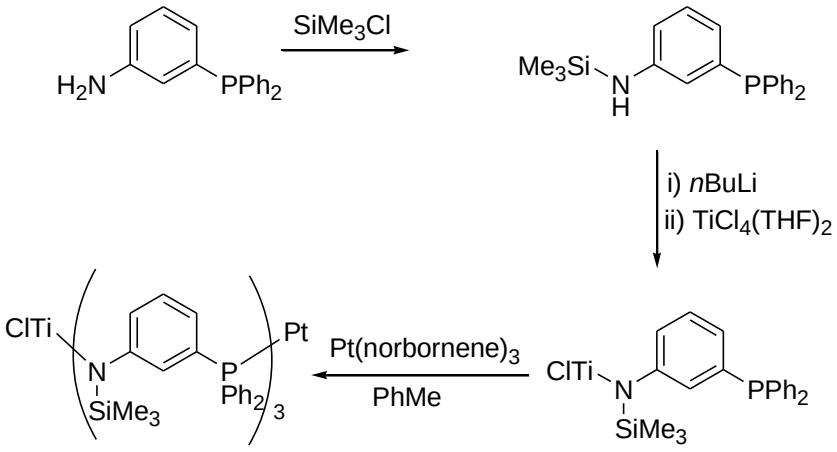

Fig.1.39 Synthesis of heterobimetallic Ti^{IV}-Pt^{0} complex.[151]

All the examples discussed above involve use of mostly bulky organic substituents, containing coordinating heteroatoms that are eligible for binding

with different metal ions. They also exemplify that a wide range of heterobimetallic complexes are possible. Due to the presence of bulky substituents in these complexes they are not water soluble. Consequently, it is impossible to use them to prepare metal nanoparticles *via* TLCT techniques. Nevertheless, if a recent example of a heteronuclear bimetallic MRI contrasting agent is considered in which a heterotrinuclear complex (**Fig. 1.32**) and heterobimetallic complexes (**Fig. 1.23** and **Fig. 1.35**) have been prepared, then there is a possibility that by using the same method of preparation a heterobimetallic complex might result. Then also, there will be prospective issues such as water solubility, hydrolysis, or stability of the complex at the step of introduction of the silica precursor. (*i.e.* at the stage of hydrolysis and methanol evolution). The stability of a complex in a lyotropic liquid-crystalline phase is an extremely important aspect as sometimes a perfectly stable complex has been seen to precipitate resulting from the bulky complexes. These are the issues which are expected to arise in experimental work and will require to be addressed.

Chapter 2
Halo-bridged Complexes

2.1. Introduction

In Chapter 1 (section 1.7), the methodologies of the formation of different types of bimetallic complexes (*i.e.* homo as well as hetero bimetallic complexes) using ditopic ligands were discussed. However, this chapter will focus only on the formation of heterobimetallic complexes of transition metals using halogens as bridging groups.

As described earlier, (Chapter 1), the aim of the project was to synthesise heterobimetallic complexes that could be used further as precursors to prepare mesoporous silicas containing heterobimetallic nanoparticles. This is because mononuclear chloridometallate complexes (*e.g.* $K_2[PdCl_4]$) had been used successfully in the preparation of such silicas containing monometallic nanoparticles,[1] one thought was that if related heterobimetallic complexes could be prepared, for example $K_2[Cl_2Pt(\mu\text{-}Cl)_2PdCl_2]$, then these may be the suitable precursors for heterobimetallic nanoparticles. Hence, halo-bridged complexes were selected as one of the main methods to attempt the preparation of such heterobimetallic systems. In addition, the possibility of including a second metal through direct ligation was also explored through complexes containing the $SnCl_3^-$ anion bound to Pt.

In the literature, various examples of halo-bridged, homo and hetero bimetallic complexes of the general formula $[M_2(\mu\text{-}X)_2L_n]$[2], $[M_2(\mu\text{-}X)_2X_2L_n]$[3] $[MM'(\mu\text{-}X)_2L_n]$[4] and $[MM'(\mu\text{-}X)_2X_2L_n]$[5,6] type have been reported,[7] where M, M′ are metals, X is a halogen, L is a π-acceptor ligand. However, these complexes possessed bulky organic ligands, which make them at best sparingly soluble in polar solvents. However, from the description given in the Introduction

(Chapter 1), the use of polar solvents, in particular water, is necessary for the preparation of porous silicas *via* TLCT. Hence, it was decided to choose potentially simpler systems and so $[X_2M(\mu\text{-}X)_2M'X_2]^{n-}$ complexes were selected instead. However, as heterobimetallic $[X_2M(\mu\text{-}X)_2M'X_2]^{n-}$ complexes are, to the best of our knowledge, completely unknown in the literature, it was decided to use the reported methods of preparation of the selected types *i.e.* $[M_2X_6]^{n-}$ and try to utilise them to synthesise $[MM'X_6]^{n-}$ - type heterobimetallic transition metal complexes.

Goodfellow and Venanzi[8] reported a method of preparation of bimetallic complexes of Pt^{II} *i.e.* $[LXM(\mu\text{-}X)_2MXL]$ type (where L = Me_3P, Et_3P, Ph_3P, Me_3As and Et_3As; X = Cl; M = Pt^{II}) by using its mononuclear metal complex (*i.e.* $[PtCl_2L_2]$). The method of preparation involved heating a finely ground mixture of $[PtCl_2L_2]$ and $[PtCl_2]$ (0.5 equivalent excess) in a boiling tube in the presence of a hydrocarbon (*i.e.* xylene or naphthalene or a mixture of the two) which was then heated (140° to 160 °C, depending on stability of $[PtCl_2L_2]$) for some time until a uniform slurry was obtained. On cooling, the slurry was filtered and washed in a Soxhlet thimble using petroleum ether (40° – 60 °C). The product obtained was extracted and crystallised from CH_2Cl_2. The method of preparation was not suitable for heterodinuclear complexes and had some serious limitations, such as decomposition of mononuclear metal complexes before melting, non-formation of a uniform slurry and difficulties in product separations *via* extraction from high-boiling solvents. Also, the characterisation of the product was done *via* elemental analysis only, and no additional supportive analytical information was reported in the literature apart from the colour of the complexes.

Goggin *et al.*[9] reported a method for the synthesis of trimethylamine complexes of Pt^{II} and Pd^{II}, of the type $[LXM(\mu\text{-}X)_2MXL]$. Later, Goggin[10] used the same method to prepare $[M_2X_6]^{2-}$ complexes of Pt^{II} and Pd^{II}. The method involved preparation of bimetallic complex by the exchange of small cations *i.e.* Na^+ or K^+ ion in Group 1 metal salts of Pt^{II} and Pd^{II} with relatively large cations such as $(Bu_4N)^+$ or $(n\text{-}Pr_4N)^+$. The method of preparation involved stirring of $K_2[MX_4]$ or $Na_2[MX_4]$ (where M = Pt^{II} or Pd^{II}) (or Group 1 metal salts of Pt^{II} or Pd^{II}) and $(R_4N)Cl$ (where R = Bu or *n*-Pr) as their aqueous solutions at room temperature. The bimetallic complex of Pd^{II} was successfully prepared and was formed instantaneously from the above method. However, the bimetallic complex of Pt^{II} required heating of the appropriate mixture under reflux for about 6 h. Alternatively, stirring $[PtBr_2]$ and $(n\text{-}Pr_4N)Br$ in DMF for 6 h resulted in a pure, homodinuclear complex of Pt^{II}, obtained after precipitation with Et_2O followed by work up and extractions with hot water and acetone.

Harris and Gray[11] reported another method of synthesis, which also involved exchange of counter ion while they were trying to synthesise neutral π-cyclopropenium complexes. They obtained homodinuclear complexes of Pt^{II} and Pd^{II} with a cyclopropenium cation and hence studied their M-X cleavage reactions. The method of preparation involved stirring $[MCl_4]^{2-}$ (as a Group 1 metal salt) with $R_3C_3^+$ (R = Me_2N or $n\text{-}C_3H_7$, **Fig. 2.1**) in water under N_2 as well as under an air atmosphere. The aim behind the synthesis was to exchange the smaller cation with a relatively large, symmetrical ion which it was hoped would enhance the stability of the resulting dinuclear system *via*

crystallisation. The method proved to be successful as $[M_2Cl_6]^{2-}$ was obtained as a product with cyclopropenium as the cation.

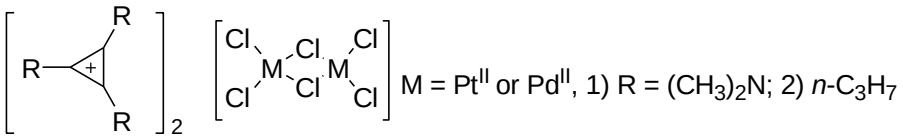

Fig. 2.1 Structure of homodinuclear complexes of Pt^{II} and Pd^{II} with different counter ions.

Usón *et al.*[12] have reported a different method of preparation of neutral bimetallic μ-chloro-bridged Au^{III} complexes of type $[M_2X_2L_n]$ system, where n = 4, L = C_6H_5, X = Cl, *via* chloride abstraction using $AgClO_4$. Another relatively recent example of chloride abstraction used to prepare homodinuclear complexes of Pt^{IV} *i.e.* $[M_2X_9]^-$ reported the use of $AlCl_3$.[13] Dell'Amico *et al*. have also shown the formation of hexanuclear μ-chloro-bridged Pd^{II} complex by the same method of preparation.[13]

In 1950, Chatt[14] synthesised a μ-chloro-bridged Pt^{II} complex of the type $[LXM(\mu\text{-}X)]_2$ *i.e.* $[\{(C_3H_7)_3P\}ClPt(\mu\text{-}Cl)]_2$, obtained by heating the two components, $[(C_3H_7)_3P]_2$ and $[PtCl_2]$, at 160 °C for 15 min in the absence of solvent. On crystallisation, this resulted in a nearly pure homodinuclear complex of the type $[M_2X_4L_n]$. The complex characterisation was not supported by any XRD data but by other analytical techniques *e.g.* elemental analysis, ebullioscopic constant and melting point. The structural assignment was based on comparison of the μ-chloro-bridged Pt^{II} complex with mononuclear *cis*- and *trans*-$[\{(C_3H_7)_3P\}_2PtCl_2]$ on the basis of their stability at high temperature (or thermal decomposition), redox potentials, isomerisation and physical properties.

Masters and Visser[15] reported formation of a heterodinuclear complex *via* a disproportionation reaction, obtained by mixing two homodinuclear complexes. The reaction was carried out in an NMR tube in $CDCl_3$ by addition of $[Pt_2Cl_4(PBu_3)_2]$ and $[Pd_2Cl_4(PBu_3)_2]$. Interpretation by ^{195}Pt NMR and ^{31}P NMR spectroscopy showed the presence of three peaks *i.e.* two of the homodinuclear starting materials and one of a new heterodinuclear complex. As the experiment was to study the kinetics of the reaction, no attempts were made to separate the heterodinuclear complex (*i.e.* $[(Cl)(Bu_3P)Pt(\mu\text{-}Cl)_2Pt(PBu_3)(Cl)]$) claimed to have been observed for the first time.

Kiffen *et al.*,[16] then tried to explain comproportionation by mixing two homodinuclear metal complexes of Pt^{II} and Pd^{II} (*i.e.* $[Pt_2Cl_4(PBu_3)_2]$ and $[Pd_2Cl_4(PBu_3)_2]$ according to the method employed previously by Masters and Visser and co-workers.[15] However, in their work they not only tried to interpret the presence of the heterodinuclear complex using ^{31}P NMR spectroscopy but also attempted to isolate the heterodinuclear complex which was thought to have formed. The results of ^{31}P NMR spectroscopy confirmed the presence of a new complex (*i.e.* $[(Bu_3P)ClPt(\mu\text{-}Cl)_2PdCl(PBu_3)]$), as observed previously but crystallisation yielded only a 1 : 1 mixture of the homodinuclear complexes of Pt and Pd used as starting materials.

Clark *et al.*[17] reported the single crystal structure of a symmetric, chloro-bridged heterodinuclear complex of Pt-Pd *i.e.* $[(PEt_3)ClPd(\mu\text{-}Cl)_2PtCl(PEt_3)]$ prepared from *trans*-$[PtCl_2(PEt_3)_2]$ with palladium(II) chloride, or from *trans*-$[PdCl_2(PEt_3)_2]$ with platinum(II) chloride *via* heating the appropriate mixture under reflux in xylene in an inert atmosphere. The results obtained confirmed

that the product obtained had a particular 1 : 1 ratio of Pt to Pd, but there was no evidence to distinguish between a mixture of two homo dinuclear complexes of Pt^{II} and Pd^{II} or the expected heterodinuclear complex, or a mixture of all three.

Steinborn and co-workers[18,19] reported methods of preparation of dinuclear complexes of Pt^{II} and Pd^{II} of the type $[M_2X_6]^{2-}$ from their Group 1 metal salts. The method of preparation involved use of $K_2[MCl_4]$ (where M = Pt or Pd) with excess of crown ether (*i.e.* [18-crown-6]) in water *via* stirring the mixture at room temperature for two days. This resulted in homodinuclear complexes of Pt^{II} and Pd^{II} *i.e.* $[K(18\text{-crown-6})]_2[Pt_2Cl_6]$ and $[K(18\text{-crown-6})]_2[Pd_2Cl_6]$, respectively. Synthesis of mononuclear complex, *i.e.* $[K(18\text{-crown-6})]_2[MCl_4]$, was carried out by stirring $K_2[MCl_4]$ and [18-crown-6] in CH_2Cl_2 for 3 h at room temperature. The reason for the use of a crown ether was not discussed in their work but it could be to allow the formation of an organic-soluble reagent/product. In addition, it is known that stable anions such as $[MCl_4]^{2-}$ have a stronger tendency to form ion pairs with complex cation *i.e.* [crown ether (alkali metal ion)]$^{+}$.[20]

2.2 Heterobimetallic Complexes

2.2.1 Synthesis

Our approach to the synthesis of a heterobimetallic complex involved two different metal centres, brought together to form a complex *via* halogeno bridges. The metals chosen for the synthesis involved Group 1 metal salts of noble metals *i.e.* $K_x[MCl_4]$, where M is Pt^{II}, Pd^{II} ($x = 2$) and Au^{III} ($x = 1$). The reason for the selection of noble metals has a correlation to the work carried out previously by King within the Bruce research group.[1] The concept of the work involved preparations of silicas[21] doped with mixed-metal nanoparticles derived from separate metal precursors. King used Group 1 metal salts of noble metals (Pt and Au), and mononuclear metal complexes of EDTA (*i.e.* $Na_x[M(EDTA)]$, where M = Cr^{III} or Co^{II}, prepared separately) to prepare heterobimetallic nanoparticles doped into porous silicas *via* TLCT. The mesoporous solids produced from the above approach successfully produced silicas doped with heterobimetallic nanoparticles such as Pt-Co, Pd-Au, and Pd-Ru. For example, it was hoped that using $K_2[PtCl_4]$ and $Na_2[Co(EDTA)]$ as separate metal precursors would lead to heterobimetallic Pt-Co nanoparticles with an equimolar ratio of the two metals. This was indeed the case but, nonetheless, the doped silicas possessed certain limitations. For example, many of the metal particles were large as observed by TEM. Further, while the overall stoichiometry across the preparation showed a 1 : 1 ratio of metals, different ratios were observed by EDX between different particles, varying between 9 : 1 and 1 : 1 (Pt-Co).[21] As Pt-Co is ferromagnetic, clearly its properties depend critically on composition requiring a narrow monodispersity in composition. Hence, the concept of

preparation of single, mixed-metal precursor originated, forming the basis of the current project. Therefore, it was decided to synthesise heterobimetallic complexes with a stoichiometric ratio of metals involved *i.e.* M : M′ = 1 : 1 hoping that they could be used as precursors in TLCT to produce heterobimetallic nanoparticles with an equivalent metallic ratio, expected to be constant throughout the mesoporous support.

In this section of the current chapter, the synthesis of a heterobimetallic Pt-Sn complex uses a literature procedure[22] with a slightly modified method of preparation in order to make the complex water soluble, necessary for further use in TLCT. The methods of preparation given subsequently also involve various attempts to obtain heterobimetallic Pt-Pd, Pt-Au and Pd-Au complexes. The attempted preparations of heterobimetallic complexes have been carried out by various methods such as halogen abstraction, counter-ion exchange, counter-ion entrapment, and mechanochemical reaction.

2.2.1.1 Heterobimetallic Pt-Sn Complexes

It is well known that $SnCl_2$ can insert into Pt-Cl bonds to give Pt-$SnCl_3$ units, and as such this represents a way into single-source Pt-Sn precursors.[22] The method of preparation involved the stirring of a solution of $[PtCl_4]^{2-}$ and $[SnCl_2]$ (1 eq. for $[PtCl_3(SnCl_3)]^{2-}$ and 2 eq. for $[PtCl_2(SnCl_3)_2]^{2-}$) in CH_2Cl_2 at room temperature for 2 h, necessitating the use of an organic-soluble derivative of $[PtCl_4]^{2-}$, such as the Bu_4N or PPh_4 salt. The solution was then evaporated to remove excess solvent so as to obtain an orange-yellow, crystalline product. The ^{195}Pt NMR spectrum (**Fig.**

2.2) shows $^{1}J_{119Sn\text{-}195Pt}$= 27.75 kHz and $^{2}J_{117Sn\text{-}195Pt}$ = 26.52 kHz, which are consistent with data for this isomer reported previously.[22]

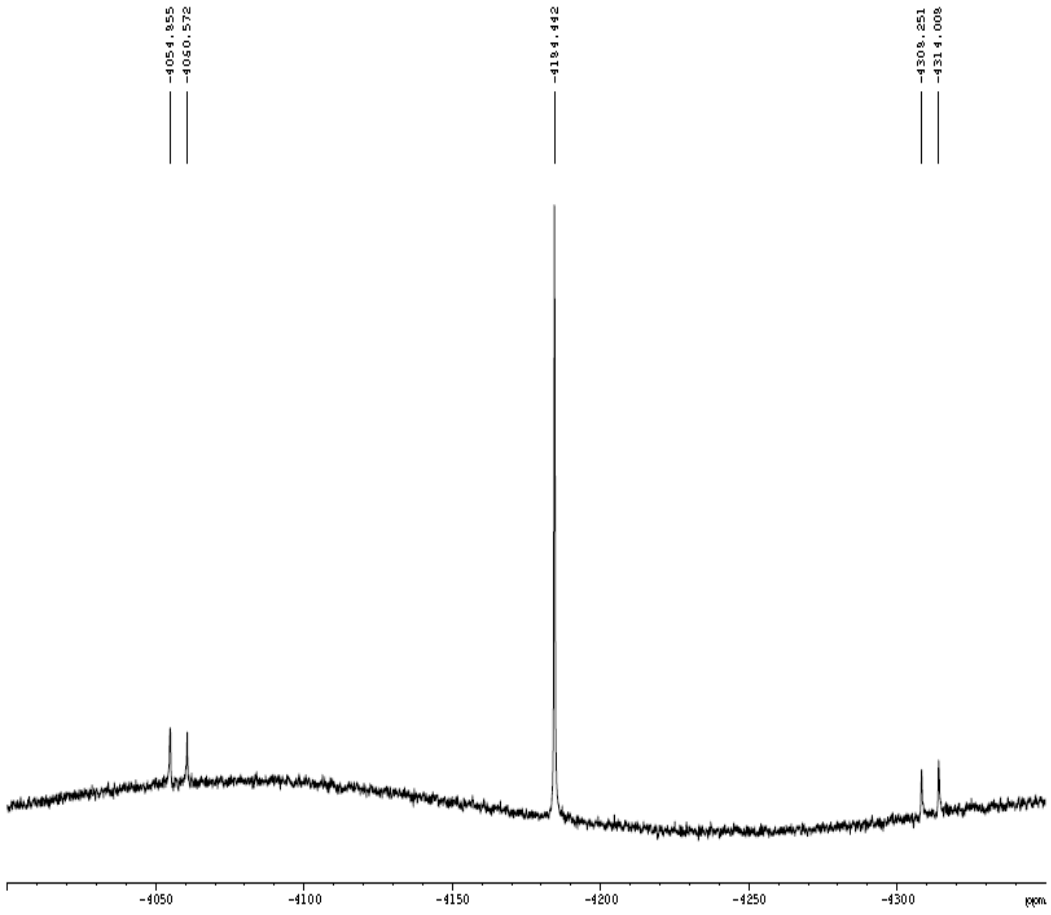

Fig. 2.2 ^{195}Pt spectrum of $[PtCl_2(SnCl_3)_2]^{2-}$ showing coupling to ^{119}Sn and ^{117}Sn, coupling constants $^{1}J_{119Sn\text{-}195Pt}$ = 27.75 kHz; $^{1}J_{117Sn\text{-}195Pt}$=26.52 kHz.

For $(Bu_4N)_2[PtCl_3(SnCl_3)]$, the product was not isolated and the mixture was treated directly with $(NH_4)PF_6$, to exchange counter cations to try to obtain $(NH_4)_2[PtCl_3(SnCl_3)]$, a water-soluble complex, which it was hoped could be used in the TLCT synthesis of silica. The reaction produced a crystalline yellow precipitate for which analysis *via* ^{195}Pt NMR spectroscopy was attempted. Unfortunately, the complex decomposed in D_2O within a few

minutes, and as a black powder settled at the bottom of the NMR tube. Attempts to prepare $(NH_4)_2[PtCl_3(SnCl_3)]$ from $(PPh_4)_2[PtCl_2(SnCl_3)_2]$ and $(NH_4)PF_6$ *via* stirring in water, led to decomposition of the yellow suspension of the complex to a black powder almost instantaneously. In both cases, decomposition is attributed to the hydrolysis of the Pt-Sn bond and then further hydrolysis of the Sn^{II}.[23] In **Fig. 2.3**, possible forms of hydrolysis products of Sn^{II} have been shown with respect to different pH range *e.g.* $[Sn(OH)_2]^0$ exists at pH 4-10 but $[Sn(OH)]^{1+}$ and $[Sn(OH)_3]^{1-}$ species occurs at pH < 4 and pH > 10, respectively, at a low concentration of tin.[23]

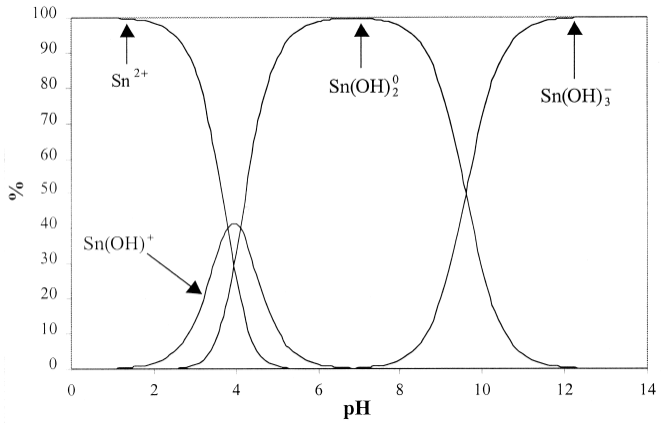

Fig. 2.3 Distribution of hydrolysed species of Sn^{II} as a function of pH.[23]

Owing to hydrolytic instability of the Pt-Sn link, this approach was not pursued further.

2.2.1.2 Attempted Preparation of Heterobimetallic Pt, Pd and Au Complexes

Attempted preparation of $K_x[MCl_2(\mu\text{-}Cl)_2M'Cl_2]$ by halogen abstraction

In this method, pairs of Group 1 metal salts of Pt^{II}, Pd^{II} or Au^{III} were added to water, followed by stirring for 30 min to ensure complete dissolution. Two molar equivalents of $AgNO_3$ were then added to abstract two chloride ligands as AgCl, which was expected to promote the formation of the binuclear complex, as proposed in the following equation.

$$[MCl_4]^{n-} + [M'Cl_4]^{m-} + 2\,Ag^{+} \xrightarrow{-2\,AgCl} [Cl_2M(\mu\text{–}Cl)_2M'Cl_2]^{x-}$$

The same concept of chloride abstraction by use of $AgClO_4$ and $AlCl_3$ to obtain homodinuclear metal complexes has been reported previously.[12,13] $AgClO_4$ has been used to abstract chlorides from 2 equivalents of $(Bu_4N)[Au(C_6H_5)_2Cl_2]$ by stirring in a CH_2Cl_2/Et_2O mixture to obtain the homodinuclear complex *i.e.* $[(C_6H_5)_2Au(\mu\text{-}Cl)_2Au(C_6H_5)_2]$. However, almost 2 equivalents of $AlCl_3$, were used to prepare the homodinuclear Pt^{IV} complex from $(Bu_4N)_2[PtCl_6]$ by simple stirring of the contents in CH_2Cl_2 at room temperature until solid $AlCl_3$ totally disappeared from the solution resulting a clear red-coloured solution, from which the product, $(Bu_4N)[Cl_3Pt(\mu\text{-}Cl_3)PtCl_3]$, was crystallised at low temperature (-30 °C) as red crystals.[13]

In the preparations in this work involving Pt^{II} and Pd^{II}, Pd^{II} and Au^{III}, the AgCl formed was removed by centrifugation and the resulting filtrate was then evaporated to obtain the precipitate, for which crystallisation was attempted from H_2O/EtOH and MeOH/H_2O, but signs of decomposition

were observed in these solvents. Prior to crystallisation, the solution of precipitate was analysed by mass spectrometry, but no peaks attributable to a mixed-metal product were observed.

In a further attempt to prepare a heterobimetallic Pt-Au complex this way, the mononuclear complexes $(Bu_4N)_2[PtCl_4]$ and $(Bu_4N)[AuCl_4]$ were added to CH_2Cl_2 followed by addition of AgOTf with continuous stirring of the contents at room temperature for 18 h. The mixture was filtered to remove the AgCl precipitate. After removal of the solvent, the residue obtained was redissolved in acetone after which Et_2O was added, resulting in an orange precipitate. Unfortunately, mass spectrometric analysis of this reaction did not indicate the presence of any heterodinuclear species.

Attempted synthesis of $(Bu_4N)_x[Cl_2M(\mu\text{-}Cl)_2M'Cl_2]$ complexes

Initial attempts involved stirring $(Bu_4N)_n[MCl_4]$ (where M = Pt^{II}, n = 2 or Au^{III}, n = 1) and $[M'Cl_2]$ (M′ = Pd or Pt) in CH_2Cl_2 at room temperature for 24 h or 48 h. The resulting mixture was then analysed *via* mass spectrometry but no dinuclear species were observed in either case. The reactions were also tried under more vigorous conditions (*i.e.* under reflux) or in different solvents (*e.g.* 1,4-dioxane) but the results obtained were no different. The reason to the unsuccessful reactions could be poor solubility of $[MCl_2]$ in solvents such as CH_2Cl_2.

Further attempts in higher-boiling solvents (*e.g.* benzonitrile, 1,4-dioxane) were used along with a different Pd source *i.e.* $[PdCl_2(NCPh)_2]$. The mixture of $K[AuCl_4]$ and $[PdCl_2(NCPh)_2]$ was heated under reflux for 48 h (under N_2, 1,4-dioxane) and then filtered. The filtrate obtained was dried and

triturated with petroleum ether and Et_2O. The results of mass spectrometry confirmed the formation of homodinuclear species such as $[Pd_2Cl_6]^{2-}$, as well as mononuclear species such as $[AuCl_2]^-$. The existence of homodinuclear species was also supported by UV-visible data in which a band corresponding to $[Pd_2Cl_6]^{2-}$ was observed at $\lambda_{max.}$ = 329 nm (in 1,4-dioxane), and 332 nm (in benzonitrile) as compared to $K_2[Pd_2Cl_6]$ (324.5, 430 nm, H_2O) and $[K(18\text{-crown-6})]_2[Pd_2Cl_6]$ (339.5 nm, CH_2Cl_2). No evidence was obtained for the formation of a heterodinuclear species, neither was it possible to obtain single crystals of the resulting solid.

In the next attempts, a method of synthesis reported by Chatt was adopted.[14] Here, $(Bu_4N)[AuCl_4]$ and $[PdCl_2(NCPh)_2]$ or $(Bu_4N)_2[PtCl_4]$ and $[PdCl_2]$, or $(Bu_4N)_2[PtCl_4]$ and $(Bu_4N)[AuCl_4]$, were heated in the absence of solvent for 15 min. On cooling, acetone was added along with a pinch of charcoal (adsorbent) followed by boiling for a few minutes. The mixture was filtered, evaporated to dryness and attempts were made to crystallise the solid from acetone but nothing was obtained for Pt-Pd or Pt-Au (an oily mass was observed), although a pinkish-brown solid was obtained from Pd-Au. Again, analysis of the solution by mass spectrometry showed no evidence of any dinuclear species.

Attempted mechanochemical preparation of $K_2[Cl_2M(\mu\text{-}Cl)_2M'Cl_2]$ in the absence of solvent

As none of the attempts with Group 1 metal salts of Pt^{II}, Pd^{II} and Au^{III} chloridometallate in solution had so far led to a heterodinuclear complex, it was decided to try to synthesise such metal complexes with a completely different approach *i.e.* by a mechanochemical reaction.[24] There are several examples reported in the literature that have used this method of synthesis, including the preparation of metal clusters,[25] metal organic frameworks,[26] mononuclear metal complexes,[27] coordination polymers,[28] coordination cages,[29] and paramagnetic species.[30] In the last of these, Group 1 metal salts of Pt^{II} were used to synthesise paramagnetic species generated during the homolytic cleavage of the M-X bond *via* a mechanochemical reaction. Therefore, using this method, a Group 1 metal salt of Pt^{II} was selected along with $PdCl_2$ as the source of second metal. The reactants were added to the reactor and were milled for a total of 2 hours. Each milling cycle was of 15 min accompanied by cooling of 15 min and the mixture was analysed by powder X-ray diffraction at each stage (**Fig. 2.4**). The reaction was non-continuous as a continuous mechanochemical reaction could result into heating up of the reactor to a very high temperature which in turn could cause decomposition.[31]

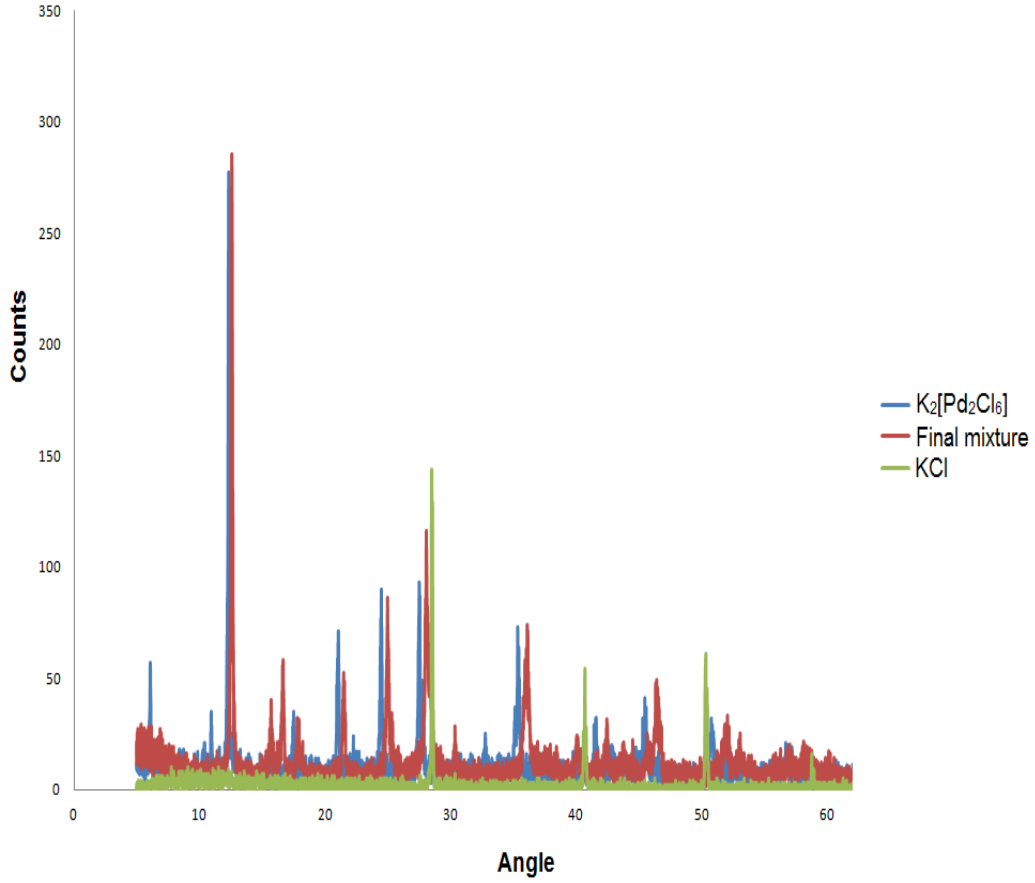

Fig. 2.4 Comparison of mixture obtained from mechanochemical reaction using powder X-ray diffraction pattern with respect to $K_2[Pd_2Cl_6]$.

In order to try to identify the complex being formed in the mechanochemical reaction, an analogous complex was prepared *i.e.* $K_2[Pd_2Cl_6]$, obtained from $[K(18\text{-crown-6})]_2[Pd_2Cl_6]$[18] (unfortunately $K_2[Pt_2Cl_6]$ could not be prepared the same way). However, a comparison was still made as it could be expected that $[Pd_2Cl_6]^{2-}$, $[Pt_2Cl_6]^{2-}$ and $[PtPdCl_6]^{2-}$ would be isostructural and, more importantly, isomorphous. Comparison did reveal a number of coincidences, but unfortunately the comparison was not precise, precluding identification in this way.

The powder was also analysed by ^{195}Pt NMR spectroscopy, from which presence of two signals at δ -1608 and -1170 were observed. The latter was

postulated as due to $[Pt_2Cl_6]^{2-}$ by comparison with separately prepared $Li_2[Pt_2Cl_6]$, while the former was $[PtCl_4]^{2-}$. There was no evidence for any other species that might have inferred reaction of palladium with platinum.

2.2.1.3 Synthesis of Heterobimetallic M-M′ Complexes

$[K(18\text{-crown-6})]_x[Cl_2M(\mu\text{-}Cl)_2M'Cl_2]$ complexes

a) Synthesis of $[K(18\text{-crown-6})]_2[Cl_2Pt(\mu\text{-}Cl)_2PdCl_2]$[32]

In the next approach, Steinborn's[18] method of preparation was adopted in which he synthesised homodinuclear complexes of Pt^{II} and Pd^{II}. Hence, by following the same method of preparation a heterobimetallic Pt-Pd halobridged complex of type $[MM'Cl_6]$ was sought. The method involved stirring of $K_2[PtCl_4]$ and $K_2[PdCl_4]$ with [18-crown-6] (1 mol eq. per K^+) in water for 2 days at room temperature. This resulted in a precipitate which was collected and then washed with water, EtOH and Et_2O to obtain the final solid. The complex formed was identified by ^{195}Pt NMR spectroscopy and by single crystal X-ray diffraction.

The results of the structure determination (X-ray crystallography) showed the expected planar di-μ-chlorido dimer and at each end the two chlorido ligands were bound to a potassium atom, itself complexed by an 18-crown-6 ligand (**Fig. 2.5**). At one end of the complex the 18-crown-6 was disordered. The disorder was modelled in two positions of relative occupancy 72 : 28 (determined independently of the Pd/Pt ratio; see below). For the minor component, the C–O bond lengths were restrained to be 1.423 Å and the

C–C bonds were restrained to 1.49 Å, these being the average of the values observed for the ordered crown ether. The anisotropic displacement parameters (adp) of the minor form were restrained to be approximately isotropic. The structure is shown in **Fig. 2.5** with this disorder removed (unmodified cif file is in Appendix A).

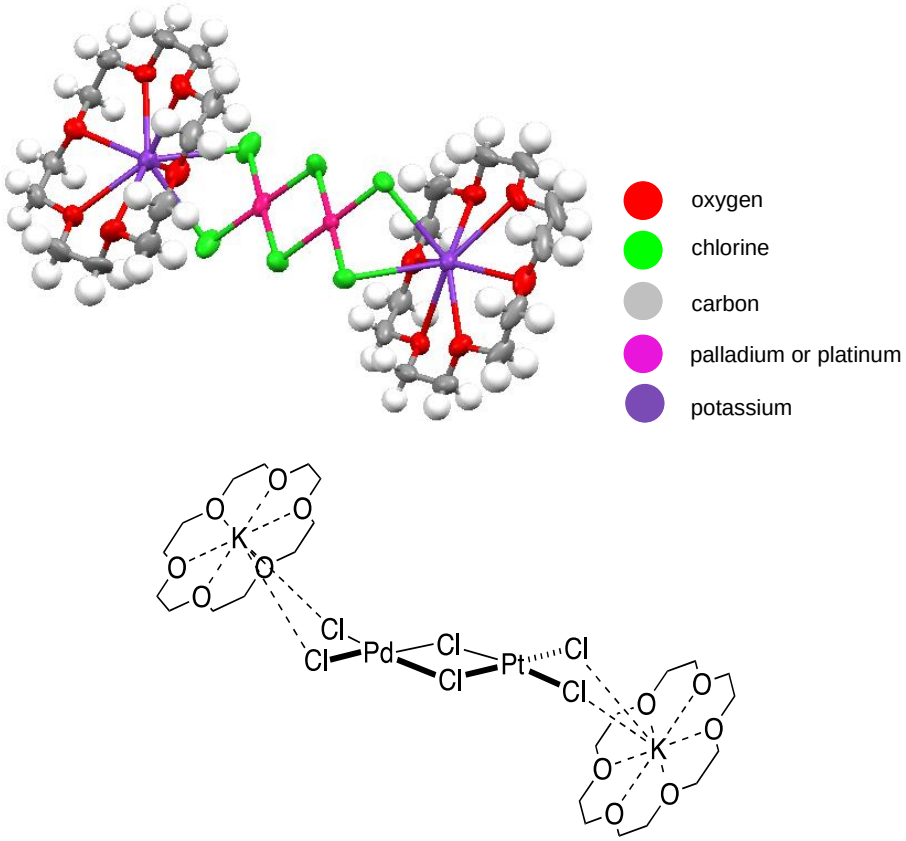

Fig. 2.5 Crystal structure of $[K(18\text{-crown-6})]_2[Pd_{1.42}Pt_{0.58}Cl_6]$.[32]

The structure contained a mixture of Pd and Pt, the ratio of which refined to 71.5 : 28.5 (which effectively corresponds to the ratio of ordered to disordered crown ethers) with the two metal atoms disordered over the two sites. The ratio of Pd/Pt at each site was allowed to refine independently but proved to be the same. Selected bond lengths are collected in **Table II.I**, in which they are compared with data for $K_2[MCl_4]$ (M = Pd or Pt),[33,34]

$[K(18\text{-crown-}6)]_2[PtCl_4]$,[35] $[K(18\text{-crown-}6)]_2[Pt_2Cl_6]$[19] and $[K(18\text{-crown-}6)]_2[Pd_2Cl_6]$.[19] The lower symmetry of the unit cell in the structure of the mixed-metal complex leads to four terminal M–Cl distances, but these are all comparable to those from the homodinuclear equivalents; interestingly, these are consistently shorter (by about 0.3 Å) than those found in the mononuclear complexes. The terminal Pt–Cl bond length does not appear to be affected by complexation of the potassium cation by the crown ether.

Table II.I Selected bond lengths and angles for $Pd_{1.42}$-$Pd_{0.58}$ and related structures.

Structure	*d(M–Cl$_t$) /Å*[§,$]	*d(K–Cl$_t$) /Å*	*d(M–Cl$_b$) /Å$*	*d(K–O) /Å*	*θ /°*
$K_2[PtCl_4]$[33]	2.3094	3.239			
$K_2[PdCl_4]$[34]	2.2931	3.233			
$[K(18\text{-c-}6)]_2[PtCl_4]$[35]	2.311(1)	3.161(1)		2.806 –2.944	84.89
$[K(18\text{-c-}6)]_2[Pd_2Cl_6]$[19]	2.270(1) 2.271(1)	3.260(2) 3.340(2)	2.327(1) 2.330(1)	2.815 – 2.956	114.57
$[K(18\text{-c-}6)]_2[Pt_2Cl_6]$[19]	2.270(3) 2.274(2)	3.259(4) 3.348(4)	2.322(2) 2.328(3)	2.788 – 2.961	112.83
$[K(18\text{-c-}6)]_2[PtPdCl_6]$[32]	2.273(1) 2.265(1) 2.262(1) 2.271(1)	3.191(1) 3.347(1) 3.222(1) 3.279(1)	2.330(1) 2.329(1) 2.325(1) 2.332(1)	2.805 –2.955 2.779 – 2.991	113.89 115.01

§ Terminal M–Cl distances; $ M = Pt or Pd as appropriate; † Angle between planes defined by MCl_4 unit and triangle of K plus 2 x Cl.

To check the reproducibility of this reaction, it was repeated on two further occasions, and single crystals were grown on each occasion. The Pd/Pt ratio was found to be 71 : 29 on one occasion and 64.5 : 35.5 on the other (see data in cif files on CD and on CCDC).[36] In both cases, the CHN data are given in the experimental section, and it should be noted that they are well within acceptable limits (not quite the case for complex $Pd_{1.42}$-$Pd_{0.58}$). Nonetheless, the fact that the analytical data predicted from the compositions found in the single-crystal structure determinations and those found from bulk crystallisations match well suggests that fractional

crystallisation would be unlikely to separate out the components and that obtaining mixtures is likely the best that can be achieved in this approach.

The X-ray data (described above) were able to provide a Pd/Pt ratio but they could not distinguish between a simple mixture of $[Pd_2Cl_6]^{2-}$ and $[Pt_2Cl_6]^{2-}$, and a mixture of $[Pd_2Cl_6]^{2-}$, $[Pt_2Cl_6]^{2-}$ and $[PdPtCl_6]^{2-}$. Therefore, to address this issue, the ^{195}Pt NMR spectrum was acquired and is reproduced as **Fig. 2.6**. The spectrum (recorded in CD_2Cl_2) shows two signals at δ = –1216 and –1278 ppm. By comparison with authentic samples prepared separately (all as the potassium crown ether salt and all data recorded in CD_2Cl_2), it was possible to ascertain that the resonance at δ = –1216 ppm corresponded to $[Pt_2Cl_6]^{2-}$, whereas the resonance for $[PtCl_4]^{2-}$ was found at δ = –1528 ppm. Given that the X-ray data clearly indicate that the only species possible are $[Pd_2Cl_6]^{2-}$, $[Pt_2Cl_6]^{2-}$ and $[PdPtCl_6]^{2-}$ and that one of the peaks in the ^{195}Pt NMR spectrum is identified as $[Pt_2Cl_6]^{2-}$, then it seems inescapable that the resonance at δ = –1278 ppm corresponds to $[PdPtCl_6]^{2-}$. Indeed, given the well-known sensitivity of ^{195}Pt chemical shifts to small changes (*e.g.*, solvent, temperature, counterion),[37] then a difference of 62 ppm between $[Pt_2Cl_6]^{2-}$ and $[PdPtCl_6]^{2-}$ is quite reasonable.

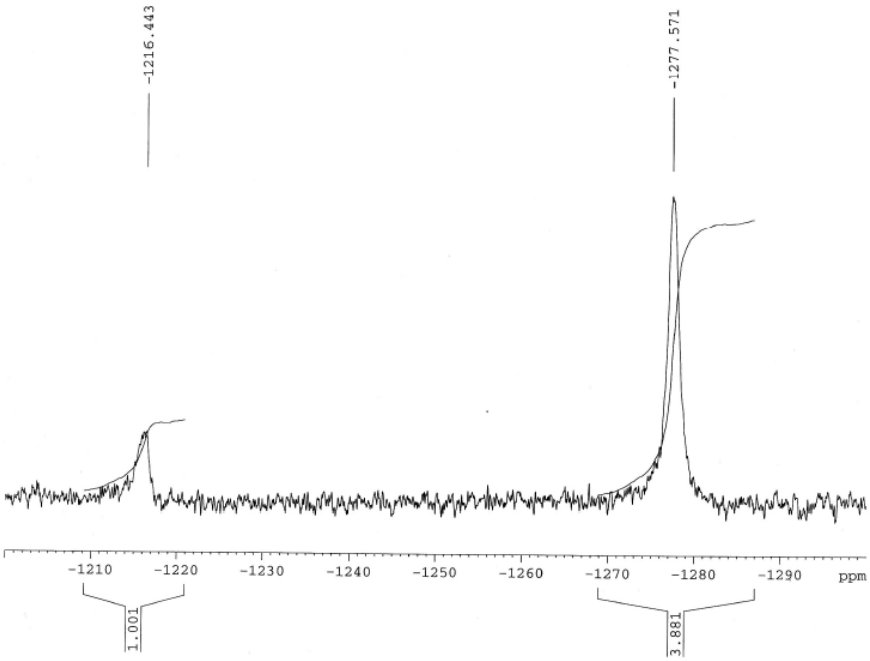

Fig. 2.6 ^{195}Pt NMR spectrum of $[K(18\text{-crown-6})]_2[Cl_2Pt(\mu\text{-}Cl)_2PdCl_2]$ complex in CD_2Cl_2 showing the presence of $[Pt_2Cl_6]^{2-}$ and $[PtPdCl_6]^{2-}$ at δ = -1216.44 and -1277.57, respectively.

This being the case, it is then possible to determine the relative quantities of $[Pd_2Cl_6]^{2-}$, $[Pt_2Cl_6]^{2-}$ and $[PdPtCl_6]^{2-}$ present in the mixture if it is assumed that the integrations from NMR spectroscopy are reasonably accurate (that the two anions are, in effect, exactly the same size gives confidence in this assumption). This is done by determining the ratio of $[Pt_2Cl_6]^{2-}$ and $[PdPtCl_6]^{2-}$ from the NMR spectrum from which a Pd/Pt ratio can be calculated. Knowing the overall ratio of the metals from the crystal structure then allows the amount of $[Pd_2Cl_6]^{2-}$ to be determined. The result was found to be:

$[Cl_2Pd(\mu\text{-}Cl)_2PdCl_2]^{2-}$	:	$[Cl_2Pd(\mu\text{-}Cl)_2PtCl_2]^{2-}$	:	$[Cl_2Pt(\mu\text{-}Cl)_2PtCl_2]^{2-}$
12	:	3.9	:	1

The reason for the observed ratio of metals can only then be the inertness of Pt with respect to Pd.[38,39] It has also been shown that $[PdCl_4]^{2-}$ is more active than $[PtCl_4]^{2-}$ in various biological systems.[40,41,42,43] In a recent study to compare dielectric constants of $K_2[PtCl_4]$ and $K_2[PdCl_4]$, it was observed that Pd^{II} showed noticeable changes in aqueous solution in comparison to Pt^{II} due to presence of greater number of H^+ and Cl^- ions.[44] Also, it is known that $[PdCl_4]^{2-}$ in solution forms the anion $[PdCl_3(OH_2)]^{1-}$[45] due to more favourable hydrolysis, which destabilises or disturbs hydrogen bonding in solution. However, the same effect is observed to be less pronounced in Pt^{II} due to difficulty in removal of the first Cl^- ion from the first coordination sphere by solvent molecules.[44] Hence, the result obtained justifies the greater lability of Pd-Cl bonds when compared to Pt–Cl bonds, which would predict a greater preponderance of the homodinuclear palladium dimer.

b) Attempts to Synthesise Heterobimetallic Pd-Au Complexes

Attempts were then made to synthesise heterobimetallic Pd-Au complexes using Steinborn's method of preparation.[18] The reaction mixture did not show any signs of decomposition, but reduction was observed in the reaction as Au^I *i.e.* $[K(18\text{-crown-6})][AuCl_2]$,[46] was recovered on crystallisation of the final reaction mixtures implying that a redox reaction had taken place, presumably with the formation of Pd^{IV}. However, metallic gold (Au^0) was not recovered from most of the reactions (except one during bulk crystallisation). Also, the oxidised product *i.e.* Pd^{IV} was never recovered from any of the mixtures, but the homodinuclear hexachlorodipalladate(II)

complex was observed every time instead being isolated by crystallisation of one of the two polymorphs. One of these was the same as that reported previously by Steinborn *et al.*, while the other showed small differences in the lattice parameters.[19] Nevertheless, formation of Pd^{IV} in the final precipitate was supported by IR spectroscopy as a band identified at 340 cm^{-1} (compared with $[K(18\text{-crown-6})]_2[PdCl_6]$, 340, 320 (w) cm^{-1}), but none of the crystallisation attempts resulted in isolation of the oxidised species. In general, the precipitates obtained from all of the attempted preparations of Pd-Au crown ether complexes in water showed the presence of a mixture of more than one products, and so the CHN data were unhelpful.

The attempted preparations of Pd-Au complexes was also carried out in CH_2Cl_2 by stirring at room temperature in the dark (Au^{III} is photosensitive) using $[K(18\text{-crown-6})]_2[PdCl_4]$ and $[K(18\text{-crown-6})][AuCl_4]$ as starting materials. The results obtained again indicated presence of an oxidised species *i.e.* $[PdCl_6]^{2-}$ ($\nu_{Pd\text{-}Cl}$ 340 cm^{-1}), a reduced species *i.e.* $[AuCl_2]^{1-}$ ($\nu_{Au\text{-}Cl}$ 350 cm^{-1}) and the homodinuclear Pd^{II} complex, $[Pd_2Cl_6]^{2-}$. Moreover, Pd^{IV} is known to be kinetically inert but thermally unstable, so that $[PdCl_6]^{2-}$ is easily reduced to Pd^{II} by H_2 and by H_2O_2.[47,48]

It is also reported that the salts of the $[PdCl_6]^{2-}$ anion are not easy to crystallise.[49] It has also been recently discovered that $[PdCl_6]^{2-}$ in solution is unstable, and can undergo disproportionation very easily to form $[Pd_2Cl_6]^{2-}$ and $[PdCl_4]^{2-}$, although this is reported to be photochemically induced.[50] In the current experiments, the reactions were carried out in the dark, but the

crystallisation was not under completely dark conditions, so that formation of $[Pd_2Cl_6]^{2-}$ could occur photochemically. Moreover, in a separate preparation of a mononuclear complex of Pd^{IV} *i.e.* $[PdCl_6]^{2-}$ using $K_2[PdCl_6]$ and [18-crown-6], the same homodinuclear complex $[Pd_2Cl_6]^{2-}$, was obtained during crystallisation of $[K(18\text{-crown-6})]_2[PdCl_6]$. The latter was confirmed by CHN and IR spectroscopy analysis, where $\nu_{Pd\text{-}Cl}$ 340 cm^{-1} corresponded to $[PdCl_6]^{2-}$.

These observations support the proposition that although Pd^{IV} is formed, it is unstable and undergoes conversion to the homodinuclear complex very easily.

$$[PdCl_4]^{2-} + [AuCl_4]^{-} \longrightarrow [PdCl_6]^{2-} + [AuCl_2]^{-}$$

$$[PdCl_6]^{2-} \longrightarrow 0.5\,[Pd_2Cl_6]^{2-} + 3\,Cl^{-}$$

In a variation of the above method, the reaction was attempted using preformed mononuclear metal complexes of Pd^{II} and Au^{III} with $[K(18\text{-crown-6})]^{+}$ as the cation. The method of preparation involved stirring of the two complexes in CH_2Cl_2 at room temperature for 48 h in the dark and the resulting solution was then treated with hexane in excess. The filtrate and precipitate obtained were analysed separately, but the results obtained were no different to the previous *in situ* preparations.

In the course of this part of the work, several single crystal structures were determined. Those that are directly relevant to the discussion are described below, while data for the others, *i.e.* $[K(18\text{-crown-6})]_2[PdCl_4]\cdot 4CH_2Cl_2$, $(PPh_4)[AuCl_4]$, $(Bu_4N)_2[PtCl_6]\cdot 3CH_2Cl_2$, $(Bu_4N)_2[PtCl_6]$,

$(PPh_4)_2[PtCl_4]\cdot H_2O$, $(PPh_4)_2[PtCl_6]\cdot 2CH_2Cl_2$ and $[K(18\text{-crown-6})]_2[Cl_2Pd(\mu\text{-}Cl)_2PdCl_2]$, are collected in the Appendix of the thesis.

c) Attempts to Synthesise Heterobimetallic Pt-Au Complexes

After the successful preparation of a heterobimetallic Pt-Pd complex and attempted Pd-Au complex preparations, the same approach was tried in an attempt to prepare a heterobimetallic Pt-Au complex. The reaction was again carried out in the dark and the amount of crown ether used was just greater than 1 crown/K^+ calculated from the total number of K^+ ions in the precursor salts, $K_2[PtCl_4]$ and $K[AuCl_4]$. The mixture of $K_2[PtCl_4]$, $K[AuCl_4]$ and [18-crown-6] was stirred in water for 48 hours in the dark, which resulted in the formation of a gold mirror (metallic gold) as a result of reduction of Au^{III} to Au^0 accompanied by the formation of a yellow precipitate, which was observed as a mixture with the gold mirror in several cases. The reaction was also carried out under the same conditions but in the absence of crown ether, this time resulting in an instantaneous reduction.

Reduction of Au^{III}

Reduction of gold complexes in the presence of light (photosensitivity) is an observation that has been known since the 18th century.[51,52] Chemical reduction of Au^{III} (or Au^{III} acting as an oxidant) is also well known.[53] In those reported examples, Au^{III} as $Na[AuCl_4]$ or $HAuCl_4$ has been employed in an attempt to synthesise mononuclear Au^{III} organometallic complexes, but due to reduction, mononuclear or polymeric Au^{I} complexes have, on occasion, been formed instead.[54,55,56,57] In some reported examples,

reduction of Au^{III} has also been observed due to thermal decomposition,[56,58] resulting in metallic gold as the final product.

The reduction observed in our work in attempting to prepare a heterobimetallic Pt-Au complex was accompanied by the oxidation of Pt^{II}. Oxidation by Au^{III} in the presence of other metals has been reported previously,[59,60] and includes metals such as Co^{II} and Pt^{II} which have resulted in the formation of the oxidised species Co^{III} and Pt^{IV}, respectively. In the latter case, the Pt^{IV} complex was formed as a result of an attempted preparation of the heterobimetallic Pt^{III}-Au^{III} complex expected from Pt^{II} as per the following equation,[60]

$$Pt^{II}, Au^{III} \xrightarrow{-e^-} Pt^{III}, Au^{III}$$

The basis of the above synthesis originated from previously reported work by Micklitz *et al.*[61] which involved synthesis of the homodinuclear Pt^{II} complex *cis*-$[(H_3N)_2Pt(\mu\text{-l-MeT})_2PtCl_2]$ (**Fig. 2.7 A**) obtained by reacting together *cis*-$[Pt(\text{l-MeT})_2(NH_3)_2]$ (where 1-MeT is 1-methylthymine anion) and $[PtCl_4]^{2-}$.[61]

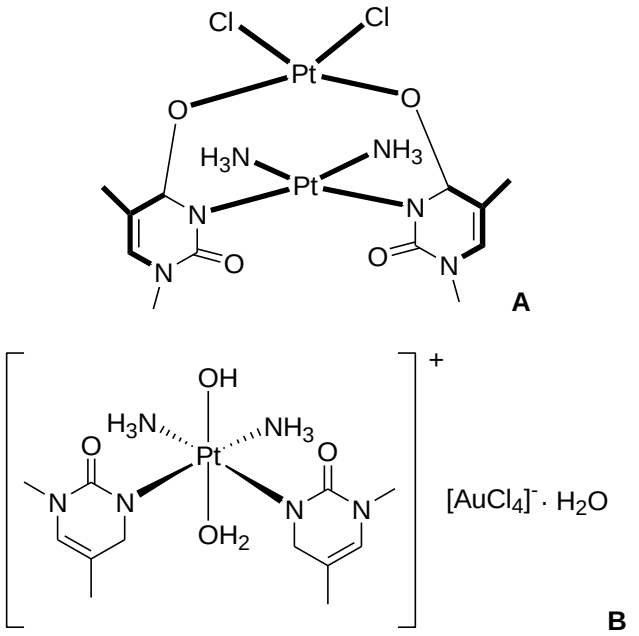

Fig. 2.7 A Structure of Pt^{II} binuclear complex, and **B** mononuclear Pt^{II} complex with $[AuCl_4]^-$ as counter anion.

Therefore, in an attempt to prepare a heterobimetallic Pt^{III}-Au^{III} complex (*i.e.* *cis*-$(NH_3)_2Pt(1\text{-}MeT)_2AuCl_4$), *cis*-$(NH_3)_2Pt(l\text{-}MeT)_2$ and $[AuCl_4]^-$ were reacted following the same method of preparation, where $[AuCl_4]^-$ was proposed to cause incomplete oxidation of Pt^{II} to Pt^{III}.[60] Unfortunately, no such heterobimetallic complex was obtained, rather, *cis*-$[(NH_3)_2Pt(l\text{-}MeT)_2(OH)(H_2O)][AuCl_4]\cdot H_2O$ (**Fig. 2.7 B**) was formed instead, where oxidisation of Pt^{II} to Pt^{IV} was observed. The structure elucidation was carried out by X-ray diffraction, but there was no evidence of a reduced gold species.

On the other hand, in our attempted preparation of a heterodinuclear Pt-Au complex, Au^0 was formed. Then, to study the redox chemistry of the reaction in more detail, the reaction was repeated several times and was analysed carefully in order to achieve the following aims:

1. To identify possible platinum species *i.e.* Pt^{III}, Pt^{IV} and Pt^{II} *via* ^{195}Pt NMR spectroscopy.
2. To obtain crystal structures of the products that could be isolated.
3. To study the stoichiometry of the reaction from the percentage yield of the reduced gold as well as by carrying out the same reaction with different ratios of the two metals.

The platinum species that might be expected from the reaction included, heterodinuclear species *e.g.* Pt^{II}-Au^{III}; Pt^{III}-Au^{III}, Pt^{IV}-Au^{I} and homodinuclear species *i.e.* Pt^{IV}-Pt^{IV}; Pt^{III}-Pt^{III}, and Pt^{II}-Pt^{II}. In order to identify the above-mentioned species, the reaction was repeated several times in water, and in different aqueous solutions, which were analysed by ^{195}Pt NMR spectroscopy.

Products isolated in reactions between Pt^{II} and Au^{III}

Various reactions were carried out with the potassium, $[K(18\text{-crown-6})]^+$ or NBu_4^+ salts of the halometallate anions of Pt^{II} and Au^{III}, which are now represented schematically. All reactions were at room temperature and were conducted in the dark with stirring for 48 h. The products obtained either from precipitates or from the filtrate were analysed mainly by ^{195}Pt NMR spectroscopy complemented by single crystal X-ray diffraction. Each reaction is described individually and then a broader discussion follows in discussion section.

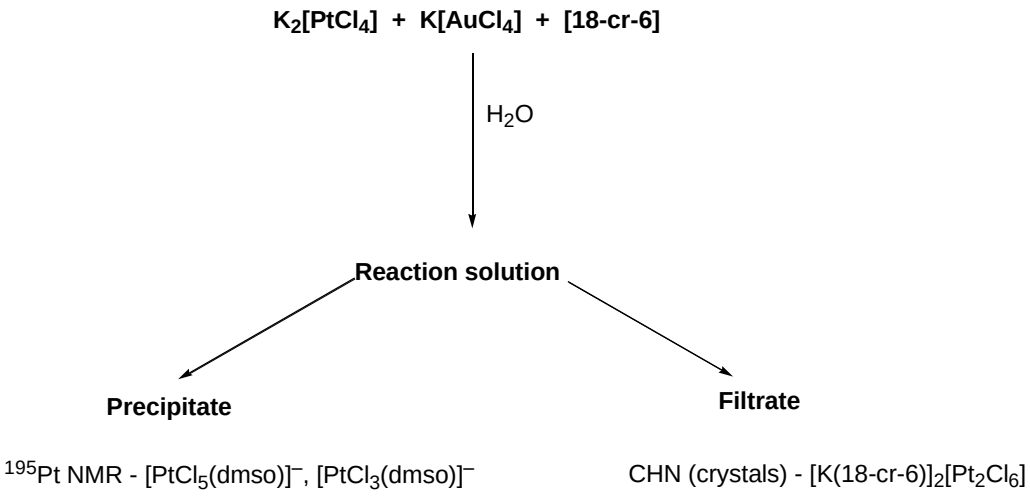

Scheme II.I Reaction carried out in water in the presence of 18-crown-6.

The reaction of potassium salts of Pt^{II} and Au^{III} in the presence of crown ether resulted in the formation of a gold mirror, a pinkish-yellow precipitate and a yellow-filtrate. The precipitate and filtrate were analysed separately. The precipitate formed was found to contain a mixture of $[PtCl_3(dmso)]^-$ and $[PtCl_5(dmso)]^-$, which was confirmed *via* ^{195}Pt NMR spectroscopy. In both cases, the solvent used to record the NMR spectrum was dmso and it is

assumed that the observed complex is formed by solvolysis of the related homoleptic chlorometallate anion, for which precedent exists.[67,68] The presence of the $[AuCl_2]^-$ anion is inferred from the stoichiometry of the reaction (Pt^{II} + Au^{III} ---> Pt^{IV} + Au^{I}), but the observation of both elemental gold and Pt^{II} salts in the product is evidence that this reaction is not totally selective. No signal was observed in the NMR spectrum of the filtrate (it is assumed that the concentration was low) but tiny crystals were obtained on standing which were confirmed to be $[K(18\text{-crown-}6)]_2[Pt_2Cl_6]$.

The above reaction was then repeated with a 3 : 2 ratio of potassium salts of Pt^{II} : Au^{III}, as such a ratio ought to ensure more complete reduction of the gold to gold metal, according to: 3 Pt^{II} + 2 Au^{III} ---> 3 Pt^{IV} + 2 Au^0. On the analysis of the resulting filtrate as well as precipitate (mixed with gold metal) again Pt^{II} and Pt^{IV} species were observed as $[PtCl_3(dmso)]^-$ and $[K(18\text{-crown-}6)]_2[PtCl_6]$ were confirmed by ^{195}Pt NMR spectroscopy and by single crystal XRD, respectively.

The 1 : 1 Pt : Au reaction was also repeated in order to analyse the filtrate of the reaction completely. However, this time the filtrate (*i.e.* filtrate I) obtained was treated with $(Bu_4N)Cl$ as in reaction II, from which the precipitate II as well as filtrate II were analysed separately by ^{195}Pt NMR spectroscopy. This analysis showed the formation of $[PtCl_6]^{2-}$ (precipitate II), $[PtCl_5(OH_2)]^-$, *cis*-$[PtCl_4(OH_2)]^{2-}$ and *trans*-$[PtCl_4(OH_2)]^{2-}$ (filtrate II).

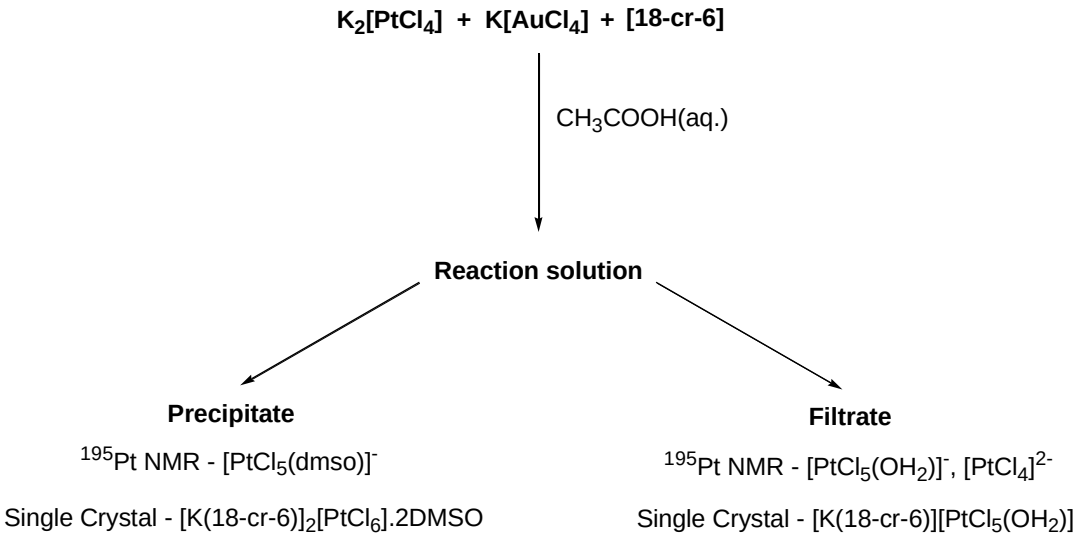

Scheme II.II Reaction carried out in aqueous acetic acid in the presence of 18-crown-6.

It is known that oxidation of Pt^{II} can also give Pt^{III} and that normally such complexes are dinuclear in nature with bridging ligands such as sulfate or acetate. Therefore, the reaction was repeated in the presence of acetate in order to determine if Pt^{III} products could be isolated. The reaction resulted in a gold mirror, a yellow precipitate and a filtrate. The precipitate and filtrate were both analysed by ^{195}Pt NMR spectroscopy and by single crystal X-ray diffraction. The precipitate showed the presence of $[PtCl_5(dmso)]^-$, $[PtCl_5(OH_2)]^-$, and $[PtCl_4]^{2-}$ while the filtrate gave $[K(18\text{-crown-}6)]_2[PtCl_6]\cdot 2DMSO$ and $[K(18\text{-crown-}6)][PtCl_5(dmso)]$. There was no evidence for Pt^{III}.

The 1 : 1 Pt : Au reaction was also repeated to analyse the products that might have formed in the filtrate which would previously have remained unanalysed. Hence, the filtrate resulting from the above reaction (*i.e.* reaction I) was then treated further with $(Bu_4N)Cl$ and was again analysed separately as filtrate II and precipitate II. On analysis of the products formed

by ^{195}Pt NMR spectroscopy, $[PtCl_5(dmso)]^-$ (precipitate II), $[PtCl_5(OH_2)]^-$ and $[PtCl_4]^{2-}$ (filtrate II) were the species observed.

The above reaction was repeated with a 3 : 2 ratio of Pt^{II} to Au^{III}. The analysis confirmed the existence of Pt^{IV} $[K(18\text{-crown-6})]_2[PtCl_6]$, $[PtCl_5(dmso)]^-$, as well as Pt^{II} $[PtCl_3(dmso)]^-$, (^{195}Pt NMR spectroscopy). Single crystals analysis showed $[K(18\text{-crown-6})]_2[PtCl_6]\cdot 2AcOH$.

The reactions given in Schemes II.I and II.II were also carried out in aqueous HCl as well as in aqueous CH_3COONa but the results obtained were not very useful. Experimental data is in the Appendix section B of the thesis.

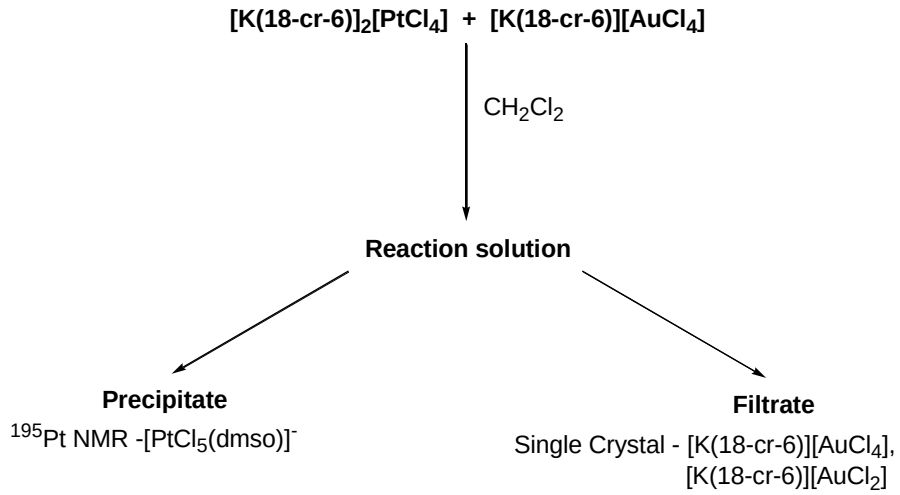

Scheme II.III Reaction carried out in dichloromethane using $[K(18\text{-crown-}6)]^+$ salts.

In this attempted preparation, mononuclear crown ether complexes of $[PtCl_4]^{2-}$ and $[AuCl_4]^-$ were reacted in CH_2Cl_2. This time no gold mirror formed: products isolated from the precipitate and the filtrate were $[PtCl_5(dmso)]^-$ (from precipitate) and $[K(18\text{-crown-}6)][AuCl_4]$ and $[K(18\text{-crown-}6)][AuCl_2]$ (from the filtrate).

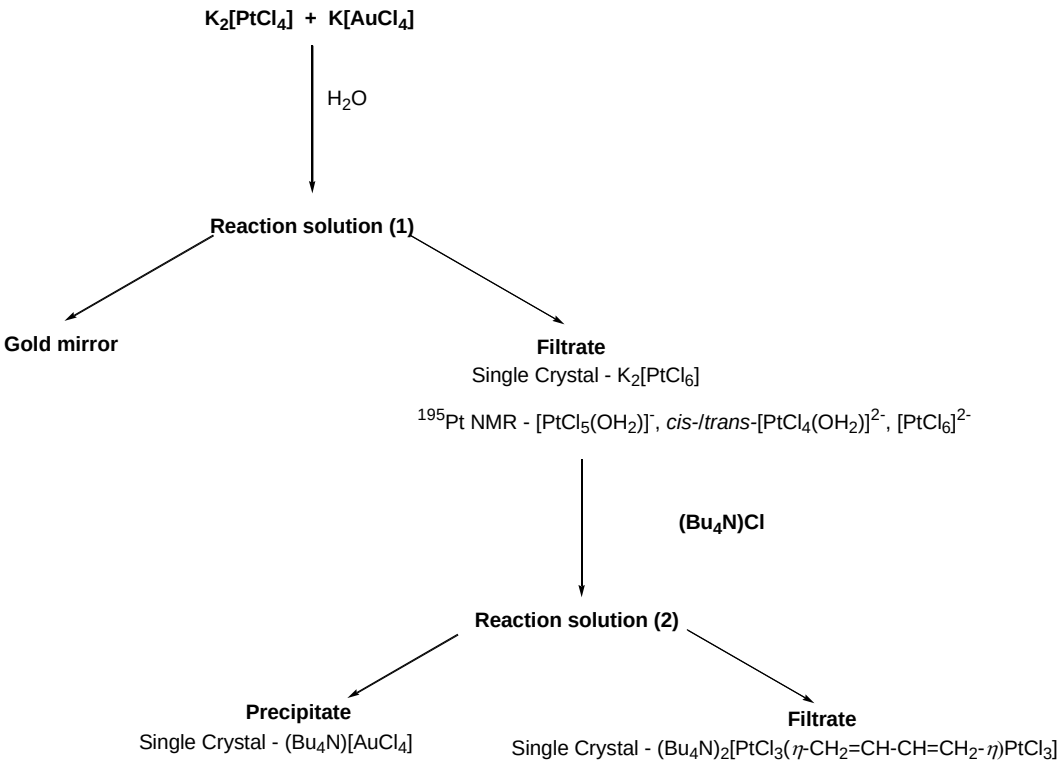

Scheme II.IV Reaction carried out in water in the absence of crown ether.

This reaction led to the formation of a gold mirror, which was separated from the filtrate. This filtrate was analysed by ^{195}Pt NMR spectroscopy and showed the presence of $[PtCl_6]^{2-}$, $[PtCl_5(OH_2)]^{2-}$ and *cis*- and *trans*-$[PtCl_4(OH)_2]^{2-}$, the aquo complexes arising from hydrolysis of $[PtCl_6]^{2-}$. While the solution was awaiting analysis by NMR spectroscopy, crystals of $K_2[PtCl_6]$ precipitated (identity confirmed by obtaining the unit cell of the single crystals). $(Bu_4N)Cl$ was added to the filtrate resulting in a precipitate and filtrate, which were analysed separately. From the solid, single crystals of $(Bu_4N)[AuCl_4]$ were recovered, while crystals of $(Bu_4N)_2[PtCl_3(\eta\text{-}CH_2\text{=}CH\text{-}CH\text{=}CH_2\text{-}\eta)PtCl_3]$ were recovered from the filtrate.

The above reaction was repeated in aqueous acetic acid. The filtrate resulted in step I contained $[PtCl_5(OH_2)]^-$ analysed by ^{195}Pt NMR spectroscopy. However, the precipitate formed in step II resulted in the formation of $[PtCl_5(dmso)]^-$ and $[PtCl_6]^{2-}$ (^{195}Pt NMR spectroscopy), while from the filtrate single crystals of $((Bu_4N)_2[PtCl_3(\eta\text{-}CH_2\text{=}CH\text{-}CH\text{=}CH_2\text{-}\eta)PtCl_3])$ and of Au^{III} as $(Bu_4N)[AuCl_4]$ were recovered.

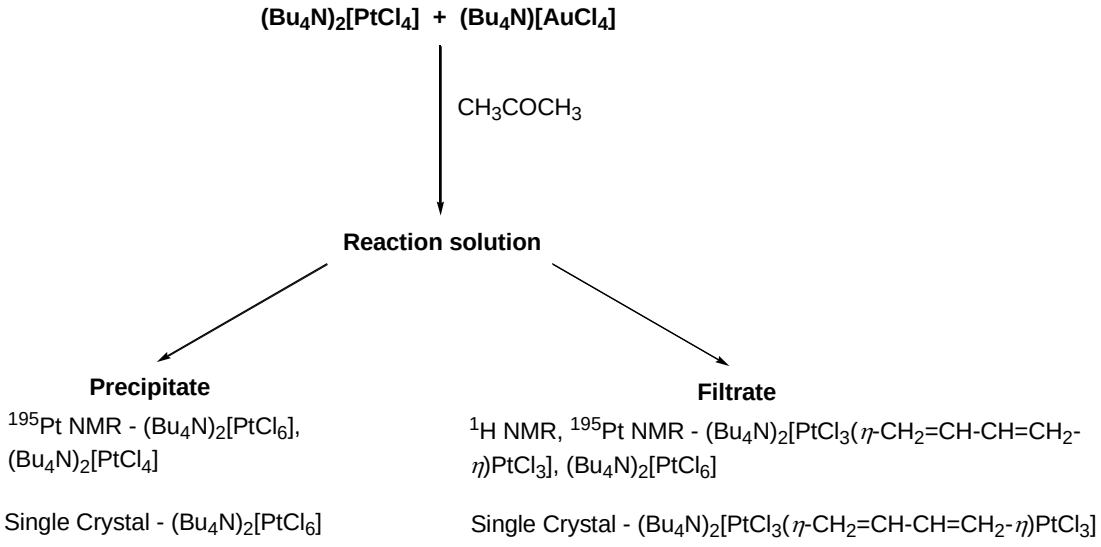

Scheme II.V Reaction of NBu_4^+ salts of Pt^{II} and Au^{III} in acetone.

In the above preparation (**Scheme II.V**), tetrabutylammonium salts of Pt^{II} and Au^{III} were used. This resulted in a precipitate and a filtrate which were analysed separately. The precipitate showed the presence of $(Bu_4N)_2[PtCl_6]$ and $(Bu_4N)_2[PtCl_4]$ when analysed by ^{195}Pt NMR spectroscopy, while the single crystal XRD results showed the presence of $(Bu_4N)_2[PtCl_6]$. The filtrate, analysed by ^{195}Pt NMR spectroscopy, showed the presence of $((Bu_4N)_2[PtCl_6])$ but also a new species *i.e.* $((Bu_4N)_2[PtCl_3(\eta\text{-}CH_2\text{=}CH\text{-}$

CH=CH_2-η)$PtCl_3$]. Two different crystal forms of $(Bu_4N)_2[PtCl_3(\eta$-CH_2=CH-CH=CH_2-$\eta)PtCl_3]$) (major) and ($(Bu_4N)_2[PtCl_6]$) (minor) were isolated, which were confirmed *via* single crystal X-ray analysis. The details of this reaction are discussed in section 2.2.1.5.

Discussion

^{195}Pt NMR spectroscopy

The ^{195}Pt NMR spectra of filtrates obtained from the reactions were analysed as obtained, while freshly prepared solutions in DMSO (dry) or CD_2Cl_2 (or $(CH_3)_2CO$ if the counter ion was not $[K(18\text{-crown-6})]^+$), were prepared from precipitates. Each analysis required a set of nine experiments covering range δ +2000 to -6000 in order to cover the complete chemical shift range of platinum.[62,63] Chemical shifts for some of the species that might be expected are shown in **Fig. 2.8.**[64,65,66]

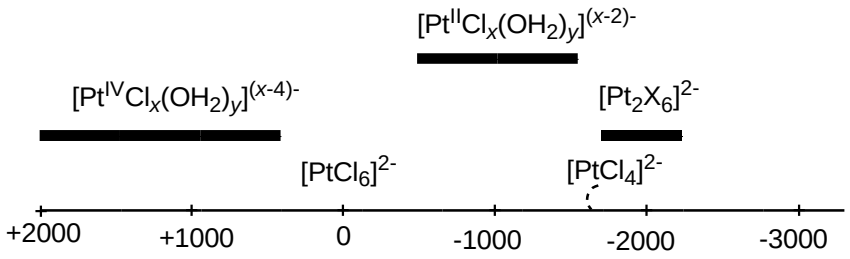

Fig. 2.8 ^{195}Pt chemical shifts for some Pt complexes in water.

The shifts of the signals obtained from each set of experiments were reconfirmed by changing the transmitter frequency (O1P) so as to avoid the drift in the chemical shift that usually occurs in an overnight run. Each experimental required 16 or 18 h to collect a full set of data and so solvolysis was observed in dmso to give $[PtCl_5(dmso)]^-$[67] (observed in Schemes **II.I**, **II.II**, **II.III**) or $[PtCl_3(dmso)]^-$[68] species (observed in

Scheme II.I) with chemical shifts of δ = -823 and -2953, respectively (**Fig. 2.9**).[69] It is known in the literature that dmso can replace chlorido groups[68] rapidly to form such solvolysed species.[67,70]

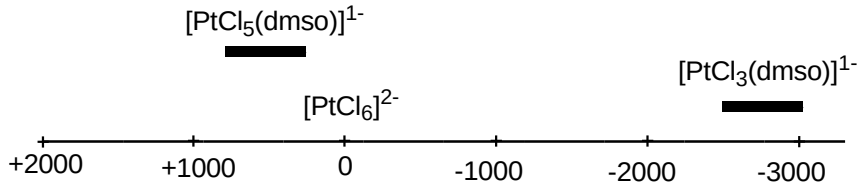

Fig. 2.9 Range of solvolysed species in dmso except $[PtCl_6]^{2-}$ (used as a reference in D_2O).

^{195}Pt NMR resonances can be heavily dependent upon the cation as has been observed in mononuclear, homodinuclear complexes mentioned in **Table II.II**. Thus, a significant change in chemical shift was observed when comparing tetrabutylammonium salts ($\Delta\delta$ = 61 ppm) and tetraphenylphosphonium salts ($\Delta\delta$ = 82 ppm) of $[PtCl_4]^{2-}$ in CD_2Cl_2.

$$(PPh_4)^+ > (Bu_4N)^+ > [K(18\text{-cr-}6)]^+$$
$$-1446 \; > \; -1467 \; > \; -1528$$

Thus, the stronger the ion pair interaction, the greater the masking (or screening) of the anionic complex and hence there is a decrease in chemical shift observed from left to right. It is known that the ion-pair effect increases due to cations like $(Bu_4N)^+$ in the presence of organic solvents as reported by Pesek and Mason.[71] This ion-pair effect in turn contributes to the screening of the anionic complex also shown above. For instance, with [K(18-crown-6)]$^+$ the cation K^+ is surrounded by a crown ether, [18-crown-6], which acts as a shell around it which effectively reduces its interaction with the counter anion. Hence, the interaction between [K(18-crown-6)]$^+$ and the anionic

metal complex is expected to decrease, thereby providing higher screening of the anion. However, for the $(Bu_4N)^+$ cation, the interaction between cation and the anionic complex is expected to be higher than for PPh_4^+, where the presence of Ph groups, play a key steric role in the reduction of ion-pair interaction between the cation and anion.

The effect of counter-cation is large for Pt^{II} complexes, but for Pt^{IV} the influence is smaller, which is most likely due to the accessibility of the Pt centre in square-planar complexes allowing approach/interaction of the cation in a way that is simply not possible in coordinatively saturated, octahedral Pt^{IV}.(**Fig. 2.10**).

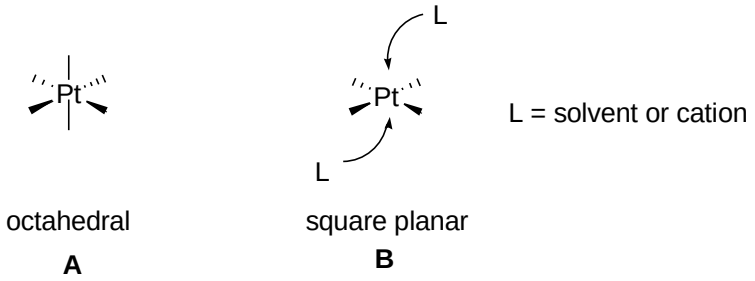

Fig. 2.10 Possible interactions of solvent or cation molecules (L) with different platinum nucleus **A** Pt^{IV} and **B** Pt^{II} having different geometry.

This is illustrated by comparing the ^{195}Pt chemical shifts for the same salts of the $[PtCl_6]^{2-}$ anion.

$$(PPh_4)^+ \sim (Bu_4N)^+ > [K(18\text{-cr-}6)]^+$$
$$+430 \sim +429 > +425$$

For homodinuclear complexes *i.e.* $[Pt_2Cl_6]^{2-}$, prominent ion-pair effects were never observed **Table II.II**. It should also be noted that the solvent, acidity or basicity of the medium and temperature have a marked effect on different

metal complexes.[71] The effect of solvent that has been observed for Pt^{IV} complexes *i.e.* $(Bu_4N)_2[PtCl_6]$, for all mononuclear Pt^{II} complexes and for homodinuclear Pt^{II} complexes is shown in the table below. Unless otherwise mentioned the values given in the table *i.e.* **Table II.II**, were obtained experimentally.

Table II.II ^{195}Pt NMR chemical shifts for various platinum complexes in different solvents.

Complex	^{195}Pt NMR chemical shifts (δ)	Solvent (T/K)
Pt^{II}		
$K_2[PtCl_4]$	-1620	H_2O (300 K)
$K_2[PtCl_4]$	-1613	D_2O (300 K)[68]
$(Bu_4N)_2[PtCl_4]$	-1418	$(CD_3)_2CO$ (300 K)
$(Bu_4N)_2[PtCl_4]$	-1467	CD_2Cl_2 (295 K)
$[K(18\text{-crown-6})]_2[PtCl_4]$	-1528	CD_2Cl_2 (295 K)
$(PPh_4)_2[PtCl_4]$	-1446	CD_2Cl_2 (295 K)
Pt^{IV}		
$K_2[PtCl_6]$	0	D_2O (300 K)[72]
$(Bu_4N)_2[PtCl_6]$	+222	CD_2Cl_2 (295 K)
$(Bu_4N)_2[PtCl_6]$	+375	$(CD_3)_2CO$ (300 K)[71]
$(Bu_4N)_2[PtCl_6]$	+429	DMSO (dry) (300 K)
$[K(18\text{-crown-6})]_2[PtCl_6]$	+425	DMSO (dry) (300 K)
$(PPh_4)_2[PtCl_6]$	+430	DMSO (dry) (300 K)
Dinuclear Pt^{II}		
$Li_2[Pt_2Cl_6]$	-1171	H_2O (300 K)
$(K[18\text{-crown-6}])_2[Pt_2Cl_6]$	-1217	CD_2Cl_2 (295 K)

^{195}Pt NMR shifts in different Pt-Au reactions

The chemical shifts obtained for Pt species from different reactions carried out in different solvents such as H_2O (**Schemes II.I**), CH_3COOH/H_2O (**Schemes II.II**), CH_3COONa/H_2O, and dil. HCl. are given in **Table II.III**. The precipitates obtained from 1 : 1 reactions carried out in H_2O (**Scheme II.I**) and CH_3COOH/H_2O (**Scheme II.II**), showed solvolysis to $[PtCl_5(dmso)]^{1-}$ and $[PtCl_3(dmso)]^{1-}$, when analysed in DMSO. However, the filtrate indicated a hydrolysed product of Pt^{IV} ($[PtCl_5(OH_2)]^-$) and some unreacted Pt^{II}, which appeared as the mononuclear as well as the homodinuclear species, $[PtCl_4]^{2-}$ and $[Pt_2Cl_6]^{2-}$, respectively. The ^{195}Pt NMR spectroscopy results obtained for 3 : 2 Pt-Au reactions in H_2O and CH_3COOH/H_2O were no different from those observed for 1 : 1 reactions. The results for the 3 h reaction (reaction conditions similar to **Scheme II.I**) indicated that the oxidation observed was fast but it did not appear that it was as complete as observed in a 48 h reaction. This was illustrated by the intensity of signals observed for Pt^{II} species relative to Pt^{IV} species, which was higher and was approximately 3 : 1 (Pt^{II} : Pt^{IV}) in a 3 h reaction in comparison to a 48 h reaction when analysed for the same duration was approximately 1 : 3 (Pt^{II} : Pt^{IV}). The idea of using CH_3COOH/H_2O as solvent was to try to trap dinuclear Pt^{III} species. As, it is known that the combination of $DMSO/H^+$ can oxidise Pt^{II} to Pt^{III}.[73,74] However, work in the group, has shown that in the presence of acetate, the oxidation stopped at Pt^{III} and metal-metal bonded, dinuclear complexes were formed that contained bridging acetate ligands (**Fig 2.11**).[75]

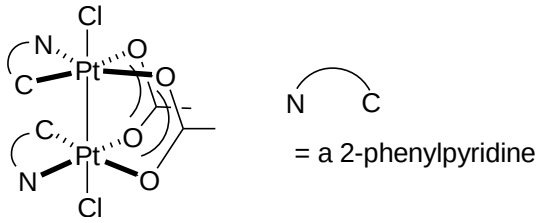

Fig. 2.11 Structure of dinuclear Pt^{III} complex.[75]

The approach was further varied by carrying out the reaction under acidic and basic conditions using HCl (dil.) (pH 2) and CH_3COONa/H_2O (pH 8), respectively. No new species were isolated from the former apart from mononuclear Pt^{IV}. However, in the latter, no Pt species were observed as peaks when analysed in the mixture as well as the filtrate at various different concentrations by ^{195}Pt NMR spectroscopy (**Table II.III**), which suggests the formation of insoluble oxide/hydroxide species.

Table II.III Data from ^{195}Pt NMR spectra obtained from different reactions.

Pt : Au	Duration	Solvent used in reaction	*δ* Peak/s observed from precipitate	*δ* Peak/s observed from filtrate
1 : 1	48 h	H_2O	-823 $[PtCl_5(dmso)]^{1-}$;[67] -2953 $([PtCl_3(dmso)]^{1-}$§)	-
1 : 1	48 h	CH_3COOH/H_2O	-823 $[PtCl_5(dmso)]^{1-}$[67]	+533.92 $[PtCl_5(OH_2)]^{1-}$,* -1512.138 $[PtCl_4]^{2-}$, -2412.56 (Pt^{II} species)
1 : 1	48 h	CH_3COONa/H_2O	*No peak was observed*	*No peak was observed*
1 : 1	48 h	HCl (dil.)	+424 $[K(18\text{-crown-6})]_2[PtCl_6]$	-2.6 $[PtCl_6]^{2-}$
1 : 1	3 h	H_2O	+815 close to $[PtCl_5(dmso)]^{-}$[67]	-1602 close to $[Pt_2Cl_6]^{2-}$, -2360 close to $[PtCl_2(OH_2)_4]^{2-}$[76]
3 : 2	48 h	H_2O	-2953 $[PtCl_3(dmso)]^{1-}$§	*No peak was observed*
3 : 2	48 h	CH_3COOH/H_2O	-424 $[K(18\text{-crown-6})]_2[PtCl_6]$; -823 $[PtCl_5(dmso)]^{1-}$;[67] -2952.19 $[PtCl_3(dmso)]^{1-}$§.	-1588 $[PtCl_4]^{2-}$

*Values given are fairly close to complex $(H_2O)[PtCl_5(OH_2)]\cdot 2[18\text{-crown-6}].6H_2O$ (δ832)[77] but the shift observed is due to the influence of counter cation *i.e.* $[K(18\text{-crown-6})]^{§}$ Values given are fairly close to reported values observed in 1 : 1 mixture of DMSO : H_2O for $[PtCl_3(dmso)]^{1-}$.[68]

Single crystal X-Ray diffraction

The list of crystal structures obtained from different Pt-Au reactions is given in **Table II.IV**. The crystals obtained indicated the presence of completely oxidised species *i.e.* Pt^{IV} either as solvolysed ([K(18-crown-6)][$PtCl_5(OH_2)$] observed[78] in **Scheme II.II** or as an unsolvolysed form ([K(18-crown-6)][$PtCl_6$]·2DMSO (**Scheme II.II**); [K(18-crown-6)][$PtCl_6$]·2AcOH. Also, crystals of reduced product *i.e.* ([K(18-crown-6)][$AuCl_2$][46] and unreacted Au^{III} ([K(18-crown-6)][$AuCl_4$]) observed in **Scheme II.III** or [K(18-crown-6)][Pt_2Cl_6][18] (**Scheme II.I**) were recovered as side products. Unfortunately, no crystals corresponding to the expected heterobimetallic complex or any other homodinuclear complex were obtained. The details of crystal structures are given in the appendix section. Crystals unsuitable for XRD were analysed *via* CHN. The structures that have not been reported previously and require a description are described below in detail, while others are in the appendix.

Table II.IV Single crystal X-ray diffraction results

Pt : Au reaction (solvent)	X-ray Diffraction	Solvent used for crystallisation
Reactions with [18-crown-6]		
1 : 1 (H_2O)	Crystals obtained were not suitable for XRD	H_2O (filtrate on standing)
1 : 1 (CH_3COOH/H_2O)	$[K(18\text{-crown-6})]_2[PtCl_6]\cdot 2DMSO$; $[K(18\text{-crown-6})][PtCl_5OH_2]$	DMSO (dry); CH_3COOH/H_2O (filtrate)
1 : 1 (CH_3COONa/H_2O)	$[K(18\text{-crown-6})][AuCl_2]$	$(CH_3)_2CO$
1 : 1 (HCl. dil.)	Crystals obtained unsuitable for XRD	HCl. dil.
3 : 2 (CH_3COOH/H_2O)	$[K(18\text{-crown-6})]_2[PtCl_6]\cdot 2AcOH$	CH_3COOH/H_2O (filtrate)

$[K(18\text{-crown-}6)]_2[PtCl_6]\cdot 2DMSO$ and $[K(18\text{-crown-}6)]_2[PtCl_6]\cdot 2AcOH$

Hexachloroplatinate(IV) with a $[K(18\text{-crown-}6)]^+$ cation was isolated from a reaction between Pt-Au in both a 1 : 1 and 3 : 2 ratio carried out in CH_3COOH/H_2O. The crystals were obtained as yellow coloured plates on standing. The two structures were very similar and even the crystallographic parameters were close to one another as shown in the appendix section.

In each case, both solvent molecules were found close to the crown ether on opposite sides of the anion (**Fig. 2.12**). The origin of $[K(18\text{-crown-}6)]_2[PtCl_6]\cdot 2AcOH$ was from the reaction mixture obtained during NMR spectroscopic analysis. However, $[K(18\text{-crown-}6)]_2[PtCl_6]\cdot 2DMSO$ was obtained from the solubilisation of the precipitate of the Pt-Au reaction mixture when DMSO was used.

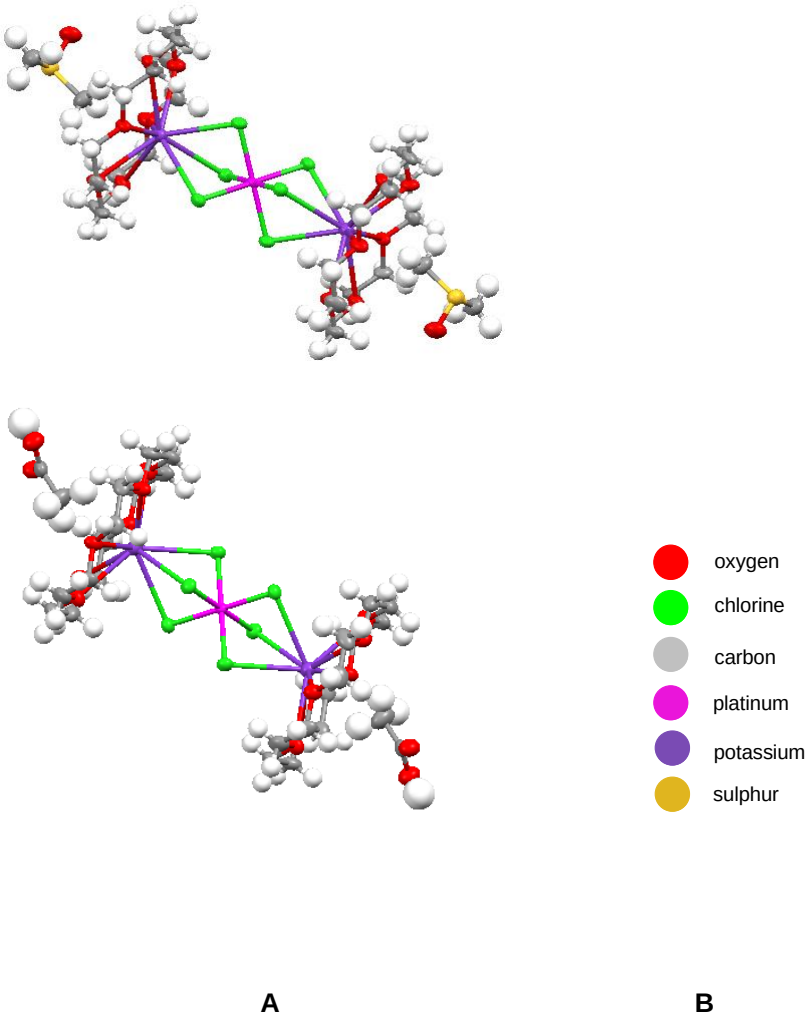

Fig. 2.12 Structures of Pt^{IV} crown ether complexes with different solvents of crystallisation **A** DMSO, and **B** CH_3COOH.

[K(18-crown-6)][AuCl$_4$]

The mononuclear Au^{III} crown ether complex ([K(18-crown-6)][$AuCl_4$]) was isolated from the preparation of the mononuclear crown ether complex of Au^{III}, carried out in H_2O from [18-crown-6] and K[$AuCl_4$] by stirring; it was crystallised from CH_2Cl_2 (under N_2, 5 °C, dark). The crystal structure has not been reported before but, previous attempts to isolate it from a mixture of K[$AuCl_4$] and [18-crown-6] in MeOH followed by crystallisation from a MeOH/Et_2O mixture, led to colourless crystals of [K(18-crown-

6)][$AuCl_2$].[46] No description was given in the paper which explains this reduction of Au^{III}. However, it was observed in this work that if the crystallisation is not carried out at low temperature and under inert atmosphere then a mixture of crystals of complex of Au^{I} (minor) and Au^{III} (major) will be obtained. If the crystallisation is carried out in the presence of light then Au^{I} will be the only product.

The final structure of the Au^{III} complex was difficult to obtain as it showed variation in data sets *i.e.* the data set collected at the beginning was significantly different from the data set obtained at the end. In fact due to the exposure to the X-ray beam a change in the molecular arrangement and hence the unit cell of the structure of [K(18-crown-6)][$AuCl_4$] was observed. The change is due to change in chloride positions in the X-ray beam and the resulting tetrachloroaurate(III) positions are randomised through the crystal (**Fig. 2.13**). This then leads to an increase in symmetry *i.e.* from *P*-1 to *C*2/*c* hence the change in the unit cell is observed. Thus, two different polymorphs are observed which is also indicated in the final structure in the cif file as well as in the appendix.

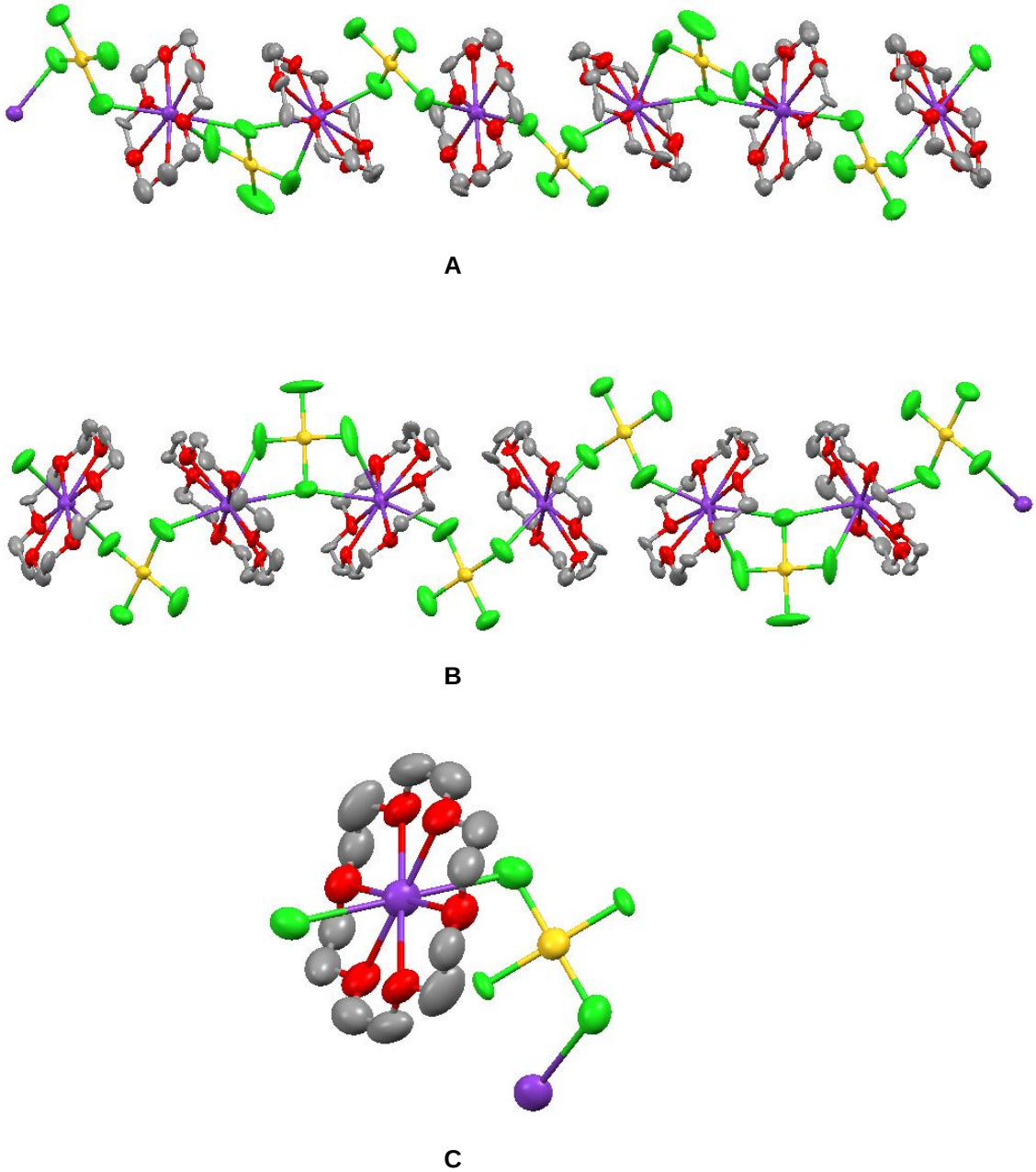

Fig. 2.13 Structure of [K(18-crown-6)][$AuCl_4$] showing different arrangement of $[AuCl_4]^{1-}$ and [K(18-crown-6)] in X-ray beam during structure analysis. **A**: Initial structure, **B**: Middle structure and **C**: Final structure, hydrogens are removed for clarity.

Stoichiometry of metals in Pt-Au reactions

Initially, reaction between Pt^{II} and Au^{III} had used a 1 : 1 ratio of starting complexes as the objective was to prepare a heterobimetallic complex of 1 : 1 stoichiometry. However, it is clear that the reaction occurring is a redox reaction as Pt^{IV}, Au^{0} and Au^{I} are all formed but characterisation of the reaction products was hampered to some degree as there is also unreacted Pt^{II} and Au^{III}. These arise as the starting stoichiometry was chosen, on the basis of the redox reaction. There were two competing possibilities:

$$Pt^{II} + Au^{III} \longrightarrow Pt^{IV} + Au^{I}$$

$$3\,Pt^{II} + 2\,Au^{III} \longrightarrow 3\,Pt^{IV} + 2\,Au^{0}$$

Therefore, the reaction was repeated using a Pt : Au ratio of 3 : 2, better to reflect the nature of the redox reaction and when the reactions were carried out in water as well as in CH_3COOH/H_2O, the results showed the presence of mononuclear oxidised Pt^{IV} species as the major product; no unreacted Au^{III} or Au^{I} was recovered in any of the reaction mixtures rather Au^{0} was the only reduced product found. On the other hand, some unreacted Pt^{II} was produced as a side product *i.e.* $[K(18\text{-crown-}6)]_2[Pt_2Cl_6]$ in CH_3COOH/H_2O mixture. In other words, the attempts were successful to eliminate the presence of different species of gold which were thought to be interfering in the product formation, but the results obtained did not show any other difference in product formation. The presence of unreacted Pt^{II} is likely due to incomplete oxidation, although it is not clear why this is the case with no Au^{III} or Au^{I} being recovered.

Attempted preparation of [K(18-crown-6)][$Cl_2Pt(\mu\text{-}Cl)_2AuCl_2$]

All attempts above to prepare heterobimetallic Pt-Au crown ether complexes were unsuccessful. Therefore, another attempt was made to synthesise the same complex using mononuclear Pt^{II} and Au^{III} complexes starting from the [K(18-crown-6)] salts. The method involved stirring the two mononuclear metal complexes (*i.e.* [K(18-crown-6)][$AuCl_4$] and $[K(18\text{-crown-6})]_2[PtCl_4]$) in CH_2Cl_2 at room temperature for 48 h in the dark. No reduced gold was formed as gold mirrors as observed in the previous attempted preparations. Instead, a clear orange-yellow solution resulted, to which was then added hexane. The precipitate obtained was insoluble in all organic solvents except dmso hence it was once again analysed by ^{195}Pt NMR spectroscopy in it, and $[PtCl_5(dmso)]^{1-}$ was observed. The results obtained were no different from the previous preparations, although use of the potassium-crown ether salts appears to have modified the reaction in that no Au^0 was formed as product.

The precipitate obtained from all the above Pt : Au reactions (either 1 : 1 or 3 : 2 ratios) carried out in the presence of crown ether showed solubility only in dmso. The latter, as discussed above, can result in solvolysis very easily. Therefore, if any of desirable homo or hetero binuclear oxidised species would have formed in any of the reaction mixtures, even at a very low concentration, they could have undergone solvolysis through the cleavage of the chloro-bridges (below). The evidence for this has been indicated by formation of $[PtCl_3(dmso)]^-$ observed from $[Pt_2Cl_6]^{2-}$ when analysed by ^{195}Pt NMR spectroscopy in DMSO as NMR solvent (δ -2952).

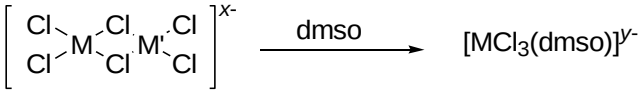

M = Pt^{II}, M' = Pt^{II}, x = 2, y = 1

To avoid this problem, it was decided to attempt to use $(Bu_4N)Cl$ as a precipitant for the filtrate recovered from the above crown ether reactions. This will be an aid to recover any other species present in the solution *e.g.* $(Bu_4N)[Cl_2Pt(\mu\text{-}Cl)_2AuCl_2]$, which are otherwise difficult to observe in the NMR spectroscopy of the mixture. Another idea was to synthesise $(Bu_4N)[Cl_2Pt(\mu\text{-}Cl)_2AuCl_2]$, the product of which in both the cases would be expected to be soluble in solvents other than DMSO.

2.2.1.4 Attempts to Synthesise Hetero-binuclear Pt-Au Complexes with a $(Bu_4N)^+$ Cation

The reaction was carried out between a 1 : 1 ratio of Pt^{II} and Au^{III} as potassium-18-crown-6 salts and after collection of the precipitate, excess of $(Bu_4N)Cl$ was added to precipitate anionic species remaining in the aqueous solution (**Scheme II.V**). The resulting precipitate was then analysed by ^{195}Pt NMR spectroscopy using a solvent other than DMSO, in this case acetone. This time, the precipitate, filtrate as well as precipitate from filtrate *i.e.* obtained after treatment with $(Bu_4N)Cl$ were analysed separately to as to confirm the presence of platinum anionic species present in any part of the reaction mixture by ^{195}Pt NMR spectroscopy. It should be noted that the ^{195}Pt NMR spectroscopy results of the first formed precipitate *i.e.* soluble in DMSO only, showed results (**Table II.V**), which were similar to those observed previously (**Table II.III**). However, this time the filtrate formed was analysed as before but the duration of analysis was for a longer period of time due to which, presence of additional peaks in an extremely small ratio which remained unanalysed in the previous experiments (**Scheme II.I**) were confirmed. In **Table II.V**, possible *cis*- or *trans*- isomers of Pt^{II} hydrolysed species (+1083 small peak, value close to *cis*-$[PtCl_4(OH_2)]^{2-}$; *trans*-$[PtCl_4(OH_2)]^{2-}$)[76] along with hydrolysed species of Pt^{IV} as main ratio (+521 $[PtCl_5(OH_2)]^{1-}$)[66] observed has been clearly represented.

In other attempts to prepare a Pt-Au hetero-binuclear complex, in absence of crown ether, $K[AuCl_4]$ and $K_2[PtCl_4]$ (at ratios 1 : 1 and 3 : 2 for Pt : Au), were stirred in water (**Scheme II.IV**) or dilute acetic acid at room

temperature for 48 h and 3 h in the dark. This resulted in the formation of metallic gold as precipitate which was filtered followed by the treatment of the yellow filtrate with $(Bu_4N)Cl$ in excess to precipitate the final product. The resulting product was analysed by ^{195}Pt NMR spectroscopy in acetone.

The ^{195}Pt NMR spectra obtained from a reaction using a Pt : Au (1 : 1) ratio showed signals that corresponded to Pt^{IV} species such as $[PtCl_6]^{2-}$. Apart from that, an unidentified peak was found at δ +94. From our knowledge of ^{195}Pt NMR spectroscopy, this comes within the range of Pt^{IV} species (see **Fig. 2.8** and **Fig. 2.9** for Pt^{IV} species existence). Hence, it is certain to possess Pt^{IV} (completely oxidised species). However, the reactions done with 3 : 2 ratio of Pt : Au, did not result in any peak other than $[PtCl_6]^{2-}$. Crystallisation of the mixtures (obtained both from H_2O as well as CH_3COOH/H_2O) of 1 : 1 or 3 : 2, Pt : Au reactions resulted in a new homodinuclear Pt^{II} butadiene complex, which is discussed separately in section 2.2.1.5. The complex formed was obtained as a mixture with $(Bu_4N)_2[PtCl_6]$.

None of the above results indicated any new species which could contribute towards the existence of any new chloro-bridged hetero or homo dinuclear complexes.

Table II.V ^{195}Pt NMR peaks obtained in attempted preparations of $(Bu_4N)^+$ salts of hetero-binuclear complexes.

Pt : Au	Reaction duration	Solvent used in reaction	δ Peak/s observed from precipitate with $(Bu_4N)^+$	δ Peak/s observed from filtrate
1 : 1	48 h	H_2O	+370 $[PtCl_6]^{2-*}$, +94 (unidentified)*	+521 (main peak) $[PtCl_5(OH_2)]^{1-}$ [66]; +1083 (small peak) (value close to *cis*-$[PtCl_4(OH_2)]^{2-}$; *trans*-$[PtCl_4(OH_2)]^{2-}$[76]; +8 (close to $[PtCl_6]^{2-}$).
1 : 1	48 h	H_2O: CH_3COOH (1 : 1)	+94 (unidentified)*, -823 $[PtCl_5(dmso)]^{1-§}$; +428 (observed initially) $[PtCl_6]^{2-§}$	+537 $[PtCl_5(OH_2)]^{1-[bb]}$
3 : 2	48 h	H_2O	+374 $(Bu_4N)_2[PtCl_6]$)*	-
3 : 2	3 h	H_2O	+374 $(Bu_4N)_2[PtCl_6]$)*	-

§ in dmso, * in acetone

Single crystal XRD

Data for the X-ray structure of single crystals obtained from the rest of the Pt-Au reactions are given in **Table II.VI**. The reactions carried out with 1 : 1, Pt : Au ratio showed the presence of unreacted Au^{III}, recuperated as side product of the reaction during crystallisation. In reactions with water a homodinuclear complex of Pt^{II} was isolated in small amounts either as side product in 1 : 1 and 3 : 2 reactions. Details are discussed separately in § 2.2.1.5.

Table II.VI Results of single crystals X-ray diffraction from the attempted Pt-Au reactions with $(Bu_4N)^+$ cation.

Pt : Au reaction (solvent)	X-ray Diffraction	Solvent used for crystallisation
(1 : 1) (CH_3COONa/H_2O)	[K(18-crown-6)][$AuCl_2$]	$(CH_3)_2CO$
1 : 1 (HCl. dil.)	Crystals obtained unsuitable for XRD	HCl. dil.
3 : 2 (CH_3COOH/H_2O)	[K(18-crown-6)]$_2$[$PtCl_6$]·2AcOH	CH_3COOH/H_2O (filtrate)
Reactions without [18-crown-6]		
1 : 1 (H_2O)*	$K_2[PtCl_6]$;	H_2O (filtrate);
	$(Bu_4N)[AuCl_4]$;	$(CH_3)_2CO$;
		$(CH_3)_2CO$/hexane
1 : 1 (CH_3COOH/H_2O)*	$(Bu_4N)[AuCl_4]$;	$CDCl_3$;
		$(CH_3)_2CO/Et_2O$

Pt^{II} butadiene complex was segregared as single crystals as *minor side product; major product with low yields in 3 : 2 reactions not mentioned in above case.

Elemental Analysis

The elemental analysis of the mixtures for most of the precipitates obtained from attempted preparations of heterobimetallic Pt-Au complexes did not correlate to any of the expected/target complexes. The reason for this was that the precipitate obtained was a mixture of more than one species as shown by NMR spectroscopy and single crystal XRD. Hence, the identification of the precipitate prior to crystallisation of the sample was based primarily on ^{195}Pt NMR and IR spectroscopy and CHN (in a few cases). Then, final identification of the product mixtures was based on the combination of all the results along with data from single crystal X-ray diffraction. However, in a few cases, it was certain that the mixture contained two components, the ratio of $M_1 : M_2$ was calculated inferred from CHN data obtained.

Homodinuclear Pt^{II} complex in Pt-Au reactions with crown ether

In the above attempted Pt-Au reactions with [18-crown-6], evidence of formation of a Pt^{II} homodinuclear complex *i.e.* $[Pt_2Cl_6]^{2-}$ has been recorded in the most of them as a side product. The latter was isolated as single crystals and was analysed by X-ray diffraction. Species arising from solvolysis, *i.e.* $[PtCl_3(dmso)]^-$ and $[PtCl_4(OH_2)_2]^{2-}$, were also found on occasions. As the reaction was carried under the conditions analogous to the Pd-Au complex synthesis, another possibility that may arise and would have resulted in the formation of such a homodinuclear complex would be the formation of $[Pt_2Cl_6]^{2-}$ from $[PtCl_6]^{2-}$ in the presence of light (see equations below) as discussed was previously in the attempted preparations of Pd-Au reactions.

$$[PtCl_4]^{2-} + [AuCl_4]^- \longrightarrow [PtCl_6]^{2-} + [AuCl_2]^-$$

$$[PtCl_6]^{2-} \longrightarrow 0.5\,[Pt_2Cl_6]^{2-}$$

Although, this has been reported in the literature for Pd^{IV} species,[50] no evidence exists for analogous chemistry with Pt^{IV} species. However, the possibility exists as the crystallisation of the mixtures was not done in perfectly dark conditions. Moreover, it has been reported by Shilov and co-workers[95] that the $[PtCl_6]^{2-}$ can be converted to $[Pt_2Cl_6]^{2-}$ in the presence of light. The same argument has been presented below to support the section 2.2.1.5.

2.2.1.5 Synthesis of a Dinuclear Zeise's Salt Analogue

While conducting reactions between $[PtCl_4]^{2-}$ and $[AuCl_4]^-$ and precipitating with $(Bu_4N)Cl$, greenish-yellow-coloured crystals were isolated along with yellow crystals of $(Bu_4N)_2[PtCl_6]$, the latter being the major product. On one occasion, a sufficient quantity of these greenish yellow crystals was isolated for analysis by single crystal X-ray diffraction. The structure obtained was remarkable, a dinuclear analogue of Zeise's salt, containing 1,3-butadiene. The structure is now described.

Crystal structure

The structure of this homodinuclear complex $(Bu_4N)_2[PtCl_3(\eta\text{-}CH_2{=}CH\text{-}CH{=}CH_2\text{-}\eta)PtCl_3]$ contains an anion possessing a $\mu\text{-}(\eta^2,\eta^2\text{-butadiene})$ moiety coordinated to two Pt^{II} nuclei. The coordination of *trans*-butadiene is orthogonal with respect to each $PtCl_3$ group as shown in **Fig. 2.14 (b)** and its coordination pattern resembles that of Zeise's salt *i.e.* $K[Cl_3Pt(\eta^2\text{-}C_2H_4)]$. The counter ion, $(Bu_4N)^+$, has been removed from **Fig. 2.14 (a)** for clarity.

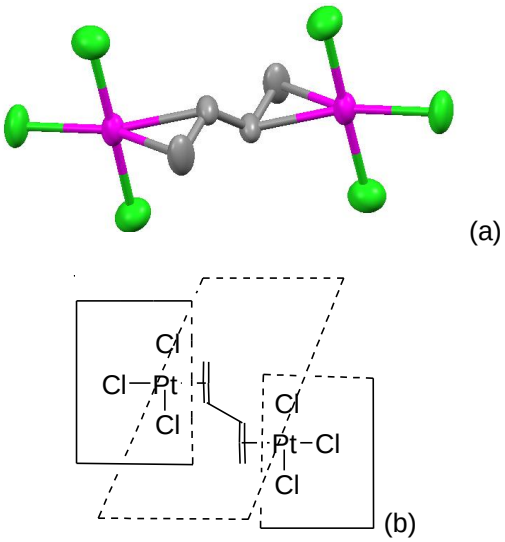

Fig. 2.14 $[Pt_2Cl_6(C_4H_6)]^{2-}$ anion showing coordination of butadiene with $PtCl_3$ groups.

Attempts were made in the past to prepare such butadiene bridged complexes using metals such as Pt^{II} and Pd^{II}.[79,80] However, the complexes formed were either unstable at room temperature[79] or it proved impossible to distinguish *cis* or *trans* conformation of the synthesised complex.[80] The existence of those complexes was based on IR spectroscopy through models[81] that were proposed for its structural elucidation. The explanation of the infrared spectrum obtained for $K_2[Pt_2Cl_6(C_4H_6)]$[82] was based on a comparison with spectra of the butadiene in $[Fe(CO)_3(\eta^4\text{-butadiene})]$[83] and the ethene in $K[Cl_3Pt(\eta^2C_2H_4)]\cdot H_2O$ (Zeise's salt).[84]

The homodinuclear Pt^{II} butadiene complex resulting from Pt-Au complex preparations was also analysed by IR spectroscopy (**Table II.VII**). An attempt was even made to distinguish the two isomers of Pt^{II} butadiene complex by IR spectroscopy results with the previously reported *cis*- and *trans*- butadiene complexes *i.e.* $K_2[Pt_2Cl_6(C_4H_6)]$,[82] and $[(CO)_3Fe(C_4H_6)]$,[83] respectively, but it was unsuccessful. However, the presence of a metal coordinated to 1,3-butadiene was confirmed. Other supporting evidence for the complex was IR spectroscopy below 400 cm^{-1} which indicated the presence of three stretching vibrations for $\nu_{Pt\text{-}Cl}$ observed at 308, 315 and 330, respectively. The values correspond to Zeise's salt and dinuclear Zeise's salt reported in the literature, **Table II.VII** and is consistent with the local C_{2v} symmetry**.**

Table II.VII Comparison of IR frequencies observed (below 400 cm^{-1}) for $K_2[Pt_2Cl_6(C_4H_6)]$[82] $[K(PtC_2H_4)Cl_3]H_2O$[91] with Dinuclear Zeise's salt.

Stretching/Assignment	$K_2[Pt_2Cl_6(C_4H_6)]$[82]	$[K(Pt(C_2H_4)Cl_3]H_2O$[91]	$(Bu_4N)_2[Pt_2Cl_6(C_4H_6)]$
ν(Pt-Cl)	308 (s)	310	308 (vw)
ν(Pt-Cl)	332 (vs)	331 (vs)	315 (w)
ν(Pt-Cl)	339 (vs)	339 (vs)	330 (s)

A crystal structure containing a $[Cl_3Pt\mu\text{-}(\eta^2,\eta^2\text{-butadiene})PtCl_3]^{2-}$ dianion has been reported with $(EtMe_3N)^+$ as cation.[85] Crystal data and selected bond lengths were given, but no coordinates. However as shown in **Table II.VIII** there is quite good agreement between those bond lengths and those found here. The method of preparation in this work was not clear.

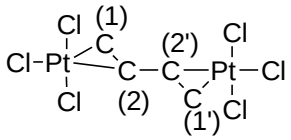

Fig. 2.15 $[Pt_2Cl_6(C_4H_6)]^{2-}$ structure used to compare bond lengths in the **Table II.VIII**.

Table II.VIII Comparison of the two differently obtained Pt^{II} butadiene complexes.

Description	$(EtMe_2N)_2[Pt_2Cl_6(C_2H_6)]$[102]	$(Bu_4N)_2[Pt_2Cl_6(C_2H_6)]$
Pt-Cl cis to diene	2.32(1), 2.29(1) Å	2.2999(11) Å
		2.3179(11) Å
Pt-Cl trans to diene	2.29(1) Å	2.3021(11) Å
C(1)-C(2)	1.51(3) Å	1.419(6) Å
C(2)-C(2')	1.36(3) Å	1.471(8) Å
Pt-C(1)	2.20(3) Å	2.110(4) Å
Pt-C(2)	2.18(2) Å	2.180(4) Å
C-C-C	118(2)°	120.5(5)°

Other relatively recently reported structures of metal-butadiene complexes include *trans*-$[Cp_2Ta(\eta^4\text{-butadiene})]^+$,[86] $[(Cp_2Zr)(\mu\text{-}CH_3)(\mu\text{-butadiene})(ZrCp_2)]^+$,[87] $[Cp_2Zr(\eta^4\text{-1,3-butadiene})]$,[88] and $[Cp_2Hf(\eta^4\text{-1,3-butadiene})]$.[88]

Preparations

The observation of a butadiene complex was unexpected and so work was undertaken to try to investigate it further. The first sample obtained was from an aqueous phase reaction between $[PtCl_4]^{2-}$ and $[AuCl_4]^-$. The solution that resulted had been treated with $(Bu_4N)Cl$ and the butadiene complex was recovered after the resulting precipitate had been allowed to remain in acetone solution for some time. This implicated Bu_4N^+ as the source of the diene ligand and so further reactions were carried out starting with NBu_4^+ salts of the complexes.

Thus, $(Bu_4N)_2[PtCl_4]$ and $(Bu_4N)[AuCl_4]$, were stirred in acetone for 48 h in the dark. No metallic gold was observed as in previous reactions between Pt^{II} and Au^{III} and a clear solution resulting in a precipitate on addition of Et_2O. This resulted in a mixture of the dinuclear Pt^{II} butadiene complex and $(Bu_4N)_2[PtCl_6]$. The two complexes were separated by crystallisation and the yield thus obtained was about 8%. Repeating the reaction with wet (5 cm^3 with 1 drop of H_2O) and rigorously dry acetone, changed the yields isolated yields from 1% to 15%, respectively.

Isomers of Pt^{II} butadiene complex

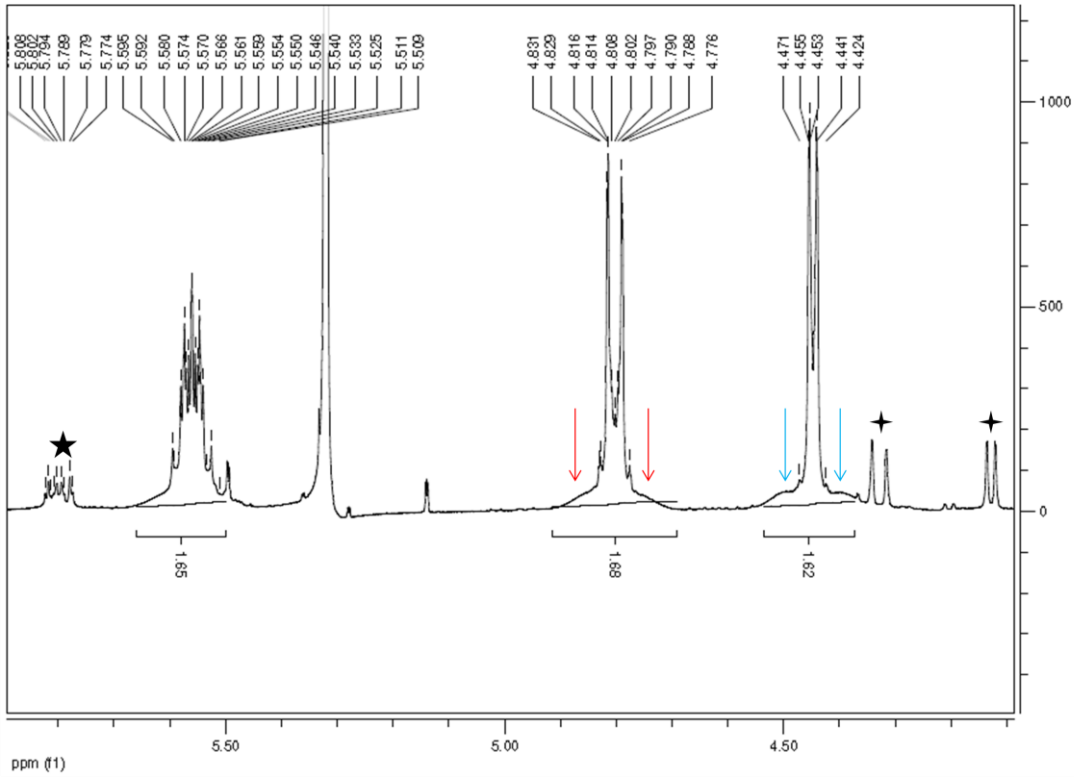

Fig. 2.16 500 MHz ^{1}H NMR spectrum of Pt^{II} butadiene complex in CH_2Cl_2, where ★ and ✦ indicates multiplet and doublets due to *cis*-conformer, respectively. The arrows in red and blue indicates regions for $J_{Pt\text{-}H}$.

The ^{1}H NMR spectrum of the Pt^{II} butadiene complex is shown in **Fig. 2.16**. and indicates the presence of two similar sets of signals (two doublets and a multiplet) in the ratio 8 : 1. It is assumed that these correspond to *transoid* and *cisoid* conformers as shown in **Fig. 2.17** and that the major conformer is the *transoid* form (**Fig. 2.17A**).

Looking at the structure, it is apparent that there are three different hydrogen environments, H_a H_b and H_c, giving rise to the three resonances, but it is clear also that while the two halves of the butadiene ligand are equivalent chemically, the two sets of three hydrogens are inequivalent magnetically.

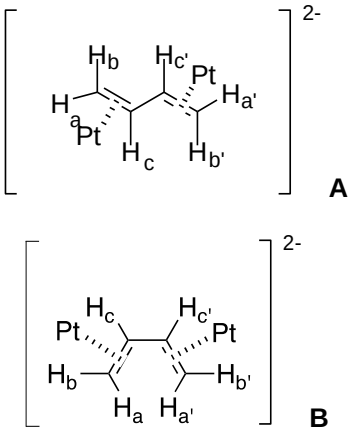

Fig. 2.17 A *cis*- and **B** *trans*- Isomers of Pt^{II} butadiene complex, chlorines are omitted for clarity.

$^3J(H_b, H_c)$ would be expected to be the largest coupling followed by $^3J(H_a, H_c)$, and for the major conformer, H_b is identified as the resonance at δ 4.80 ($^3J(H_b, H_c)$ = 12.0 Hz) and H_a as the resonance at δ 4.45 ($^3J(H_a, H_c)$ = 6.0 Hz). That these appear as simple doublets means that $^2J(H_a, H_b) \approx 0$, although the small peaks to either side of the main resonance suggest some coupling (unassigned) to $H_{a'}$, $H_{b'}$ or $H_{c'}$. Coupling to ^{195}Pt is not well resolved but the broad shoulders would give a value of ^2J(Pt-H) of *ca* 66 Hz, which is quite close to the value of 64.0 Hz obtained for $[Pt_2Cl_4(PPr_3)_2(\mu\text{-}C_2H_6)]$ by Briggs *et al.*[89]. However, the second coupling constant *J*(Pt-H) indicated by red-arrows is not well-resolved as for ^2J(Pt-H) and is difficult to assign its value from the spectrum. The remaining resonance at δ 5.55 is assigned to H_c and is a multiplet with coupling to H_a and H_b as well as to some or all of the magnetically inequivalent hydrogens $H_{a'}$, $H_{b'}$ and $H_{c'}$.

The other set of signals, assumed to the *cisoid* conformer (**Fig. 2.17B**), can be analysed analogously, so that the resonance at δ 4.13 is assigned as H_a, while that at δ 4.33 is assigned as H_b. The coupling constants are $^3J(H_a, H_c)$ = 13.5 Hz and $^3J(H_b, H_c)$ = 7.0 Hz. The resonance at δ 5.79 is assigned as H_c and appears to have a simpler coupling pattern when compared with the equivalent hydrogen in the major isomer, which may well be consistent with the proposal that this is the *cisoid* form.

As noted above, a somewhat similar range of coupling constants was reported for $[Pt_2Cl_6(PPr_4)_2(\mu\text{-}C_2H_6)]$[89] in $CDCl_3$ at 100 MHz and give confidence in the assignments made. This paper[89] also reported the synthesis and CHN data for $[NBu_4]_2[Pt_2Cl_6(\mu\text{-}C_2H_6)]$, but did not contain any NMR data.

Molecule	J_{bc} (Hz)	J_{ac} (Hz)	J_{ab} (Hz)
1,3-butadiene[90]	17.05	10.17	1.74
$[Pt_2Cl_6(PPr_4)_2(\mu\text{-}C_2H_6)]$[89]	13.2	6.6	~0
$[Cl_3Pt\mu\text{-}(\eta^2,\eta^2\text{-butadiene})PtCl_3]^{2-}$	12	6	~0

^{195}Pt NMR spectra of the mixture solutions (acetone/Et_2O) obtained from the precipitate, and of the filtrate prior to crystallisation showed the existence of the complex at δ = -2723 with an unidentified peak at δ = -2527 being observed in acetone/Et_2O mixtures, attributed to the minor *cisoid* conformer. However, a peak of $[PtCl_6]^{2-}$ was also observed at δ +375 only in acetone. A repetition of ^{195}Pt NMR spectroscopy experiment in CD_2Cl_2 revealed the presence of two peaks at δ -2546 and δ -2543. The peaks were expected to

be the *transoid*- or *cisoids*- conformers. However, without the separation of the conformeric mixture it is not possible to distinguish between the two.

From the reactions carried out with Pt^{II} and Au^{III}, it is evident that in these reactions, oxidation of Pt^{II} to Pt^{IV} appears to take place rapidly. Also, if the tetrabutylammonium ion is present in the reaction mixture in any form (*i.e.* as a precipitant or as a counter cation) then the formation of the Pt^{II} butadiene complex is found to occur *i.e.* observed as a single crystal. From these two observations, it appears that the formation of the homodinuclear Pt^{II} butadiene complex is somehow linked with the formation of Pt^{IV} (*i.e.* oxidised product) and the presence of tetrabuylammonium cation. It is important to mention here that the concept of C-H activation by the involvement of higher oxidation state metals do exist and it has been reported by Shilov and co-workers in the past.[95] Interestingly, such C-H activation reactions of alkanes can also involve Pt^{II}/Pt^{IV} mixtures.

In the light of above observations and the possibility of the involvement of a Pt^{II} and Pt^{IV} mixture in C-H activation in our reaction, the reaction was repeated under similar conditions but with Pt^{II} and Pt^{IV} tetrabutylammonium salts. The reaction was successful, resulting in an overall yield of pure Pt^{II} butadiene complex *i.e.* 18%.

Mechanistic possibilities and other experimental evidences

From the success of the reaction between tetrabutylammonium salts of Pt^{II} and Pt^{IV}, it is clear that the possibility of C-H activation similar to Shilov's chemistry exists. However, the introduction of a C_4 fragment *i.e.* butadiene into the system can be possible either by $(Bu_4N)^+$ and also by acetone

(solvent). The latter is less likely (*i.e.* forming a C_4 fragment from a C_3 fragment) but this doubt can be cleared up if the reaction is repeated in d_6-acetone.

Another concept that also exists in the literature is the Hoffmann elimination. Tetrabutylammonium fluoride has been reported to be prone to decompose when vigorous attempts are employed to dry it.[92] This decomposition occurs due to a Hoffmann elimination as shown by the mechanism below, which results into 1-butene and tributylamine.

$$(n\text{-}C_4H_9)_4N^+F^-.3H_2O \longrightarrow (n\text{-}C_4H_9)_4N^+F^- + 3\,H_2O \quad (1)$$

$$2\,(n\text{-}C_4H_9)_4N^+F^- \longrightarrow \underset{\text{adduct}}{(n\text{-}C_4H_9)_4N^+FHF^-} + (n\text{-}C_4H_9)_3N + \underset{\text{olefin}}{CH_3CH_2CH{=}CH_2} \quad (2)$$

Hence, if the origin of C_4 fragment is the $(Bu_4N)^+$ cation, then a mechanism analogous to Hoffmann elimination reaction is possible and the above equations might hold. Nevertheless, this elimination requires an extremely basic anion, whereas $(Bu_4N)^+$ cation relies on the presence of stronger affinity of counter anion *i.e.* F^-. However, in this case, the counter anion is Cl^-, which is rather less effective. Then also, to prove that the C_4 fragment originated from of $(Bu_4N)^+$ cation through its activation with a different source, attempted preparations with mononuclear complexes of Pt^{II}, Au^{III} and Pt^{II}, Pt^{IV} (with $(PPh_4)^+$ cation) were carried out in $(CH_3)_2CO$ *via* stirring at room temperature in the dark. The precipitates as well as filtrates obtained from these reactions were analysed as well as crystallised separately. No homodinuclear complex was isolated from any of the two reactions. Nevertheless, oxidation of Pt^{II} to Pt^{IV} was observed in the Pt-Au reaction as

observed previously for reaction carried out with [18-crown-6] and tetrabutylammonium.

With relevance to the Hoffmann elimination, if the C_4 fragment did originate from $(Bu_4N)^+$ then the nitrogen containing product should be (NBu_3) or possibly $(NHBu_3)^+$, but the identification of such species would be difficult by ^1H NMR spectroscopy due to presence of excess of $(Bu_4N)^+$. Hence, ^{14}N NMR spectroscopy was chosen as a tool to try to identify the species formed. ^{14}N being quadrupolar with I = 1, possesses a signal line width which is strongly dependent on the symmetry of the environment. Consequently, it is known that the line width of the resonance in the ^{14}N NMR spectrum of NMe_3 and NMe_4^+ are ~100 Hz and ~1 Hz, respectively.[93] This is because in a low symmetry environment (NMe_3), the ^{14}N nucleus relaxes quickly leading to broad lines, whereas this is slowed in a high-symmetry environment $(NMe_4)^+$. Therefore, ^{14}N NMR spectra were recorded for NBu_3, NBu_4^+ and NBu_3H^+, showing chemical shifts of δ = 0, +22, and +12, respectively. As predicted, the spectrum of NBu_3 showed the greatest line width (1020 Hz), while those for $HNBu_3^+$ and Bu_4N were narrower at 347 Hz and 11 Hz, respectively.

The reaction was carried out as described above and the ^{14}N NMR spectrum of the resulting solution was recorded, but unfortunately there was evidence only for $(NBu_4)^+$. Therefore, no definite conclusion could be drawn.

In an alternative approach, it was decided to repeat the above Pt^{II}, Pt^{IV} reaction in the absence of $(Bu_4N)^+$ but in the presence of a different cation, $(PPh_4)^+$. An alkene (hex-1-ene) was added externally and it was hoped that it

would produce a different homodinuclear Pt^{II} olefinic complex possessing olefin which would be long chained *i.e.* C_6 fragment. A mononuclear Pt^{II} hexadiene complex[94] ($PtCl_2$(1,5-hexadiene)) has been recently reported in the literature. The latter was synthesised in an attempt to prepare a dichloro-bridged homodinuclear Pt^{II} π-allyl complex from $K_2[PtCl_4]$ and allyl chlorides *via* reduction using NaOAc in EtOH under reflux. The complex was analysed further after XRD with ^{1}H NMR, ^{195}Pt NMR and ^{13}C NMR. The results from the mononuclear Pt^{II} hexadiene complex would have been used to compare with the peaks obtained from the expected homodinuclear Pt^{II} hexadiene complex. Unfortunately, the attempt did not prove successful and no such homodinuclear complex was analysed.

From the above E2 elimination mechanism (given in the above two equations (1) and (2)), a mechanism for the formation of but-1-ene was clear but the formation of second double bond was still unclear. Hence, it was thought that presence of Pt^{IV} (as formed in excess) might be involved in the activation of the C-H bond for H^{+}elimination of the alkene formed. It has been reported that activation of an olefinic C-H bond due to π-complexation by different metals is possible, and C-H activation by Pt^{II} was reported by Shilov and co-workers, although this was and H/D exchange process.[96] However, only a few examples are known in the literature which have reported C-H activation with metals with higher oxidation states. Olefins are known to be more reactive than alkanes, due to weakening of C-H bond present in allylic position to double bond.[96] Hence, it is expected to undergo dehydrogenation reactions easily. It has also been reported that alkanes can

undergo dehydrogenation reactions in the presence of Pt^{IV} to form more stable alkenes.[97]

Possible mechanism:

The formation of the bridging butadiene complex was an unexpected outcome of these reactions and requires further discussion. The product was isolated from reactions in acetone between $[Bu_4N]_2[PtCl_4]$ and $[Bu_4N][AuCl_4]$, and also between $[Bu_4N]_2[PtCl_4]$ and $[Bu_4N]_2[PtCl_6]$. No reaction was found simply by stirring/heating $[Bu_4N]_2[PtCl_4]$ or $[Bu_4N]_2[PtCl_6]$ under reflux in acetone. It should be stated at the outset that the notion that the butadiene originates from the solvent, acetone, is discounted as it is more difficult (although admittedly not impossible) to understand the origin of a C_4 fragment from a C_3 fragment.

As mentioned above, there is precedent for extrusion of 1-butene from rigorously anhydrous samples of Bu_4NF *via* a Hoffmann mechanism[92] in which F^- acts as a base.[98] The present system does not contain fluoride, and neither is there another recognisable strong base present so it seems that a mechanism of this type has to be discounted.

An alternative view is then needed and, given the presence of both Pt^{II} and Pt^{IV} then the conditions are correct for Shilov chemistry, which allows for C–H activation of saturated alkanes. Typical Shilov chemistry relates to H/D exchange in saturated alkanes, although catalytic synthesis of methanol has been reported. A Shilov mechanism would almost certainly require C–H activation in the Bu_4N^+ cation probably leading to initial formation of $[PtCl_3(\eta^2\text{-1-butene})]^-$ and then a second activation to give the diene. With

low yields (typically <20%), there is still much to learn of this intriguing reaction, but one way forward would be to use regiospecifically deuteriated Bu_4N^+, whose preparation has been reported previously.[99] Used in cross-labelling studies with acetone-d^6, this would first allow demonstration that the source of the butadiene was indeed Bu_4N^+ and secondly, it may allow (depending on any scrambling processes that occur) some greater comprehension of the mechanism by following deuterium incorporation by NMR spectroscopy. This study would then be complemented by employing Pr_4N^+ and Et_4N^+ which ought to lead to $[PtCl_3(\eta^2\text{-1-propene})]^-$ and $[PtCl_3(\eta^2\text{-1-ethene})]^-$, respectively and then Me_4N^+, which ought to give no reaction at all.

2.2.2 Future Work

The experiments performed for the preparation of Pt^{II} butadiene complex gave low yields of the product. However, the experiment using $[PtCl_6]^{2-}$ and $[PtCl_4]^{2-}$ provided evidence that the product could be formed according to Shilov's mechanism. Hence, repetition of the same reaction in dry acetone is essential. Another suggestion would be heating $[PtCl_6]^{2-}$ under reflux in dry acetone, which was incomplete in this work. However, it did give evidence of the formation of a Pt^{II} butadiene complex along with other unidentified products observed within the same range of the ^{195}Pt NMR spectroscopy experiment, which remained unidentified at this stage. Moreover, a product could not be crystallised from the mixture of components. Also, repeating these reactions in d_6-acetone will give another advantage in being able to provide additional evidence for the involvement or otherwise of acetone in the formation of this dinuclear analogue of Zeise's salt.

2.2.3 Conclusion

In this Chapter, attempts to prepare halo-bridged heterobimetallic complexes were mostly unsuccessful. In spite of that, a new heterobimetallic Pd-Pt complex was obtained successfully and analysed. Immense efforts were made to understand Pd-Au and Pt-Au chemistry *via* different techniques, during which different crystal structures were obtained. However, in attempts to prepare heterobimetallic Pt-Au complex, a dinuclear Pt^{II} butadiene complex (*i.e.* Zeise's type analogue) was isolated. The complex was analysed by single crystal X-ray diffraction and by NMR spectroscopic techniques. Nevertheless,

the possible mechanistic details suggest that the origin of the C_4 fragment is none other than tetrabutylammonium cation, which requires further evidence through possible repetition of reactions under best conditions.

2.3 Experimental

2.3.1 Instrumentation

^{195}Pt NMR Spectroscopy

The ^{195}Pt NMR spectra were recorded on a JEOL 500 MHz spectrometer. Experiments were done at 300 K or 313 K in DMSO. However, for samples in CH_2Cl_2 and d_6-acetone or acetone/diethyl ether 295 K and 298 K were used, respectively. Standards used involved $K_2[PtCl_4]$ in D_2O, $K_2[PtCl_6]$ in d_6-DMSO and in D_2O. However, for samples in acetone $(Bu_4N)_2[PtCl_4]$ was used as the standard.

^{1}H and ^{13}C NMR Spectroscopy

^{1}H and ^{13}C spectra were recorded using Jeol ECX400 (^{1}H, 400 MHz; ^{13}C 100 MHz), running Delta software or on a Jeol ECX500 (^{1}H 500 MHz; ^{13}C 100 MHz) also running Delta software.

Single crystal X-ray diffraction

The X-ray data for the single crystal were collected with a Bruker SMART Apex CCD type X-ray diffractometer system, while for others an Oxford Diffraction SuperNova diffractometer was used. The diffractometers were fitted with monochromated graphite MoK_α radiation (λ = 0.71073 Å) with the radiation source of a fine focused sealed tube. The diffractometers were connected to an Oxford cryostream cooling system for cooling crystals down to 115 K. Structure solution used SHELTX-97 running Olex2.[100] The structures were solved with the XS[101] structure solution program using direct or Patterson method (details in cif files) followed by refinement with the XL[102] refinement package using least squares minimisation.

Powder X-ray diffraction

Powder X-ray diffraction patterns (low angle) were recorded by using a Bruker D8 diffractometer (Bruker D8) equipped with a CuK_α source of radiation (λ = 1.54 Å) with dynamic scintillation detector. The parameters used were I = 40 A, V = 40 V; slit width: 1.00 mm; angles 30 and 60°. A PTFE sample holder was used for the samples of mechanochemical reaction.

Mechanochemical reaction

The mechanochemical reactions were done by using Specac miniature ball mill with an operating frequency of 50 MHz and amplitude of 5.5 mm. In a mechanochemical reaction, the metal salts were enclosed in an agate reactor with stainless steel balls and were milled for 15 min followed by 15 min cooling cycle.

Atomic Absorption Spectroscopy (AAS)

The atomic absorption spectroscopy (AAS) used a Z-5000 series polarised Zeeman atomic absorption spectrophotometer (Hitachi). The source of radiation was a hollow cathode lamp and the flame was an acetylene/air mix. The solutions prepared for analysis were not acidified. The solutions for standards were prepared as per the sensitivity of the instrument towards the metal ion.

Elemental Analyser

Elemental analysis for carbon, hydrogen and nitrogen was done on Exeter Analytical Inc., CE-440 Elemental Analyser. The analyser was calibrated by running standards of acetanilide which was further checked by *S*-benzyl-thiouronium chloride (an internal standard). The samples to be analysed were

weighed into disposable tin capsules *via* Sartorius SE2 analytical balance, with weighing accurately up to four decimal places on a milligram. The combustion and carrier gases *i.e.* O_2 and He (CP-grade) were from BOC. Some of the data were obtained from Newcastle University on a Carlo Erba 1108 Elemental Analyser controlled with CE Eager 200 software, and weighed using a certified Mettler MX5 Microbalance. The analyser was calibrated with Acetanilide Organic Analytical Standard.

IR Spectroscopy

Infrared spectral data for solid samples below 400 cm^{-1} were obtained at the University of Hull. CsI discs were used for data collection and the spectra were recorded on a Bruker IFS66 FTIR instrument with a 6 micron mylar beamsplitter and DTGS detector. For the range above 400 cm^{-1}, spectra were recorded on a Mattson research series FTIR spectrometer fitted with a CsI beam splitter linked to a PC. The sample chamber was purged with dry, CO_2-free air.

UV-visible spectroscopy

Absorbance measurement was carried out by using Shimadzu UV-visible-2400 PC series spectrophotometer using quartz cells with 10 mm path length.

ESI Mass Spectrometric Analysis

Bruker micrOTOF with electrospray was used for negative ion mass spectral analysis with automated high throughput sample delivery and an LCQ ion trap with ESI source.

2.3.2 Materials

All precious metal salts (*i.e.* $K_2[PtCl_4]$, $K_2[PdCl_4]$ and $K[AuCl_4]$) were obtained as loans from Johnson Matthey. [18-crown-6], $(Bu_4N)Cl$ and Atomic Absorption Spectroscopic grade standards (Pt, Pd, Au) were ordered from Sigma Aldrich. Other basic solvents were from Fisher Scientific and were of HPLC grade. DMSO (dry) used for ^{195}Pt NMR spectroscopy was dried over $CaSO_4$ followed by distillation over CaH_2; acetone was dried over drierite. Dried solvents were stored under nitrogen over activated 4 Å molecular sieves. All deuterated solvents used for nuclear magnetic resonance spectroscopy were obtained from Sigma Aldrich.

2.3.3 Synthesis

The experimental data from this chapter are collected partly here and partly in Appendix B. The chapter outlines that the attempts to prepare mixed-metal, chloro-bridged complexes did not lead to the target products. However, on many occasions valuable NMR data and/or single crystals were obtained demonstrating the products obtained from these reactions. On occasions where single crystals were obtained (some being identified by structure solution and some simply from their unit cell dimensions), the experimental is given here in almost every case. Similarly, the experimental detail is reported here in cases where the ^{195}Pt NMRs were crucial. In all other cases, the experimental details are retained for consultation in the Appendix.

2.3.3.1 Synthesis of heterobimetallic Pt-Sn complexes[22]

2.3.3.1.1 Preparation of $(NH_4)_2[PtCl_3(SnCl_3)]$, ammonium (trichloro(trichlorostannyl)platinate(II)*[22]*(1)

$K_2[PtCl_4]$ (1.046 mmol, 0.4343 g) was dissolved in water (10 cm^3) *via* stirring. To this another solution of $(Bu_4N)Br$ (2.09 mmol, 0.6745 g) in water (10 cm^3) was added and the mixture was stirred at room temperature for 2 h. This resulted in a pasty solid left at the bottom of the flask which was then dissolved in CH_2Cl_2 (30 cm^3). The halogenated layer was collected and dried over Na_2SO_4 followed by crystallisation in the freezer (-5 °C). The brown crystals obtained were filtered and dried under vacuum for 24 h. The product, $(Bu_4N)_2[PtCl_4]$ (Yield: 30% (0.31 mmol, 0.255 g)) was then dissolved in CH_2Cl_2 (10 cm^3), $SnCl_2$ (anhydrous, 0.31 mmol, 0.0588 g) was added and the mixture was stirred at room temperature for 24 h. To the resulting solution was added $(NH_4)[PF_6]$ (0.09 mmol, 0.01474 g) and the mixture was stirred further for 3 h. Excess of solvent was removed under vacuum, during evacuation a yellow solid began to crystallise as $(NH_4)_2[PtCl_3(SnCl_3)]$ (Yield: 18% (0.0547 mmol, 0.0308 g). The characterization of the complex formed was attempted by ^{195}Pt NMR, 107.5 MHz, D_2O: No peak was obtained as the sample was decomposed after a few minutes, observed as black solid at the bottom of NMR tube As the product decomposed so a CHN was not performed.

2.3.3.1.2 Preparation of cis-$(PPh_4)_2[PtCl_2(SnCl_3)_2]$, cis-tetraphenylphosphonium(dichlorobis(trichlorostannyl)platinate(II) (2)

$K_2[PtCl_4]$ (1.2 mmol, 0.5 g) was dissolved in water (50 cm^3), after which a solution of $(Ph_4P)Cl$ (2.4 mmol, 0.9 g) in water (10 cm^3) was added. The mixture was stirred at room temperature for 2 h. A peach-coloured precipitate resulted, which was recovered by filtration and dried under vacuum in a desiccator (overnight). The solid was crystallised from CH_2Cl_2 at low temperature (-5 °C) and the light orange-solid product was filtered off and dried under vacuum. The product, $(Ph_4P)_2[PtCl_4]$ (Yield: 37.6% (4.56 mmol, 0.4631 g)), was then dissolved in CH_2Cl_2 (20 cm^3) and $SnCl_2$ (anhydrous, 8.91 mmol, 1.69 g) was added followed by stirring of the mixture at room temperature for 24 h. Excess of solvent was removed under vacuum, during this process a yellow solid began to crystallise: *cis*-$(PPh_4)_2[PtCl_2(SnCl_3)_2]$, Yield: 30% (0.383 mmol, 0.432 g).

Analysis: Elemental analysis, found (expected): C 41.33, H 3.35 % (C 40.43, H 2.84 %). ^{195}Pt NMR, 107.5 MHz, CD_2Cl_2: δ +4184 ($^1J_{Pt\text{-}Sn\text{-}119}$ = 27.75 kHz; $^1J_{Pt\text{-}Sn\text{-}117}$ = 26.52 kHz). MS[ESI^-], found (expected), m/z: 785.2 $[Cl_{10}PtSn_2]$ (m/z: 784.46. $[Cl_{10}PtSn_2]$).

2.3.3.2 Synthesis of heterobimetallic Pt-Pd complexes

$(Bu_4N)_2[PtCl_4]$ ***(4)***

To an aqueous solution (10 cm^3) of $K_2[PtCl_4]$ (0.964 mmol, 0.400 g) was added another solution of $(Bu_4N)Cl$ (1.928 mmol, 0.536 g) in water (10 cm^3). The contents were then left to stir for 2 h. To this solution was added CH_2Cl_2 (30 cm^3) and the halogenated layer was separated and dried over Mg_2SO_4 and was concentrated to dryness. The resulted sticky pasty solid was triturated with Et_2O (10 cm^3) which resulted in a pink solid which was filtered off and dried under vacuum for 10 h. Yield: 87.6% (0.844 mmol, 0.6937 g).

Analysis: Elemental analysis, found (expected): C 46.94, H 8.81, N 3.27 % (C 46.77, H 8.83, N 3.41 %). ^{195}Pt NMR, 107.5 MHz, $(CD_3)_2CO$: δ -1418 (s). ^{1}H NMR, 400 MHz, $(CD_3)_2CO$: δ 0.98 (t, $-CH_3$, 24 H), 1.45-1.54 (m, $-CH_2-$, 16 H), 1.85-1.93 (m, $-CH_2-$, 16 H), 3.67-3.71 (m, $-NCH_2-$, 16 H). IR (ν_{Pt-Cl}): 310 cm^{-1}.

2.3.3.2.1 Attempted mechanochemical preparation of $K_2[Cl_2Pt(\mu-Cl)_2PdCl_2]$

$K_2[PtCl_4]$ (0.506 mmol, 0.210 g) and $[PdCl_2]$ (0.506 mmol, 0.0897 g) were added together as solids to the milling reactor and were milled for 15 minutes accompanied by cooling. After each cycle the powder X-ray diffraction pattern was recorded. The milling was carried out for a total of 2 h (excluding time of cooling cycles). The brown solid obtained was analysed by ^{195}Pt NMR spectroscopy. The solid obtained was not stable

and showed signs of decomposition owing to the presence of a black solid in the mixture. The identity of the black solid remained unknown.

Analysis: ^{195}Pt NMR, 107.49 MHz, H_2O: δ -1608 corresponds to $[PtCl_4]^{2-}$; -1171 corresponds to $[Pt_2Cl_6]^{2-}$. No peak attributable to $[PtPdCl_6]^{2-}$ was observed.

An attempt was made to crystallise the sample used for ^{195}Pt NMR spectroscopy by adding EtOH to it but this resulted in the sample decomposition, observed after 24 h, indicated as a shiny black powder and colourless solution. Attempts were also made to crystallise the sample from a H_2O/MeOD solution (deuterated methanol was used so that the sample could be analysed further by NMR spectroscopy) black powder was obtained (decomposed part) along with a yellow solution, which was then analysed *via* ^{195}Pt NMR spectroscopy and by UV-visible spectroscopy.

Analysis: ^{195}Pt NMR, 107.49 MHz, H_2O/MeOD: No peak corresponding to any of the possible species *i.e.* $[PtCl_4]^{2-}$ or $[Pt_2Cl_6]^{2-}$ or $[PtPdCl_6]^{2-}$ was observed. λ_{max}: 260 and 204 corresponds to $[PtCl_6]^{3-}$, could not be identified further by ^{195}Pt NMR spectroscopy as sample was prone to decomposition.

2.3.3.2.2 Preparation of [K(18-crown-6)]$_2$[Cl$_2$Pt$_{0.58}$(μ-Cl)$_2$Pd$_{1.42}$Cl$_2$]

$K_2[PtCl_4]$ (0.25 mmol, 0.104 g) was stirred to dissolve in water (6 cm^3). To this solution, solid [18-crown-6] (1.085 mmol, 0.287 g) was added, and the mixture was stirred for one hour. To the resulting mixture, was added solid $K_2[PdCl_4]$ (0.25 mmol, 0.0816 g) followed by stirring at room temperature for 48 h. This resulted in a brown precipitate which was filtered, washed with water (2 cm^3), EtOH (4 cm^3) and Et_2O (4 cm^3). The precipitate was dried under vacuum for 16 h. Yield: 78% (0.196 mmol, 0.2126 g).

Analysis: Elemental analysis, found (expected): C 26.15, H 4.31 % (C 25.71, H 4.32 %, with respect to Pt : Pd ratio 1 : 1). ^{195}Pt NMR, 107.5 MHz, CD_2Cl_2: δ -1277 and -1216 (observed as 3 : 1 corresponds to [K(18-crown-6)]$_2$[PtPdCl$_6$]) and [K(18-crown-6)]$_2$[Pt$_2$Cl$_6$] complex respectively). ^{1}H NMR, 400 MHz, $CDCl_3$: δ 3.80 (s). IR: 340 cm^{-1} ($\nu_{Pd\text{-}Clter}$); 315 cm^{-1} ($\nu_{Pt\text{-}Clter}$). Crystals suitable for X-ray diffraction were obtained from CH_2Cl_2 at room temperature. Yield (crystals): 52% (0.1307 mmol, 0.1417 g). AAS metal concentration (ppm), found: Pd 19, Pt 6.9. This reaction could be repeated to give a mixture with very similar composition.

The repeated preparations gave a similar ratio of metals (*i.e.* 3 : 1) in the X-ray diffraction analysis. For (K[18-crown-6])$_2$[Pt$_{0.71}$Pd$_{1.29}$Cl$_6$] (CCDC reference no. 905394), *Analysis*: Elemental analysis, found (expected): C 26.2, H 4.4 % (C 26.3, H 4.4 %). For (K[18-crown-6])$_2$[Pt$_{0.58}$Pd$_{1.42}$Cl$_6$] (CCDC reference no. 905393), *Analysis*: C 26.2, H 4.3 % (C 26.6, H 4.5 %).

2.3.3.3 Attempted synthesis of heterobimetallic Au-Pd complexes

2.3.3.3.1 Attempted preparation of [K(18-crown-6)][$Cl_2Pd(\mu$-$Cl)_2AuCl_2$]

$K_2[PdCl_4]$ (0.25 mmol, 0.0816 g) and [18-crown-6] (0.814 mmol, 0.2152 g) were stirred in water (6 cm^3) at room temperature for an hour. To this brown solution was added solid $K[AuCl_4]$ (0.25 mmol, 0.0945 g), and the mixture was stirred at room temperature for 48 h in the dark. This resulted in a brownish-yellow precipitate, which was filtered, washed with water (2 cm^3), EtOH (4 cm^3) and Et_2O (4 cm^3) followed by drying under vacuum for 18 h. The filtrate was placed in a freezer (-5 °C) under inert atmosphere which resulted in yellow crystals which were analysed *via* XRD.

XRD (single crystals), CH_2Cl_2: yellow crystals corresponds to $[K(18\text{-crown-6})]_2[Pd_2Cl_6]$ (details in the appendix section). MS[ESI] (crystals), found (expected): m/z: 226.9814 ($C_6H_{26}O_8$), m/z: 282.1910 ($C_8H_{26}O_{10}$), m/z: 303.1211$[K(18\text{-crown-6})]^+$, no identifiable peaks were observed in the negative region.

The solid obtained was redissolved in CH_2Cl_2 for crystallisation in bulk, resulting in a clear brown solution and a greyish solid (*i.e.* Au^0), which was removed by filtration. Yield: 41% (0.102 mmol, 0.020 g) of Au^0 with respect to Au^{III} used initially. From the solution that resulted, the solvent was removed under vacuum which produced a sticky brown solid, which was triturated with acetone (8 cm^3) resulting into a light brown solid which was dried under vacuum for a few days.

0.165 g of a brown solid was obtained. ^{1}H NMR, 400 MHz, $CDCl_3$: δ 3.69 (s). IR shown for structure from structure vibration 320 and 330 cm^{-1} (ν_{Pd-Cl}) corresponds to $[PdCl_4]^{2-}$; 340 cm^{-1} (ν_{Pd-Cl}) corresponds to $[PdCl_6]^{2-}$, 350 cm^{-1} (ν_{Au-Cl}) corresponds to $[AuCl_2]^{1-}$. ^{1}H NMR shows the crown ether. CHN is consistent with $[PdCl_6]^{2-}$, but we don't know if this is consistent with the IR data in the absence of a reference.

2.3.3.3.2 Attempted preparation of [K(18-crown-6)][$Cl_2Pd(\mu$-$Cl)_2AuCl_2$]

To an aqueous solution of [18-crown-6] (0.814 mmol, 0.2152 g) was added $K_2[PdCl_4]$ (0.25 mmol, 0.0816 g) and the contents were stirred for 1 h at RT. To this mixture was then added solid $K[AuCl_4]$ (0.25 mmol, 0.0945 g), which was then left to stir at RT in the dark for 3 h. The brown precipitate that resulted was then filtered and washed with water, EtOH and Et_2O followed by drying under vacuum for 48 h. Yield: 0.1354 g.

Analysis, (precipitate): Elemental analysis, found (expected): C 24.39, H 3.98 (does not correspond to the expected product/s C 27.92, H 4.69 $[K(18\text{-crown-6})]_2[Pd_2Cl_6]$, or C 25.23, H 4.23 $[K(18\text{-crown-6})][AuCl_2]$). ^{1}H NMR, 400 MHz, $CDCl_3$: 3.72 (s). The precipitate was crystallised from CH_2Cl_2**.** *Analysis (crystals from precipitate)*: XRD (single crystals), CH_2Cl_2: yellow, corresponds to $[K(18\text{-crown-6})]_2[Pd_2Cl_6]$ (different polymorph from previously reported $[K(18\text{-crown-6})]_2[Pd_2Cl_6]$.[19].Yellow and colourless single crystals corresponding to $[K(18\text{-crown-6})]_2[Pd_2Cl_6]$ and $[K(18\text{-crown-6})][AuCl_2]$, respectively were isolated from the NMR solution in $CDCl_3$.

2.3.3.3.3 Attempted preparation of [K(18-crown-6)][$Cl_2Pd(\mu$-$Cl)_2AuCl_2$] from mono-nuclear metal complexes of Pd^{II} and Au^{III}

*[K(18-crown-6)][$AuCl_4$] (**6**)*

To a solution of [18-crown-6] (0.50 mmol, 0.132 g) in water (2 cm^3) was added another solution of K[$AuCl_4$] (0.25 mmol, 0.0945 g) in water (2 cm^3) followed by stirring of the contents for 24 h in the dark. A yellow-coloured precipitate was observed which was filtered off, washed with water (4 cm^3), EtOH (2 cm^3) and Et_2O (2 cm^3) and then dried under vacuum for 18 h. Yield: 84% (0.2099 mmol, 0.1348 g). The above reaction was also carried out in CH_3COOH : H_2O *i.e.* 1 : 1 (v/v %) to obtain the final structure of the complex *i.e.* [K(18-crown-6)][$AuCl_4$].

Analysis: Elemental analysis, found (expected): C 22.25, H 3.69 % (C 22.44, H 3.77 %). ^{1}H NMR, 400 MHz, $CDCl_3$: δ 3.66 (s). XRD (single crystals) from CH_2Cl_2: yellow crystals correspond to [K(18-crown-6)][$AuCl_4$] (major) and some colourless crystals were also obtained corresponding to [K(18-crown-6)][$AuCl_2$] (minor) determined by analysis of the unit cell.

*[K(18-crown-6)]$_2$[$PdCl_4$] (**7**)*

To CH_2Cl_2 (3 cm^3) was added [18-crown-6] (0.6675 mmol, 0.1764 g), and K_2[$PdCl_4$] (0.25 mmol, 0.0816 g) and the suspension was left to stir for 3 h until a brown coloured solution was formed. To this solution was added hexane in excess which resulted in a light-brown precipitate, which was filtered off and dried under vacuum for 18 h. Yield: quantitative. Single

crystals were obtained from $CDCl_3$ or CH_2Cl_2 at room temperature after one week.

Analysis: Elemental analysis, found (expected): C 33.48, H 5.50 % (C 33.71, H 5.66 %). ^{1}H NMR, 400 MHz, $CDCl_3$: δ 3.73 (s). IR ($\nu_{Pd\text{-}Cl}$): 320 (s) and 330 cm^{-1} (w), two signals seen attributed to lowering of the D_{4h} symmetry as K^+ binds to two Cl ligands.

[K(18-crown-6)][$Cl_2Pd(\mu$-$Cl)_2AuCl_2$]

To a brown solution of $[K(18\text{-crown-6})]_2[PdCl_4]$ (**7**) (0.15 mmol, 0.1283 g) in CH_2Cl_2 (2 cm^3) was added a yellow solution of $[K(18\text{-crown-6})][AuCl_4]$ (**6**) (0.15 mmol, 0.0963 g) in CH_2Cl_2 (2 cm^3). This mixture was then left to stir at room temperature for 48 h in the dark. No precipitate was observed. Hexane (12 cm^3) was then added which resulted in a dark yellow precipitate. The precipitate was then dried under vacuum. Yield: 0.1066 g.

Analysis, (precipitate): Elemental analysis, found: C 26.18, H 4.33 %. ^{1}H NMR, 400 MHz, $CDCl_3$: δ 3.72 (s). MS[ESI], found (expected): No peak attributable to the product *i.e.* $[PdAuCl_6]^{1-}$ was observed.

The precipitate obtained was crystallised from CH_2Cl_2/hexane to give colourless crystals and a yellow oil. The crystals were analysed *via* XRD as $[K(18\text{-crown-6})][AuCl_2]$.

The filtrate obtained also yielded a brown precipitate on standing, Yield: 0.0268 g *Analysis*: Elemental analysis, found (expected): C 33.07, H 5.52 % (C 33.71, H 5.66 %) corresponds to $[K(18\text{-crown-6})]_2[PdCl_4]$. ^{1}H NMR,

400 MHz, $CDCl_3$: δ 3.73 (s). IR ($\nu_{Pd\text{-}Cl}$): 320 and 330 cm^{-1} corresponds to $[PdCl_4]^{2-}$. λ_1: 286.9,[103] λ_2: 471.5 nm corresponds to $[PdCl_4]^{2-}$.

On crystallisation from $CDCl_3$, two different coloured crystals *i.e.* yellow and colourless crystals were obtained. XRD (single crystals), $CDCl_3$: colourless crystals $[K(18\text{-crown-6})][AuCl_2]$ and yellow crystals $[K(18\text{-crown-6})]_2[Pd_2Cl_6]$. Also, crystals obtained from the same precipitate after dissolving in CH_2Cl_2 produced yellow crystals of different type. XRD (single crystals), CH_2Cl_2: $[K(18\text{-crown-6})]_2[PdCl_4]$ (details in appendix section).

2.3.3.4 Attempted synthesis of heterobimetallic Au-Pt complexes

2.3.3.4.1 ***Attempted preparation of $[K(18\text{-crown-6})][Cl_2Pt(\mu\text{-}Cl)_2AuCl_2]$ in acetic acid: water (1 : 1 v/v) with Pt : Au (3 : 2)***

To a mixture of CH_3COOH : H_2O ((1 : 1), 6 cm^3) was added [18-crown-6] (0.814 mmol, 0.215 g), with stirring followed by $K_2[PtCl_4]$ (0.25 mmol, 0.104 g), and the mixture was left to stir for 1 h. To the resulting red-coloured solution was added solid $K[AuCl_4]$ (0.167 mmol, 0.063 g), and the contents were then left to stir at room temperature for 48 h in the dark. The precipitate contained gold which could not be separated. Thereafter, the precipitate was filtered off, washed with H_2O (2 cm^3), EtOH (4 cm^3), Et_2O (4 cm^3) followed by drying it under vacuum for a few days. After washing, golden-coloured precipitate could not be distinguished from that of reduced gold. Yield: 0.070 g.

Analysis (precipitate): ^{195}Pt NMR, 107.5 MHz, DMSO: δ -424 corresponds to $[K(18\text{-crown-6})]_2[PtCl_6]$; -823 corresponds to $[PtCl_5(dmso)]^{1-}$; -2952.19 corresponds to $[PtCl_3(dmso)]^{1-}$. IR (M-X str.): ($\nu_{Pt\text{-}Cl}$) 325 cm^{-1} corresponds to $[PtCl_6]^{2-}$.

Analysis (filtrate): ^{195}Pt NMR, 107.5 MHz, CH_3COOH/H_2O: δ -1588 $[PtCl_4]^{2-}$. XRD (crystals from filtrate), CH_3COOH : H_2O (1 : 1): pale yellow plates corresponds to $[K(18\text{-crown-6})]_2[PtCl_6]\cdot 2AcOH$, were obtained in an overnight NMR experiment in an NMR tube, this is why no Pt^{IV} peak could be observed in the experiment. Then, it was placed in the fridge which resulted in pale yellow coloured crystals after a few days.

2.3.3.4.2 Attempted preparations of $(Bu_4N)[Cl_2Pt(\mu\text{-}Cl)_2AuCl_2]$

$(Bu_4N)[AuCl_4]$ (**5**)

$H[AuCl_4]$ (1.47 mmol, 0.500 g) was dissolved in water (25 cm^3) and solid $(Bu_4N)Cl$ (1.47 mmol, 0.4085 g) was added followed by stirring at room temperature for 3 h in the dark. A yellow precipitate was collected, washed with water (10 cm^3) and dried under vacuum for 48 h. Yield: quantitative.

Analysis: Elemental analysis, found (expected): C 32.98, H 6.14, N 2.19 % (C 33.06, H 6.24, N 2.41 %). ^{1}H NMR, 400 MHz, $(CD_3)_2CO$: δ 0.98 (t, $-CH_3$, 12 H), 1.39-1.48 (m, $-CH_2-$, 8 H), 1.79-1.88 (m, $-CH_2-$, 8 H), 3.42-3.49 (m, $-NCH_2-$, 8 H).

General Preparation

Different ratios of $K_2[PtCl_4]$ and $K[AuCl_4]$ were added to a solvent (6 cm^3) and the mixture was left to stir at room temperature in the dark. This resulted in gold (Au^0) observed as gold mirrors along with a yellow solution obtained *via* filtration. To the filtrate was added $(Bu_4N)Cl$ (0.75 mmol, 0.208 g), and the mixture was stirred for 2 h at room temperature. This resulted in a yellowish precipitate which was filtered, washed with water, and dried under vacuum for 48 h. Both the filtrate as well as the precipitate were analysed.

a) In water, Pt : Au (1 : 1)

$K[AuCl_4]$ (0.25 mmol, 0.0945 g) and $K_2[PtCl_4]$ (0.25 mmol, 0.104 g).

Au^0 was obtained as a gold mirror which was filtered and dried under vacuum for a few hours. Yield: 81% (0.203 mmol, 0.040 g) of Au^0 with respect to Au^{III} used initially. The yellow filtrate was analysed, ^{195}Pt NMR, 107.5 MHz, H_2O: δ +521 (main peak) corresponds to $[PtCl_5(OH_2)]^{1-}$[66] and +1083 (small peak) (value close to *cis*-$[PtCl_4(OH_2)]^{2-}$ and *trans*-$[PtCl_4(OH_2)]^{2-}$[76]; +8 (close to $[PtCl_6]^{2-}$). Yellow crystals separating from the NMR solution were shown to be $K_2[PtCl_6]$ by XRD.

To the yellow filtrate was added $(Bu_4N)Cl$ (0.75 mmol, 0.208 g), and the mixture stirred for 2 h. This resulted in a dark yellow precipitate. *Analysis (precipitate)*: Elemental analysis, found: C 34.60, H 6.51, N 2.36 %. Crystals suitable for X-ray diffraction were obtained from $(CH_3)_2CO$ at

room temperature. XRD (single crystals), $(CH_3)_2CO$: yellow crystals correspond to $(Bu_4N)[AuCl_4]$.

Again, to the yellow filtrate obtained from above was added $(Bu_4N)Cl$ (0.75 mmol, 0.208 g), and the mixture was stirred at room temperature for 48 h. This resulted in a yellow precipitate, which was filtered and dried under vacuum for 48 h. *Analysis (precipitate)*: Elemental analysis, found (expected): C 37.33, H 6.99, N 2.59 % (C 37.87, H 6.89, N 2.45 %, corresponds to $(Bu_4N)_2[PtCl_3(\eta\text{-}CH_2{=}CH\text{-}CH{=}CH_2\text{-}\eta)PtCl_3]$). ^{195}Pt NMR, 107.5 MHz, $(CD_3)_2CO$: δ +94. ^{1}H NMR, 400 MHz, $CDCl_3$: δ 0.99 (t, $-CH_3$, 24 H), 1.43-1.52 (m, $-CH_2-$, 16 H), 1.59-1.70 (m, $-CH_2-$, 16 H), 3.33-3.37 (m, $-NCH_2-$, 16 H), no peak corresponding to olefinic complex was observed, hence it was reanalysed in dichloromethane. ^{1}H NMR, 500 MHz, CD_2Cl_2: δ 1.03 (t, $-CH_3$, 24 H, J = 7.5 Hz), 1.43-1.50 (m, $-CH_2-$, 16 H, J = 7, 14.5 Hz), 1.62-1.68 (m, $-CH_2-$, 16 H, J = 8, 15.5 Hz), 3.18-3.22 (m, $-NCH_2-$, 16 H), 4.45 (d, $=CH_2$, 2 H, H_aH_c, J = 6.0 Hz), 4.80 (d, $=CH_2$, 2 H, H_bH_c, J = 12.0 Hz), 5.55 (m, =CH, 2 H, H_c, H_c', J difficult to interpret); ^2J(Pt-H) of *ca* 66 Hz. Crystals for X-ray diffraction were obtained for the precipitate from $(CH_3)_2CO$/hexane mixture. XRD (single crystals), $(CH_3)_2CO$/hexane: Pale yellow crystals, corresponds to $(Bu_4N)_2[PtCl_3(\eta\text{-}H_2C{=}CH\text{-}CH\text{-}CH_2\text{-}\eta)PtCl_3]$. IR ($cm^{-1}$): 308, 315, 330 ($\nu_{Pt\text{-}Cl}$) and 382 ($\nu_{Pt\text{-}olefin}$); 738 (sharp), 877 (sharp), 992 (sharp), 1173 (small, sharp), 1239, 1345, 1379 (sharp), 1459, 1483, 2855 (w), 2873 (s), 2924 (s), 2964 (s).

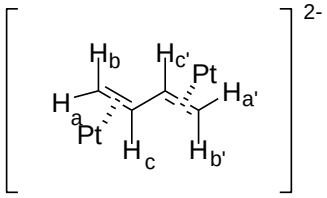

b) In H_2O : CH_3COOH (1 : 1 v/v) Pt : Au (1 : 1)

$K[AuCl_4]$ (0.25 mmol, 0.0945 g), $K_2[PtCl_4]$ (0.25 mmol, 0.104 g).

Au^0 was obtained as tiny balls which were filtered off, dried under vacuum for 48 h. Yield: 29% (0.059 mmol, 0.0117 g) of Au^0 with respect to Au^{III} used initially. The yellow filtrate obtained on filtering off Au^0 was analysed. *Analysis (filtrate)*: ^{195}Pt NMR, 107.49, (H_2O : CH_3COOH) (1 : 1): δ +537 correspond with $[PtCl_5(OH_2)]^{1-}$.

To the yellow filtrate was added $(Bu_4N)Cl$ (0.75 mmol, 0.208 g), and the mixture was stirred for 2 h. This resulted in a yellow precipitate. Yield: 0.0790 g. *Analysis (precipitate)*: Elemental analysis, found: C 40.38, H 7.59, N 2.75 %.^{195}Pt NMR, 107.49 MHz, $(CD_3)_2CO$: δ +94 (unidentified peak). ^{195}Pt NMR, 107.49 MHz, DMSO (dry): δ -823 corresponds to $[PtCl_5(dmso)]^{1-}$; +428 (observed initially) corresponds to $[PtCl_6]^{2-}$. The peak at +428 was observed only in an instantaneously prepared sample, which disappeared after an hour or so and a peak at -823 appeared instead. ^{1}H NMR, 400 MHz, $CDCl_3$: δ 1.04 (t, $-CH_3$, 24 H), 1.46-1.53 (m, $-CH_2-$, 16 H), 1.61-1.71 (m, $-CH_2-$, 16 H), 3.21-3.31 (m, $-NCH_2-$, 16 H). MS[ESI] m/z: 338.84 $[H_2AuCl_4]^{1+}$, m/z: 382.78 ($[H_{11}AuCl_5]^{9+}$, m/z: 426.73 $[H_2AuCl_6(H_2O)]^{1-}$, m/z: 468.25 $[H_5Au_2Cl_2]^{9+}$,

m/z: 608.79 [$H_5Au_2Cl_6$] (unidentified). IR: 325 cm^{-1} ($\nu_{Pt\text{-}Cl}$) corresponds to $[PtCl_6]^{2-}$.

Crystals suitable for X-ray diffraction were obtained from a $(CH_3)_2CO/Et_2O$ mixture obtained from filtrate were shown by XRD to correspond to $(Bu_4N)_2[PtCl_3(\eta\text{-}H_2C{=}CH\text{-}CH\text{-}CH_2\text{-}\eta)PtCl_3]$. Single crystals were also obtained from the solution used for ^1H NMR spectroscopy. XRD (single crystals), $CDCl_3$: yellow crystals corresponds to $(Bu_4N)[AuCl_4]$.

Single crystals for X-ray diffraction were obtained from a $(CH_3)_2CO/Et_2O$ mixture (mentioned before). However, samples analysed for NMR spectroscopy produced colourless crystals in DMSO (dry) and yellow crystals in $CDCl_3$ which were not suitable for X-ray diffraction. *Analysis (crystals)*: Elemental analysis, found (expected): C 36.63, H 6.51, N 2.12 % (C 37.87, H 6.89, N 2.45 % correspond to $(Bu_4N)_2[PtCl_3(\eta\text{-}H_2C{=}CH\text{-}CH\text{-}CH_2\text{-}\eta)PtCl_3]$). XRD (single crystals), $(CH_3)_2CO/Et_2O$: pale yellow also correspond to $(Bu_4N)_2[PtCl_3(\eta\text{-}H_2C{=}CH\text{-}CH\text{-}CH_2\text{-}\eta)PtCl_3]$. ^1H NMR, 400 MHz, CD_2Cl_2: same as observed previously for $(Bu_4N)_2[PtCl_3(\eta\text{-}H_2C{=}CH\text{-}CH\text{-}CH_2\text{-}\eta)PtCl_3]$.

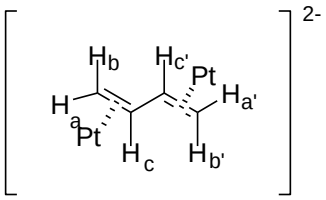

c) In H_2O, Pt : Au (3 : 2)

$K_2[PtCl_4]$ (0.25 mmol, 0.104 g) and $K[AuCl_4]$ (0.167 mmol, 0.063 g).

The resulting gold metal was filtered off and was dried under vacuum for a few hours. Yield: 46% of Au^0 (0.113 mmol, 0.0223 g) with respect to Au^{III} used initially. Orange-yellow precipitate obtained after filtering off gold. Yield: 0.0124 g. *Analysis (precipitate)*: Elemental analysis, found (expected): C 41.85, H 7.78, 2.41 % (C, 43.05, H 8.13, N 3.14 % correspond to $(Bu_4N)_2[PtCl_6]$). ^{195}Pt NMR, 107.5 MHz, $(CD_3)_2CO$: δ +374 corresponds to $[PtCl_6]^{2-}$. IR (ν_{Pt-Cl}): 325 cm^{-1} correspond to $[PtCl_6]^{2-}$.

Single crystals were obtained from the orange-yellow precipitate above by recrystallisation from a mixture of $(CH_3)_2CO/Et_2O$. *Analysis (crystals)*: XRD (single crystals), $(CH_3)_2CO/Et_2O$: corresponds to $(Bu_4N)_2[PtCl_3(\eta\text{-}H_2C{=}CH\text{-}CH\text{-}CH_2\text{-}\eta)PtCl_3]$. ^1H NMR, 400 MHz, CD_2Cl_2: same as observed previously for $(Bu_4N)_2[PtCl_3(\eta\text{-}H_2C{=}CH\text{-}CH\text{-}CH_2\text{-}\eta)PtCl_3]$.

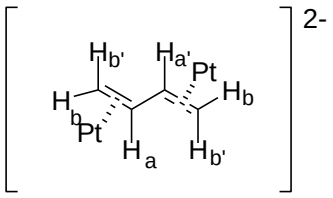

d) In water, Pt : Au (3 : 2)

$K[AuCl_4]$ (0.167 mmol, 0.063 g), and $K_2[PtCl_4]$ (0.25 mmol, 0.104 g).

The resulting gold metal was filtered off and dried under vacuum. Yield: 86% of Au^0 (0.143 mmol, 0.0282 g) with respect to Au^{III} used initially. To the filtrate obtained was added $(Bu_4N)Cl$ (0.828 mmol, 0.230 g), stirred for 2 h. The resulting precipitate was then filtered off and was washed

with water (excess) followed by drying under vacuum. $(Bu_4N)_2[PtCl_6]$, Yield: 5.6% (0.0138 mmol, 0.0124 g). *Analysis (precipitate)*: Elemental analysis, found (expected): C 42.46, H 7.81, N 2.69 % (C 43.05, H 8.13, N 3.14 % corresponds $(Bu_4N)_2[PtCl_6]$). ^{195}Pt NMR, 107.5 MHz, $(CD_3)_2CO$: δ +374 (corresponds to $(Bu_4N)_2[PtCl_6]$). ^{1}H NMR, 400 MHz, $(CD_3)_2CO$: δ 0.98 (t, $-CH_3$, 24 H), 1.41-1.50 (m, $-CH_2-$, 16 H), 1.76-1.85 (m, $-CH_2-$, 16 H), 3.45-3.49 (m, $-NCH_2-$, 16 H). ^{13}C NMR, 100 MHz, $(CD_3)_2CO$: δ 14.03 ($-CH_3$), 20.45 ($-CH_2-$), 24.76 ($-CH_2-$), 59.54 ($-NCH_2-$). IR (ν_{Pt-Cl}): 325 cm^{-1} corresponds to $[PtCl_6]^{2-}$.

Crystals suitable for XRD of the precipitate (above) were obtained from an acetone/Et_2O solution. XRD (single crystals), $(CD_3)_2CO/Et_2O$: pale yellow crystals correspond to $(Bu_4N)_2[PtCl_3(\eta\text{-}H_2C{=}CH\text{-}CH\text{-}CH_2\text{-}\eta)PtCl_3]$. (minor), orange-yellow crystals corresponds to $(Bu_4N)_2[PtCl_6]$.

2.3.3.5 Synthesis of $(Bu_4N)_2[PtCl_3(\eta\text{-}H_2C{=}CH\text{-}CH{=}CH_2\text{-}\eta)PtCl_3]$

In attempts to prepare Pt-Au heterobimetallic complexes, mononuclear metal complexes of tetrabutylammonium salts of Pt^{II} and Au^{III} were also employed. However, in these preparations, the expected complex could not be synthesised but a Pt^{II} butadiene complex was obtained as a product in a mixture of Pt^{IV} mononuclear complex in low yields.

*Preparation of $[K(18\text{-crown-}6)]_2[PtCl_4]$ (**8**)*

To CH_2Cl_2 (3 cm^3) was added [18-crown-6] (0.6675 mmol, 0.1764 g) and $K_2[PtCl_4]$ (0.25 mmol, 0.104 g). This suspension was left to stir at room temperature for 3 h and to the resulting red solution was added hexane in excess, resulting in a light pink precipitate, which was then filtered off and dried under vacuum for 18 h. Yield: quantitative.

Elemental analysis, found (expected): C 30.86, H 5.08 % (C 30.54, H 5.13 %). ^{1}H NMR, δ400 MHz, $CDCl_3$: 3.74 (s). ^{195}Pt NMR, 107.5 MHz, CD_2Cl_2: δ-1528. ^{195}Pt NMR, 107.5 MHz, DMSO (dry): δ-2952 (peak corresponds to $[PtCl_3(dmso)]^{1-}$[67]). ^{195}Pt NMR, 107.5 MHz, CD_2Cl_2: δ -1528 (peak corresponds to $[PtCl_4]^{2-}$). MS[ESI], found (expected): m/z: 889.21 ($[K(18\text{-crown-}6)]_2[PtCl_2(OH_2)]$), m/z: 965.25 ($[K(18\text{-crown-}6)]_2[PtCl_3(OH_2)_3H_5]$). IR (M-X) cm^{-1}: ($\nu_{Pt\text{-}Cl}$) 320 and 335 (short).

$[K(18\text{-crown-}6)][Cl_2Pt(\mu\text{-}Cl)_2AuCl_2]$ (attempted)

To a solution of $[K(18\text{-crown-}6)]_2[PtCl_4]$ (**8**) (0.15 mmol, 0.142 g) in CH_2Cl_2 (2 cm^3) was added a solution of $[K(18\text{-crown-}6)][AuCl_4]$ (**6**) (0.15 mmol, 0.0963 g) in CH_2Cl_2 (2 cm^3) and the contents were stirred at room

temperature for 48 h in the dark. This resulted in a light-yellow coloured precipitate which was filtered off and dried under vacuum. Yield: 0.067 g. *Analysis (precipitate)*: Elemental analysis, found: C 24.57, H 4.10 % corresponds to calculated overall concentration of Pt^{IV} and Au^{I} as 6.61 and 2.65 ppm, respectively. MS[ESI] found (expected): m/z: 641.21 ($[K(18\text{-crown-6})]_2Cl)^+$, m/z: 719.22 ($([K(18\text{-crown-6})]_2[K_2Cl])^{3+}$, m/z: ($[K(18\text{-crown-6})][Au_2H_4(OH_2)]$). ^{1}H NMR, 400 MHz, d_6-DMSO: δ 3.54 (s). ^{195}Pt NMR, 107.5 MHz, DMSO (dry): δ -823 corresponds to $[PtCl_5(dmso)]^{1-}$. IR ($\nu_{Pt\text{-}Cl}$): 325 cm^{-1} corresponds to $[PtCl_6]^2$.

The filtrate (CH_2Cl_2) resulted in two different types of crystals, yellow and colourless, at low temperature (-5 °C), (inert atmosphere) after a few days which were analysed *via* XRD. *Analysis (filtrate)*: XRD (single crystals), filtrate (CH_2Cl_2): yellow corresponds to $[K(18\text{-crown-6})][AuCl_4]$ and colourless corresponds to $[K(18\text{-crown-6})][AuCl_2]$. Unfortunately, the precipitate obtained did not result in crystals suitable for analysis by XRD.

In attempting to prepare heterobimetallic Pt-Au species, it was found that a homodinuclear platinum complex of 1,4-butadiene with $PtCl_3$ η-bound to each ethylenic bond was obtained in a low yield. The following experimental details its preparation.

General Preparation

$(Bu_4N)_2[PtCl_4]$ (**4**) (0.122 mmol, 0.100 g), was dissolved in acetone (2.5 cm^3). To this was added a solution of $(Bu_4N)[AuCl_4]$ (**5**) (0.122 mmol, 0.070 g) in acetone (2.5 cm^3) followed by stirring at room temperature for 48 h in the dark resulting a clear orange solution. To this solution was added Et_2O in

excess which resulted in a yellowish-orange precipitate and a yellow filtrate. The filtrate as well as precipitate were analysed separately by ^{195}Pt NMR spectroscopy for product identification. Crystals suitable for X-ray diffraction were obtained both from filtrate as well as precipitate by separate crystallisations from a $(CH_3)_2CO/Et_2O$ mixture at room temperature. Both the crystallising mixture of the solutions of filtrate and precipitate produced a mixture of crystals of $(Bu_4N)_2[PtCl_6]$ (orange-yellow) and $(Bu_4N)_2[PtCl_3(\eta\text{-}H_2C{=}CH\text{-}CH{=}CH_2\text{-}\eta)PtCl_3]$ (pale-yellow), separated by their differing solubility in solvents *i.e.* acetone and CH_2Cl_2 respectively. The mixture of crystals was filtered, washed with acetone to dissolve the orange-yellow crystals of $(Bu_4N)_2[PtCl_6]$ and to separate the pale-yellow crystals of $(Bu_4N)_2[PtCl_3(\eta\text{-}H_2C{=}CH\text{-}CH{=}CH_2\text{-}\eta)PtCl_3]$ which were insoluble in acetone. The crystals of $(Bu_4N)_2[PtCl_6]$ were crystallised again from the solution. The same solution was re-crystallised many times to obtain the final yield of both the products.

2.3.3.5.1 $(Bu_4N)_2[PtCl_3(\eta\text{-}H_2C{=}CH\text{-}CH{=}CH_2\text{-}\eta)PtCl_3]$ preparation in acetone

Pale yellow crystals, $(Bu_4N)_2[PtCl_3(\eta\text{-}H_2C{=}CH\text{-}CH{=}CH_2\text{-}\eta)PtCl_3]$, Yield: 7.9% (0.0097 mmol, 0.011 g) and orange crystals, $(Bu_4N)_2[PtCl_6]$, Yield: 17.5% (0.022 mmol, 0.019 g).

Analysis (filtrate): ^{195}Pt NMR, 107.5 MHz, $(CH_3)_2CO/Et_2O$: δ -2723 (main peak) and -2527 and +345 (a weak peak is observed) corresponds to $(Bu_4N)_2[PtCl_6]$. XRD (crystals from filtrate): $(CH_3)_2CO/Et_2O$ corresponds to $(Bu_4N)_2[PtCl_3(\eta\text{-}H_2C{=}CH\text{-}CH{=}CH_2\text{-}\eta)PtCl_3]$.

Analysis (precipitate), Elemental analysis, found (expected): C 41.00, H 7.56, N 2.72 % (C 43.05, H 8.13, N 3.14 % corresponds to $(Bu_4N)_2[PtCl_6]$). ^{1}H NMR, 400 MHz, $(CD_3)_2CO$: δ 0.98 (t, $-CH_3$, 24 H), 1.41-1.50 (m, $-CH_2-$, 16 H), 1.78-1.86 (m, $-CH_2-$, 16 H), 3.47-3.51 (m, $-NCH_2-$, 16 H). ^{195}Pt NMR, 107.49 MHz, $(CD_3)_2CO$: δ +368 corresponds to $(Bu_4N)_2[PtCl_6]$; +92 (unidentified peak); -1424 corresponds to $(Bu_4N)_2[PtCl_4]$.

Analysis (pale yellow crystals), Elemental analysis, found (expected): C 37.82, H 6.74, N 2.38 % (C 37.87, H 6.89, N 2.45 %). ^{1}H NMR, 400 MHz, CD_2Cl_2: as observed previously for $(Bu_4N)_2[PtCl_3(\eta\text{-}H_2C{=}CH\text{-}CH{=}CH_2\text{-}\eta)PtCl_3]$. ^{195}Pt NMR, 107.5 MHz, CD_2Cl_2: δ -2546 (s) (main peak) and -2543 (s). MS[ESI], found (expected): m/z: 839.4871 $((Bu_4N)_2[PtCl_3(C_4H_6)])^+$ (m/z: 838.49 $(Bu_4N)_2[PtCl_3(C_4H_6)])^+$), m/z: 855.50 $((Bu_4N)_2[PtCl_3(C_4H_6)(OH_2)])^+$ (m/z: 856.50 $(Bu_4N)_2[PtCl_3(C_4H_6)(OH_2)])^+$), m/z: 929.3878 $((Bu_4N)_2[PtCl_5(C_4H_6)(OH_2)H_2])^+$ (m/z: 928.45 $(Bu_4N)_2[PtCl_5(C_4H_6)(OH_2)H_2])^+$).

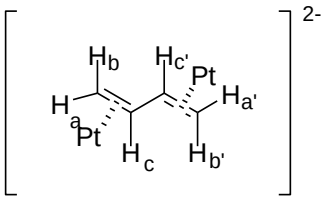

The preparation was then repeated using rigorously dried acetone, which yielded the butadiene complex with 24% yield (0.0289 mmol, 0.033 g), with 0.0136 g of $(Bu_4N)_2[PtCl_6]$ being recovered (12.5% with respect to starting Pt). Repeating the preparation in wet acetone (5.0 cm^3 with 1 drop of water) lowered the yield to 15%.

An attempt was made to increase yield by using a base (*i.e.* 1,6-lutidine) in the above preparation involving acetone. Unfortunately, no difference in results could be observed.

2.3.3.6 Synthesis of $(Bu_4N)_2][PtCl_3(\eta\text{-}H_2C{=}CH\text{-}CH{=}CH_2\text{-}\eta)PtCl_3]$ from tetrabutylammonium complexes of Pt^{II} and Pt^{IV}

*$(Bu_4N)_2[PtCl_6]$(**12**)*

To acetone (10 cm^3) was added solid $(Bu_4N)Cl$ (4.12 mmol, 1.143 g) and $K_2[PtCl_6]$ (2.058 mmol, 1.00 g) and the mixture was stirred overnight. This resulted in a clear orange solution along with white precipitate of KCl. The precipitate was the filtered followed by removal of solvent under vacuum, which resulted in an orange crystalline solid, which was dried under vacuum. Yield: quantitative.

Analysis: Elemental analysis, found (expected): C 43.37, H 8.24, N 3.04 % (C, 43.05; H, 8.13, N 3.14 %). ^{195}Pt NMR, 107.5 MHz, $(CD_3)_2CO$: δ +374 (s). ^{1}H NMR, 400 MHz, $(CD_3)_2CO$: δ 0.98 (t, $-CH_3$, 24 H, J = 14.8 Hz), 1.42-1.50 (m, $-CH_2-$, 16 H, J = 7.2, 14.4 Hz), 1.77-1.85 (m, $-CH_2-$, 16 H, J = 8.4 Hz, 7.6 Hz), 3.45-3.51 (m, $-NCH_2-$, 16 H, J = 5.6, 10.8 Hz). IR ($\nu_{Pt\text{-}Cl}$): 325 cm^{-1}.

General Preparation

To acetone (5 cm^3) was added solid $(Bu_4N)_2[PtCl_4]$ (**4**) (0.122 mmol, 0.100 g), and $(Bu_4N)_2[PtCl_6]$ (**12**) (0.122 mmol, 0.109 g), and the mixture was stirred at room temperature in $(CH_3)_2CO$ (5 cm^3) for 48 h in the dark. To the

resulting orange solution was added Et_2O in excess (~12 cm^3) which resulted in an orange precipitate. Then, the filtrate and the precipitate were separately crystallised from an acetone/Et_2O mixture. This resulted in a mixture of $(Bu_4N)_2[PtCl_6]$ and $(Bu_4N)_2[PtCl_3(\eta\text{-}H_2C{=}CH\text{-}CH{=}CH_2\text{-}\eta)PtCl_3]$ observed as orange and yellow crystals, respectively. The crystals of $(Bu_4N)_2[PtCl_6]$ were washed off or were dissolved in acetone to obtain pale yellow crystals of the $(Bu_4N)_2[PtCl_3(\eta\text{-}H_2C{=}CH\text{-}CH{=}CH_2\text{-}\eta)PtCl_3]$. Yield**:** 17.6% (0.0214 mmol, 0.0244 g). *Analysis (crystals)*: Elemental analysis, found (expected): C 37.48, H 6.76, N 2.29 % (C 37.87, H 6.89, N 2.45 %).^{195}Pt NMR, 107.5 MHz, CD_2Cl_2: δ -2546 (s) corresponds to $(Bu_4N)_2[PtCl_3(C_4H_6)PtCl_3]$; -2615 (unidentified peak). ^{1}H NMR, 107.5 MHz, CD_2Cl_2: data same as observed previously. ^{13}C NMR, 100 MHz, CD_2Cl_2: δ 13.94 ($-CH_3$), 20.21 ($-CH_2$), 24.63 ($-CH_2$), 59.43 ($-NCH_2$), 63.78 ($=CH_2$), 86.2 (=CH).

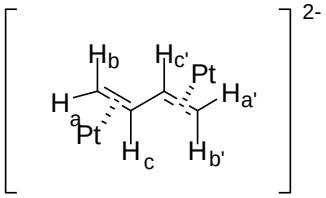

The reaction was repeated in rigorously dried acetone and in wet acetone (5 cm^3 with a drop of water), which resulted in a yield of Pt^{II} butadiene complex 17.6 % to 1 %, respectively.

2.3.3.7 Attempted preparation of Pt^{II} butadiene type complex

Another attempt was made to synthesise Pt^{II} butadiene complexes with a different counter cation *i.e.* PPh_4^+. The reactions were carried out with mononuclear metal complexes of Pt^{II}, Pt^{IV} and Au^{III} as previously for

tetrabutylammonium complexes. Unfortunately, they were all unsuccessful, hence their experimental details are in the Appendix section B.

Chapter 3
TTHA Metal Complexes

3.1 Introduction

The attempts to prepare heterobimetallic halo-bridged complexes as described in Chapter 2 were largely unsuccessful and so another approach was sought for the preparation of heterobimetallic complexes. The methodology chosen used a chelate ligand with multiple coordination sites, which has the propensity to coordinate with metals of high coordination number. The details of this approach are described in this Chapter.

3.1.1 The Chelate Effect

Metal ions, when coordinated by more than one coordination site or donor atom of the same ligand, form cyclic structures or rings known as *chelate rings*, hence the phenomenon is termed *chelation*. The molecules that participate in chelation are usually organic with multiple coordination sites. They are therefore known as *multidentate* or *polydentate* ligands and are said to be *chelating agents*. The *chelate effect* is a phenomenon where metal ions favour the formation of complexes with polydentate ligands in comparison to the monodentate ligands. The factors contributing towards the stability of such complexes involve entropy as well as enthalpy:

$$\Delta G^\circ = - RT \ln K = \Delta H^\circ - T\Delta S^\circ \qquad (1)$$

where K is the equilibrium constant, ΔG° is the change in free energy, ΔH° is the change in enthalpy, and ΔS° is the change in entropy. K increases when ΔG° is more negative and ΔG° can only be more negative when the balance of ΔH° and $T\Delta S^\circ$ is negative.

A variety of models[1,2] have been proposed to describe the chelate effect through structural characteristics such as the number of rings involved in the complex, the stability of the chelate and the size of the chelate rings, CFSE, metal ion charge, and last and most importantly, the entropic contributions to the effect. The chelate effect is usually a result of more than one of the contributing factors listed above. However, the major factors driving the effect are described in this chapter with the help of selected examples given below.

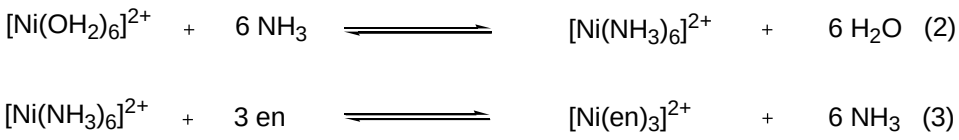

Enthalpic as well as entropic contributions to the chelate effect can be explained with the complex formation of Ni^{II} with ammonia (monodentate ligand) and ethylene diamine (bidentate ligand).[3] (**Fig. 3. 1**).

For equation (2),[3]	For equation (3),[3]
$\Delta G° = -12.39$ kJ mol^{-1}	$\Delta G° = -12.70$ kJ mol^{-1}
$\Delta H° = -24$ kJ mol^{-1}	$\Delta H° = -4$ kJ mol^{-1}
$\Delta S° = -39$ J mol^{-1}K^{-1}	$\Delta S° = +29$ J mol^{-1}K^{-1}

The chelate effect is observed as an entropy-driven process and to some extent it is also dependent on enthalpy. In equation (2) the size of the two ligands *i.e.* H_2O and NH_3 is almost the same. As the total number of free, as well as coordinated ligands, is the same on both the sides of the equilibrium, the entropic contribution towards the stability of the complex is very little. Therefore, the driving force of the reaction is dependent on the nature of coordination bonds of the resulting complex. In this case, ammonia binds more strongly with Ni^{2+} as compared H_2O and so, $\Delta G°$ is negative largely due to the favourable enthalpic contribution of a stronger bond formation between nickel and nitrogen.

In equation (3), two ammine ligands are replaced by one *en* and this reduces the entropy of the *en* ligand as its freedom to rotate is reduced because both ends are now tethered.[4] However, counting of the number of free species formed along with the associated complex increases the entropy of the overall system. As in equation (3), the total number of species on the right-hand side of the equilibrium is seven, but in comparison, the number of species on the left side is four. This creates a positive contribution to the entropy hence, ΔS is positive.

Another contribution is the basicity of the donor atom[5] also termed *intrinsic basicity i.e.* of the nitrogen of amine in ethylenediamine ligand. It is due to the +I effect of ethylene group of the *en* ligand which intensifies the electron density on the nitrogen. It is observed to bond with the metal strongly in comparison to NH_3, which leads to a negative enthalpy change further contributing to the final value of $\Delta G°$.

3.1.2 Aminopolycarboxylates

Aminopolycarboxylates are known to form stable complexes with a range of metal cations due to their strong binding affinity towards them. Therefore, such ligands possess a wide range of applications in catalysis,[6] therapeutics[7] (*e.g.* treatment of anaemia,[8] contrast agents in MRI,[9] radiopharmaceuticals[10]), water treatment,[11] sequestering agents,[11,12] industrial masking agents,[13] molecular magnets[14] and paper chromatography.[10] The smallest, simplest and most extensively used aminopolycarboxylic acid is EDTA, but its higher analogues do exist, including H_4DTPA (diethylenetriamine-*N*, *N*′, *N*″-pentaacetic acid)[15] and H_6TTHA (triethylenetetraamine-*N*, *N*′, *N*″, *N*‴-hexaacetic acid)[16] with eight and ten coordination sites, respectively **(Fig. 3.1)**.

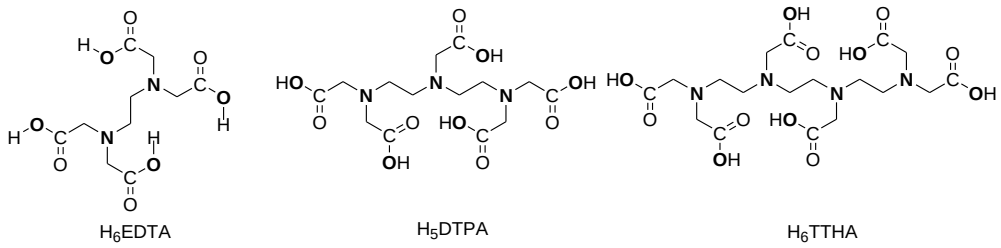

Fig. 3.1 Structures of the common aminopolycarboxylic acids with donor atoms indicated in bold.

Ligands that possess multiple coordination sites can complex with metals that have low as well as high coordination numbers. For example, $TTHA^{6-}$, a symmetrical decadentate ligand, is known to form 1 : 1 complexes with rare-earth metals to form eight-, nine- and ten-coordinate complexes.[17,18] There are also some examples in the literature that show the existence of homo- as well as hetero- dinuclear metal complexes of $TTHA^{6-}$ and a few of those reported

examples include Co-Co,[19] Ni-Ni,[20,21] Cu-Cu[22,23] and Zn-Zn.[24] However, only one example of heterobimetallic complex has been reported as a crystal structure in the literature in which $TTHA^{6-}$ is coordinated to Co-Ni,[25] which is discussed below.

Apart from these examples, there are reported examples of homodinuclear as well as heterodinuclear transition metal complexes in solution form but their isolation has never been reported. Rather, their existence was inferred by various other methods which mainly include potentiometry and EPR measurements.

For example, Grimes *et al*.,[26] were the first to study the interactions between alkaline earth metals and H_6TTHA, and other aminopolycaboxylates *via* potentiometric titrations, where they calculated chelate stability constants from the data obtained. From these data they even tried to describe the structure of the complex formed.

Soon after, Bohigian and Martell[27] also studied metal-ligand interactions *via* potentiometric titrations, in which mononuclear as well as homodinuclear metal complexes were described but in a relatively improved manner in comparison to previously studied complexes by Grimes *et al*.[26] The aim of the study *i.e.* metal-ligand interactions was achieved by varying metal-to-ligand ratios *via* metal complexations. Metals studied include rare-earth metals (Ln^{III}, Th^{IV}), transition metals (Co^{II}, Ni^{II}, Cu^{II}) as well as alkaline earth metals (Ca^{II}, Mg^{II}). It was observed from the M : H_6TTHA ratio, *via* potentiometric titrations, that a 2 : 1 ratio of M : H_6TTHA is required to obtain a peak that

corresponds to a homodinuclear complex *e.g.* $(Cu^{II})_2$ and $(Ni^{II})_2$. However, for Co^{II} a homodinuclear complex was suggested from the potentiometric curve with a 1 : 1 as well as 2 : 1, M : H_6TTHA ratio. From the results obtained, the existence of a homodinuclear complex was very well formulated but no attempt was made at any step to try to isolate any of these complexes from the mixture. However, the results obtained gave a general idea according to which, formation of a homodinuclear complex requires a M : H_6TTHA ratio of 2 : 1.

Concurrently, Schrøder[28] also discovered the existence of homodinuclear iron (Fe^{II} and Fe^{III}) TTHA complexes in aqueous solutions by controlled addition of NaOH *i.e.* by pH titration. The species formed were identified by redox potential measurement, polarography and spectrophotometric titrations. The possible structure of the final homodinuclear complex of ferric and ferrous ion as $[Fe^{III}_2(TTHA)(OH)_2]^{2-}$ and $[Fe^{II}_2(TTHA)]^{2-}$ were confirmed from the titration data. The aim of the experiment was to confirm the formation of different forms of iron TTHA complexes *i.e.* mononuclear non-protic forms ($[Fe^{III}(TTHA)]^{3-}$, $[Fe^{III}(OH)(TTHA)]^{4-}$, $[Fe^{III}(OH)_2(TTHA)]^{5-}$, $[Fe^{II}(TTHA)]^{4-}$ $[Fe^{II}(OH)(TTHA)]^{5-}$, $[Fe^{II}(OH)_2(TTHA)]^{6-}$), mononuclear protic forms ($[Fe^{III}(HTTHA)]^{2-}$, $[Fe^{III}(H_2TTHA)]^{1-}$, $[Fe^{II}(HTTHA)]^{3-}$, $[Fe^{II}(H_2TTHA)]^{2-}$, $[Fe^{II}(H_3TTHA)]^{1-}$), and homodinuclear forms ($[Fe^{III}_2(TTHA)(OH)_2]^{2-}$ and $[Fe^{II}_2(TTHA)]^{2-}$). Nonetheless, no attempt was made to isolate any of the homodinuclear species observed. Similarly, homodinuclear and other mononuclear complexes of Hg^{II} were also analysed and identified by Schrøder[29] as done for the previously reported Fe^{II} and Fe^{III} complexes. Thus,

various homodinuclear species were identified such as $[Hg^{II}_2(TTHA)]^{2-}$, $[Hg^{II}_2(OH)(TTHA)]^{3-}$ and $[Hg^{II}_2(OH)_2(TTHA)]^{4-}$. However, no possible structural formulation was described and no isolation was attempted.

Bohigian and Martell[30] reported the existence of homodinuclear Fe^{III} and Cu^{II} complexes but with mixed-ligand chelates identified *via* potentiometric titrations. The ratio of 2 : 1 : 2 for M : H_6TTHA : L (where L = 3,5-pyrocatecholdisulfonic acid (Tiron) (**Fig. 3.2. A**) or 8-hydroxyquinoline-5-sulfonic acid (**Fig. 3.2. B**)) was used.

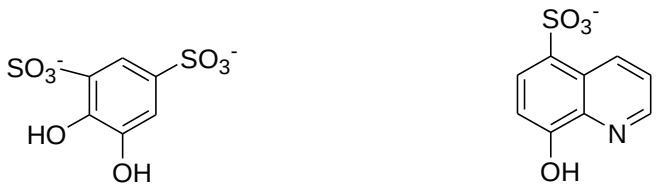

A **B**

Fig. 3.2 A. Tiron, **B.** 8-hydroxyquinoline-5-sulfonic acid (deprotonated).

The two homodinuclear complexes formed were compared with the potentiometric curve of M : H_6TTHA (1 : 1), where differences in the inflection points were observed for the both of the dinuclear complexes and so existence of the complexes were confirmed. Again, no attempt was made to try to separate the complexes.

Harju and Ringbom[31] described the existence of the homodinuclear metal complexes of Cu^{II} (*i.e.* Cu : H_6TTHA in the ratio 2 : 1) by complexometric titration. The method reported was only to test the validity of the previously described theory of formation of 1 : 1 and 2 : 1, M : L complexes *via* complexometric titrations.[32] Hence, various different transition metals such as

Co^{II}, Cd^{II}, Hg^{II}, Cu^{II}, Mn^{II}, Zn^{II}, Ni^{II} and Fe^{III} were used in the experiment. The different metals showed a different behaviour in the formation of 1 : 1 and 2 : 1, M : H_6TTHA complex formation as shown by the curves obtained. The use of different metal combinations gave different titration curves, which illustrated that their propensity to form either 1 : 1 or 2 : 1 M : H_6TTHA complexes was a function of pH. Nonetheless, the only evidence for the formation of the complex was from the titration curves.

Smith and Martell[33] also reported the existence of mononuclear as well as homodinuclear Cu^{II}-TTHA metal complexes observed *via* EPR measurements. It is known that EPR measurements are capable of determining the distance between two Cu^{2+} ions in dimeric or polynuclear species. The dipole-dipole interactions between the two copper ions of the complex in the solution form were used to calculate the distance between the two copper ions. The spin Hamiltonian ($\mathcal{H}$) given in the equation below was used in the calculation:

$$\mathcal{H} = g_{\parallel}\beta H_z S_z + g_{\perp}\beta(H_x S_x + H_y S_y) + A S_z I_z + B(S_x I_x + S_y I_y) \qquad (4)$$

where β is the Bohr magneton; H is the dc magnetic field; S = 1/2 is effective electronic spin; I =3/2 is nuclear spin; $g_{\parallel}$ and $g_{\perp}$ are electronic g factors parallel and perpendicular to the *z*-axis, respectively; A and B are hyperfine interaction parameters parallel and perpendicular to the *z*-axis. The above equation is for uncoupled Cu^{II} complexes described by a spin Hamiltonian assuming axial symmetry along the *z*-axis.[34]

However, when pairs of Cu^{II} centres come into proximity, then dipole-dipole coupling occurs and is the main factor to be considered in EPR measurements. Therefore, the following equation is used.[34]

$$\mathcal{H} = \mathcal{H}_1 + \mathcal{H}_2 + \mathcal{H}_{ex} + \mathcal{H}_d \quad (5)$$

where, $\mathcal{H}_1$ and $\mathcal{H}_2$ are the Hamiltonians for the two copper ions and are calculated as equation (4), respectively. While $\mathcal{H}_{ex}$ and $\mathcal{H}_d$ are exchange and dipolar terms, respectively. The term $\mathcal{H}_d$ is calculated as follows:

$$\mathcal{H}_d = \frac{1}{r^3}[\mu_1\mu_2 - 3(\mu r^0)(\mu_2 r^0)] \quad (6)$$

where μ_1 and μ_2 are magnetic dipole moments for ions 1 and 2, respectively; r is the distance between the two ions or the dipoles; r^0 is the unit vector along the line joining the dipoles.

From equation (6), by evaluation of all the above factors, the distance was calculated. The calculations were based on relative orientations of the principal axis of the g tensor with dipoles (assumed to have the same principle axis). All three axes were calculated on the basis of the same principle.

Hence, EPR spectroscopy was used as a tool to identify as well as to elucidate the structure of the possible homodinuclear species formed in the mixture of Cu^{II} and $TTHA^{6-}$. The EPR measurements were obtained for Cu : H_6TTHA ratios of 1 : 1 as well as 2 : 1 over a wide pH range to obtain well-resolved spectra for both mononuclear and homodinuclear complexes. In the EPR measurement, in the region of $g \approx 2$, the presence of a single species indicated

one of the most probable forms of a homodinuclear Cu^{II} species, which was observed when the spectrum was analysed at a low field *i.e.* ~ 1500 G at room temperature. The existence of the single species has been accounted for by the dipolar coupling of the homodinuclear chelate. On the basis of the results obtained, two structures were proposed for homodinuclear $[Cu^{II}_2(TTHA)]$ complex described as closed (**Fig. 3.3 a)**) and open (**Fig. 3.3 b)**) structural forms.

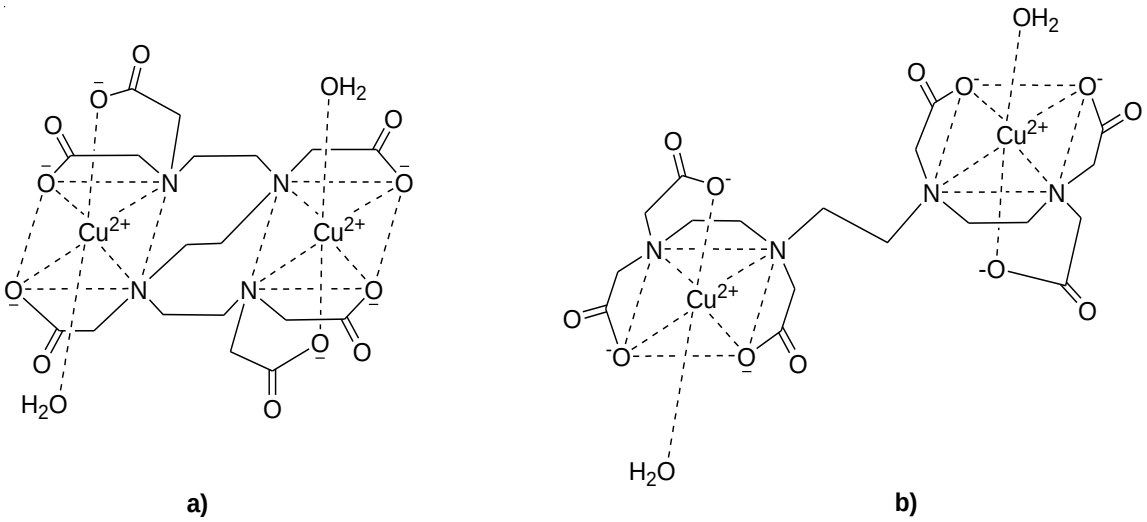

Fig. 3.3 Structures proposed for $[Cu_2(TTHA)]$ complexes **a)** closed form, **b)** open form.

The closed form (**Fig. 3.3 a)**) was found to possess a more rigid framework and a shorter distance between the two Cu atoms, and the value of distance obtained was comparable with the distance value obtained experimentally from (4) to (6). However, in the open form (**Fig. 3.3 b)**), free rotation was possible around the ethylene group of the two encapsulated Cu^{II} centres *i.e.* the overall framework was less rigid in comparison to the structure

represented by a closed form (**Fig. 3.3 a)**), the distance of separation between the two Cu atoms was found to be higher than its experimental value. The EPR spectrum obtained for a homodinuclear species was confirmed by observation of a single species at room temperature. However, in the previously reported investigations, it was noted that the signal found due to the existence of homodinuclear species usually disappeared at room temperature or was replaced by a rather broader signal at $g \sim 2$, which was reported as a definite confirmation of the formation of a dinuclear complex.[34,35,36,37,38,39] Sometimes, the disappearance of the mononuclear complex and the instantaneous appearance of another broad signal was also an indication of the appearance of a homodinuclear complex, which did not persisted for long at room temperature before disappearing. Nevertheless, the EPR data obtained by Smith and Martell in this report contradicted the earlier reported investigations,[33] as their reported complex proved that the homodinuclear complex formed was stable at room temperature in the solution form. Also, in the earlier reported investigations, the authors did not give a reason for the disappearance of the peak which might have occurred due to conversion of paramagnetic species to some diamagnetic copper species which could not possibly be identified in EPR measurement. Although, it has been proved previously that due to rapid electron transfer between two different oxidation states of copper *i.e.* Cu^{I} and Cu^{II}, the disappearance of EPR signal can be seen.[36] Also, to justify these results in support of the formation of a stable homodinuclear complex, no attempt was made either to analyse it any further or to try to isolate the complex (*e.g.* by

precipitation). Hence, the existence of a stable homodinuclear complex remains to be confirmed.

Zhang *et al.*[40] proposed the existence of a stable heterodinuclear Fe^{II}-Cu^{II} TTHA (1) complex (**Fig. 3.4 A** 1)) in solution using data from EPR and UV-visible spectroscopy. The complex formed (**Fig. 3.4 A** 1) was found to undergo oxidation and disproportionation to form the final species as homodinuclear complexes *i.e.* $[Cu^{II}_2(TTHA)(OH_2)_2]^{2-}$ and $[Fe^{III}_2(O\text{-}TTHA)]^{2-}$. This conversion of the analysed heterodinuclear species to the two homodinuclear complexes was reported to have occurred by autooxidation of complex (1) *via* cross metal exchange to an intermediate oxidised complex $[Fe^{III}Cu^{II}(TTHA)]^{1-}$ (2) (**Fig. 3.4 A**) and an isomeric complex $[Fe^{III}Cu^{II}(TTHA)]^{1-}$ (3) (**Fig. 3.4 B**) detected in the two different methods of preparations described in their work.

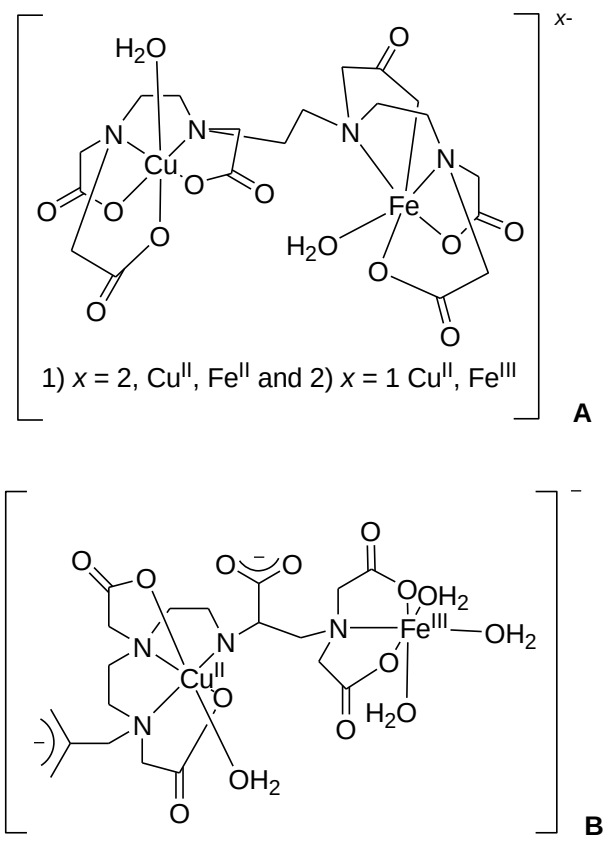

Fig. 3.4 Structure of $[CuFe(TTHA)]^{2-}$ complexes as **A** 1) Cu^{II}, Fe^{II} and 2) Cu^{II}, Fe^{III}; **B** $[Fe^{III}Cu^{II}(TTHA)]^{1-}$ complex isomer.

The UV-visible as well as EPR spectra obtained from those reaction solutions (taken at different time intervals) were compared with solutions of the homodinuclear complex of Cu^{II} *i.e.* $[Cu_2TTHA]^{2-}$, a mixture of solutions of Fe^{II} and Cu^{II} *i.e.* $[Fe_2TTHA]^{2-}$ and $[Cu_2TTHA]^{2-}$ and the final mixture solution of the product. In the UV-vis spectrum of the reaction mixture an absorption band was observed which corresponded to the $[Cu_2TTHA]^{2-}$ complex. This observation raised doubts about the existence of the heterobimetallic complex as no band corresponding to the expected heterobimetallic complex was obtained. However, a slight variation in the

EPR spectrum was observed in the nature of peak width along with a peak drift with respect to $[Cu_2TTHA]^{2-}$. Nonetheless, two possible mechanisms were described with respect to the formation of the two intermediates hence, the formation of the two homodinuclear complexes as products. The formation of final products or the stability of the heterodinuclear complex was demonstrated by carrying out the reaction in the presence of oxidising agents such as O_2 and H_2O_2. No strong supporting evidence for the existence of the heterodinuclear complex apart from the presence of an EPR peak has been discovered.

Xu *et al.*[25] reported the crystal structure of a proposed heterodinuclear complex of Co^{II}-Ni^{II} TTHA, which is hydrogen bonded to a hexaaquamanganese(II) cation (**Fig. 3.5**). There is, however, some doubt over the identity of this complex. In this reported heterodinuclear complex of $TTHA^{6-}$, the ligand is described to bind with both Co as well as Ni. However, the experimental conditions simply report adding Co, Ni and Mn salts (there is a separate Mn^{II} cation) to the ligand.

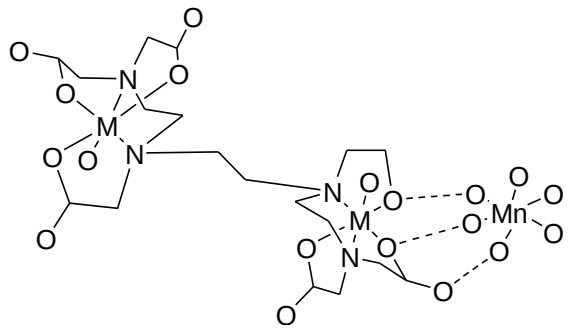

Fig. 3.5 Structure of $[Mn(OH_2)_6][NiCo(TTHA)(H_2O)_2]$, where M = Ni or Co. Water molecules are removed to show the coordination pattern.[25]

Elemental analysis and X-ray diffraction (single crystal) methods cannot separate the possibilities (Ni_2, Co_2, NiCo). However, by metal analysis (AAS) the distinction between the two metals is definitely possible as two different lamp sources would have been used for the identification in the latter case. Nevertheless, this was not carried out at this stage due to in availability of the same single crystal. The structure elucidation by single crystal X-ray diffraction technique is based on the number of diffracted electrons, but it is impossible to distinguish between two similar metal atoms that differ by only one electron difference. In addition, elemental analysis is a bulk analysis which would not readily separate possibilities differing by only by one mass unit. There is also a reference to there being low-spin Co^{II}, which is not expected to be the case as it is shown that the analogous EDTA complex of Co^{II} is high spin.[41] Electronic spectroscopy would identify the composition better, but the data were not provided.

3.2 Heterobimetallic Chelate Complexes

3.2.1 Ligand Selection

Chapter 2 describes the attempted synthesis of heterobinuclear halo-bridged complexes involving platinum group metals. However, this chapter introduces an alternative route to the synthesis of heterobinuclear metal complexes that involves the polydentate ligand, $TTHA^{6-}$,[16] selected due to its structural resemblance to EDTA used earlier by King in this research group. Thus, as described in Chapter 1, King prepared mononuclear, anionic EDTA complexes of some metal salts which were then employed as metal precursors in the preparation of nanoparticle-doped, mesoporous silicas using a TLCT approach.[42]

$TTHA^{6-}$ possesses properties similar to those of EDTA but also has a relatively high binding affinity towards a wide range of different metal ions including alkaline earth metals [26,27,31] and rare-earth metals [43,44] as well as transition metals.[19,20,21,22,23,24] A few examples of post-transition metals complexing to higher analogues have also been reported in the past years.[45,46] Thus, as well as binding to single metal centres, TTHA had the attraction that, as a ligand that possesses two interconnected, five-coordinate binding sites, it represented a possible approach to the target heterobinuclear complexes that might lead to porous silicas doped with well-defined bimetallic nanoparticles. (**Fig. 3.6**).

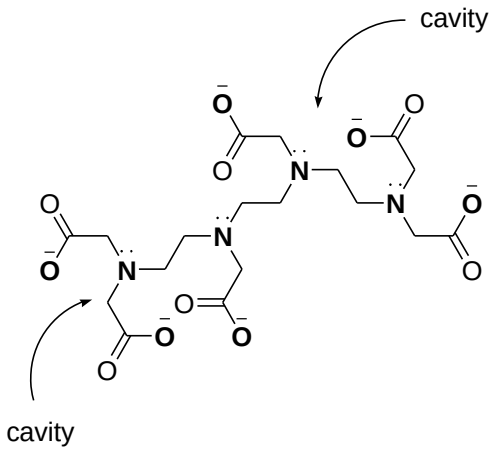

Fig. 3.6 $[TTHA]^{6-}$ showing two cavities with five coordination sites each (atoms in bold).

Using this approach, a wide range of metals with +2 as well as +3 oxidation states have been employed to synthesise the heterobimetallic complexes, discussed in the following sections.

3.2.2 Metal-Ligand Complexation, a stepwise approach

From the reported examples of dinuclear complexes, discussed above, it was clear that such complexes were, in spite of their thermodynamic stability, kinetically rather labile. Therefore, a strategy was sought to prepare the heterodinuclear complexes in a stepwise fashion (**Scheme III.I**). The concept involved was to try first to form a 1 : 1 complex with $TTHA^{6-}$ and a more inert metal (*e.g.* Rh^{III}, Cr^{III}, Ir^{III}) and then react it with a more labile second metal (*e.g.* Ni^{II}, Co^{II}, Pd^{II}, Cu^{II}) to form the desired heterobinuclear complex selectively. For comparison, the reverse was also tried. Thus, a 1 : 1 ratio of H_6TTHA and the desired metal salt was reacted *via* heating under reflux in water, after which the solution was treated with six molar equivalents of base (NaOH) to neutralise acid produced and leave the sodium salt of the complex.

One molar equivalent of the second metal was then added and the reaction continued, being monitored at each step by negative-ion mass spectrometry. Ethanol was then added to precipitate the product which, after drying was analysed by atomic absorption spectroscopy, infrared spectroscopy and CHN analysis. The precipitate was then crystallised from either water or a water/ethanol mixture.

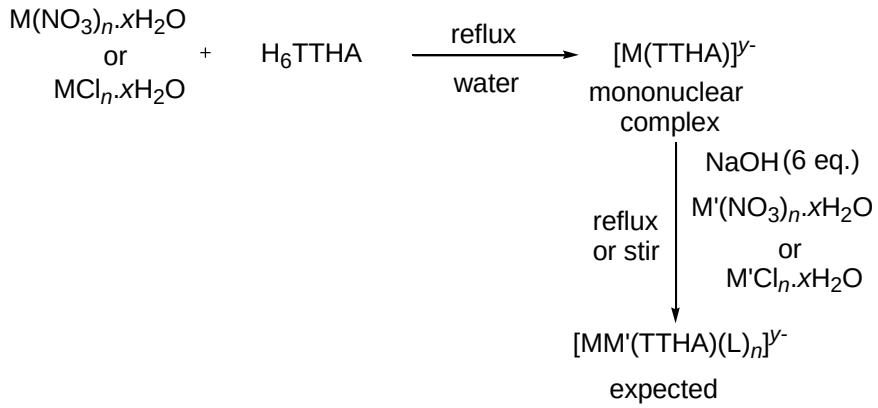

Scheme III.I Typical preparation of heterobimetallic complex, where, L = coordinated H_2O and Cl, *n* = number of ligands (H_2O/Cl).

On addition of metal salts such as those containing Pd^{II}, which were prone to decomposition at higher temperatures, the contents were stirred at a lower temperature.

Therefore, the preparation of various heterobimetallic complex was tried with the following combinations: Rh-Ni, Rh-Zn, Rh-Pd, Rh-Cu, Rh-Co, Rh-Cr, Cr-Pd, Cr-Co, Ni-Pd, Cr-Ni, Ni-Co, Ir-Pd and Ir-Rh. In these metal mixtures, a Na^+ ion (from the base *i.e.*, NaOH) was expected to act as the counter ion where the complexes were anionic. Hence, no other counter ion or external

precipitant was added. All the complexes prepared were crystallised from either water or from a water/ethanol mixture. The crystals obtained were analysed along with the precipitate for quantitative estimation of the metallic ratio in a complex by X-ray diffraction as well as by AA spectroscopy (details below). However, in a few cases where precipitates were not obtained, PPh_4^+ was added as a large counter cation to precipitate the complex.

Using these approaches, several crystal structures were obtained,[47] which are now described.

3.3 Heterodinuclear Complexes

3.3.1 $Na[RhZnCl(TTHA)(H_2O)_4]\cdot xH_2O$ (**1**)

This was the only heterobimetallic complex prepared successfully by using the step-wise approach. Single crystals of the complex were obtained from an extended crystallisation period, although, the ratio of metals observed in bulk (see **Table III.II**) was different from that of the single crystal. In the crystal structure, the position of the two metals is not disordered. Supporting evidence was provided by negative ion mass spectrometry

The yellow crystals of this heterodinuclear complex contain a great deal of disordered lattice water, which means that the *R*-factor is rather high. However, the formula given through the solution of the structure does not give a balanced charge as the dimeric TTHA unit is dianionic and the given formula shows only a single sodium. This is probably explained by the large amount of disordered solvent/ions which was modelled using the SQUEEZE algorithm.[48] The latter predicts a volume of 1084 $Å^3$ of disordered material

with an electron count of 574 within the unit cell. This means around 110 atoms (including hydrogens) so there may well be sodium ions included in this. These channels of water are found in the *ac* plane as indicated in **Fig. 3.7**.

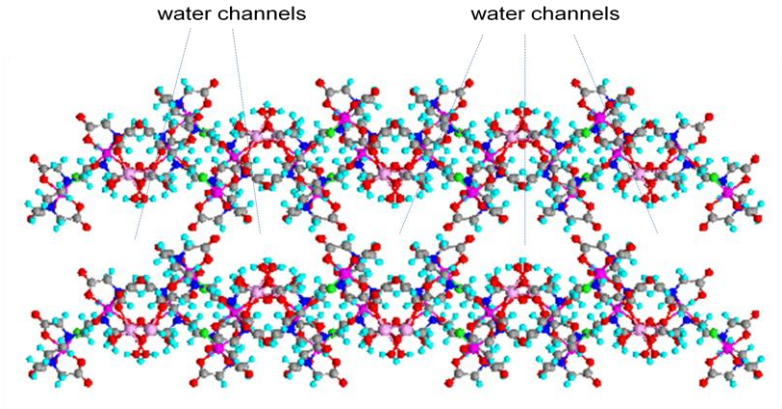

Fig. 3.7 Structure of complex **1** showing the water channels.

The probability that sodium ions in the unit cell balancing the charge is higher than that of protons (oxonium ions) as the solution used for the complex preparation was alkaline, but confirmation of this proposal is not possible due to the poor structural data indicated by the *R*-factor (wR_2 = 0.1340). Another possibility would be the presence of a protonated carboxylate oxygen, and attempts were made to model this before 'squeezing' the crystallographic model, but no evidence could be found supporting its existence. From the literature, the C-O and C=O bond lengths of a neutral carboxylic acid *i.e.* in formic acid are reported to be 1.26(3) and 1.23(3) Å, respectively.[49] The bond lengths of an uncoordinated neutral carboxylic acid may vary between 1.31 and 1.21 Å for C-O and C=O on average, depending upon the coordinating groups.[50] On the other hand, for monodentate coordinated anionic carboxylates, the values of d(C-O) and d(C=O) are reduced to 1.277(17) Å

(M-O-C) and 1.234(15) Å (M-O=C), respectively.[50] In the current case (Rh-Zn), most of the values of the bond lengths of the metal-coordinated carboxylate oxygens (M-O-C) correspond closely to the anionic case *i.e.* 1.269(8), 1.254(8) and 1.244(7) Å, for, Zn-O(1), Zn-O(5), Zn-O(3), respectively (**Fig. 3.8**). Similarly, the Zn-O=C *i.e.* Zn-O(2) (1.236(8)) and Zn-O(6) (1.234(9)), also have close correspondence to the values of the two bond lengths were reported for a protonated carboxylate. However, one of the bond lengths showed consistent difference from the rest of the reported metal coordinated C=O bond lengths *i.e.* Zn-O(4) (1.275(7)). From this difference in bond length, a doubt was raised about the possibility of the existence of a protonated carboxylate oxygen around Zn-O(4). So, to eliminate this doubt, the crystallographic model was closely looked at using an electron density map, which showed no indication whatsoever of the presence of hydrogen around that carboxylate oxygen (*i.e.* O(4)).

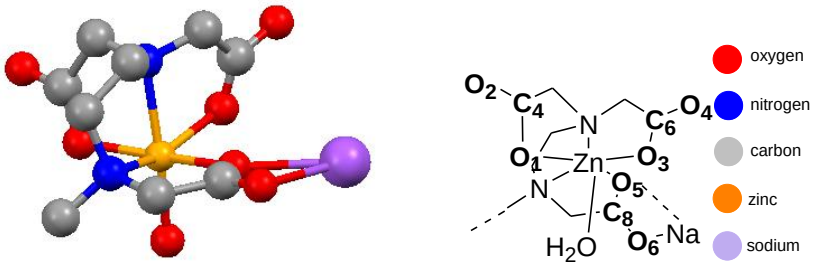

Fig. 3.8 Showing a part of crystal structure of the Rh-Zn complex, where the probability of protonated carboxylate was examined and the groups discussed are highlighted in bold. (located hydrogens are removed for clarity).

Despite of the disordered lattice water, data relating to the positions of atoms in the complex are good (note that the ADP of C10 was restrained to be approximately isotropic)[51] and so it is realistic to offer a description of the

structure. Thus, each $TTHA^{6-}$ is bound at one end to a Rh^{III} centre with its sixth coordination site occupied by a chlorido ligand, while at the other end it is bound to Zn^{II} whose sixth coordination site is occupied by coordinated water. This gives each dinuclear complex a 2- charge and the basic structure is shown as **Fig. 3.9**.

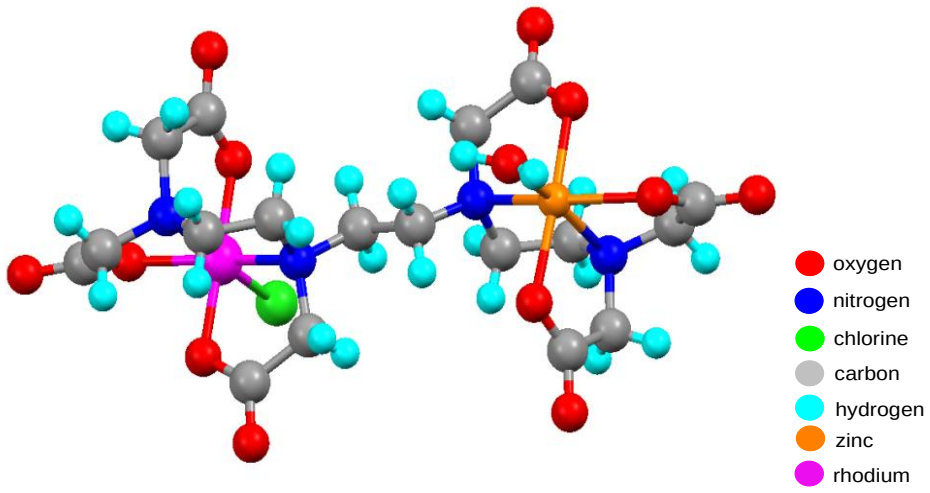

Fig. 3.9 Structure of the heterobimetallic $[Rh(Cl)Zn(TTHA)]^{2-}$ anion.

These complexes are then linked in one of two ways to give a non-covalently linked polymeric arrangement, which is now described. The 'zinc ends' of two dinuclear complexes are linked *via* a pair of sodium atoms in a staggered arrangement that are themselves linked by an oxygen that sits on a 2-fold axis, although it is difficult to know if this bears one or more hydrogen atoms. Each sodium is five coordinate, being bound by one precisely located water molecule, the aforementioned bridging oxygen and an exogenous κ^2 interaction with one of the carboxylate groups that binds η^1 to zinc. The fifth site is occupied by an oxygen atom that is the carbonyl oxygen of a

carboxylate group bound to the Rh^{III} centre of a neighbouring complex. In addition, the representation shows two other water molecules 'associated' with each sodium, although the Na···O separation is >2.6 Å (ΣvdW radii = 2.32 Å). The overall picture and that localised around the two sodium ions are shown in **Fig. 3.10 A–C.**

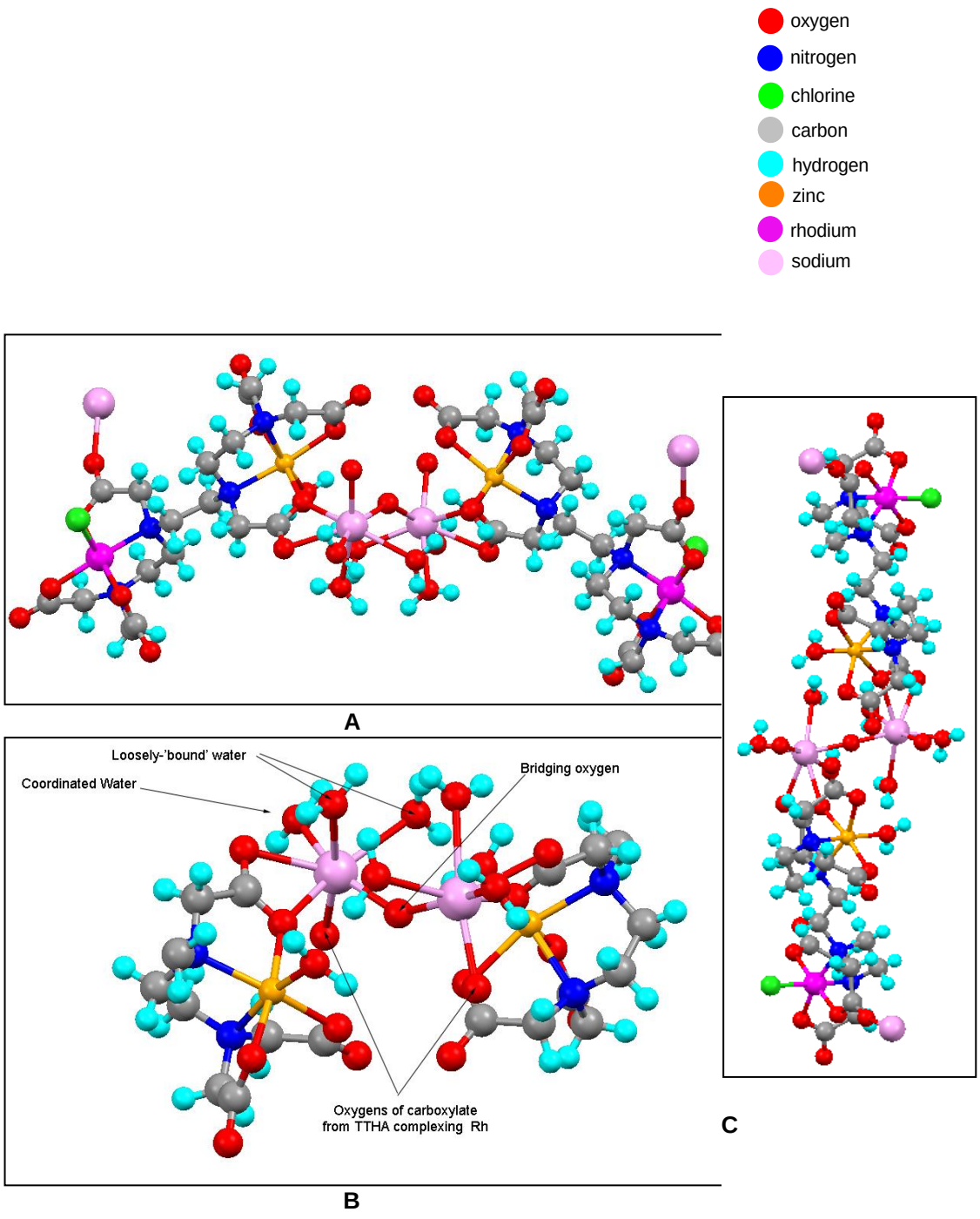

Fig. 3.10 Different views of the structure of $Na_2[Rh(Cl)Zn(TTHA)]$ emphasising the arrangement of the sodium cations in the structure.

If for the sake of this description, the fragment shown in **Fig. 3.10 A** is taken as a notional repeat unit, then one of its 'rhodium ends' is bound to the

bridging sodium unit of another repeat unit *via* the carbonyl oxygen of an η^1-carboxylate group bound to the rhodium and, in turn, the 'rhodium end' of this second fragment binds to the bridging sodium unit of the first. This is shown in **Fig. 3.11** with part of the structure and also schematically. This arrangement persists to form the polymer and different polymer units are linked together through hydrogen-bonding arrangements (not illustrated).

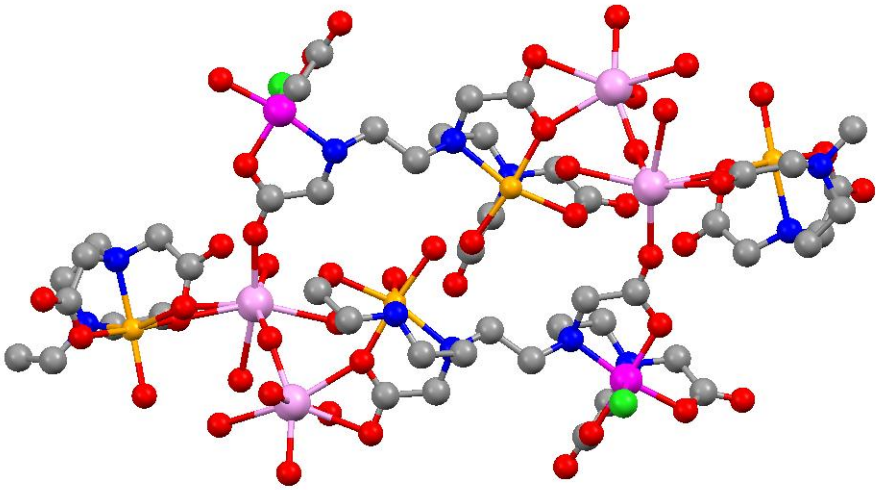

(a)

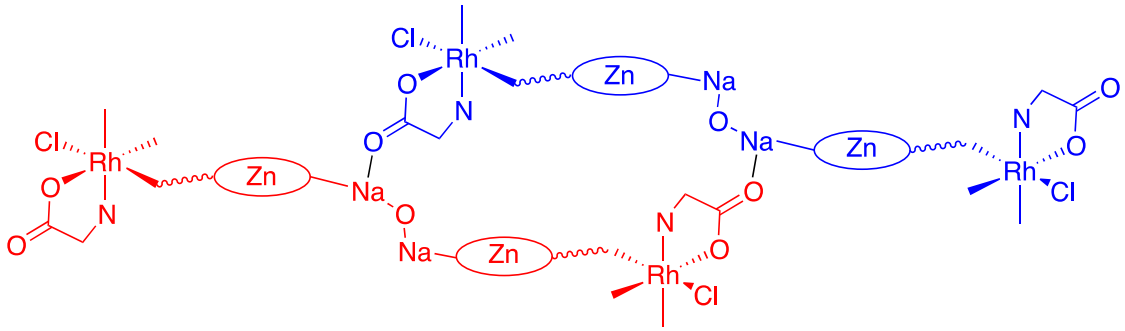

(b)

Fig. 3.11 Illustration of the linking together of fragments *via* the Rh-end of the TTHA heterodimer **(a)** from the structure with hydrogens and selected other atoms removed to give a clear picture and **(b)** a schematic of the same showing how the polymer extends.

3.3.2 $[Cr_{1.50}Rh_{0.50}(TTHA)(OH_2)_2]\cdot 6H_2O$ (**2**)

The binuclear Cr^{III}-Rh^{II} complex (**2**), which was obtained by the sequential addition of metals as described in section 3.2.2, was analysed to possess a Cr : Rh ratio of 3 : 1 from single crystal X-ray diffraction and by atomic absorption studies. In this case, the crystal structure of the complex reflects the composition of the product (metals) in bulk *i.e.* 3 : 1 (Cr : Rh) as shown in **Table III.II**. However, the structure obtained cannot differentiate between a mixture of two homodinuclear complexes of Cr_2 and Rh_2, and a mixture of the two homodinuclear and heterodinuclear complexes *i.e.* Cr_2, Rh_2 and Cr-Rh, respectively. Nevertheless, unlike the other attempted preparations of heterodinuclear complexes, the yield of this complex was relatively high (52%). The complex was crystallised several times to verify the ratio of the two metals and atomic absorption analyses of the precipitated product as well as the crystallised product were carried out separately to determine the final ratio *i.e.* 3 : 1, Cr-Rh. Thus, with two rather inert metal centres, while it is not possible precisely to identify the species contributing to the observed ratio of metals, it is at least a well-behaved system with defined composition.

The asymmetric unit consists of half the complex, with the metal centre being modelled as disordered Cr : Rh in 0.75 : 0.25 ratio (Rh/Cr disorder appears random as an ordered solution could not be obtained in the *P*1 space group). Combined with the observation of an inversion centre at the mid-point of the C–C bond joining the two halves of the TTHA, then there is no discrimination in bond lengths.

To test the crystallographic model, the effect on the *R*-factor of varying the metal ratio was studied and results are shown in **Table III.I.** In the first case, **I.** the percentage of each metal as determined by analysing was entered into the program, for which, the data are shown. The ratio determined by refining occupancy factors is shown as entry **II**, which gives the best fit with lowest *R*-factor and residual electron density. Other possibilities (entries **III** to **V**) were also tried but resulted in a significantly higher value for the *R*-factor along with ADP values for non-metal atoms that were too small, especially when compared to that of the metal (which is large). Thus, in modelling a homodinuclear Cr_2 complex (*i.e.* **III**), the presence of high residual density adjacent to Cr was indicated while modelling and the ADP for the Cr was very small, while for the other atoms it was too large. This is the characteristic of a model with too light a metal. Conversely, modelling a homodinuclear Rh_2 complex (*i.e.* **IV**), gave a residual density near the oxygens, with the deepest hole near the Rh atom, characteristic of a model with too heavy a metal. The ADP on the non-metal atoms was too small. Another possibility was of a 50 : 50 mixture of Cr : Rh (*i.e.* **V**), whose modelling gave an ADP of non-metal atoms too small in comparison to metal (which is somewhat large), as well as, high residual density near the oxygens, with a deepest hole near the metal. Thus, the disordered model with a 3 : 1 Cr : Rh ratio is clearly the best solution to the data. Nonetheless, further discrimination is not possible with the data in hand.

Table III.I Possible structures of homo- and hetero- dinuclear complexes with main (collected) crystallographic data.

Sr. No.	%Cr	%Rh	*R*1 (all)	*wR*2	GooF	Residual density
I	75	25	2.70	6.85	1.034	0.6/-0.54
II	75.95	24.05	2.69	6.75	1.035	0.58/-0.54
III	100	0	5.04	15.087	1.085	1.79/-0.64
IV	0	100	8.45	27.90	1.085	3.38/-2.73
V	50	50	4.33	14.30	1.100	0.99/-0.90

The coordination around each metal is as expected for TTHA, with the sixth site taken up by a water ligand so that the dinuclear complex is neutral (**Fig. 3.12**). There are six lattice water molecules in the structure, three associated with each half, and these appear to play a partly structural role as in the following description, which refers to one half of the dinuclear complex only. The waters are numbered to aid the description (**Fig. 3.13**).

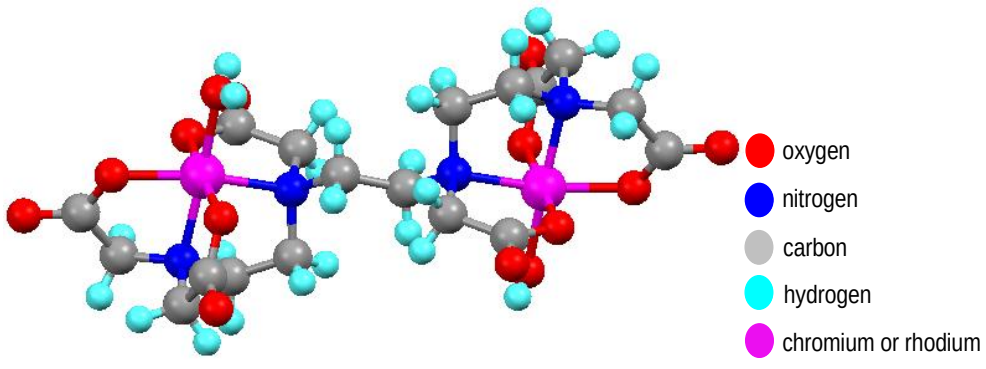

Fig. 3.12 Structure of the dinuclear unit of $[Cr_{1.50}Rh_{0.50}(TTHA)(OH_2)_2]$ showing a heterobimetallic dimer (metals indistinguishable).

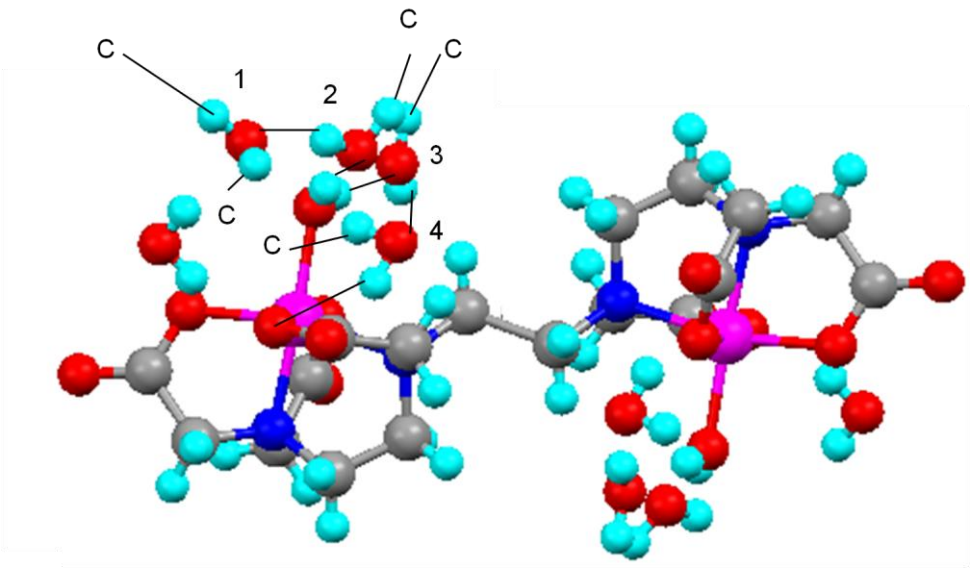

Fig. 3.13 Arrangement of water molecules around the $[Cr_{1.50}Rh_{0.50}(TTHA)(OH_2)_2]$ dinuclear complex.

Thus, two water molecules (2 and 3) are hydrogen bonded to the coordinated aqua ligand. Each of these is then bound to a further lattice water (1 and 4, with 4 coming from a different asymmetric unit) through one hydrogen, with the other being hydrogen-bonded to the oxygen of a bound carboxylate from another TTHA dimer in the lattice (indicated **C**). The two hydrogens of molecule 1 and one hydrogen of molecule 4 are also hydrogen bonded to such carbonyl oxygen atoms, while the remaining hydrogen of 4 is bound to a carbonyl oxygen of the dimer in the description. Thus, the overall arrangement of dinuclear complex in the lattice is moderated by the arrangement of the lattice water molecules.

3.4 Homodinuclear Complexes

3.4.1 $Na_2[Rh_2Cl_2(TTHA)]\cdot 8\ H_2O$ (**3**)

The homobimetallic complex **3** was obtained as yellow block crystals from attempted preparations of Rh-Co, Rh-Ni and Rh-Cu through a step-wise approach.

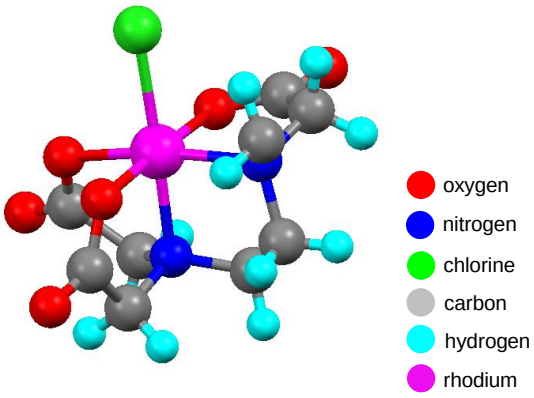

Fig. 3.14 Organisation of one half of TTHA around the Rh–Cl unit (the other half is related through an inversion centre halfway along the central C–C bond in TTHA.

The organisation of the ligand around each rhodium is shown as **Fig. 3.14** (the two halves are related by an inversion centre). Thus, one half of the TTHA occupies five coordination sites with a *mer* arrangement of the three oxygen atoms, *cis* nitrogens and the chloride ligand *trans* to the nitrogen atom bearing two $-CH_2CO_2^-$ groups. The three oxygens and the rhodium can be considered as sitting in a plane and the nitrogen *trans* to the oxygen sits about 0.36 Å below that plane. When half of the TTHA functions as a pentadentate ligand it places certain strains on the coordination, so that none of the angles is 90°, although metal-ligand bond distances are not abnormal. The presence of two chloride ligands creates a dianionic complex and the charge is balanced by two sodium cations. Thus, at each end of the complex, a sodium

ion is bound (2.445 Å) to the hydroxylate oxygen of a carboxylate group that is attached directly to the rhodium (**Fig. 3.15 A**).

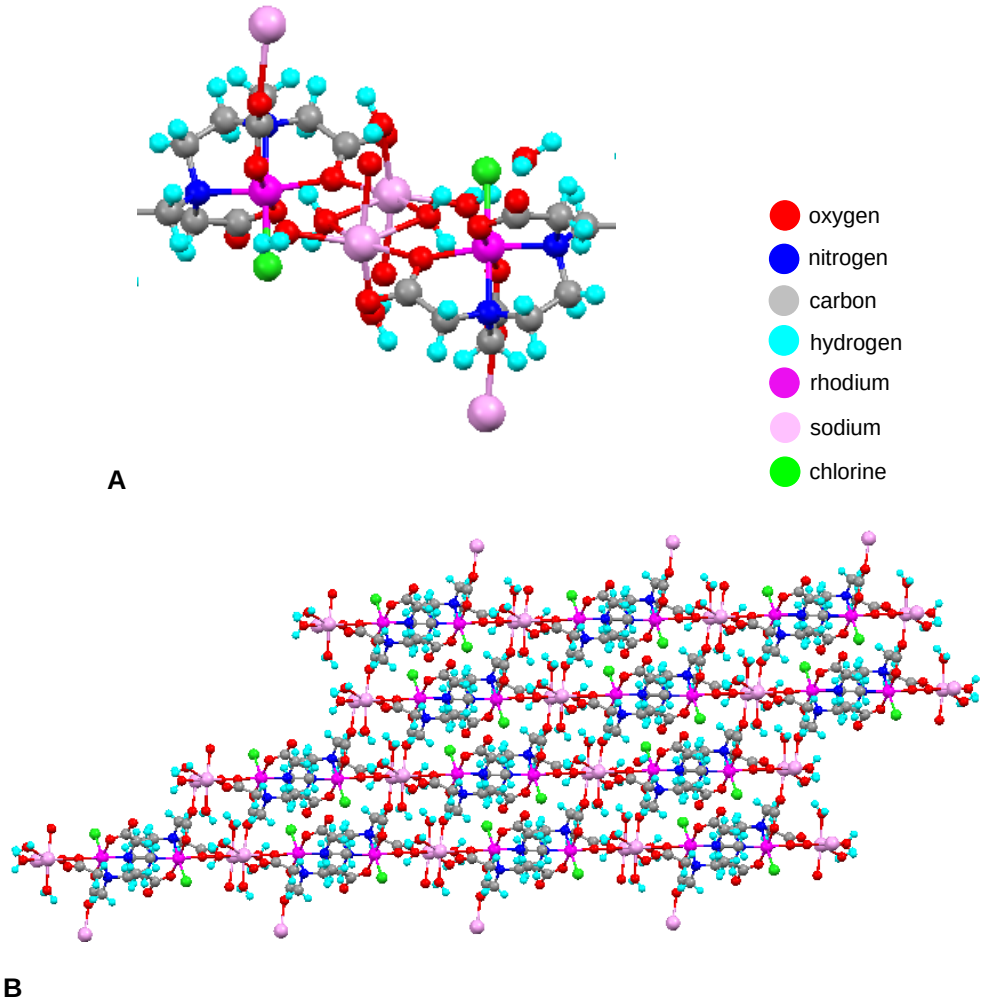

Fig. 3.15 A Sodium bridging unit between two Rh_2(TTHA) units and **B** four, parallel 'polymeric chains'.

This sodium is then part of a Na_2 unit that is held together by two μ-OH_2 groups with the second sodium being symmetry-equivalent and so bound to the next $Rh_2(TTHA)Cl_2$ unit. In this way, a polymeric chain is created that propagates in the *ab* plane. For each sodium, two other coordination sites are taken up by terminal OH_2 ligands, with the sixth site being bound to a TTHA

oxygen in the next 'polymer chain'. Four of these chains are shown in **Fig. 3.15 B**.

3.4.2 $[PPh_4]_2[Rh_2Cl_2(TTHA)]\cdot 11H_2O$ (**4**)

This complex was obtained by the addition of an aqueous solution of PPh_4Cl to a solution prepared as for **3**; the complex crystallised as fine yellow needles. The asymmetric unit contained eleven waters of crystallisation (not shown below), four of which were disordered and modelled over two sites. The hydrogen atoms for these waters could not be located owing to disorder. The organisation around rhodium is similar to that found in **3** and all metal–atom distances around the metal are statistically identical except Rh-Cl distances which are 2.3609(13) and 2.3656(13) (**Fig. 3.16**).

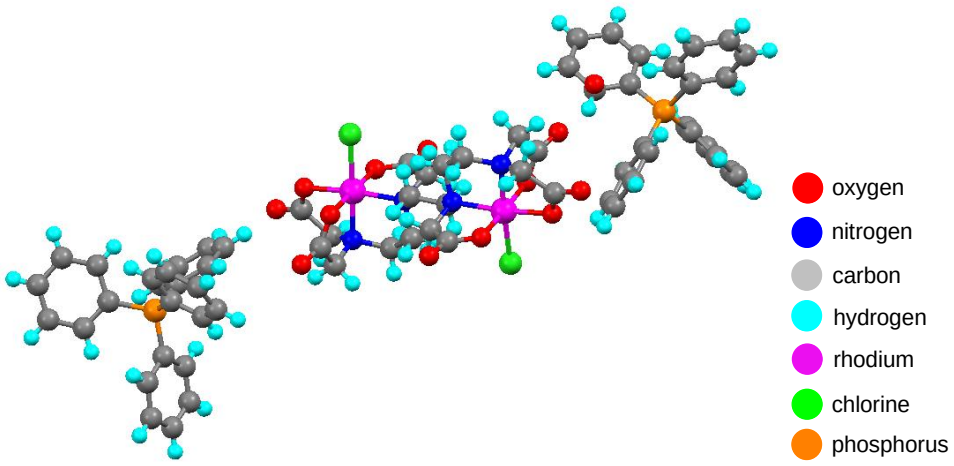

Fig. 3.16 Structure of $[PPh_4]_2[Rh_2Cl_2(TTHA)]$ without water of crystallisation.

However, in the present case there is no inversion centre between the two halves of the complex. The tetraphenylphosphonium cations are disposed at each 'end' of the dinuclear complex and ipso-C–P–ipso-C angles are all close to the expected value. There are no short interactions between cation and

anion. Interestingly, when viewed down the *b*-axis, it is apparent that the dirhodate(III) anions and the phosphonium cations are arranged in alternating layers (**Fig. 3.17**).

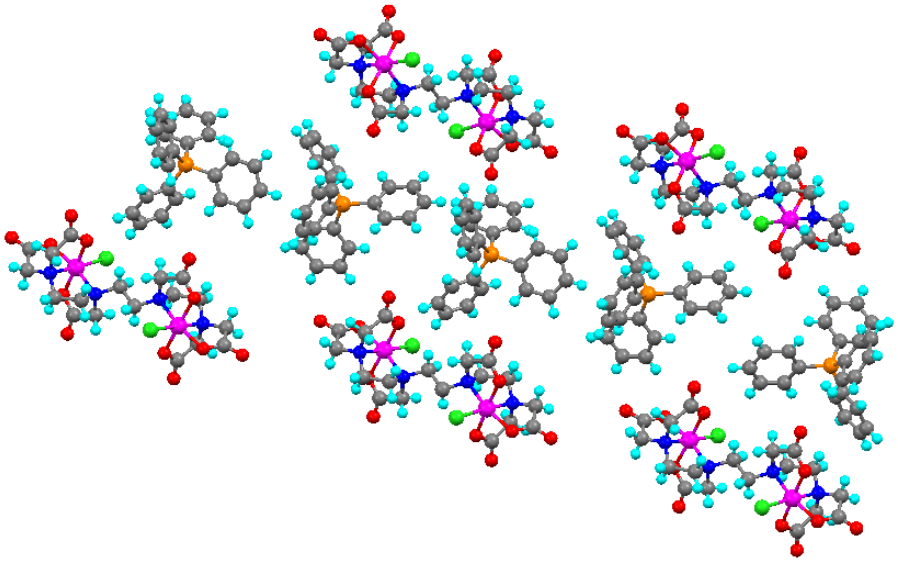

Fig. 3.17 View of complex **4** along the *b*-axis, showing the organisation into alternating cation-anion layers.

3.4.3 $[Cr_2(TTHA)(OH_2)_2]\cdot 6H_2O$ (**5**)

The complex crystallised as purple plates from a reaction that had used Cr^{III} and then Ni^{II} in a stepwise fashion. A similar complex was also obtained from an attempted heterobimetallic Cr-Co complex in which Cr was added first.

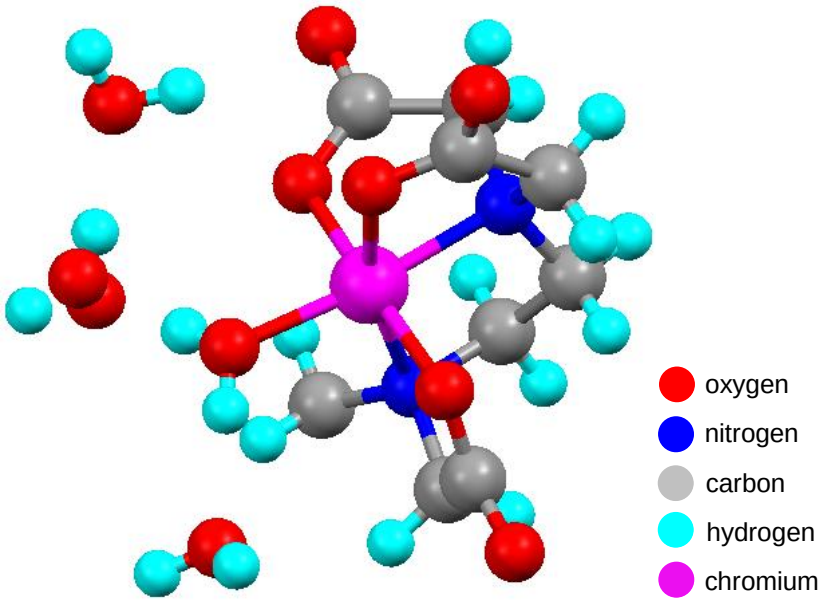

Fig. 3.18 Structure of one half of the $[Cr_2(TTHA)(OH_2)_2]$ dimer showing the three water molecules of crystallisation associated with that half, one of which is disordered.

Once more, the TTHA provides an N_2O_3 donor set, but this time the sixth position is taken up by coordinated water, resulting in a neutral dinuclear complex, the two halves being related by an inversion centre. Each half of the dinuclear complex is associated with three water molecules of crystallisation, and the oxygen of one of these is modelled as disordered over two sites, although the hydrogen positions are not disordered (**Fig. 3.18**). Thus, each hydrogen of the coordinated water is hydrogen bonded to a water molecule in the lattice (O···O separation of 2.616 Å to the non-disordered oxygen), while

the third lattice water is hydrogen-bonded through one of its hydrogens to the carbonyl oxygen of one of the carboxylates.

3.4.4 $C_{18}H_{34}KN_4NaNi_2O_{21.27}$ (**6**)

This complex was prepared by using nickel(II) ($Ni(NO_3)_2 \cdot 6H_2O$) followed by palladium(II) (K_2PdCl_4). The colour of the crystals was bluish-green. However, the precipitate of the complex was olive-green. The mixture did not correspond well when analysed for its metallic ratio *via* AA spectroscopic analysis as **Table III.II**.

The crystal contained substantial disorder. In the asymmetric unit, the sodium was disordered over two sites and the associated complexing waters were also disordered. The relative occupancy was refined to 58 : 42. O9 was also disordered and modelled over two sites with equal occupancy. In addition there is another disordered water this was only partially modelled; the other sites could not be identified. As such, the level of detail of the description is moderated to account for the most significant features.

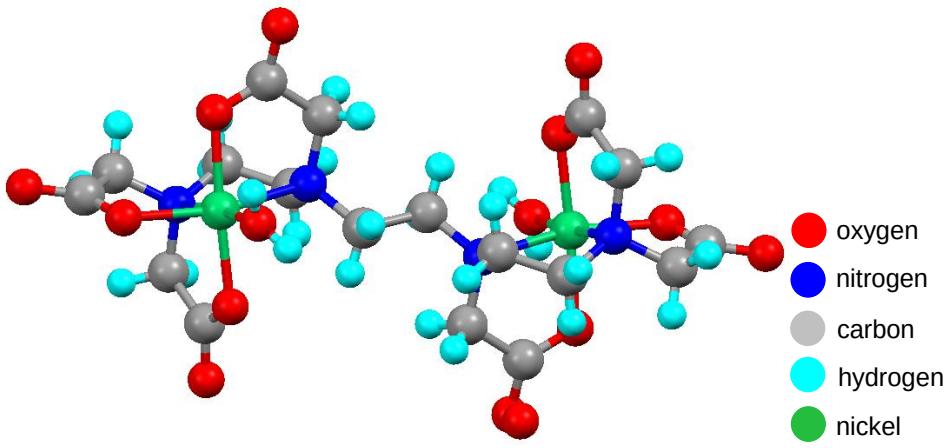

Fig. 3.19 Structure of the dinuclear $[Ni_2(TTHA)]^{2-}$ unit.

Thus, the dinuclear M_2TTHA unit (**Fig. 3.19**) is arranged as expected and as found above, with the sixth coordination site taken up by a bound water molecule. These dinuclear complexes forms non-covalently bound ribbons through the structure which are linked at each side to channels containing the sodium and potassium counter cations. Disorder precludes a very detailed description of the channels, but a schematic is given in **Fig. 3.20 A**, which shows fairly well-behaved, six-coordinate sodium ions that bridge facially to potassium on one side through three oxygen atoms and edge bridge on the other *via* two oxygen atoms. The sixth oxygen appears hydrogen bonded into disordered water. These interactions in turn describe five oxygens bound to potassium and a further two coordination sites are taken up bridging to nickel *via* a coordinated oxygen, with what is believed to be an adventitious contact to the carboxylate carbon. A further oxygen from a neighbouring oxygen bound to Ni completes the coordination sphere. Viewed down the *a*-axis, the ion channels are mutually disposed as a parallelogram (**Fig. 3.20 B**).

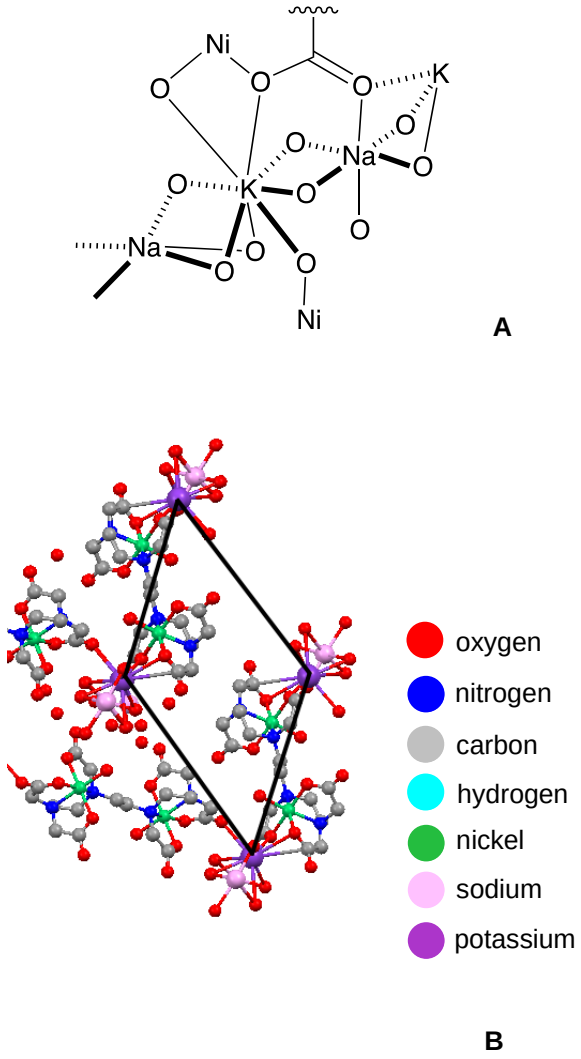

Fig. 3.20 Arrangement of the sodium and potassium cations in the structure of complex **6**.

3.4.5 $Na_2[M(TTHA)(OH_2)_2]\cdot 6H_2O$ (**7**) (where M = Ni_2 or Co_2 or Ni-Co)

This complex was prepared by using nickel(II) followed by cobalt(II). The analysis of the bulk sample (**Table III.II**) shows the two metals in a ratio of about 1.25 : 1, but crystallographically it has not been possible to distinguish between Co and Ni in the final structure.

The complex was obtained as faint grey to colourless fine needles. The metal was reported to be either nickel or cobalt by us in the current work. The poor

quality of data meant that it was not possible to distinguish between the two (no difference was observed in the quality for either metal). The metal was therefore arbitrarily assigned as nickel.

Two ordered water molecules were observed although it was not possible to locate the hydrogen atoms on either of these water molecules. The crystals contained a large amount of disordered water in large channels running through the crystals parallel to the *z*-axis. A suitable model for this water could not be obtained so the SQUEEZE[48] algorithm was again used to take account of these waters. There is the equivalent of three voids per unit cell each with a volume of about 1397 $Å^3$, each containing 768 electrons equivalent to about 43 water molecules.

The large amount of disorder meant that the crystals diffracted poorly and hence the crystallographic quality is poor. The arrangement of the TTHA around the two metal centres is as expected with the sixth position again taken up with an aqua ligand (**Fig. 3.21 A**). Beyond this, it is not intended to give much further description of the structure owing to the level of disorder, except to observe that six dinuclear complexes arrange themselves hexagonally around a water channel, giving an indication of the extent of the disorder (**Fig. 3.21 B** – cations removed for clarity).

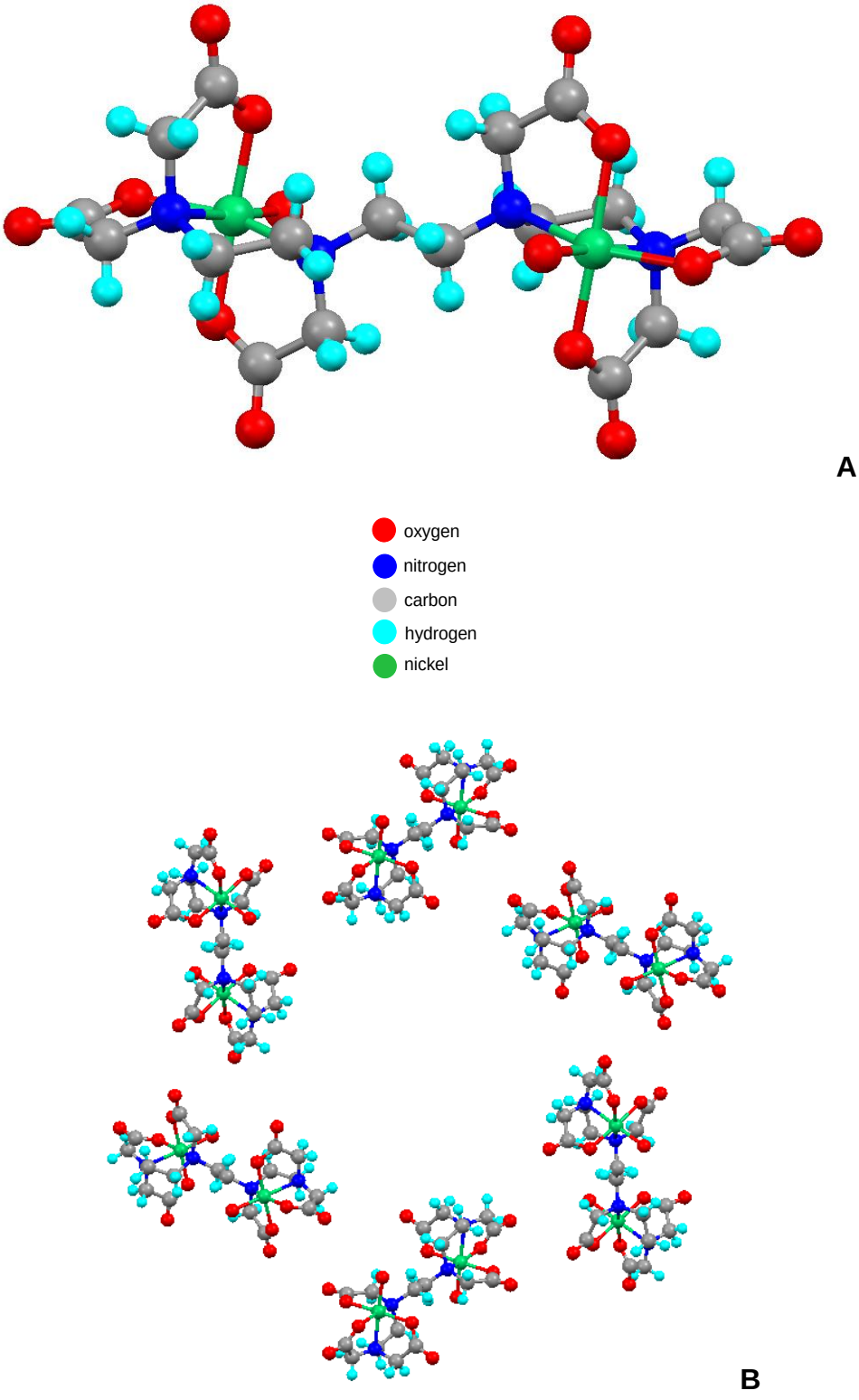

Fig. 3.21 Structure of $Na_2[Ni_2(TTHA)(OH_2)_2]$ showing the homodinuclear dianion **(A)** and the water channel **(B)**.

3.5 Composition of the Bimetallic Complexes

The crystals isolated here (details shown above) represent the least soluble components of the preparation, so that their composition is not necessarily representative of the bulk solution. To this end, for some preparations atomic absorption measurements were undertaken in order to determine the ratio of metals in the bulk sample and so to make a comparison with the composition of the single crystal (**Table III.II**). Thus, it seems that only in the case of complex **2** did the crystal obtained reflect the composition of the bulk. However, in viewing these complexes as possible precursors for the preparation of nanoparticle-doped silicas, it is also instructive to note that only in one case mentioned in **Table III.II** did the preparation lead to a bulk material with the same metal ratio as used in the experiment.

Table III.II Results obtained from atomic absorption measurements for the solid obtained at the end of reactions compared with metal ratios found in the isolated single crystals.

Complex	Metals used in preparation[†]	Ratio from AA	Ratio from Crystal Structure
1	Rh/Zn	1 : 3	1 : 1
2	Cr/Rh	3 : 1	3 : 1
2[*]	Cr/Rh	3 : 1.2	3 : 1
5	Cr/Co	3 : 5	Cr only
5[*]	Cr/Ni	1 : 1	Cr only
6	Ni/Co	1.25 : 1	Ni&Co indistinguishable
7	Ni/Pd	1.2 : 1	Ni only

[†] The order in which they are written corresponds to the order in which they were used in the reaction and in each case 1 : 1 ratios were used.

[*] X-ray data are from separate preparations from which single crystals were also obtained. Structures are not described here as the data sets are less good than those reported although structures have been deposited at CCDC.

3.6 Discussion and Conclusions

The attempts to prepare heterobimetallic complexes employing TTHA described in this chapter using a two-stage, one-pot synthesis were mostly unsuccessful except in one case where a Rh-Zn (1 : 1) complex was isolated as a single crystal. The mixtures for the rest of them led to the isolation of homo- as well as hetero-bimetallic complexes recovered as single crystals. The precipitates obtained from each of these syntheses were analysed by CHN (for overall stoichiometry) and AAS (for determination of the metallic ratio). The results of the metallic composition obtained from the above were then compared with the ratio obtained from single crystal X-ray diffraction analysis. The results obtained by atomic absorption were straightforward, but the CHN analyses were not very helpful as the method could not distinguish mixtures. In addition, the number of random water molecules found in the solids was extremely high, which also raises the chances of error in the calculations of CHN data. For these reasons, from these two methods, only AAS results were used as a standard for comparison Therefore, the data obtained from AAS were used as a representative of the bulk sample, and these ratios were used to describe final sample composition throughout Chapter 4. In contrast, the single crystal X-ray diffraction results corresponded to the bulk only in the case of the Cr-Rh complex. Moreover, one is aware of the fact that crystallisations result from a particular solvent mixture that has more than one complex present leads to precipitation of the least soluble component and is not essentially representative of the bulk sample.

From the above explanation, it is then clear that this method of synthesis is much less selective than we had anticipated and the successful synthesis would require a robust route to a pure, monometallic complex of TTHA with an inert metal, which could then be functionalised selectively with a second metal.

3.7 Experimental

3.7.1 Instrumentation

Single crystal X-ray diffraction

The X-ray data were collected with a Bruker SMART Apex CCD type X-ray diffractometer system using monochromated graphite MoK_α radiation (λ = 0.71073 Å) with the radiation source of a fine focused sealed tube. The single crystal structure elucidation was done by direct methods using SHELXS-97. Structures were refined by using SHELXL-97.[51]

Atomic Absorption Spectroscopy (AAS)

The atomic absorption spectrophotometric analysis was carried out using a Z-5000 series polarised Zeeman atomic absorption spectrophotometer (Hitachi). The source of radiation was a hollow cathode lamp. The flame used was acetylene/air.

The standards were prepared directly from the metal solution obtained by diluting them to a particular concentration considering the detection limits (sensitivity) of metal. The solutions of the complexes (to be analysed) were not prepared in acidified water. However, the standards were in acidic solution (%w/w).

Elemental Analysis

Elemental analysis for carbon, hydrogen and nitrogen was performed on an Exeter Analytical Inc., CE-440 Elemental Analyser. The description is the same as that in Chapter 2.

IR spectrophotometry

The IR spectra were obtained by using a Shimadzu IR spectrophotometer.

UV-visible spectrophotometer

UV–Vis spectra were measured with a Schimidzu (UV-2401PC) spectrophotometer using quartz cells with 10 mm path length.

ESI Mass Spectroscopic analysis

Bruker microTOF with electrospray with an LCQ ion trap was used for negative ion ESI analysis.

3.7.2 Materials

The reagents *N*, *N′*, *N″*, *N‴* - triethylenetetramminehexaacetic acid (H_6TTHA), zinc(II) chloride (anhydrous), cobalt(II) nitrate hexahydrate, chromium(III) nitrate nonahydrate, copper(II) nitrate hydrate, nickel(II) nitrate hexahydrate and iron(III) nitrate nonahydrate were purchased from Sigma Aldrich. Potassium tetrachloroplatinate(II), potassium tetrachloropalladate(II), iridium(III) chloride trihydrate and rhodium(III)

chloride trihydrate were gifts from Johnson Matthey Chemicals. However, other chemicals including tetraphenylphosphonium chloride and sodium hydroxide were from Fisher Scientific. The AAS standards (Pt, Pd, Cu, Co, Cr, Ni, Rh and Zn) were purchased from Sigma Aldrich.

3.7.3 Synthesis of $Na_x[MM'(TTHA)]$ complexes

General

An aqueous solution of H_6TTHA (0.5 mmol, 0.247 g, 15 cm^3) was prepared to which was added an aqueous solution of $MCl_n{\cdot}xH_2O$ or $M(NO_3)_n{\cdot}xH_2O$ (0.5 mmol, 5 cm^3) and the mixture was heated under reflux for 20 h. NaOH solution (3 cm^3, 1 mol dm^{-3}) was added and the solution was stirred for 30 min. A solution of a second metal – $MCl'_n{\cdot}xH_2O$ or $M'(NO_3)_n{\cdot}xH_2O$ (0.5 mmol, 5 cm^3) – was added and the mixture was again heated under reflux for 20 h. Addition of ethanol (*ca* 250 cm^3) led to precipitation of a solid and single crystals were obtained either from ethanol/water mixture or from water in the fridge (5 °C).

It should be noted that the CHN data given in the following sections, wherever obtained, have been used in conjunction with the ratio of metals obtained from AAS and those calculated values are based on the expected structure, ignoring the possibility of adventitious solvent molecules. This is important as it should also be noted that several precipitates obtained contained excess of solvent of crystallisation (*i.e.* as random water molecules), which was difficult to remove.

The AAS values are given in a concentration (ppm) format to avoid any confusion if regeneration of the data are required. The values given have been worked out of the graphs and equations using MS excel. The values have also been corrected for their percentage error with respect to the graphs of standards used for each metal. The ratios given in the **Table II.II** earlier in discussion section were calculated straightway from these ppm values.

3.7.3.1 Attempted preparation of sodium triethytetraamine-N,N',N'',N''' hexaacetatonickel(II)rhodium(III), $Na_x[Rh_yNi_z(TTHA)]$

H_6TTHA (0.5 mmol, 0.247 g), $RhCl_3.3H_2O$ (0.5 mmol, 0.1317 g), NaOH (3 cm^3, 1 mol dm^{-3}) and $Ni(NO_3)_2.6H_2O$ (0.5 mmol, 0.1454 g) were used.

To the green-coloured solution was added ethanol (*ca* 200 cm^3) to precipitate a light green solid, which was filtered and dried under vacuum. Yellow-coloured crystals of $(PPh_4)_2[Rh_2TTHA]\cdot 11H_2O$ suitable for X-ray analysis were then obtained from an ethanol/water mixture after addition of PPh_4Cl used to crystallise the light-green precipitate. The details of the crystal structure are given in appendix A.

Analysis: AAS metal concentration (ppm), found: Rh 1.63, Ni 6.3. Elemental: found, C 25.94, H 3.96, N 7.46 %. MS[ESI^-], found (expected), mixture: m/z: 649.0 [$C_{18}H_{24}N_4NiO_{12}Rh$] (m/z: 648.98) [$C_{18}H_{24}N_4NiO_{12}Rh$] *i.e.* $[RhNi(TTHA)]^{1-}$). IR (ν cm^{-1}): 1636 (C=O str.).

3.7.3.2 Preparation of sodium triethylenetetraamine-N,N',N'',N''' hexaacetatorhodium(III)zinc(II), Na[ZnRh(TTHA)]

H_6TTHA (0.5 mmol, 0.247 g), $RhCl_3.3H_2O$ (0.5 mmol, 0.1317 g), NaOH (3 cm^3, 1 mol dm^{-3}) and $ZnCl_2$ (0.5 mmol, 0.0682 g) were used.

The yellow solution was filtered while hot and ethanol was added in excess (*ca* 200 cm^3). A light-yellow-coloured precipitate was obtained which was filtered and dried under vacuum. The single crystal for this complex suitable for X-ray analysis was obtained from ethanol/water. The details of the X-ray analysis are given in the appendix A, but the crystal obtained was of a 1 : 1 complex with no disorder in the metal positions.

Analysis: AAS metal concentration (ppm), found: Zn 0.38, Rh 1.26. Elemental: found, C 26.15, H 4.07, N 6.70 % would correspond to a calculated overall ratio of Rh : Zn of 13 : 1 if only Rh-Cl, Zn and TTHA were present. MS[ESI^-], found (expected), crystal: m/z: 654.97 [$C_{18}H_{24}N_4O_{12}RhZn$] (m/z: 654.97 [$C_{18}H_{24}N_4O_{12}RhZn$] *i.e.* $[RhZn(TTHA)]^{1-}$). λ_1: 336 nm, λ_2: 307 nm. IR (ν cm^{-1}): 1744 (C=O str.).

3.7.3.3 Attempted preparation of sodium triethyltetraamine-N,N',N'',N'''-hexaacetatopalladium(II)rhodium(III) $Na_x[Pd_yRh_z(TTHA)]$

H_6TTHA (0.5 mmol, 0.2472 g), $RhCl_3.3H_2O$ (0.5 mmol, 0.13171 g), NaOH (3 cm^3, 1 mol dm^{-3}) and $K_2[PdCl_4]$ (0.5 mmol, 0.1633 g) were used.

Ethanol (*ca* 200 cm^3) was added to the solution, and a deep yellow precipitate resulted which was isolated by filtration and dried under vacuum. Attempts to crystallise from an ethanol/water mixture were unsuccessful.

Analysis: AAS metal concentration (ppm), found: Pd 8.06, Rh 1.67. Elemental, found: C 25.70, H 3.65, N 6.63 % which also corresponds to a calculated overall ratio of Rh : Pd of 1 : 4, which is in approximate agreement. MS[ESI^-], found (expected): m/z: (699.0) [$C_{18}H_{26}N_4O_{12}RhPd$] (m/z: 698.96 [$C_{18}H_{26}N_4O_{12}RhPd$] *i.e.* $[RhPd(TTHA)]^{1-}$). IR (ν cm^{-1}): 1690 (C=O str.).

3.7.3.4 Attempted preparation of sodium triethylenetetraamine-N,N',N'',N'''-hexaacetatocopper(II)rhodium(III), $Na_x[Rh_yCu_z(TTHA)]$

H_6TTHA (0.5 mmol, 0.2472 g), $RhCl_3.3H_2O$ (0.5 mmol, 0.1317 g), NaOH (3 cm^3, 1 mol dm^{-3}) and $Cu(NO_3)_2.2.5H_2O$ (0.5 mmol, 0.1163 g) were used.

To the resulting green solution was added ethanol (*ca* 200 cm^3) to form a dark green precipitate. The crystal suitable for X-ray structure analysis was obtained from aqueous solution of the complex after several weeks at room temperature. The unit cell analysis of the crystals corresponded to the data of the crystals of $[Rh_2Cl_2(TTHA)]^{2-}$ complex (with Na^+ cation) obtained from X-ray analysis are given in the Appendix A.

Analysis: AAS metal concentration (ppm), found 2.7 : 12.8, Rh : Cu. MS[ESI^-], found (expected), (mixture): m/z: 672.0 [$C_{18}H_{26}N_4O_{12}RhCuCl$]

(m/z: 671.99 [$C_{18}H_{26}N_4O_{12}RhCuCl$]; (crystal): m/z: 764.9 [$C_{18}H_{25}Cl_2N_4O_{12}Rh_2$](m/z: 763.8 [$C_{18}H_{25}Cl_2N_4O_{12}Rh_2$]); m/z: 381.9 [$C_9H_{12}ClN_2O_6Rh$] (m/z: 381.9 [$C_9H_{12}ClN_2O_6Rh$]). λ_{max}: 353 nm. IR (ν cm^{-1}): 1636 (C=O str.).

3.7.3.5 Attempted preparation of sodium triethylenetetraamine-N,N',N'',N'''-hexaacetatocobalt(II)rhodium(III), $Na_x[Rh_yCo_z(TTHA)]$

H_6TTHA (0.5 mmol, 0.247 g), $RhCl_3.3H_2O$ (0.5 mmol, 0.1317 g), NaOH (3 cm^3, 1 mol dm^{-3}) and $Co(NO_3)_2.6H_2O$ (0.5 mmol, 0.1455 g) were used.

To the resulting purple-coloured solution was added ethanol (*ca* 200 cm^3) to form in a deep purple precipitate. The crystal suitable for X-ray structure analysis was obtained from ethanol/water of the complex after several weeks at low temperature (5 °C). The data obtained for $[Rh_2Cl_2(TTHA)]^{2-}$ (with Na^+ cation) X-ray analysis are given in Appendix A.

Analysis: AAS metal concentration (ppm), found: Rh 2.16, Co 6.9. Elemental, found: C 23.76, H 4.28, N 6.37 % would correspond to a calculated overall ratio of Rh : Co of 2.15 : 1, if only Rh-Cl, Zn and TTHA were present. MS[ESI^-], found (expected): m/z: 668.0 [$C_{18}H_{26}N_4O_{13}RhCo$]$^{1-}$ (m/z: 667.99 [$C_{18}H_{26}N_4O_{13}RhCo$]$^{1-}$); crystal, m/z: 746.9 [$C_{18}H_{27}N_4O_{12}RhCoCl_2$] (m/z: 745.93 [$C_{18}H_{27}N_4O_{12}RhCoCl_2$]). λ_{max}: 357 nm. IR (ν cm^{-1}): 1636 cm^{-1} (C=O str.).

3.7.3.6 Preparation of triethyltetraamine-N,N′,N″,N‴-hexaacetatochromium(III)rhodium(III), [Rh_xCr_y(TTHA)]

H_6TTHA (0.5 mmol, 0.247 g), $Cr(NO_3)_3.9H_2O$ (0.5 mmol, 0.200 g) and $RhCl_3.3H_2O$ (0.5 mmol, 0.1317 g) were used.

To the resulting purple solution was added ethanol (*ca* 200 cm^3) to form a purple-coloured precipitate. The precipitate was filtered and dried under vacuum. Yield: 52.2% (0.261 mmol, 0.1678 g). On repetition of the reaction in order to confirm the crystallisation the yield of complex crystals found to be 0.1497 g (0.208 mmol, 42%). Crystals suitable for X-ray structure analysis were obtained from an aqueous solution of the complex after 3 weeks at room temperature. The data obtained from X-ray analysis of [$Cr_{1.50}Rh_{0.50}$(TTHA)] are given in the Appendix A.

Analysis: AAS metal concentration (ppm), found: Cr 10.93, Rh 2.92. Elemental, found: C 28.14, H 4.46, N 7.26 % would correspond to a calculated overall ratio of Rh : Cr of 1 : 7.3. MS[ESI^-], found (expected): m/z: 649.0 [$C_{18}H_{24}N_4O_{12}RhCr$] (m/z: 642.99 [$C_{18}H_{24}N_4O_{12}RhCr$]). λ_1: 371 nm, λ_2: 301 nm. IR (ν cm^{-1}): 1636 (C=O str.). XRD (single crystal) metal ratio, found (expected): 3 : 1, Cr : Rh (1 : 1 Cr : Rh).

3.7.3.7 Attempted preparation of sodium triethyltetraamine-N,N′,N″,N‴-hexaacetatochromium(III)palladium(II)

H_6TTHA (0.5 mmol, 0.2473 g), $Cr(NO_3)_3.9H_2O$ (0.5 mmol, 0.200 g), $K_2[PdCl_4]$ (0.5 mmol, 0.1633 g), NaOH (3 cm^3, 1 mol dm^{-3}) were used.

Addition of ethanol (*ca* 200 cm^3) to the purple-coloured solution gave a violet-coloured precipitate, which was filtered and dried under vacuum. Attempts to crystallise the solid from an ethanol/water mixture were unsuccessful.

Analysis: AAS metal concentration (ppm), found: Cr 6.29, Pd 15.25. Elemental, found: C 26.49, H 3.81, N 7.02 % corresponds to a calculated overall ratio of Cr : Pd of 1 : 2.5, which is in good agreement. MS[ESI^-], found (expected): m/z: 645.99 [$C_{18}H_{24}N_4O_{12}PdCr$] (m/z: 645.98 [$C_{18}H_{24}N_4O_{12}PdCr$]). IR ($\nu$ cm^{-1}): 1636 (C=O str.).

3.7.3.8 Attempted preparation of sodium triethyltetraamine-N,N′,N″,N‴-hexaacetatochromium(III)cobalt(II)

H_6TTHA (0.5 mmol, 0.247 g), $Cr(NO_3)_3.9H_2O$ (0.5 mmol, 0.200 g), NaOH (3 cm^3, 1 mol dm^{-3}) , $Co(NO_3)_2.6H_2O$ (0.5 mmol, 0.1455 g) were used.

Ethanol (*ca* 200 cm^3) was added to the solution, resulting in a purple precipitate, which was retrieved by filtration, and then dried under vacuum. The product was crystallised from the aqueous solution at low temperature (5 °C) after three months in the form of purple-coloured needles as

$[Cr_2(TTHA)(OH_2)_2]$. The details of the crystal structure are given in appendix A.

Analysis: AAS metal concentration (ppm), found (expected): Co 18.6, Cr 11.45. Elemental, found: C 29.21, H 4.38, N 7.76 % corresponds to a calculated overall ratio of Cr : Co of ~ 1 : 2, which is in good agreement. MS[ESI^-], found (expected) (crystal): m/z: 601.03 [$C_{18}H_{27}N_4O_{12}CrCo$] (m/z: 599.01 [$C_{18}H_{24}N_4O_{12}CrCo$]). IR ($\nu$ cm^{-1}): 1589 (C=O str.).

3.7.3.9 Attempted preparation of sodium triethyltetraamine-N,N',N'',N'''-hexaacetatonickel(II)palladium(II)

H_6TTHA (1.0 mmol, 0.495 g) in 30 cm^3, $Ni(NO_3)_2.6H_2O$ (1.0 mmol, 0.229 g) in 2 cm^3, NaOH (6 cm^3, 2 mol dm^{-3}) in 4 cm^3 and $K_2[PdCl_4]$ (1.0 mmol, 0.3264 g) in 2 cm^3 were used.

To the prepared solution was added ethanol (*ca* 200 cm^3), and a deep yellow precipitate resulted which was isolated by filtration and dried under vacuum. The precipitate was crystallised from ethanol/water mixture. The details of crystal structure of the $[Ni_2TTHA]^{2-}$ complex are given in the Appendix A.

Analysis: AAS metal concentration (ppm), found: Pd 34.32, Ni 12.46. Elemental, found: C 24.61, H 3.90, N 6.59 % corresponds to a calculated overall ratio of Ni : Pd of 1 : 3.4. MS[ESI^-], found (expected), (mixture): m/z: (655.0) [$C_{18}H_{24}N_4O_{12}NiPd$] (m/z: 653.99 [$C_{18}H_{26}N_4O_{12}NiPd$]); (crystal): m/z: 627.0 [$C_{18}H_{30}N_2Ni_4O_{13}$]. IR ($\nu$ cm^{-1}): 1589 (C=O str.).

3.7.3.10 Attempted preparation of sodium triethylenetetraamine-N,N′,N″,N‴-hexaacetatochromium(III)nickel(II)

H_6TTHA (0.5 mmol, 0.247 g), $Cr(NO_3)_3.9H_2O$ (0.5 mmol, 0.200 g), NaOH (3 cm^3, 1 mol dm^{-3}) and $Ni(NO_3)_2.6H_2O$ (0.5 mmol, 0.145 g) were employed.

To the resulted violet solution ethanol (*ca* 200 cm^3) was added which resulted in a violet precipitate. Crystals suitable for single crystal X-ray analysis was obtained from the aqueous solution of the mixture at reduced temperature (-5 °C). The detailed data of the crystals of $[Cr_2(TTHA)(OH_2)_2]$ are given in the Appendix A.

Analysis: AAS metal concentration (ppm), found: Cr 11.29, Ni 11.54. Elemental, found: C 28.63, H 4.50, N 7.43 % corresponds to a calculated overall ratio of Cr : Ni of 1 : 2.1. MS[ESI^-], found (expected), (mixture): m/z: 638.0 [$C_{18}H_{31}CrN_4O_{14}Ni$] (m/z: 637.06 [$C_{18}H_{31}CrN_4O_{14}Ni$]); (crystal): m/z: 627 [$C_{18}H_{28}N_4O_{14}Cr_2$]. IR ($\nu$ cm^{-1}): 1589 (C=O str.).

3.7.3.11 Attempted preparation of sodium triethylenetetraamine-N,N′,N″,N‴-hexaacetatocobalt(II)nickel(II)

H_6TTHA (0.5 mmol, 0.247 g), $Ni(NO_3)_2.6H_2O$ (0.5 mmol, 0.145 g), NaOH (3 cm^3, 1 mol dm^{-3}) and $Co(NO_3)_2.6H_2O$ (0.5 mmol, 0.145 g) were used.

To the mixture was added ethanol (*ca* 200 cm^3). The grey-coloured precipitate was filtered and dried under vacuum. The precipitate was re-

dissolved in water and colourless, needle-shaped crystals were obtained by diffusion of ethanol into the water. The data of the single crystal X-ray diffraction analysis for $[Ni_2TTHA]^{2-}$ are given in the Appendix A.

Analysis: AAS metal concentration (ppm), found: Co 12.02, Ni 15.1. Elemental, found: C 24.82, H 4.59, N 6.33 % corresponds to a calculated overall ratio of Co : Ni of 1 : 1.25. MS[ESI^-], found (expected), (mixture): m/z: 607.0 [$C_{18}H_{26}N_4O_{12}NiCo$] (m/z: 607.02 [$C_{18}H_{26}N_4O_{12}NiCo$]); (crystal): m/z: 606.0181[$C_{18}H_{25}CoN_4NiO_{12}$] . IR ($\nu$ cm^{-1}) 1585 (C=O str.).

3.7.4 Synthesis of $(PPh_4)_x[MM'(TTHA)]$ complexes

General

The method of preparation is similar to the general method of preparation mentioned earlier in section 3.7.3. However, in these preparations an additional step of adding an aqueous solution of $(PPh_4)Cl$ (3.0 mmol,′x′ g) after the NaOH addition and stirring was completed. The amount of $(PPh_4)Cl$ is equal to that of NaOH (*i.e.* 3.0 mmol) added to the contents of the mixture initially. The contents were again stirred for 30 min. The rest of the procedure is mentioned in section 3.7.3. The crystallisation details are mentioned in each complex preparation given in the subheadings below. The yields given in each section correspond to the respective complex in the subheadings.

3.7.4.1 Preparation of tetraphenylphosphonium triethytetraamine-N,N′,N″,N‴-hexaacetatorhodium(III), $(PPh_4)_2[Rh_2(TTHA)]$

H_6TTHA (0.5 mmol, 0.247 g), $RhCl_3.3H_2O$ (0.5 mmol, 0.1317 g), NaOH (3 cm^3, 1 mol dm^{-3}) and $(PPh_4)Cl$ (3.0 mmol, 1.123 g) were used.

To the yellow solution was added ethanol (*ca* 200 cm^3) resulting a light-yellow precipitate. The precipitate was crystallised from water as light yellow-coloured needles. The data of the single crystal X-ray analysis for $(PPh_4)_2[Rh_2(TTHA)Cl_2]\cdot 9H_2O$ are given in the appendix. Yield: 0.82 %.

Analysis: Elemental, found (expected) (crystals): C 48.31, H 4.27, N 2.53 % (C 48.27, H 5.28, N 3.41 %). MS[ESI^-], found (expected): (mixture) m/z: 593.1[$C_{18}H_{26}N_4O_{12}Rh$] (m/z: 593.06 [$C_{18}H_{26}N_4O_{12}Rh$]); (crystal): m/z: 785.2 [$C_{18}H_{29}Cl_2N_4O_{13}Rh_2$].

3.7.4.2 Preparation of tetraphenylphosphonium triethytetraamine-N,N′,N″,N‴-hexaacetatoplatinum(II), $(PPh_4)_2[Pt_2(TTHA)]$

$K_2[PtCl_4]$ (0.415 g, 1.0 mmol), H_6TTHA (0.2472 g, 0.5 mmol), NaOH (3 cm^3, 1 mol dm^{-3}) PPh_4Cl (1.123 g, 3.0 mmol) were used.

A solution of H_6TTHA (0.2472 g, 0.5 mmol) was prepared by dissolving in water (15 cm^3, 100 °C). To this solution was added $K_2[PtCl_4]$ (0.415 g, 1.0 mmol, 2 mol. eq.), in water (6 cm^3). Then, the contents were stirred at room temperature overnight (16 h). To the resulting solution was added another solution of NaOH in water (3.0 cm^3), stirred for 30 min. Thereafter, a

solution of PPh_4Cl (1.123 g, 3.0 mmol) in water (6 cm^3) was added, resulting in a light-yellow precipitate, which was filtered and dried under vacuum. Yield: 0.69 g. The precipitate was crystallised from CH_2Cl_2 after drying the halogenated layer over Na_2SO_4 at room temperature. After one week, yellow needles of the complex ($(PPh_4)_2[PtCl_4]$) resulted. The single crystal data are given in the appendix.

Analysis: Elemental, found (expected): C 55.63, H 3.93 % (C 55.76, H 3.97 %). MS[ESI^-], found (expected): m/z: 879.1 [$C_{18}H_{25}N_4O_{12}Pt_2$] (m/z: 879.08 [$C_{18}H_{25}N_4O_{12}Pt_2$]).

Chapter 4
Mixed-Metal Silicas

4.1 Introduction

4.1.1 True Liquid Crystal Templating and Nanoparticle Functionalised Mesopores

The TLCT technique was introduced by Attard *et al.*,[1] who described the formation of lyotropic liquid-crystalline phases at the high concentrations of surfactants, that are used as templates in the synthesis of mesoporous silicas (Chapter 1, section 1.5.3). They also demonstrated a methodology to introduce metal particles *e.g.* Sn[2] and Pt,[3] to the mesoporous domains by the reduction (either by a chemical[3] route or by electrodeposition[2]) of metal salts dissolved in an aqueous liquid-crystalline phase (H_1, hexagonal) of oligoethylene oxide surfactants such as $C_{16}(EO)_8$. Later, this group also demonstrated the use of the same methodology by employing a different non-ionic surfactant $C_{18}(EO)_{10}$, highlighting the possibility to incorporate alloyed Pt-Ru nanoparticles into an inorganic framework.[4] In the above examples, the liquid-crystalline phase of the oligoethylene oxide surfactants was attained from a 50% w/w mixture of water and surfactant, and the concentration of the metal precursor was usually kept low in order to maintain the liquid-crystalline behaviour of the system. They also demonstrated the applicability of such materials in electrochemical sensor devices and used the same non-ionic surfactants with hexachloroplatinic acid to prepare mesoporous thin films[5] *via* electroplating.

Stupp and co-workers used a similar approach in the preparation of different nanoscale semiconducting superlattices such as CdS,[6] CdSe,[6] ZnS,[6] and $CaPO_4$.[7] Their work used an organic precursor acting as a template, which

was usually an oligoethylene oxide, which then assisted the synthesis of a periodically nanostructured inorganic framework that replicated the symmetry as well as the dimensionality of the template used. Their methodology was also known as a *direct approach*.

Dag and co-workers, introduced metal particles (*e.g.* Li)[8] through a 'one-pot synthesis' of the silica framework using TLCT. Later, they used transition metal aqua complexes $[M(OH_2)_n]X_2$ (where M is a transition metal (first- or second- row); X is NO_3^-, Cl^-, or ClO_4^-) and a non-ionic surfactant ($C_{12}EO_{10}$, $C_{12}H_{25}(CH_2CH_2O)_{10}OH$).[9,10,11]. From this technique, they successfully illustrated the direct formation of liquid-crystalline phases of nitrate metal salts in the presence as well as absence of water. The hypothesis behind the formation of such liquid-crystalline phases is explained below.

The formation of liquid crystalline phases as per the results obtained can be explained on the basis of interactions involved in the salt-surfactant system. In a salt-surfactant system, ligand exchange reactions are observed between coordinated water molecules and the counter anions. This ligand exchange reaction in turn influences the ionic strength of the liquid-crystalline medium as well as affecting the solubility of the surfactant and the counter ion. To explain this, the Hofmeister series[12] for anions influencing surfactants is of considerable importance.[13,14]

$$SO_4^{2-} > HPO_4^{2-} > CrO_4^- > CO_3^{2-} > Cl^- > Br^- > NO_3^- > I^- > ClO_4^- > SCN^-$$

(Hydrotropic) (Lyotropic)

The anions to the left make the surfactant hydrophobic, hence a reduction in the solubility of the salts is observed in the salt-surfactant medium. This reduced solubility is due to the weak interaction of the surfactants and the anions observed hence, anions on the left are also termed 'hydrotropic'. However, an opposite behaviour, *i.e.* stronger interactions, is observed for the anions on the right or lyotropic part. In other words, when the interactions between the anion and the metal part increase, then the ionic strength of the medium decreases. This decrease in ionic strength in turn reduces the number of ions in the system. On the other hand, if the ionic strength is increased along with the charge density, then the salt-surfactant system experiences phase separation as crystallisation. This explains the solubility of nitrate salts in metal aqueous complexes in non-ionic surfactants. However, chlorides and sulfates were observed as insoluble. An exception to the solubility of nitrates was $AgNO_3$, which was also observed by Dag and co-workers, in an attempt to prepare a LC phase in the absence of water or less water with non-ionic surfactant.[15] This unexpected behaviour was explained by of loss of coordinated water molecule (to the silver ion) on evaporation of the mixture of silver-containing LC phase, giving rise to free silver ions, which crystallised out as the complex $[Ag(C_{12}EO_{10})_x](NO_3)$. The latter was formed due to interactions between the free Ag^+ ion and EO head groups.

From the above results Dag proved that the presence of coordinate water molecules is important for the process of self assembly. Also, the interactions between ions and the surfactant play a lead role and hence affect liquid crystalline-phase formation.

Later, Dag used the TLCT approach to synthesise mesoporous silicas containing noble metal particles[16] *i.e.* Ag, Au and Pt from $AgNO_3$, $H[AuCl_4]$ and $H_2[PtCl_6]$, respectively. In the preparation, $C_{12}EO_{10}$ and TMOS were used as non-ionic surfactant and silica precursor, respectively. Their preparation successfully produced silicas doped with well-dispersed nanoparticles over the inorganic framework. The effect of the anion was not considered in this work. The low-angle X-ray diffraction data showed the absence of well-defined, long-range pore order, expected due to the presence of high acidity in the medium. Thus, it is known that acidic conditions are essential for a particular mesophase formation[17] but extremely high acidic conditions result in rapid condensation of silica. This also affects the mesophase as the silica formation occurs earlier than the reformation of mesophase by methanol removal *via* evacuation, causing deformities such as mechanical instability, ill-defined pore structure, and thicker walls. Nonetheless, the resulting mesoporous silicas successfully led to nanoparticles of Pt (2-3 nm) and Ag (up to 6 nm), observed by TEM. However, the Au nanoparticles formed grew bigger in size (20 nm) during the process of reduction.

Thereafter, King in this research group modified Dag's approach and used chloridometallate anions or anionic EDTA complexes of Group 1 metal salts of different metals to prepare metal-containing silicas. The methodology used $C_{12}EO_8$ as template, TMOS as silicate precursor and aqueous acid (pH 2) to dissolve the metal precursors to make the mesophase. Their approach successfully produced metal-doped silicas of Pd, Pt, Rh, Re, Ru, Ir, and Au,[18,19] from $A_z[MCl_y]$, M = transition metal and A = K^+ or Na^+ (for Ir) exhibiting uniform silica pores. For first-row metals, where chloridometallate

anions readily hydrolyse, mononuclear metal complexes of EDTA (Na_z[MEDTA], where M is transition metal) were used instead.

Using the same approach, silicas doped with bimetallic nanoparticles were prepared starting from mixture of chloridometallate and/or EDTA anions. The methodology proved successful and well-dispered bimetallic nanoparticles of Pd-Au, Pt-Co, and Pd-Ru, were observed within well-defined mesopores.[20] Nevertheless, in several cases the particles obtained were large in size and not present within the mesopores.

Furthermore, when one of the silicas (Pt-Co) was analysed previously by King[20] through EDX analysis, it was found that the selected molar ratio used in the starting preparation was reproducible. However, on averaging over the whole sample of the selected silica (Pt-Co), a very wide range of compositions was found, when the individual nanoparticles were being analysed. This was expected to have occurred due to the use of two different metal precursors as the metal source. Hence, to try to overcome this, it was decided to target the use of single-source, bimetallic precursors which would hopefully lead to greater homogeneity in particle composition.

Therefore, the focus of this chapter will be the generation of mesoporous silicas doped with mixed-metal nanoparticles by the use of heterobimetallic complexes of the TTHA ligand discussed in Chapter 3.

Unfortunately, the preparation of these heterobimetallic complexes was not as successful as had been hoped. However, despite the fact that the complexes turned out not to have well-defined compositions, it was nonetheless decided to work with them as sources of metals in order to evaluate the possibility of

using such complexes. In each case, four preparations were carried out, first used the solution of the two metals with TTHA resulting from the attempted preparation of the heterobimetallic complex. Then, the preparation was repeated using two discrete precursor complexes together. Finally, two preparations were carried out- one each using the separate metal precursor.

4.1.2 Methods of Characterisation Used in the Study

4.1.2.1 Polarised Optical Microscopy

The technique most commonly used to identify liquid-crystalline phases is *Polarised Optical Microscopy* (POM); it is the most convenient and easy way to identify phases. Generally, all liquid-crystalline mesophases are birefringent except the cubic phase. Hence, their first identification is based on the presence of birefringence under the optical microscope. The birefringence originates from the difference between the different components of the refractive index of anisotropic substances. When passed through an anisotropic substance and after interacting with it, polarised light gives rise to two different refractive indices *i.e.* perpendicular ($n_{\perp}$) and parallel ($n_{\parallel}$), to the direction. The birefringence, Δn, is given by

$$\Delta n = n_{\parallel} - n_{\perp} \qquad (1)$$

To analyse this birefringence, a small amount of sample is placed on a cover slip or slide under the objective lens of the microscope and then covered by another cover slip. The polariser and the analysers are adjusted orthogonal to each other as shown in **Fig. 4.1**.

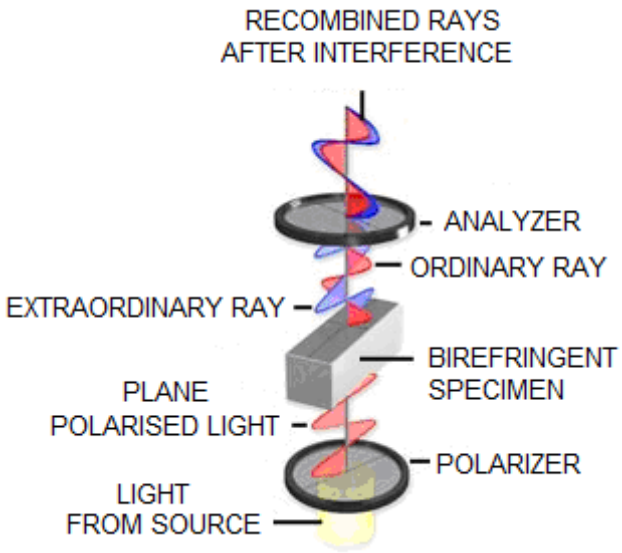

Fig.4.1 Configuration of a working polarised optical microscope[21]

The plane polarised light interacts with the sample in the mesophase producing birefringence. Thus, the two rays interfere, plane polarization is lost, and an interference pattern is seen through the analyser. That recombined resultant pattern is then observed through the eye piece (binoculars) giving an optical texture. **Fig. 4.2.** shows the texture of the normal hexagonal phase (H_1) observed for $C_{12}EO_{10}$ and water (1 : 1) mixture as seen under the optical microscope.

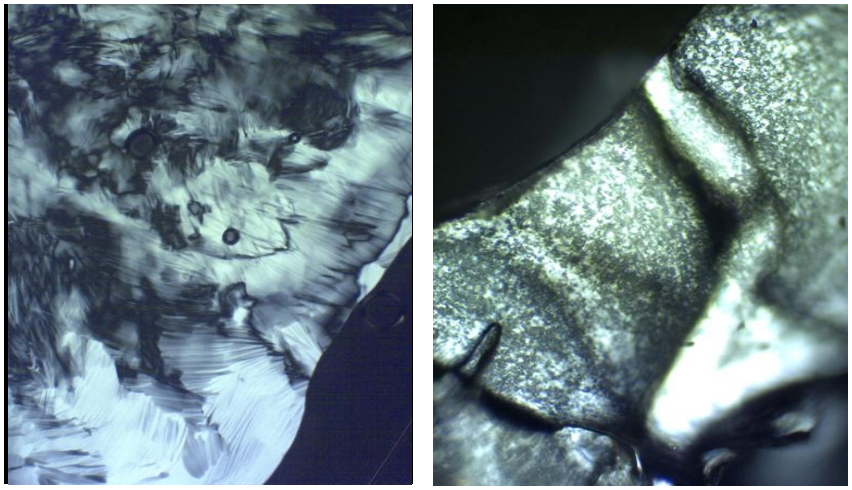

A **B**

Fig. 4.2 Fan like texture of the normal hexagonal (H_1) lyotropic liquid crystalline phase of $C_{12}EO_{10}$ in **A** after removal of MeOH; **B** in monolith after completion of sol-gel condensation.

4.1.2.2 Brunauer, Emmett, and Teller (BET)[22,23] Adsorption Measurement

The BET method is based on physical adsorption of gases on the internal and external surfaces of a porous solid. The material to be analysed is surrounded by, and is in equilibrium with, a gas (N_2/ Kr/ O_2/ He/ methane), which has a relative vapour pressure (p/p_0). The material adsorbs a certain amount of gas, which is proportional to the internal as well as the external surface of the porous solid but is also dependent on p/p_0. The measurement is carried out with varying pressures at low temperature and by the application of vacuum. The nature of the adsorption-desorption curve produced is dependent on the interactions between adsorbate and adsorbent. The adsorption isotherms have been divided into six types by IUPAC Types I-VI (**Fig. 4.3)**,[22] and the first five correspond with the classification of Brunauer.[23] The BET method can be used for the surface area identification of isotherm types, II (*e.g.* non-porous materials), IV (*e.g.* mesoporous

materials) and VI (*e.g.* uniform solids). However, the method is not suitable for solids displaying type I (*e.g.* microporous adsorbents such as zeolites and carbon), type III (*e.g.* graphitised carbon) and type V (*e.g.* macroporous solids, mesoporous solids with interconnected pores) isotherms due to the comparatively weak interactions between adsorbate and adsorbent.

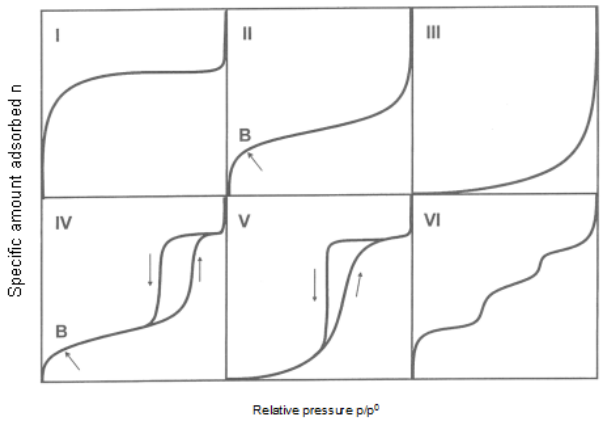

Fig. 4.3 Adsorption isotherms (I-VI) as per IUPAC classification[24]

The equation (2) governing the BET process is:

$$\frac{p}{v(p_0 - p)} = \frac{1}{v_m c} + \frac{c-1}{v_m c}\frac{p}{p_0} \qquad (2)$$

where v is the volume of gas adsorbed; c is the BET constant, dependent on isotherm shape; p is the pressure of adsorbate at equilibrium; p_0 is the pressure of adsorbate at saturation; v_m is the volume of monolayer gas adsorbed.

From the BET equation, a linear relationship is obtained from the plot of $p/v(p_0\text{-}p)$ against p/p_0 *i.e.* the BET plot. From this plot, v_m can be obtained

which is then used in the next step as the surface area can be calculated from equation (3):[25]

$$S = n_{mono}\, v_m \, \mathrm{N} \qquad (3)$$

where S is the surface area ($m^2\ g^{-1}$), n is monolayer capacity (mol g^{-1}), v_m volume of monolayer gas adsorbed and N is Avogadro's number (molecules per mol). The area occupied by N_2 = 0.162 nm^2/molecule.

This surface area measurement technique can also be used for determining pore size and pore volume quantitatively. The sample required for the surface area determination by BET is approximately 100 mg or more. If the amount of the sample is less than this, then precise results cannot be expected due to the limitation of the instrument. The samples have to be degassed before introducing them to the measurement ports for a minimum of 6 h under an inert atmosphere (N_2) at a set temperature (*e.g.* 150 °C for doped SiO_2). The degassing removes gases adsorbed at the surface of the material or within the pores at room temperature. The temperature used for degassing the porous solids may vary depending upon the stability of sample.

The BET isotherm for a mesoporous solid is shown in **Fig. 4.4**. In this figure, **A** is a rounded part, which illustrates monolayer formation, **C** is the hysteresis region which depicts capillary condensation in the mesopores and **B** is the saturation point used for calculation of the total pore volume. The adsorption part of the isotherm corresponds to multilayer formation however, desorption relates with meniscus formation.

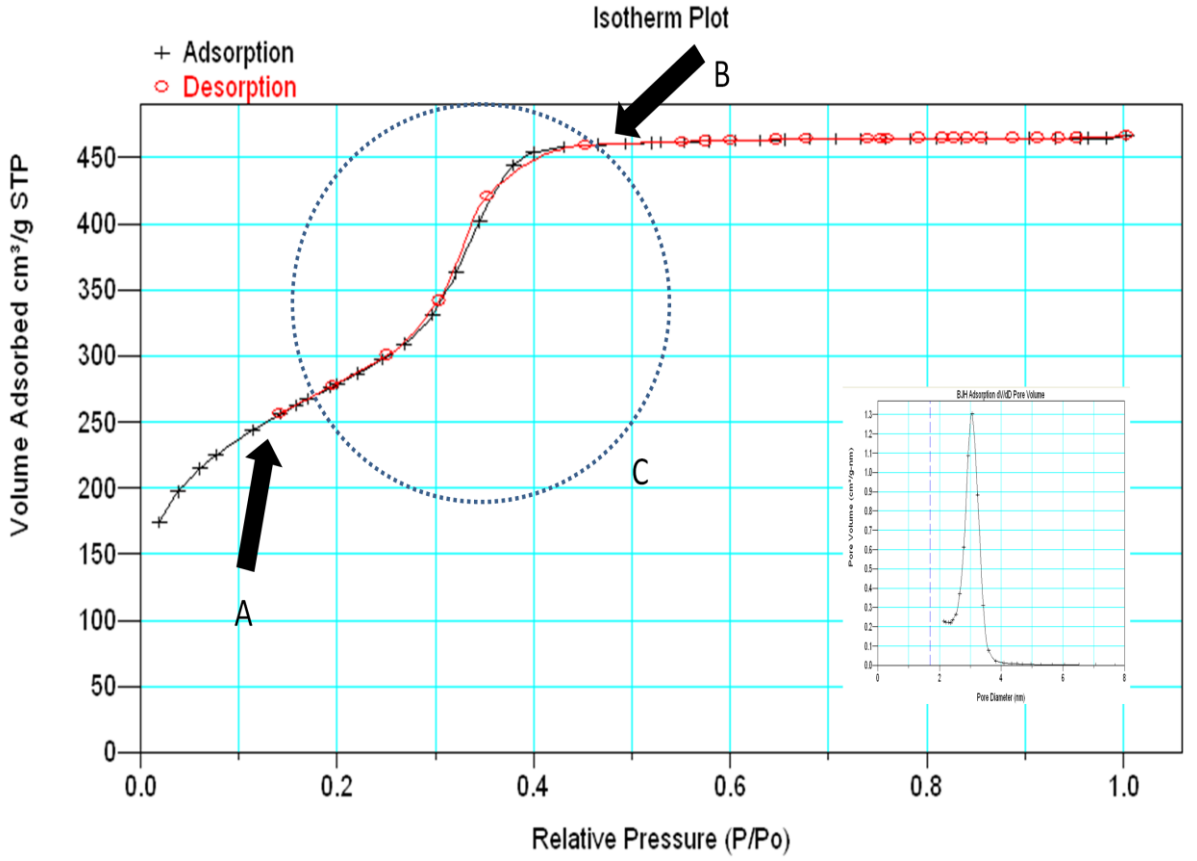

Fig. 4.4 Adsorption (black) - desorption (red) isotherm for a mesoporous solid prepared from $C_{12}EO_{10}/H_2O$/TMOS with pore diameter obtained *via* BJH adsorption.

The nature of the porosity of the material can be identified from the capillary condensation at a medium relative pressure (p/p^0).[26] However, the presence or absence of hysteresis identifies the nature of pores in the porous solid. If the N_2 adsorption/desorption curves show no hysteresis (as shown **Fig. 4.4**) it indicates that the pores formed are highly uniform in size during desorption.

The N_2 adsorption data are used further to obtain the size distribution of the mesopores by employing computational procedures which involve the Barret-Joyner-Halenda (BJH) method (**Fig. 4.4**). The basis of this procedure involves conceptual emptying of mesopores by stepwise reduction of p/p^0, thereby thinning of the multilayer in the pores which have been already vacated by the condensate. It has been assumed that the pore morphology controls the meniscus curvature, the pores are rigid within the mesopore range and the pore blocking effects are completely absent. Moreover, the pore size distribution is dependent on the branch of adsorption-desorption hysteresis loop used for computation. The BJH method uses the Kelvin equation[27] (equation 4) for the calculations.

$$ln\frac{p}{p_0} = \frac{2\gamma V_m}{\gamma RT} \qquad (4)$$

where γ is the surface tension; R is the universal gas constant; V_m, p and p_0 are the same parameters found in the BET equation.

The surface area of an undoped silica prepared *via* TLCT from TMOS and $C_{12}EO_{10}$ (template) is typically around 1000 $m^2\ g^{-1}$ with an average pore volume and pore diameter of 0.72 $cm^3\ g^{-1}$ and 2.87 nm, respectively.

4.1.2.3 X-ray Diffraction (XRD)

This is a widely used technique for the quantitative estimation of porous solids. The instrument consists of an X-ray generator with radiation sources mostly Mo or CuK_α, a slit (range 0.01 to 2 mm), a sample holder, a detector and an analyser, connected to the computer.

The X-ray beams of suitable wavelength (CuK_α = 0.154 nm) with a definite intensity are used for the characterisation of the mesoporous solids by diffraction. The mesoporous silicas are amorphous and they do not tend to show peaks corresponding to the silica. However, the peaks seen reflect the organised array of pores with a specific diameter in a particular nanometer range. In other words, the difference in the electron density of the pore walls and the vacant pores produce such reflections.[28] Hence, the data collected are used to identify and confirm the pore distribution and the crystalline nature of the inorganic framework. **Fig. 4.5** illustrates the formation of a silica template on the H_1 hexagonal phase obtained by the use of a 1 : 1 : 2 ratio of surfactant ($C_{12}EO_{10}$), water (pH 2) and silicate precursor (TMOS), respectively.

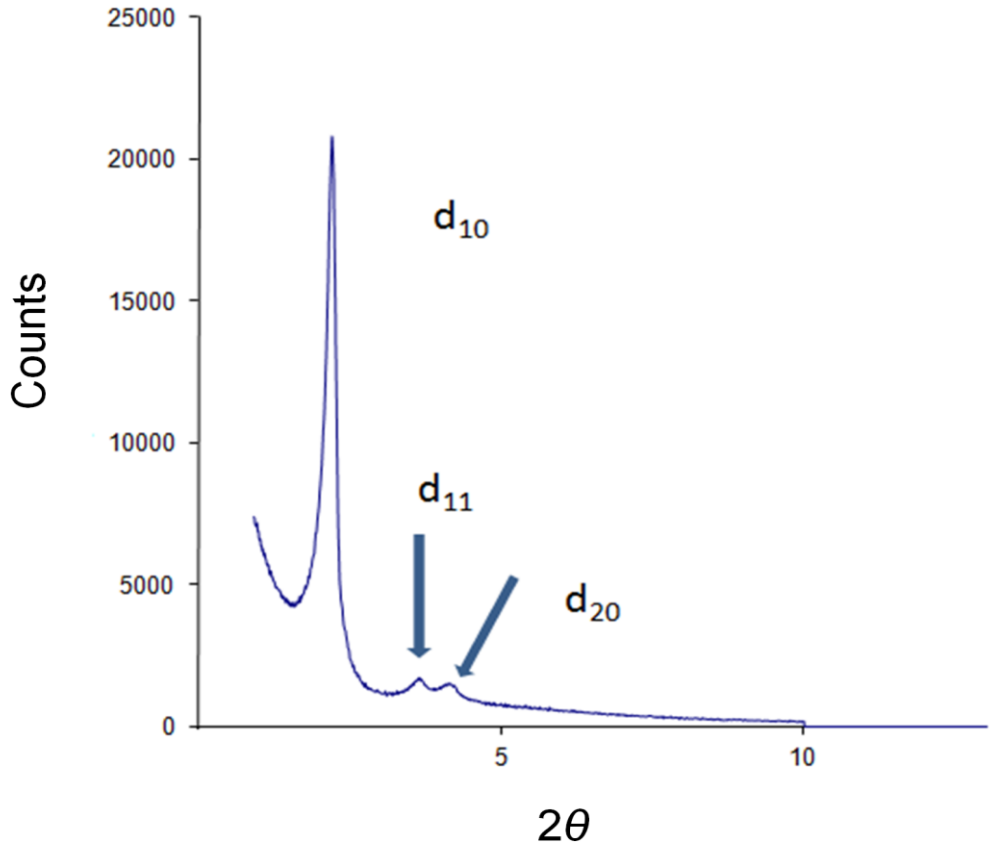

Fig. 4.5 Small-angle X-ray diffraction pattern showing diffraction lines observed for a silica with hexagonal pore distribution.

The diffraction peaks are assigned on the basis of Miller indices which are different for different unit cells. In the current silica framework, the Miller indices correspond to the parameters of a 2D hexagonal unit cell (**Fig. 4.6**). The parameters involved are *hk0* (as its two dimensional) and the resulting diffraction pattern (**Fig. 4.5**), represents well-resolved diffraction lines that can be indexed to d_{10}, d_{11}, and d_{20}, of 2D hexagonal lattices (**Fig. 4.6**). On analysing the samples containing metal nanoparticles at high-angle, sharp and well-defined peaks are produced, which correspond to crystalline nanoparticles incorporated within the silica framework.

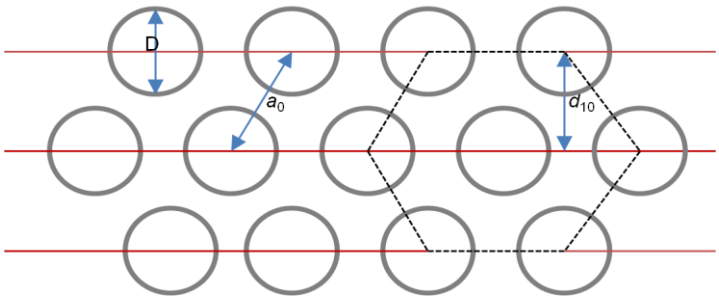

Fig. 4.6 Characteristic packing of hexagonal array of pores in a mesporous solid.

From the X-ray diffraction data, the *d* value corresponding to the periodicity can be calculated from peak positions at the respective angle, 2θ by using Bragg's Law of Diffraction:

$$n\lambda = 2d \sin\theta \qquad (5)$$

where, *n* is the integer, λ is the wavelength (nm), *d* is the distance between the lattice planes, θ is the diffraction angle (Bragg's angle). The lattice parameter (a_0) that is distance between the two mesopores (**Fig. 4.6**) can be calculated by using equation (6).

$$a_0 = \frac{2d_{10}}{\sqrt{3}} \qquad (6)$$

The relative peak positions of a hexagonal unit cell can be calculated from equation (7). However, relative peak positions of different peaks for a 2D hexagonal phase are given in **Table IV.I**.

$$\frac{1}{d_{hk^2}} = \frac{4}{3a^2}(h^2 + k^2 + hk) \qquad (7)$$

Table IV.I relative peak positions of reflections of the 2D hexagonal lattice

Relative values of 1/d	*hkl*
1	10
√3	11
√4	20
√7	21
√9	22

From the lattice parameter calculated from equation (6), the wall thickness (*t*) can be obtained from equation (8).

$$t = D - a_0 \qquad (8)$$

where *D* is the pore diameter (BET data), and a_0 is the lattice parameter.

The size of the crystallite or the crystalline nanoparticles can be calculated from a high-angle XRD *via* the Scherrer formula[29,30] (equation (9)).

$$t = \frac{\mathrm{K} \times \lambda}{B \cos \theta_B} \qquad (9)$$

where, t = thickness of the particle; K = Scherrer constant, dependent on crystallite shape, 0.89; λ = X-ray wavelength; B = integral breadth or full width at half max (FWHM); θ_B = Bragg's angle (equation (5)).

However, B can be calculated as the difference in the angles at half maximum as shown below in equation (10). The values of B can be obtained from high-angle X-ray diffraction of the sample as shown in **Fig. 4.7**. The

width of the peak may vary from broad to fine lines as it is dependent on the size of the particle. It has been observed that the broader the peak the smaller will be the size of the particle. It should be noted that the Scherrer equation can only give an average size of the particles present. However, it cannot be used to calculate size of the particles if they are amorphous or are too small.

$$B = 2\theta_{high} - 2\theta_{low} \qquad (10)$$

The peaks of the crystallite obtained from the high angle X-ray diffraction method were identified *via* peak matching. Peak matching is carried out by using the raw data in a software (*i.e.* EVA or Match 2), which then compares them with the peaks of metals or metal mixtures or its different forms such as oxides or hydroxides *etc.* that have been reported in the literature, which may or may not be in a particular shape *e.g.* cubic, hexagonal *etc.* The same technique has been used throughout the data sets reported in the current work for comparison details in the discussion section of this chapter.

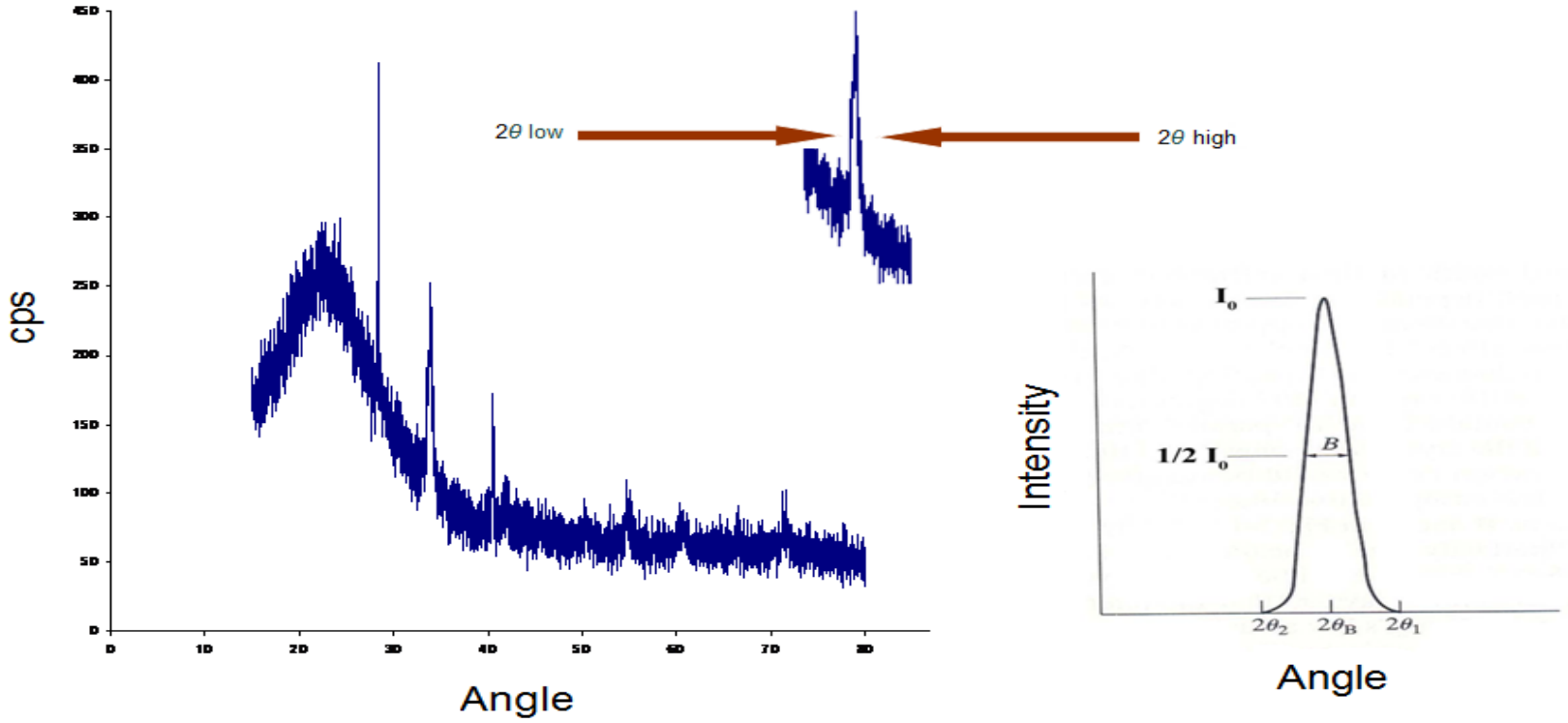

Fig. 4.7 High-angle X-ray diffraction pattern of Pd-doped mesoporous solid.

4.1.2.4 Transmission Electron Microscopy (TEM)

Transmission Electron Microscopy is a well-known technique used for the atomic-level resolution of the solids *via* imaging. The principle of this technique involves an accelerated electron beam (under high potential, range 100 to 1000 kV) (anode), which is passed through different condenser lenses (I and II) and strikes the sample. The transmitted electrons are detected by the detectors mounted behind the sample through a thin section (< 100 nm), resulting in the formation of an image commonly known as an *electron micrograph* (**Fig. 4.9**). The components of the instrument are shown in **Fig. 4.8**.

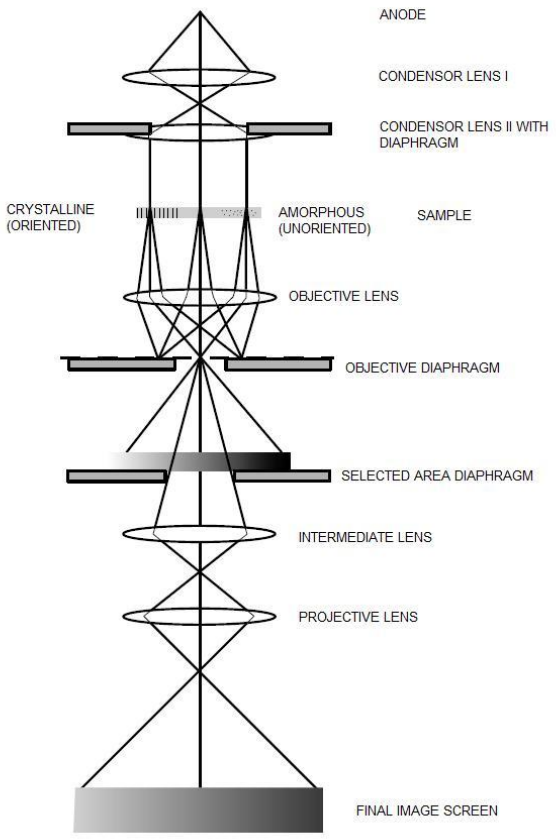

Fig. 4.8 Working of transmission electron microscope (TEM) in light mode.[31]

The aim of the objective diaphragm is to assist the selection of the transmitted beam, the intermediate lens helps to avoid lens aberration and the projective lens projects the final image produced on the screen. The objective diaphragm also helps to obtain a well contrasted image. This technique can be used at different angles *i.e.* horizontally as well vertically and therefore it alleviates the identification of the size and the shape of the pores from different angles.[32]. The micrographs can display the presence of various metal particles of different sizes. The technique in conjugation with EDX can also identify the comparative ratios of the metals involved in such materials.[19] The results obtained from the TEM can be used to substantiate and complement the results obtained from BET and SAXS analysis.

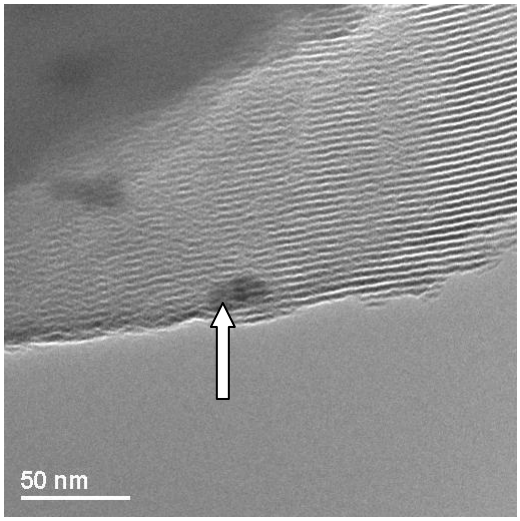

Fig. 4.9 TEM image showing wide, parallel pores with incorporated metal particle highlighted with an arrow.

4.2 Mixed-Metal Silica Synthesis and Characterisation

4.2.1 Using Bimetallic Metal Precursors

Mesophases were prepared by making a 50% w/v mixture of surfactant and acidified stock solution of the mixed-metal complex (Rh-Ni, Rh-Pd or Cr-Pd), according to the method described in the experimental section (§ 3.7.3). The metal ratios present in these solutions were determined by atomic absorption measurements and issues regarding these and also the precise composition in terms of metal/ligand ratios are discussed in Chapter 3. To this end and to simplify presentation, only the metal ratio will be given in regard of each preparation described. In the preparation, the mixture was heated gently, resulting in the formation of a hexagonal H_1 phase, characterised by optical microscopy. To the resulting phase was added the silica precursor, TMOS, and the whole sample was mixed again by gentle heating of the contents resulting in an alcohol by-product *i.e.* MeOH due to hydrolysis of the TMOS. The by-product was removed instantaneously by the application of gentle, dynamic vacuum so as to reform the viscous, birefringent H_1 phase (re-analysed by optical microscopy). The evolution of methanol was observed as bubbles and usually ended when the alcohol was removed completely from the mixture, resulting in a viscous gel. The gel was left at room temperature for 2 days to allow the sol-gel condensation to proceed, resulting in a coloured, translucent monolith. This was then calcined at 400 °C, (1 h under N_2 followed by air for 5 h) to remove the organic part of the template so as to obtain a solid silica with well-defined pores and crystalline nanoparticles. The resulting dark-coloured solid was characterised by BET surface area analysis,

XRD (low- and high- angle), and TEM for characteristics of mesopores and metal particles.

The mesophases prepared from the bimetallic stock solutions of Rh-Ni, Cr-Pd and Rh-Pd did not show any signs of metal leeching, as large crystalline metal particles were not observed during phase formation or on completion. Also, none of them showed any signs of decomposition or change in colouration of the solidifying viscous layer during and after sol-gel condensation or before subjecting them to calcination. A significantly different colour change was observed for each of them after calcinations as noted below.

To obtain the mixed-metal doped silicas, a bimetallic mixture of Rh-Ni that had ratio 1 : 4, was selected for use. Higher loadings of the stock solution led to precipitation of the metal precursor as observed by POM during the mesophase formation. It is important to mention that the preparation of the mixed-metal silicas described in the current chapter illustrates an attempt to synthesise mixed-metal silicas from the bimetallic mixtures. However, we were aware of the fact that it is unlikely that uniform and truly bimetallic nanoparticles would result from such bimetallic mixtures as they are likely a mixture of homo- and hetero- dinuclear complexes.

4.2.1.1 Cr-Pd

Borgna *et al*.[33] were the first to report a Cr-Pd catalyst on a SiO_2 support, chosen for its unique selectivity towards hydrogenation of symmetric alkenes. For instance, 1,3-butadienes were analysed for partial hydrogenation to form alkenes on a Cr-Pd/SiO_2 catalyst and, in spite of showing excellent selectivity, their activity was found to be extremely low. Later, a Cr-Pd catalyst on HY-Al_2O_3[34] was investigated thoroughly for its ability of being resistant to sulfur poisoning in the hydrogenation of aromatic hydrocarbons *i.e.* in the petroleum refining process. Soon after, the same bimetallic catalyst was also studied on different supports *e.g.* Al_2O_3 and (Ce,Zr)O_2/Al_2O_3 (mixed support)[35], for its influence on CO and NO elimination from Cr-Pd catalyst in different reactions. All the reported examples exhibited a catalytic role of Cr-Pd bimetallic nanoparticles in different chemical reactions. However, the methods of preparation involved in almost each of them were post-synthetic impregnation, which used salts of the two metals to dope 'off-the-shelf' support materials. Conversely, in the current work, a completely different methodology has been used in an attempt to synthesise Cr-Pd bimetallic nanoparticles *in situ* which are of truly bimetallic nature. The particles formed were then compared with Cr-Pd particles synthesised by following King's method of preparation using separate metal precursors.[20]

In this work, the silica was synthesised from a stock solution of bimetallic mixture, that had a metallic ratio of 2.33 : 1 of Pd : Cr. The appearance of liquid-crystalline phase was a homogenous brownish purple, while the

colour of silica after calcination was fawn. The data obtained by BET surface area analysis are given in **Table IV.II**. The characterisation showed the presence of well-defined diffraction peaks corresponding to d_{10}, d_{11} and d_{20} reflections, which indicate well-defined pores (**Fig. 4.10**), which were further characterised by TEM (**Fig. 4.12 A** and **B**).

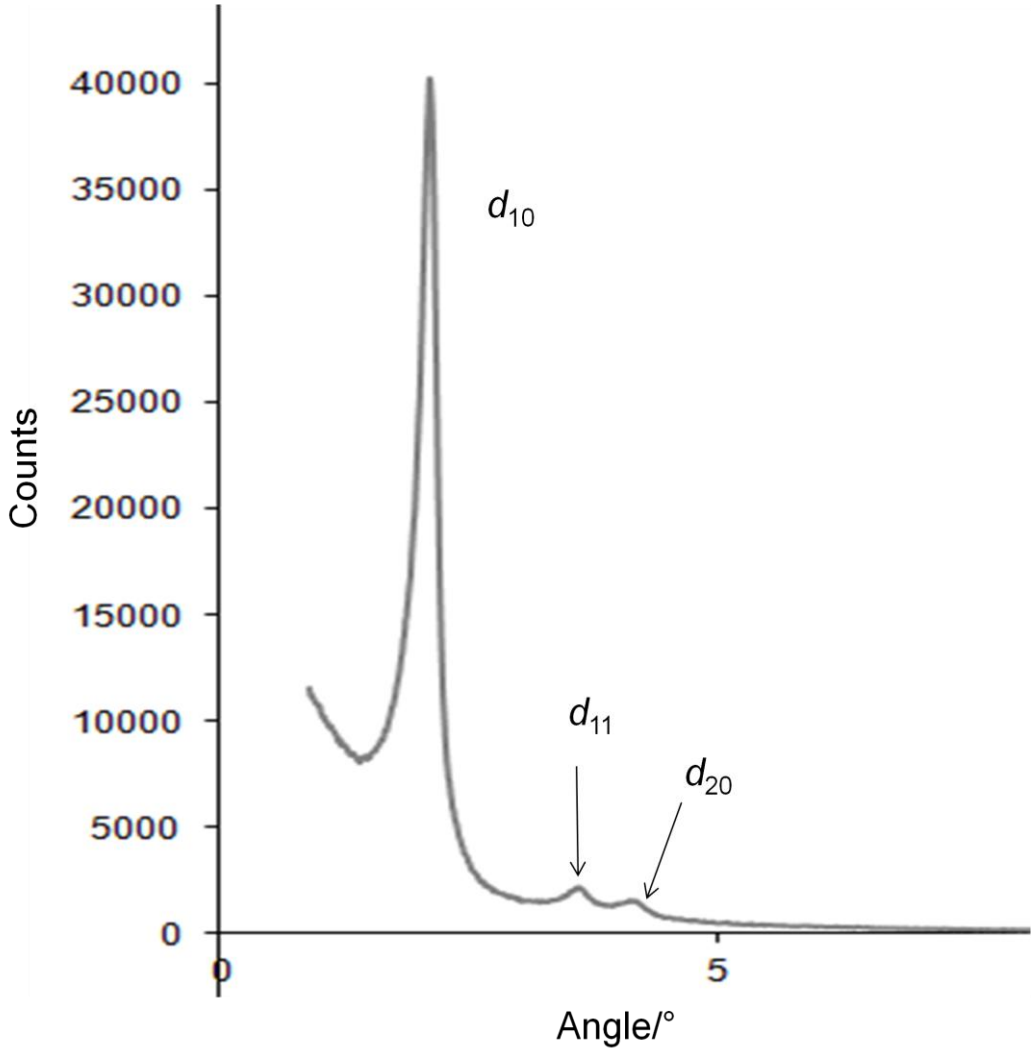

Fig. 4.10 Low-angle X-ray diffraction pattern of the hexagonal silica prepared by TLCT using a Cr-Pd precursor.

High-angle X-ray diffraction data showed the presence of Pd, PdO and Cr_2O_3 by peak matching (**Fig. 4.11 A** and **B**) with particles described in literature possessing trigonal,[36] tetragonal[37] and cubic symmetry,[38] respectively. The particle sizes calculated from wide angle X-ray diffraction data by applying the Scherrer equation were 10.3, 17.8 (Pd) and 10.2 nm, (PdO). Cr_2O_3 and PdO reflections were observed together as shown in **Fig. 4.11 A** and **B**, Therefore, the size of Cr_2O_3 particles could not be determined.

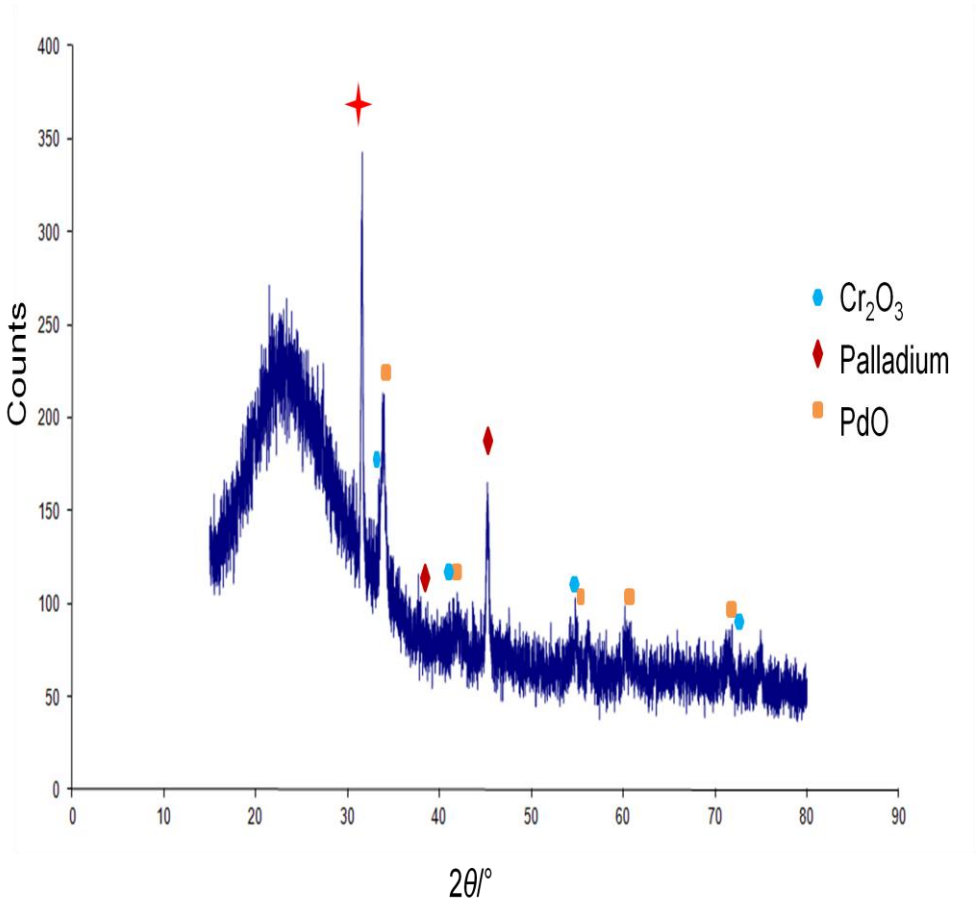

Fig. 4.11 High-angle X-ray diffraction showing peaks of carbon (+),[67] and Cr_2O_3 (⬣), PdO (▬), and Pd (◆) particles under **A** low magnification and **B** high magnification.

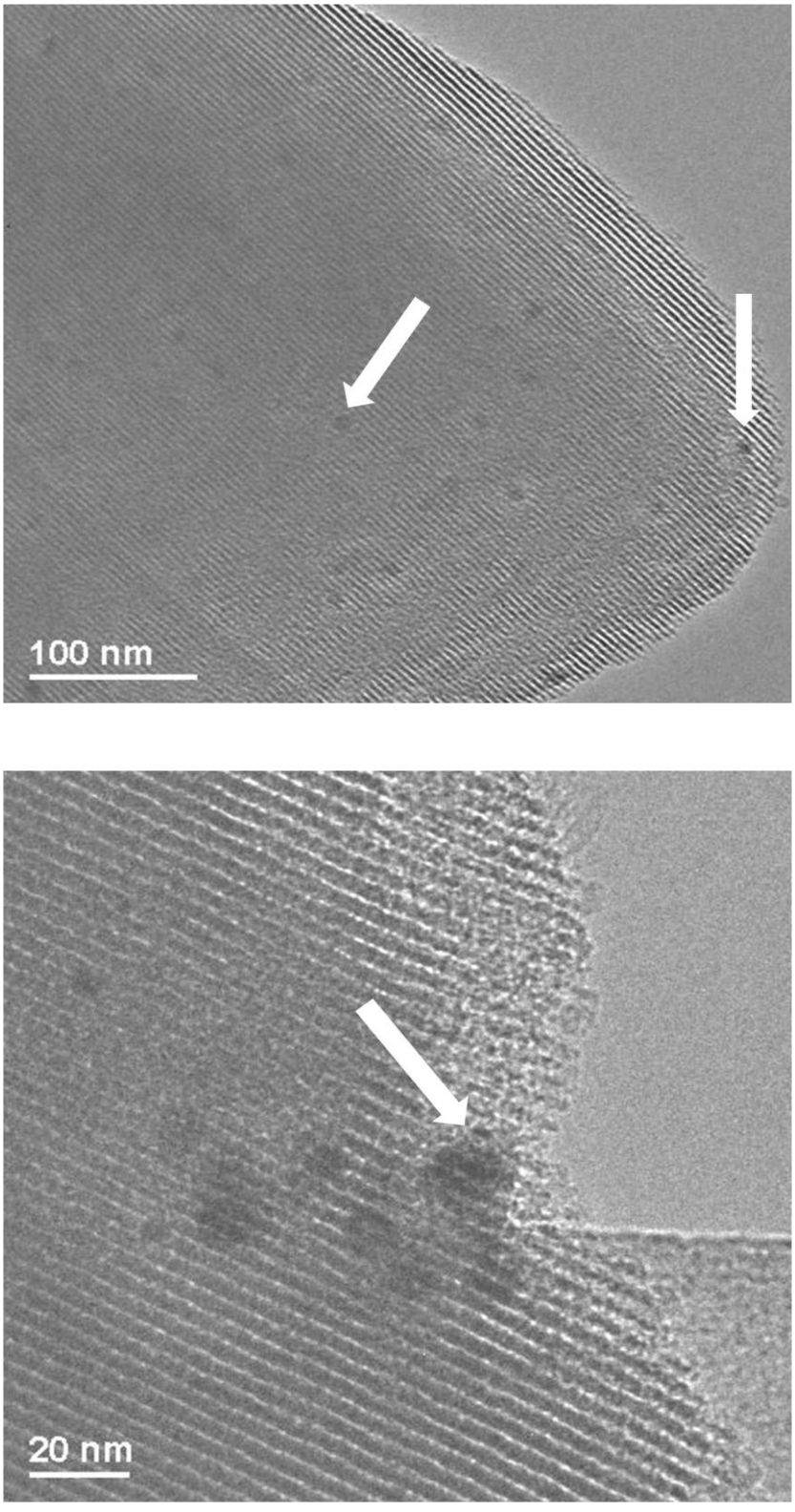

Fig. 4.12 TEM micrograph showing nanoparticles indicated by arrows. **A:** long-range order and uniform distribution of nanoparticles; **B:** different sized nanoparticles.

The TEM data (**Fig. 4.12**) indicated the presence of large as well as small particles and no evidence was obtained which could show that the particles had been incorporated into the inorganic framework. The presence of different sized particles as shown in the TEM micrographs was in agreement with the results of high-angle XRD. Also, the presence of large sized particles illustrates the presence of metal oxides *i.e.* Cr_2O_3 and PdO. Besides, the oxides of chromium and palladium have been reported in the literature as large sized particles.[39] Consequently, we can conclude that the probability to observe bimetallic Cr-Pd here is negligible.

Table IV.II BET N_2 adsorption data of Cr-Pd bimetallic and Cr, Pd monometallic nanoparticles.

Precursor	Loading (wt%)	Surface area ($m^2 g^{-1}$)	Pore volume ($cm^3 g^{-1}$)	Pore Wall thickness (nm)	Lattice parameter (nm)	Pore diameter (nm)	d-spacing (nm)
$Cr_1Pd_{2.33}$	Cr 0.48; Pd 1.00	817	0.60	1.89	4.84	2.95	4.19
Na[Cr(EDTA)]; $K_2[PdCl_4]$	Cr 0.48 1.00 Pd	997	0.62	2.15	4.65	2.50	4.03
Na[Cr(EDTA)]	Cr 0.48	812	0.61	1.57	4.56	2.99	3.95
$K_2[PdCl_4]$	Pd 1.00	873	0.62	1.97	4.82	2.85	4.18

The data obtained from the above silica were then compared with a silica prepared by using separate metal precursors (*i.e.* $K_2[PdCl_4]$ and Na[Cr(EDTA)]). This material on being analysed by porosimetry, showed a significant difference in surface area, close to that of an undoped silica *i.e.* 1001 $m^2\ g^{-1}$ (**Table IV.II**), suggesting that the nanoparticles formed are not incorporated within the pores. However, for the nanoparticles prepared from the bimetallic precursor solution some decrease in the surface area was observed, suggesting that in this case the nanoparticles have been incorporated into the pores. However, the TEM micrographs of silicas prepared from individual metal precursors showed that there were nanoparticles present on the surface of silica, which were all rather large. The average size of the nanoparticles calculated from the Scherrer equation was 22.2 nm. The high-angle X-ray diffraction analysis also showed that the particles formed from separate metal precursors were the same as observed for the TTHA metal precursor *i.e.* Cr_2O_3 and PdO except they did not show presence of metallic palladium.

The results obtained from these two different preparations were then compared further with separate Cr- and Pd- doped silicas prepared by using Na[Cr(EDTA)] and $K_2[PdCl_4]$, From the high-angle XRD data of the Cr sample, no peak was obtained which was an indication that either the particles are very small, amorphous in nature or that the Cr has been incorporated into the silica framework. When the material was analysed by TEM, particles could hardly be seen. In the Pd sample, the particles formed were observed in the TEM micrographs but they were quite large, their size

was calculated from the Scherrer equation as 21.7 nm, and the presence of PdO and not reduced palladium was shown.[40]

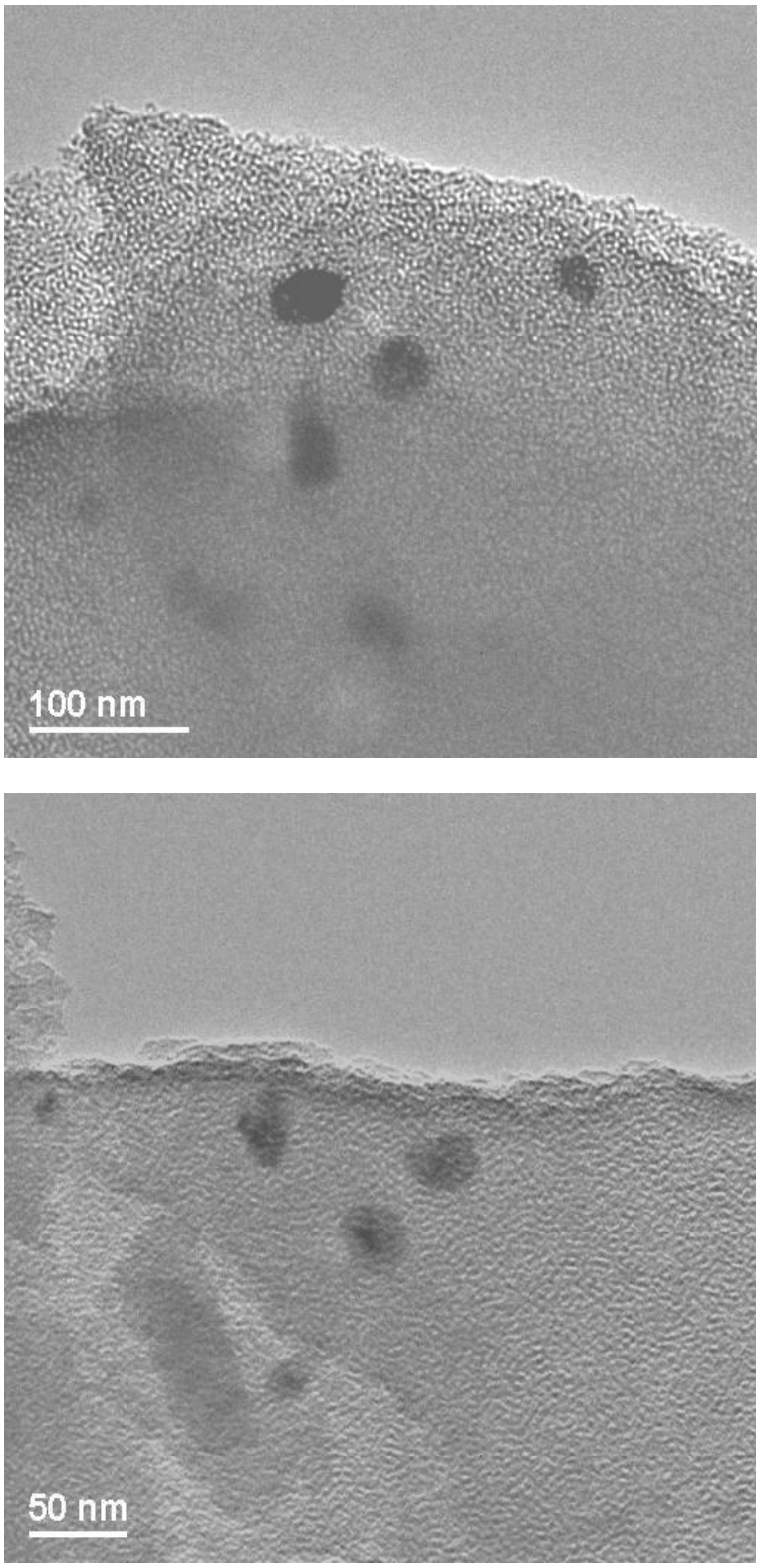

Fig. 4.13 Silica doped with Cr-Pd nanoparticles

4.2.1.2 Rh-Pd

Bimetallic Rh-Pd nanoparticles have been reported as catalysts in various chemical reactions such as oxidation of CO with O_2,[41] hydrogenation of aromatic[42,43,44] as well as aliphatic[44] alkenes, and hydrogenation of arenes.[45] All the reported examples include nanoparticles prepared from different forms of separate metal precursors *i.e.* having different sources of Rh and Pd through known techniques such as sequential impregnation[46,47] and co-impregnation.[41,48] The synergistic effects of these nanoparticles have been studied by carrying out different experiments to analyse them by techniques such as X-ray photoelectron spectroscopy.[49] Thus, Renzas *et al*.[49] have recently reported examples of Rh-Pd nanoparticles doped on silicon wafers of up to five different composition of Rh to Pd as shown by XPS and TEM. The particles observed were bimetallic in nature, but again an overall uniform distribution of particles was not observed. No attempt has been reported in the literature to prepare nanoparticles by use of a single precursor of Rh-Pd.

In our attempt to produce uniformly distributed Rh-Pd bimetallic nanoparticles, a stock solution containing a ratio of 1 : 4 of Rh : Pd with TTHA was prepared as described before in section **4.1.1**, its detailed description is in § **4.3.3**. The details of the complex preparation are in Chapter 3 § **3.7.3**. The liquid-crystalline phase formed was a homogenous orange/yellow colour, but after calcination it appeared black.

The low-angle X-ray scattering pattern (**Fig. 4.14**) showed the presence of three strong reflections indicating a persistent and well-correlated hexagonal

pore arrangement. The results of surface area analysis, including calculated parameters such as lattice parameters, *d*-spacing, surface area pore diameter as well as wall thickness are given in **Table IV.III.**

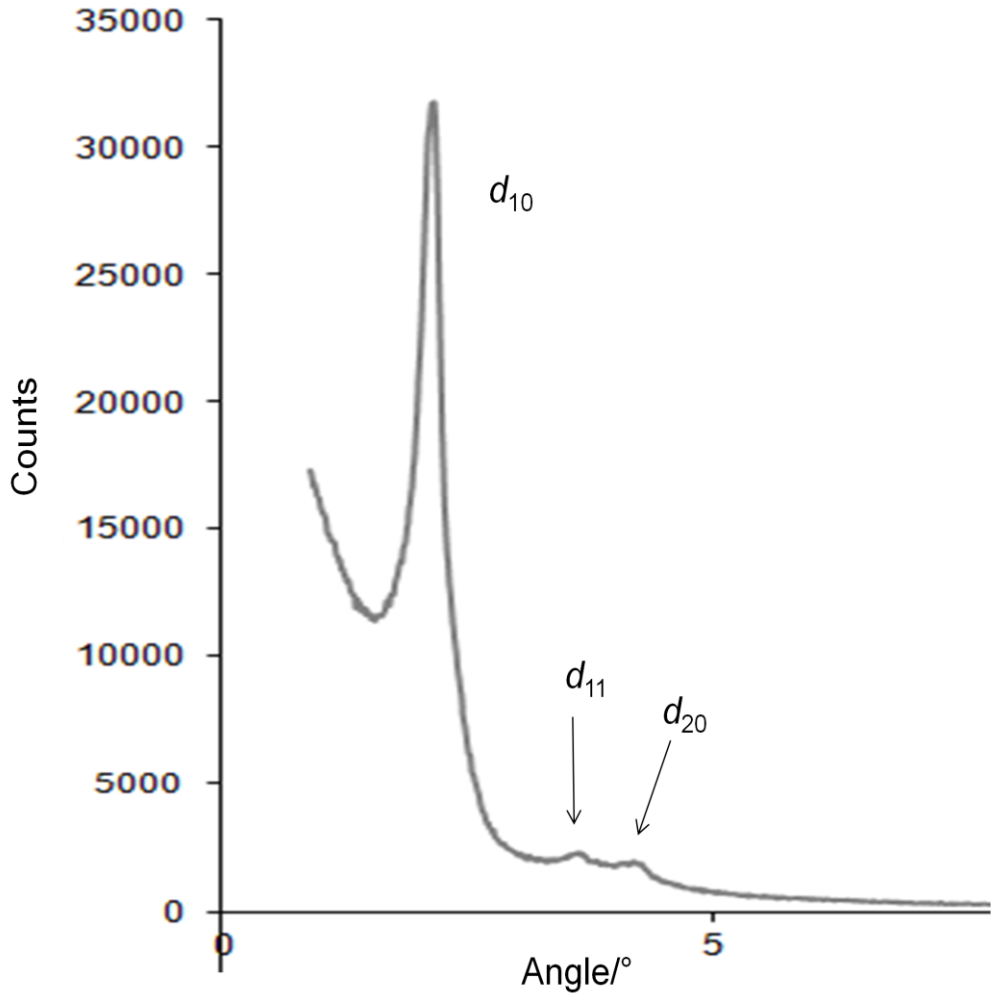

Fig. 4.14 Low-angle X-ray diffraction pattern of Rh-Pd doped silica

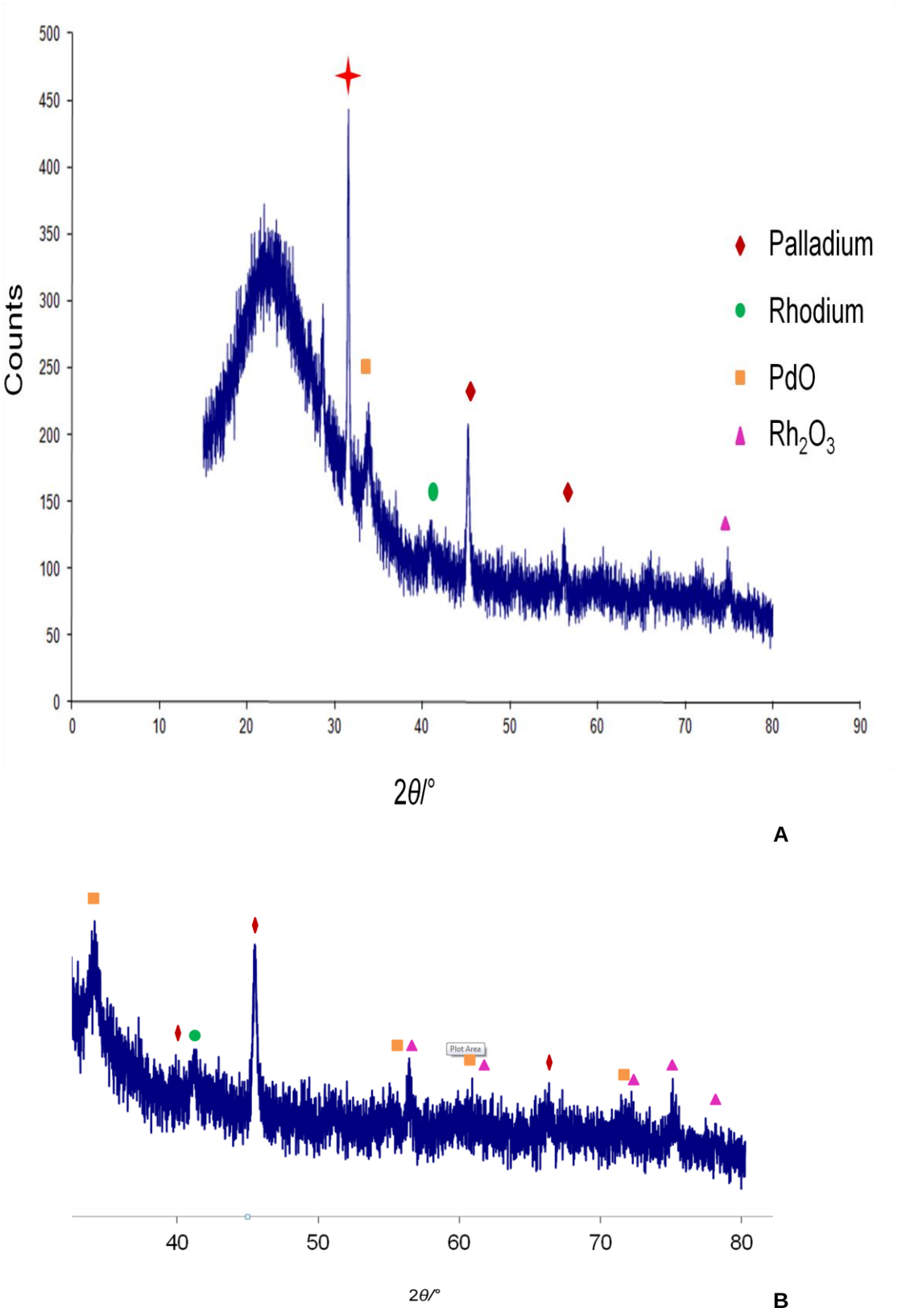

Fig. 4.15 A Wide-angle X-ray diffraction of doped Rh-Pd nanoparticles silica showing carbon (✦),[67] Palladium (♦) PdO(■), Rhodium (●) and Rh_2O_3 (▲) peak positions. **B** Magnified area showing small peaks which are otherwise difficult to observe.

Wide-angle X-ray diffraction data are shown in **Fig. 4.15**, from which the average size of the nanoparticles formed was calculated by using the Scherrer equation. The particles of Rh and Pd were identified by phase matching with the pattern of particles reported in the literature that possesses cubic symmetry.[50,51] Rh_2O_3 and PdO showed matching with particles possessing trigonal and tetragonal symmetry,[52,37] respectively. The average particle sizes calculated from the Scherrer equation using the high-angle XRD data for Rh, Rh_2O_3, Pd and PdO were 11.4, 15.4, 22.13 and 7.3 nm, respectively.

The TEM images of Rh-Pd doped (**Fig. 4.17**) mesoporous silica prepared from the TTHA precursor (single source precursor) exhibit large as well as small nanoparticles present outside as well as incorporated within the silica pores as shown in **Fig. 4.16. A** and **B.**

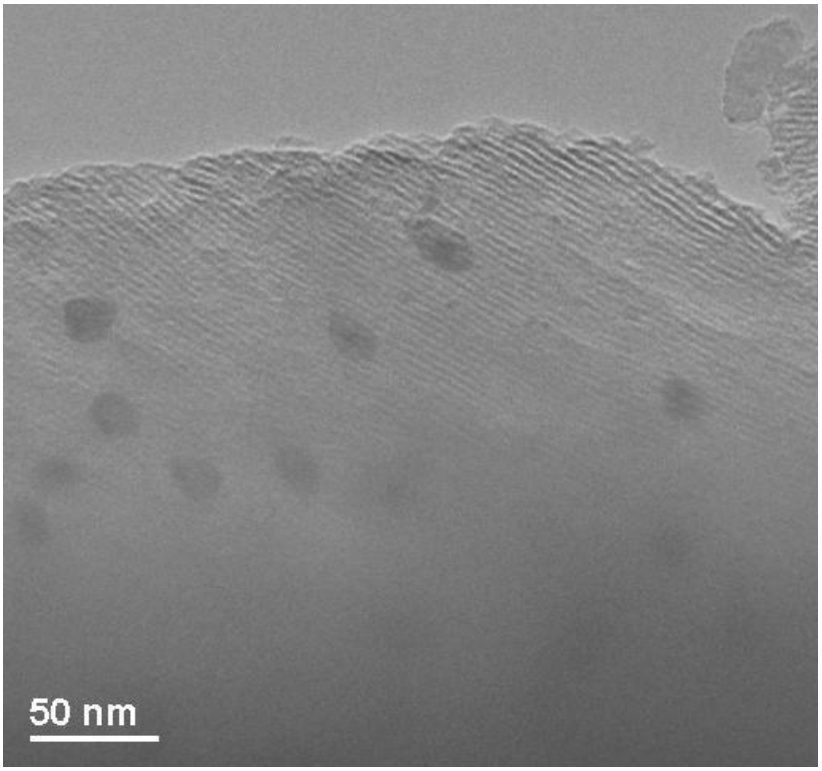

Fig. 4.16 A Rh-Pd nanoparticles and **B** inserted and surface metal particles shown by arrows in white and red.

Again, to compare with the above data, a silica doped with Rh-Pd nanoparticles was prepared by using separate metal precursors, namely $K_2[PdCl_4]$ and $Na_3[RhCl_6]\cdot 12\ H_2O$. The results obtained showed the presence of large particles that were occupying multiple pores as shown in the TEM micrographs (**Fig. 4.17**).

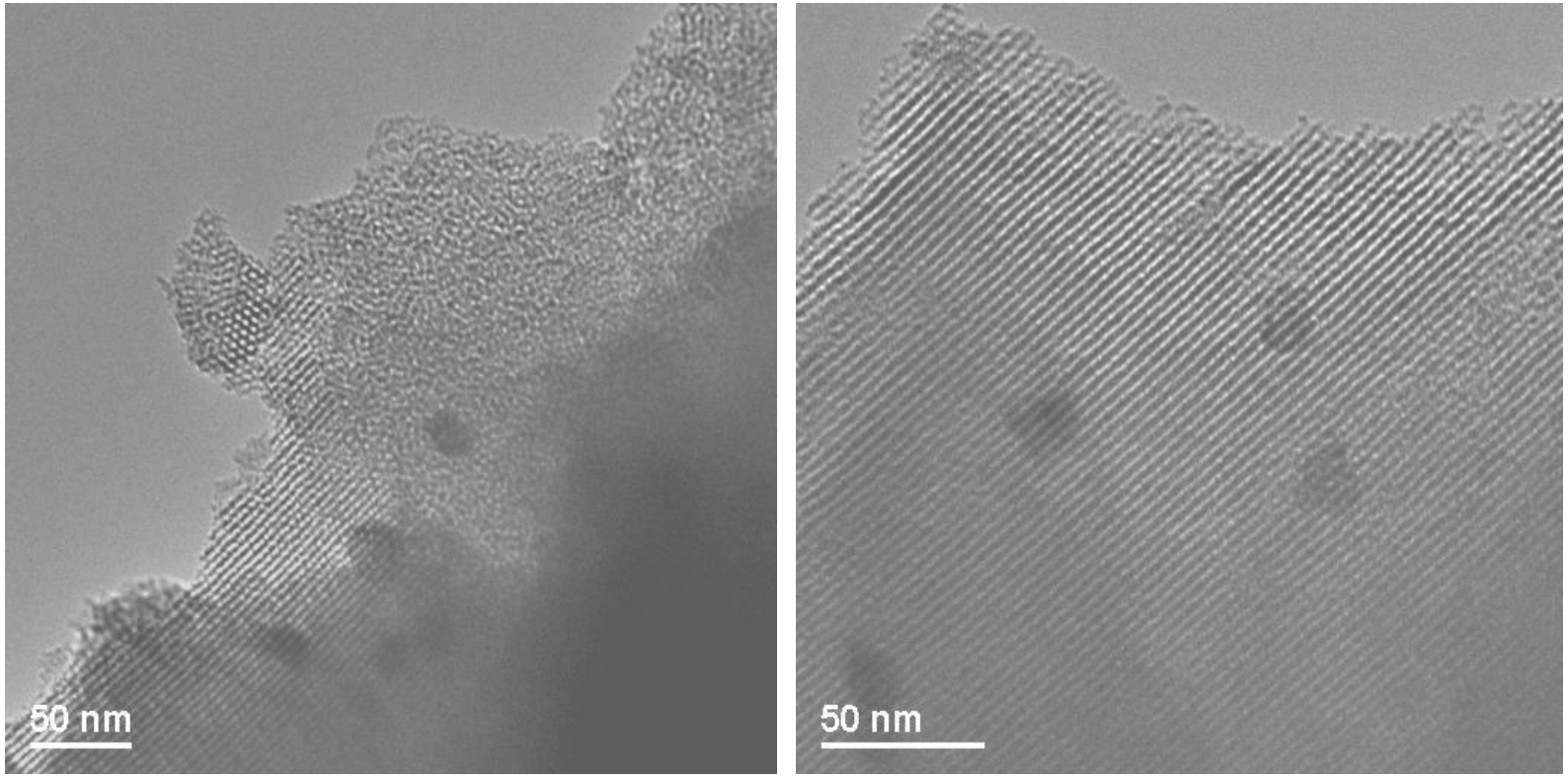

Fig. 4.17 TEM micrographs of a mesoporous silica doped with Rh-Pd nanoparticles prepared using separate metal precursors.

The average size of the particles calculated for Rh, Pd and PdO using the Scherrer formula and high-angle XRD data was 15.47, 10.6 and 9.3 nm, respectively. The palladium and rhodium particles observed were identified by phase matching with particles reported to possess a cubic symmetry.[38,50] The palladium oxide particles matched those that were reported to have tetragonal symmetry[53] as observed previously in the Rh-Pd bimetallic nanoparticles prepared from a single source precursor. The materials were characterised by BET-N_2 surface area and X-ray diffraction techniques with the data given in **Table IV.III**.

Table IV.III Data showing differences observed in silica doped with Rh-Pd nanoparticles prepared by single as well as separate metal precursors.

Precursor	Loading (wt%)	Surface area (m^2g^{-1})	Pore volume (cm^3g^{-1})	Pore Wall thickness (nm)	Lattice parameter (nm)	Pore diameter (nm)	d-spacing (nm)
Rh_1Pd_4	Rh 0.96 Pd 1.00	830	0.54	2.10	4.71	2.61	4.08
$Na_3[RhCl_6].12H_2O$ $K_2[PdCl_4]$	Rh 0.94 Pd 1.00	714	0.51	1.80	4.65	2.85	4.03
$Na_3[RhCl_6].12H_2O$	Rh 0.94	936	0.67	2.01	4.88	2.87	4.23
$K_2[PdCl_4]$	Pd 1.00	873	0.62	1.97	4.82	2.85	4.18

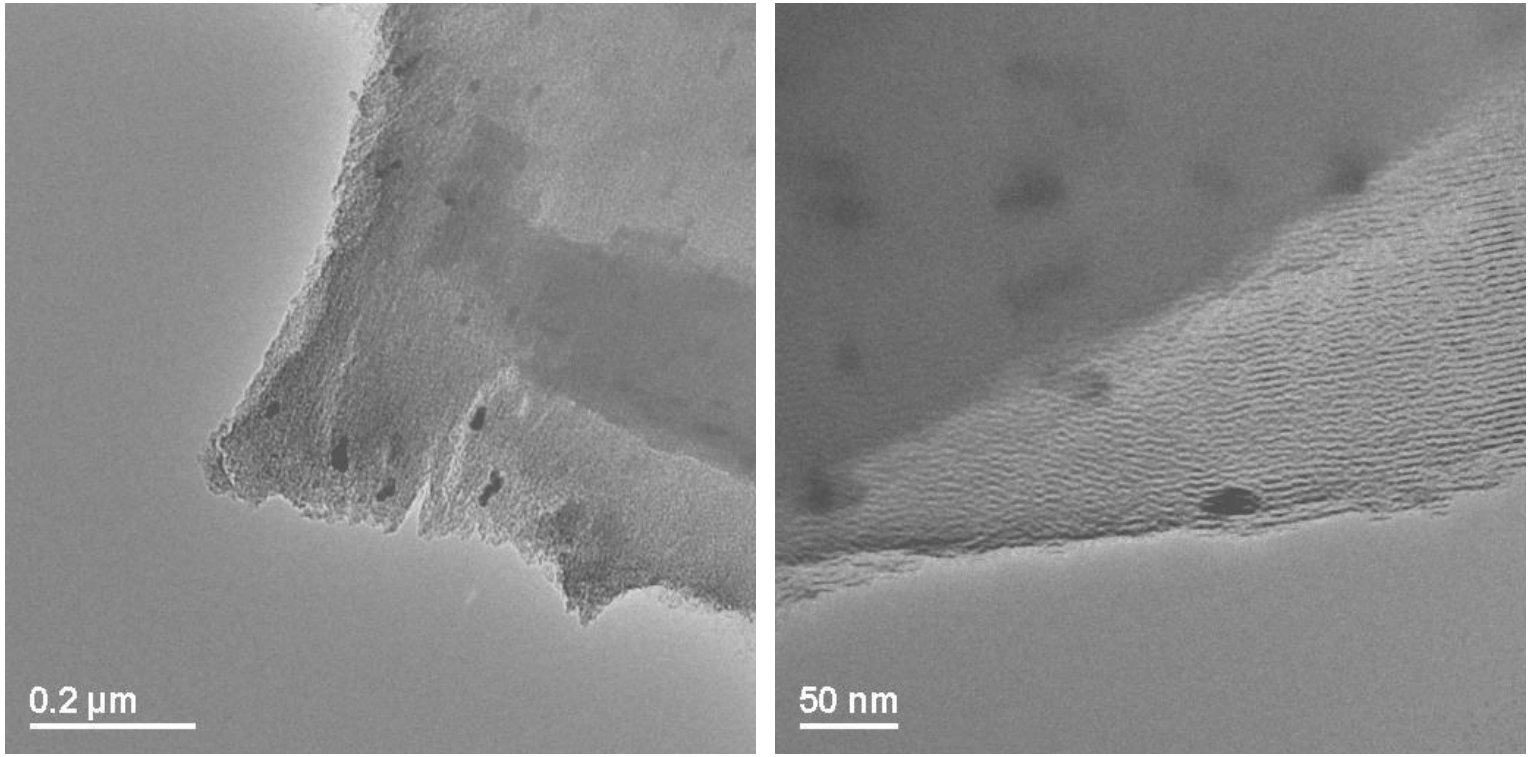

Fig. 4.18 Silica doped with Rh showing nanoparticles **A** end on pores, and **B** parallel pores.

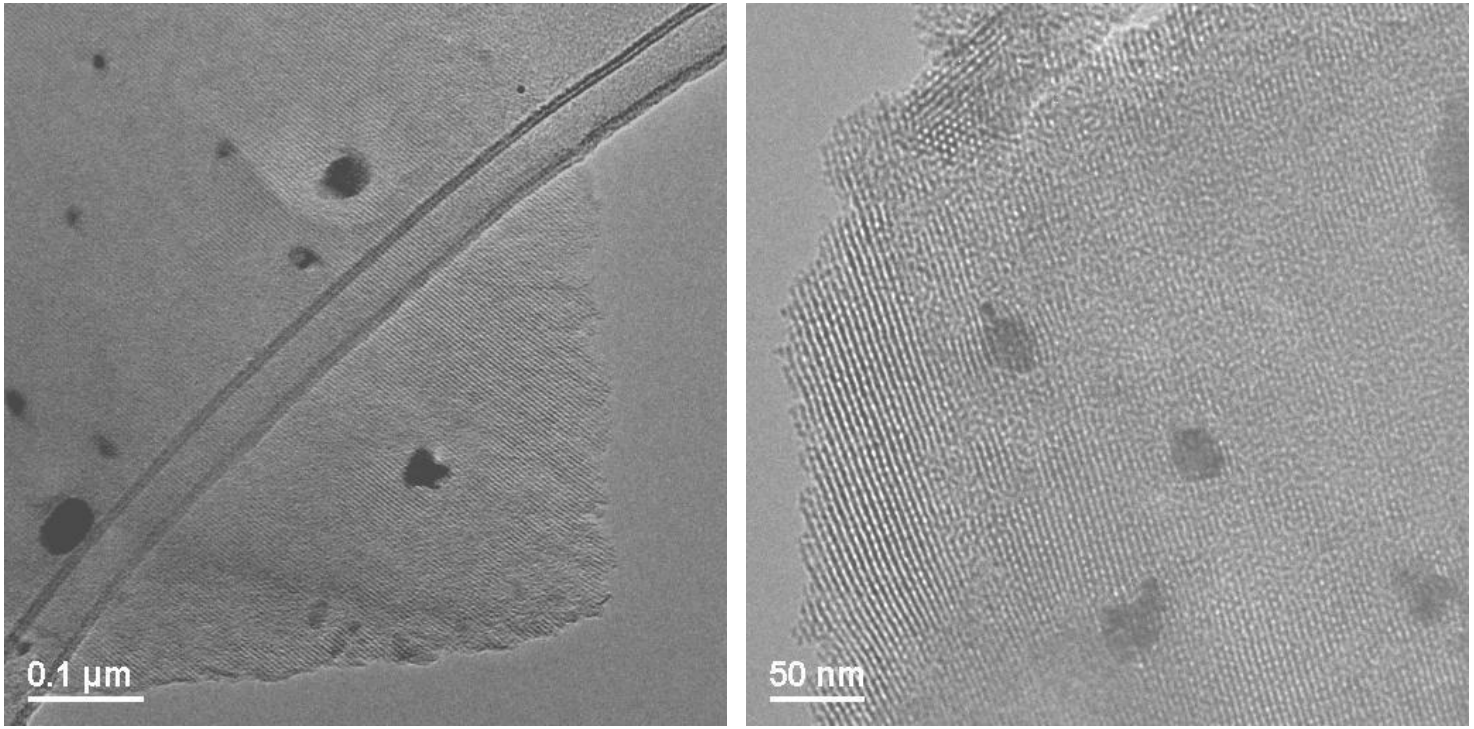

Fig.4.19 TEM micrograph of Pd-doped mesoporous silica

All the micrographs of Rh, Rh-Pd (1 : 4) (prepared by different and the same metal precursor) and Pd silica showed long, well-defined pores with a hexagonal pattern. The particles obtained were not present within the pores for the most of them but the lower surface area than the original undoped silica which indicates that the particles are either too small and are amorphous or are present onto the surface of pores occupying more than one pores. Moreover a mixture of oxidised and reduced particles was observed indicating that the particles formed are not truly bimetallic in nature.

4.2.1.3 Rh-Ni

Bimetallic Rh-Ni catalysts are well known in the dry reforming of methane.[54,55]

$$CO_2 + CH_4 \longrightarrow 2\,CO + 2\,H_2$$

The interest in this bimetallic catalyst began with the discovery of less expensive nickel-based catalysts, which have been studied on various catalytic supports *e.g.* CeO_2,[56,57] La_2O_3,[58] ZrO_2,[59] Al_2O_3,[60,61] and SiO_2.[54] Bimetallic Rh-Ni catalysts have been known to participate in reactions such as propane steam reforming,[62] oxidative steam reforming of ethanol[63] and CO_2 reforming of methane.[64]

Jóźwiak *et al*. were the first to use commercial SiO_2[54] as the catalytic support for the preparation of bimetallic Rh-Ni catalysts and to study their catalytic behaviour. They used the incipient impregnation method to synthesise their catalyst, and the nature of nanoparticles formed in the doped

silica were analysed using high-angle X-ray diffraction analysis. This analysis showed the presence of a mixture of Rh, Ni and Rh-Ni alloy (shown in **Fig. 4.20**) in the sample.

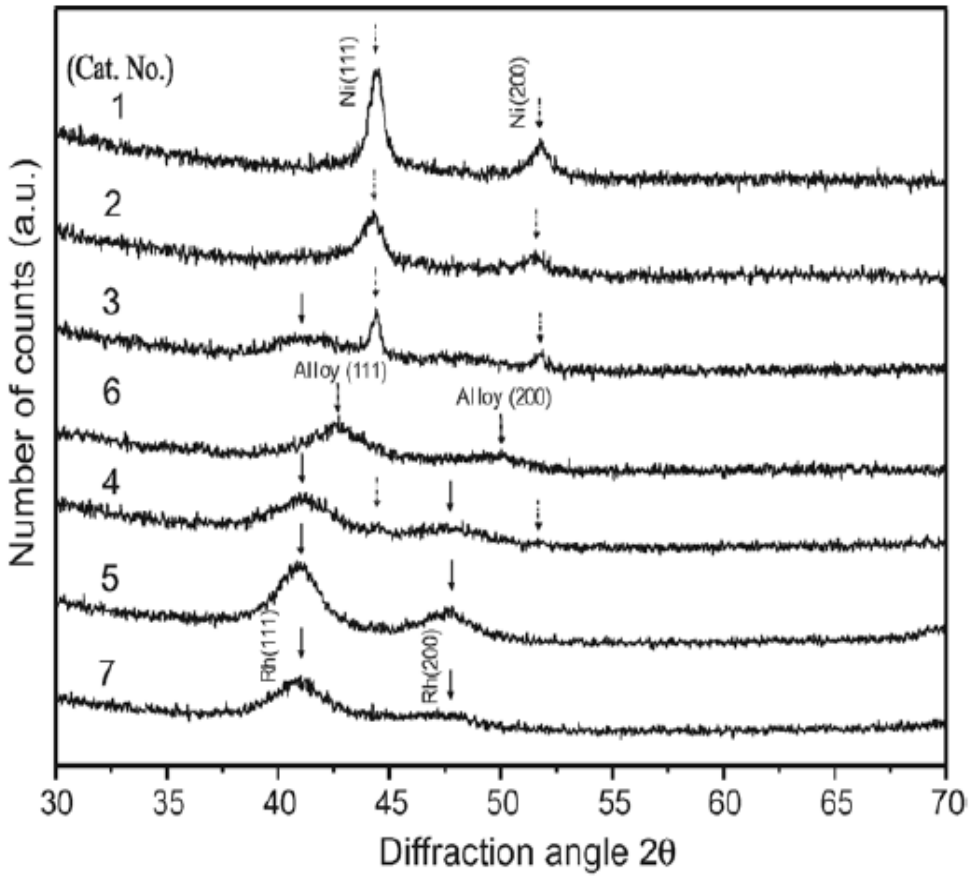

Fig. 4.20 XRD patterns of Rh-Ni/SiO_2 catalysts after calcination at 500 °C (3 h), followed by reduction at 600 °C (1 h).[54]

The composition of metals in the material was thoroughly studied and was also analysed for the catalytic process. However, the effect of metal precursors on the nature of inorganic framework was never discussed or investigated with low-angle X-ray diffraction. The size of the particles formed was observed to vary according to the wt% of metals being used (*i.e.* 30.1 nm for Rh : Ni (1.25 : 3.75) and 20.8 nm for Rh : Ni (2.5 : 2.5)) and to

some extent with the nature of metal precursor (*i.e.* for $RhCl_3$ precursor, the particle size is 16.5 nm for Rh : Ni (2.5 : 2.5 wt%). The size of the nanoparticles was calculated from an assumption based on the stoichiometric coefficient of hydrogen chemisorption. It was not then compared by any other appropriate analysis such as TEM.

In the current work, the bimetallic Rh-Ni nanoparticles were prepared from the stock solution of mixed-metal precursor possessing a ratio of Rh: Ni of 1 : 4 using the strategy described in section **4.3.3**. Details of the metal complex preparations are given in § **3.7.3** (Chapter 3). The appearance of the liquid-crystalline phase was a homogenous green, which after calcination turned black. The data obtained from the BET-surface area analyser are given in **Table IV.IV**. For comparison, Rh-Ni silica was also prepared by the use of separate metal precursors of Rh and Ni, but the results obtained (**Table IV.IV**), did not show any noticeable variation in the parameters other than surface area from those for Cr-Pd and Rh-Ni bimetallic mixtures of TTHA. The small difference in surface areas shown can be accounted for by the presence of more nanoparticles within the pores of silica than on the surface of the inorganic framework. Other minor variations observed are largely within the bounds of the accuracy of the techniques used or some experimental error.

Table IV.IV Data obtained from BET-N_2 surface area analyser for Rh-Ni and Rh and Ni nanoparticles

Precursor	Loading (wt%)	Surface area (m^2g^{-1})	Pore volume (cm^3g^{-1})	Pore Wall thickness (nm)	Lattice parameter (nm)	Pore diameter (nm)	d-spacing (nm)
Rh_1Ni_4	0.94 Rh 0.54 Ni	872	0.57	2.04	4.63	2.59	4.01
$Na_3[RhCl_6].12H_2O$ $Na_2[Ni(EDTA)]$	0.94 Rh 0.54 Ni	952	0.57	2.27	4.68	2.41	4.05
$Na_3[RhCl_6].12H_2O$	0.94 Rh	936	0.67	2.01	4.88	2.87	4.23
$Na_2[Ni(EDTA)]$	0.54 Ni	934	0.67	1.78	4.65	2.87	4.03

The low-angle X-ray diffraction data of the silica doped with Rh-Ni (4 : 1) nanoparticles showed three reflections corresponding to d_{10}, d_{11} and d_{20} observed at 4.01, 2.32 and 1.97 nm, respectively. All three are characteristic of the hexagonal pore structure of the silica (**Fig. 4.21**).

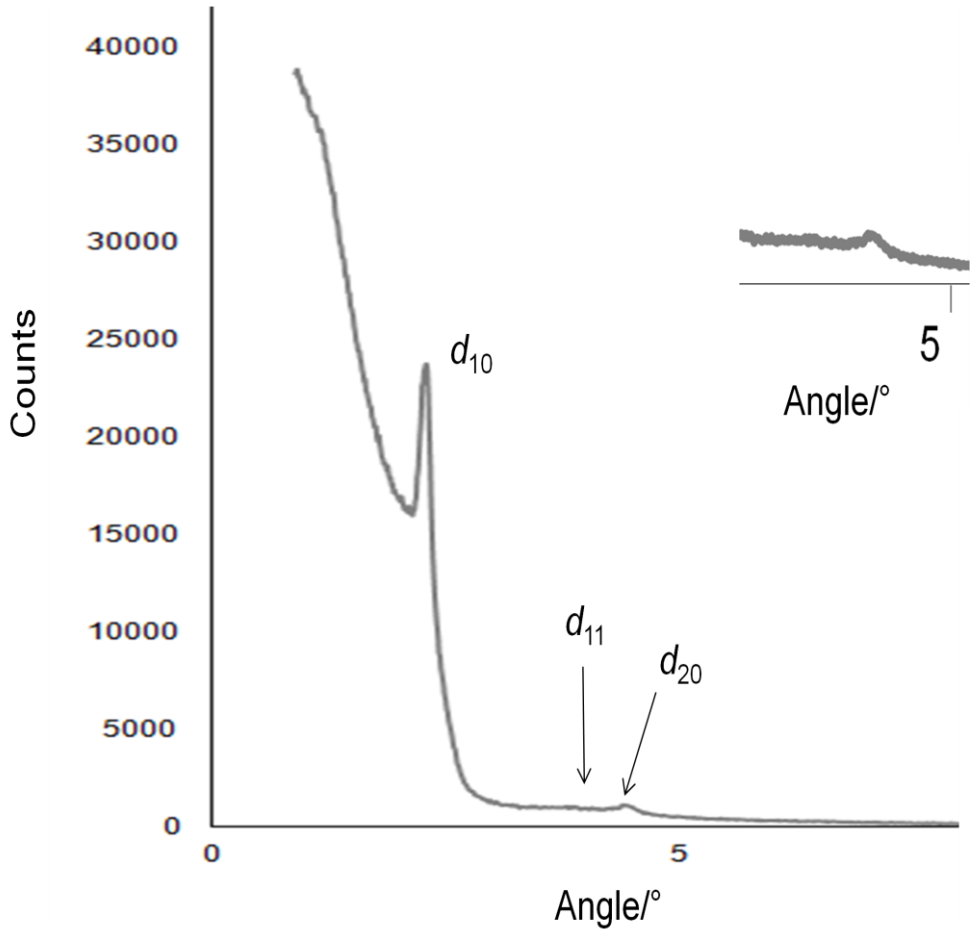

Fig. 4.21 Low-angle X-ray diffraction pattern of silica doped with Rh-Ni bimetallic nanoparticles prepared from bimetallic precursor.

The high-angle X-ray data (**Fig. 4.22**) were used further to determine the size of the nanoparticles using the Scherrer equation. Peak matching was again used as a tool to indentify the type of the particles obtained from the high-angle X-ray diffraction data present in the bulk of sample. The average size of the nanoparticles calculated from the Scherrer equation was 13.1 nm

but that observed with the TEM micrographs 5.28 nm. The peak matching depicts the presence nickel and rhodium nanoparticles with hexagonal[65,66] and cubic symmetry,[50] respectively. The size of the nanoparticles obtained by using separate precursors, observed from TEM images is 10.45 nm. Unfortunately, few peaks were observed in the high-angle XRD which indicated most of the particles formed were very small in size or were poorly crystalline. Hence, the data could not be used any further in the Scherrer equation for average particle size calculation. Only a single peak corresponding to Ni nanoparticles was observed which matches with particles with hexagonal symmetry,[60] for which, the average size was calculated as 21.3 nm by employing the Scherrer formula.

To confirm the existence of the bimetallic Rh-Ni nanoparticles if formed in the current metal mixture prepared from a bimetallic precursor mixture containing Rh : Ni ratio 1 : 4 it was compared with the Rh-Ni alloy formed in the previously reported preparation shown in **Fig. 4.20**. The presence of the peak of Rh-Ni alloy at approximately $2\theta = 43°$ supports the bimetallic nature of nanoparticles in the current sample. Nevertheless, the exact nature of particles formed still requires further confirmation. Oxides of Rh and Ni were not observed in the high-angle X-ray diffraction data indicating that the particles have been completely reduced even in the air atmosphere and in the absence of H_2.

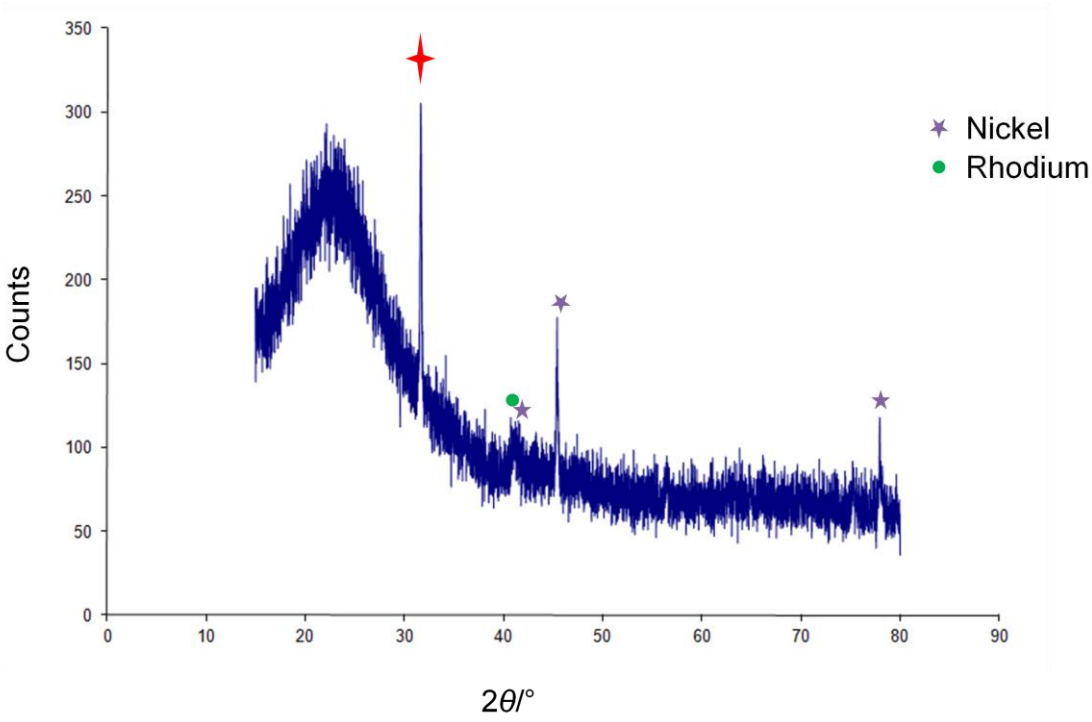

Fig. 4.22 High-angle X-ray diffraction of Rh-Ni doped silica showing peaks of rhodium (●) and nickel (✶). Peak shown by (✦) is carbon.[67]

The TEM images show long, straight pores but the size of nanoparticles as shown in **Fig. 4.23 A** and **B**, (Rh-Ni prepared from single source precursor), clearly indicate the presence of particles on the surface and incorporated within the pores of the silica. The latter can be clearly seen having a diameter equivalent to single silica pore in **Fig. 4.23 A**. On the other hand, some of the nanoparticles were also observed as dark patches shown with a square in **Fig. 4.23 B**. It was not easy to determine the size of those tiny particles as the pore walls of silica appeared to have destroyed with the electron beam.

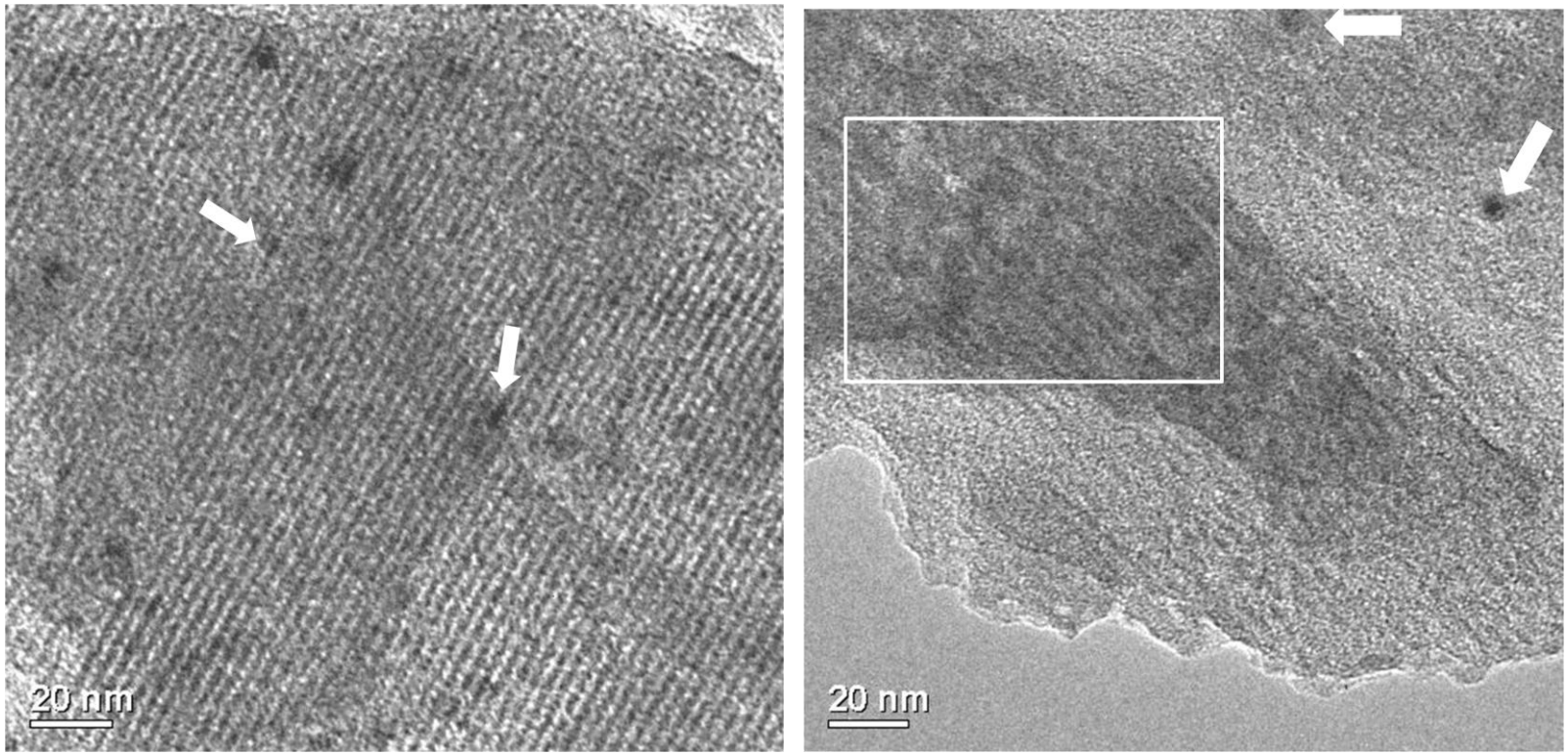

Fig. 4.23 TEM micrographs of Rh-Ni doped silica nanoparticles A incorporated into mesopores shown by arrows on the left and B by a square, where particles appear to be forming a dark patch.

For Rh-Ni doped silica prepared using separate metal precursors, the presence of large as well as small nanoparticles was found; the particle size is clearly shown in **Fig. 4.24 B**, highlighted in red.

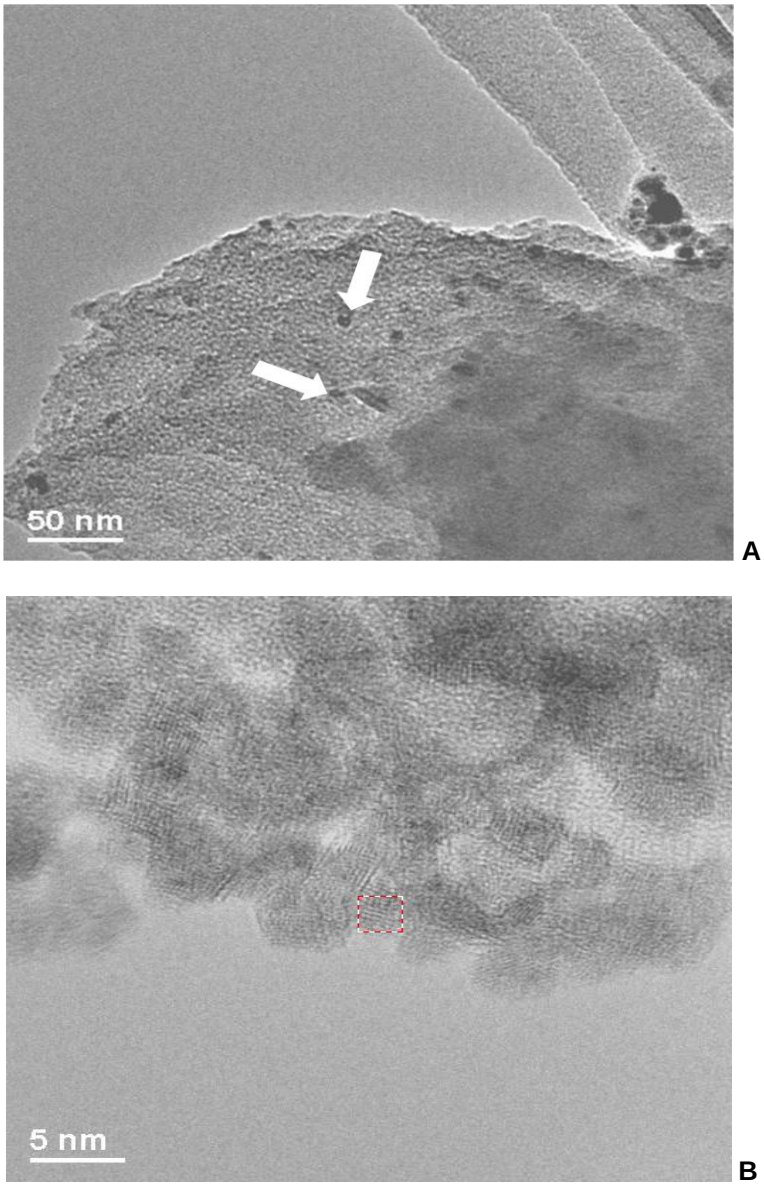

Fig. 4.24 TEM micrographs of silica doped with Rh/Ni prepared by separate metal precursors.

If the above TEM data for Rh-Ni nanoparticles prepared by single and separate metal precursors are compared with TEM images of Rh and Ni, respectively, then, it is found that Rh produces large-sized particles but Ni gives rise to extremely small particles which are almost invisible in the electron micrograph. However, as a bimetallic particle the size was in between the Rh and Ni nanoparticles. The absence of any metal oxides or complete reduction of the metal mixtures indicates that the possibility of formation of bimetallic particles is higher in the above two cases.

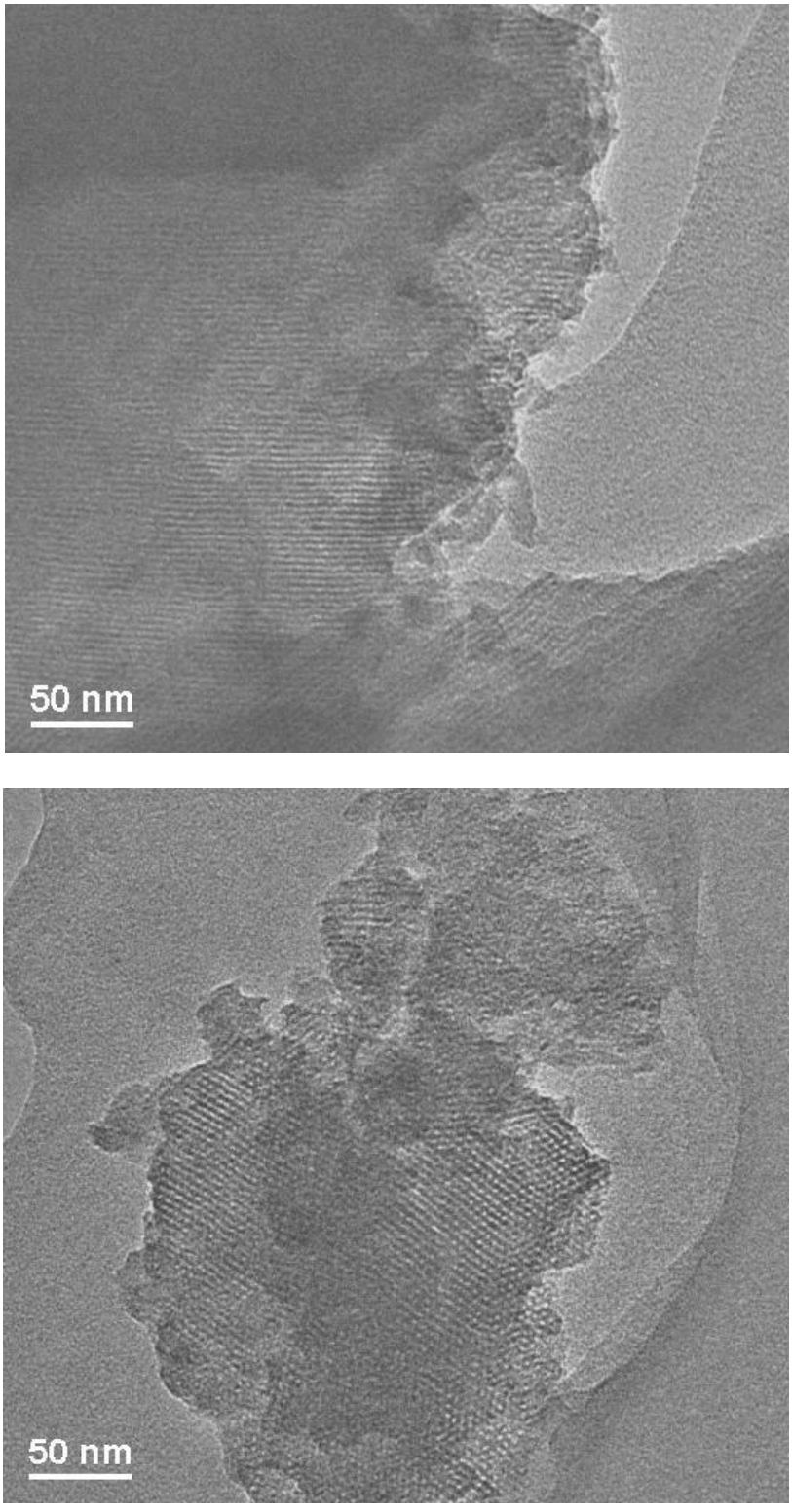

Fig. 4.25 TEM micrographs obtained from Na_2[Ni(EDTA)] precursor.

4.2.2 Application of Polyethylene Oxides in a Template-Mechanism

In the self-assembly process, electrostatic interactions between the head group of the non-ionic surfactant *e.g.* C_nEO_m and the water molecules dissolving metal ions from the metal ligand complex play a lead role in the formation of the mesophase. The electrostatic interactions assist in the organisation of the sol-gel mixture to form a mesophase. In oligoethylene oxide surfactants, the EO head groups organise themselves in such a way so that they can interact with cations in a manner analogous to crown ether (**Fig. 4.26**).

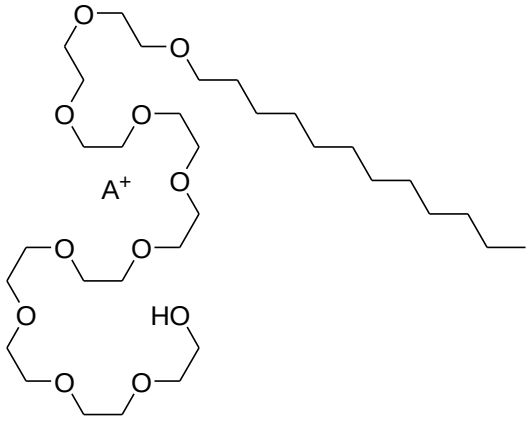

Fig. 4.26 Structure of $C_{12}EO_{10}$ showing interaction of EO head group to the counter ion (A^+).

Therefore, when a complex metal anion is introduced into such system then it should reside close to the interacting cation in the hydrophilic part. On interaction with TMOS with the surfactant, hydrolysis will take place resulting in the formation of methanol (by-product). The latter could be removed under gentle, dynamic vacuum, and the mesophase reformed. The sol-gel condensation should begin with the silica formed outside the mesophase acquiring its shape. On complete drying, the monolith formed with solidified silica around the surfactant and the metal ligand complex

could then be subjected to calcination. This should remove all the hydrocarbon content *i.e.* the ligand of the complex, surfactant and counter anions if present leaving behind the reduced metal nanoparticles incorporated within the pores of silica (**Fig. 4.27**). However, the final observation showing large surface adhering nanoparticles in **Fig. 4.28**, which is detected for the most of them.

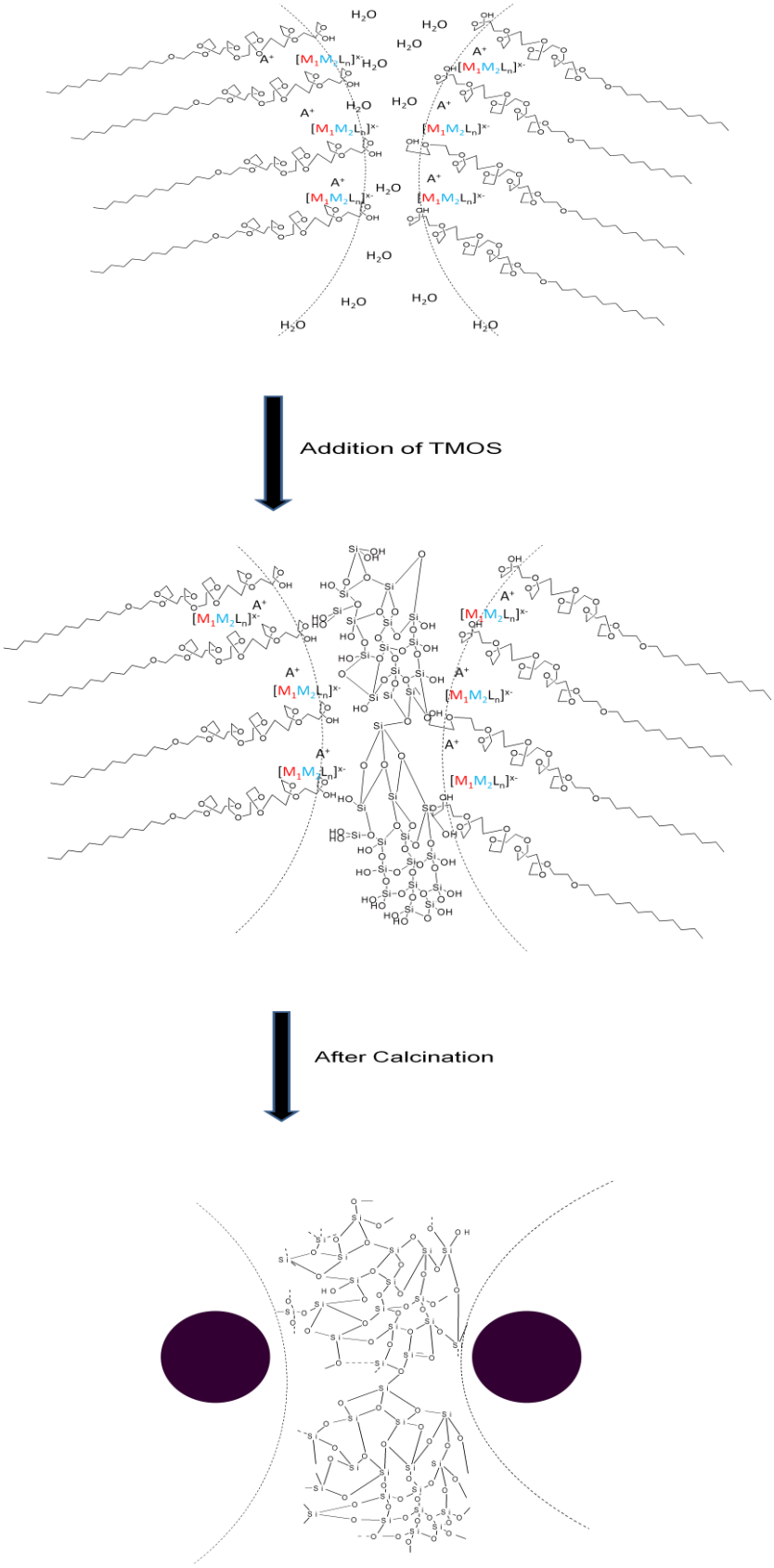

Fig. 4.27 Schematic representation of metal incorporation *i.e.* M_1 and M_2, to the mesophase of non-ionic surfactant ($C_{12}EO_{10}$) resulting doped bimetallic silica.

The results obtained for the Cr-Pd, Rh-Pd silicas, did not show any strong evidence to suggest that the particles formed were always present within the silica framework. This had been expected due to particle aggregation occurring before completion of sol-gel condensation or before solidification of silica walls was complete. The same behaviour of particle aggregation has also been observed previously by King.[18] Particle aggregation is very common in nanoparticles due to their extremely high surface area. The control of aggregation is known to be achieved by temperature, pH, solubility of metal particles in solvent, dispersity of particles, time required for the solidification of silica walls as well as surface stabilisation.[68] Well-dispersed and well-solubilised metal particles make the intermolecular interactions less probable in comparison to the interaction with the other functional groups such as PEO and zwitterionic silica, and as a consequence, the formation of particle aggregates is reduced to minimum. However, due to prolonged duration of silica walls formation or sol-gel condensation can promote cluster formation.

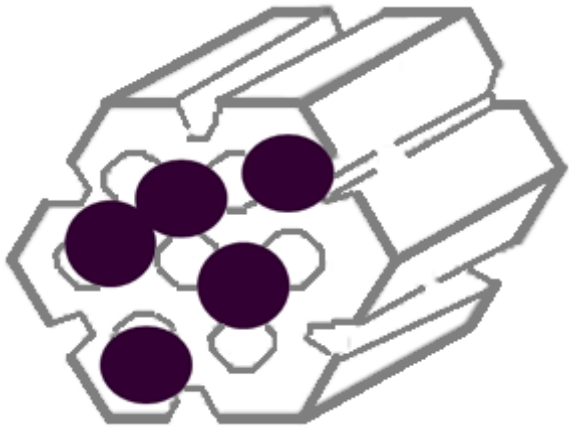

Fig. 4.28 Schematic representation of mesoporous silicate doped with large sized bimetallic nanoparticles.

4.2.3 Conclusion

The sections above describe the attempts made to synthesise uniformly distributed bimetallic nanoparticles using single metal precursors as a source of the two metals. The experiments used a strategy that involved the use of single-source precursor stock solutions containing bimetallic complex mixtures (Cr-Pd, Rh-Pd and Rh-Ni) and TTHA. The attempts successfully produced doped silicas with well-defined pores that possess long-range order, but reduced nanoparticles were not found in all cases. For instance, the Cr-Pd and Rh-Pd systems showed signs of incomplete reduction and formation of metal oxides observed as large particles present outside the silica framework, which was expected to have occurred due to particle aggregation and oxidation during calcination. However, for Rh-Ni the particles formed were relatively small and were even observed as small black patches indicating them to be present within the pores.

The general conclusion is that the aim to produce two different metals in reduced form present close to one another as a bimetallic nanoparticle or at a certain distance was not accomplished. However, the method has established a potential new route of using single metal precursors which has shown a possibility of obtaining bimetallic nanoparticles provided the ratio of metals in the precursor employed is the same.

4.3 Experimental

4.3.1 Instrumentation

Polarised Optical Microscopy

Polarised Optical Microscopy for liquid-crystalline phase identification was carried out with an Olympus BX50 microscope at magnifications x100 and x200 on a Linkam Scientific LTS 350 heating stage. All samples were analysed on borosilicate glass microscope cover slips (thickness no. 1).

Calcination

Calcination was carried out using a Carbolite tube furnace (made by Eurotherm) with a temperature controller 3216. The samples prepared were roughly crushed and then degassed with N_2 for 20 min. The degassed samples were then heated at 3 K min^{-1} to 673 K, where they were held isothermally for an hour under N_2 and then a further 5 h in air, after which they were allowed to cool to room temperature.

BET surface area measurement

Surface areas, average pore volumes and average diameters were determined for the prepared silica samples by using BET adsorption desorption measurements *via* a Micromeritics Tri-Star 3000 surface area and porosimetry analyser. The measurement was carried out at 77 K (liquid nitrogen), using nitrogen as the adsorbing gas.

Powder X-ray Diffraction

A Bruker D8 diffractometer equipped with a CuK_α source of radiation (λ = 0.154 nm) with dynamic scintillation detector was used for the powder XRD. Low- and high- angle XRD measurements were carried out using slit widths of 0.6 and 1.00 mm, respectively.

Transmission Electron Microscopy (TEM)

The TEM micrographs were obtained from high-resolution Transmission Electron Microscope (JEM 2010 TEM) with installed ISIS system analysed by Professor Wuzong Zhou at the University of St. Andrews.

4.3.2 Materials

The reagents, chromium(III) nitrate nonahydrate, nickel(II) nitrate hexahydrate, decaethylene glycol monodecyl ether ($C_{12}EO_{10}$), tetramethylorthosilicate (TMOS), were purchased from Sigma Aldrich, while sodium hexachlororhodate(III) dodecahydrate, sodium hexachloroiridate(III) hydrate were purchased from Alfa Aesar. Potassium tetrachloropalladate(II), was obtained as gift from Johnson Matthey Chemicals. Basic reagents *e.g.* hydrochloric acid *etc.* were from Fisher Scientific.

4.3.3 Preparation of Doped Mesoporous Silicas

General method of preparation using MM'TTHA as precursors

A stock solution (5 cm^3, 8 mmol%) of Na[M′(MTTHA)] was prepared using the methodology as given in § 3.7.3. An aliquot (1 g) of solution was taken and its pH adjusted to 2 by addition of HCl (conc., typically 1 drop). Then,

$C_{12}EO_{10}$ (1.0 g) was added to the solution, which was warmed gently and mixed well until a viscous gel formed. The homogeneity of the gel was then characterised by polarised optical microscope and found to show a hexagonal H_1 phase. To this mixture was added TMOS (2.0 g) and the contents were mixed *via* gentle heating which resulted to the evolution of MeOH which was removed by applying a partial dynamic vacuum in order to avoid the disruption of phase being formed. After the MeOH had been removed completely from the mixture, it was again examined under the polarising microscope for the presence of hexagonal H_1 phase. The gel was left in the same flask undisturbed for 48 h at room temperature for completion of the sol-gel condensation. After condensation, the gel was dried to give a coloured, translucent monolith, which was calcined. After calcination, a coloured silica (*i.e.* black (Rh-Ni and Rh-Pd), and fawn (Cr-Pd)) resulted. All the silicas of Rh-Pd, Rh-Ni and Cr-Pd were prepared in the similar way. The quantities used in their synthesis and the amounts of silicas are given below.

Metals	Metal precursor	Quantities of metals (wt%)	Mass of dried monolith (g)	Mass of calcined silica (g)
Cr-Pd	$Na_x[Pd_y(Cr_zTTHA)]$	Cr 0.48% Pd 1.00%	2.039	0.825
Rh-Pd	$Na_x[Pd_y(Rh_zTTHA)]$	Rh 0.96% Pd 1.00%	1.788	0.749
Rh-Ni	$Na_x[Ni_y(Rh_zTTHA)]$	Rh 0.94% Ni 0.54%	1.713	0.759

General method of preparation using $Na_x[MEDTA]$ and $K_y[MCl_n]$ as separate metal precursors

A stock solution (5 cm^3) of $Na_x[M(EDTA)]$ was prepared by using the method of preparation described by King[18] and according to the details below.

Preparation of $Na_x[MEDTA]$ stock solution

$[Na_2H_2EDTA].2H_2O$ (0.40 mmol, 0.151 g) was dissolved in water (35 cm^3). To it an aqueous solution (15 cm^3) of $M(NO_3)_n{\cdot}xH_2O$ (0.40 mmol, 0.040 mol%) was added and the contents of the flask were heated under reflux for 20 h. The resulting solution was concentrated to 4 cm^3 by evaporating the solvent under vacuum at (40 °C). The volume of this solution was then made up to 5 cm^3 in a volumetric flask. This stock solution was used to carry out the preparations of separate metal precursors.

Preparation of mixed-metal silica from separate metal precursors

A quantity (1 cm^3, 0.08 mmol, 0.008 mol%) of the stock solution of the complex was transferred to a round-bottomed flask followed by the addition of the second metal salt *i.e.*, solid $Na_m[M'^{n+}Cl_{(1-n)}]^{m-}\cdot xH_2O$ (0.08 mmol, 0.08 mol%) and the contents were mixed by stirring at room temperature. This resulted in a different coloured solution to which a drop of HCl (conc.) was added with stirring. The surfactant *i.e.* $C_{12}EO_{10}$ (1.0 g) was added to the mixture, which was then mixed and heated gently until it was homogenous. The rest of the methodology is same as given in section **4.3.3**. (mixed-metal precursors). The following mixtures were prepared in an analogous manner.

Metals	**Metal precursor**	**Quantities of metals (wt%)**	**Mass of dried monolith (g)**	**Mass of calcined silica (g)**
Cr-Pd	Na[Cr(EDTA)]	Cr 0.48%	1.550	0.641
	$K_2[PdCl_4]$	Pd 1.00%		
Rh-Pd	$Na_3[RhCl_6].12H_2O$	Rh 0.94 %	1.941	0.834
	$K_2[PdCl_4]$	Pd 1.00 %		
Rh-Ni	$Na_3[RhCl_6].12H_2O$	Rh 0.94%	1.762	0.781
	$Na_2[Ni(EDTA)]$	Ni 0.54%		

General method of preparation of silicas from monometallic precursor

A stock solution (1 cm^3, 0.08 mmol, 0.008 mol%) of the complex $Na_x[M(EDTA)]$ (where M = Cr or Ni) was transferred to a round-bottomed flask, to which a drop of HCl (conc.) was added to acidify the solution to pH 2. For salts of Rh and Pd, (0.08 mmol, 0.008 mol%) was dissolved in acidified water (1 cm^3, pH 2) resulting in a coloured solution. Then, to either of the coloured solution was added $C_{12}EO_{10}$ (1.0 g) followed by gentle heating until a homogenous, viscous layer was obtained. The rest of the methodology then follows section **4.3.3**. (mixed-metal precursors). The details of the relevant materials are tabulated below.

Metals	**Metal precursor**	**Quantities of metals (wt%)**	**Mass of dried monolith (g)**	**Mass of calcined silica (g)**
Cr	Na[Cr(EDTA)]	Cr 0.48%	1.723	0.697
Ni	$Na_2[Ni(EDTA)]$	Ni 0.54%	1.364	0.552
Pd	$K_2[PdCl_4]$	Pd 1.00%	1.931	0.788
Rh	$Na_3[RhCl_6].12H_2O$	Rh 0.94%	1.610	0.666

Conclusions

The aim of the project had been to prepare well-defined, water-soluble, heterodinuclear metal complex anions that could be used in the true liquid crystal templating of mesoporous silicas. These metal complexes would act as metal sources which, when decomposed during calcination would generate well-defined bimetallic nanoparticles of homogeneous composition. Such complexes were sought as earlier work within the group had shown that the use of two different, single-source metal complexes led to bimetallic nanoparticles with a very heterogeneous composition.

Heterobinuclear chlorometallate anions

In defining the true liquid crystal templating approach that had led to this project, a common source of metal had been the various inert chlorometallate anions formed by the second- and third-row transition elements of Groups 7-11. Therefore, the first approach that was tried was to prepare heterobimetallic analogues. Thus, for example, the homobinuclear complex anion $[Cl_2M(\mu\text{-}Cl)_2MCl_2]^{2-}$ (M = Pd, Pt) is known and so possible routes to heterobimetallic analogues $[Cl_2M(\mu\text{-}Cl)_2M'Cl_2]^{2-}$ (M, M' = Pd, Pt, Au) were sought. It turned out that this was not straightforward, but during the course of this work, the following observations were made:

i) It did prove possible to prepare the complex $[Cl_2Pd(\mu\text{-}Cl)_2PtCl_2]^{2-}$ with $[K(18\text{-crown-}6)]^{+}$ as the counter-cation, but the heterobinuclear complex was not isolated pure and formed part of a mixture with the two homodinuclear analogues *i.e.* $[Cl_2Pt(\mu\text{-}Cl)_2PtCl_2]^{2-}$ and $[Cl_2Pd(\mu\text{-}Cl)_2PdCl_2]^{2-}$. The mixture was characterised by a combination of

single crystal X-ray crystallography and ^{195}Pt NMR spectroscopy and the ratio of the three components was found to be:

Pd_2	PtPd	Pt_2
12	3.9	1

A pure heterodinuclear complex was not obtained from this method and this was consistent with related studies that have attempted to prepare mixed-metal Pd/Pt complexes with other ligand sets. This work has been published.[1]

ii) In attempting to prepare similar mixed-metal complexes containing gold by reacting $[AuCl_4]^-$ with $[PdCl_4]^{2-}$ or $[PtCl_4]^{2-}$, it was found that Au^{III} acted as an oxidising agent leading to the formation of $[PtCl_6]^{2-}$ (detected directly *via* ^{195}Pt NMR spectroscopy and single crystal X-ray diffraction) or $[PdCl_6]^{2-}$ (inferred from subsequent reactions). The reduced product was mainly $[AuCl_2]^-$, although Au^0 was often found and, indeed, changing the stoichiometry of the reaction could lead to Au^0 as the preferred gold product. This reaction was studied in most detail for combination of platinum and gold under a variety of conditions, in different solvents and with different counter-cations. One result of this work was numerous single crystal structures of complexes of gold and platinum with these different cations.

iii) Another interesting result was the formation of a butadiene dimer that was formed while reacting $[AuCl_4]^-$ and $[PtCl_4]^{2-}$, in the presence of tetrabutylammonium counter-cation, which was obtained during crystallisation of the solid obtained from these reactions. This dinuclear Pt^{II}-butadiene complex was found to contain a *trans*-1,3-butadiene unit in which each alkene was bound η^2 to a $PtCl_3^-$ unit, like a dimeric version of

Zeise's salt. Further investigation showed that the same complex could also be obtained from a reaction using $[PtCl_4]^{2-}$ and $[PtCl_6]^{2-}$.

In order to explore this further, the reactions with $[AuCl_4]^-$ and $[PtCl_4]^{2-}$ were repeated under different sets of conditions and the results obtained showed that the percentage yield of the dimer tended to increase if vigorously dry conditions were employed. In the course of this study, the mechanism of the reaction could not be elucidated, however the results obtained showed that the complex is formed because of C-H bond activation by Pt^{IV} as reported by Shilov and co-workers.[2]

The discovery of an interesting dimeric Zeise-type analogue has given a new direction to the synthesis of such a unique complex. Hence, to determine the interesting chemistry involved in these preparations it will be useful to repeat the reactions under completely dry conditions in order to attain good yields and to understand the mechanistic details of the reactions. To repeat the reactions with selectively deuteriated alkene would be another advantage as it will assist in the direct analysis of the reaction mixture by ^1H NMR spectroscopy. Evidence was also found for what was believed to be the related *cis*-conformer and it would be of interest to isolate this and prove its identity by a mixture of NMR spectroscopy and single-crystal X-ray methods.

Dinuclear TTHA complexes

As the above approach did not lead to a route which could generate a true heterodinuclear complex, another different approach was sought. In this approach, a homologue of EDTA *i.e.* TTHA was used to coordinate with two different metal ions. TTHA is formally a decadentate ligand, but with

complexes with lower coordination number requirements, it is known to form dinuclear complexes, encapsulating each metal in a five-coordinate N_2O_3 pocket. The method attempted was by trying to first to make a mononuclear complex and then to add the second metal. The chemistry of TTHA did not lend itself to such a simple approach, but during the course of this work, it was found that:

i) Due to the lack of selectivity in TTHA, true heterobimetallic complexes could not be generated in bulk.

ii) Nonetheless, a new heterobimetallic Rh-Zn complex was obtained as single crystal. Other preparations led either to disordered, non-stoichiometric complexes, *e.g.* a Cr-Rh TTHA complex that had a Cr and a Rh in a 3 : 1 ratio disordered over the two coordination sites and which was obtained in good yield, or to homobimetallic complexes containing only one of the metals used in the preparation.

iii) In the course of this work, many (mainly) homodinuclear TTHA complexes were obtained as single crystals and had their structure confirmed by single crystal X-ray diffraction. However, analysis by atomic absorption methods of the bulk material from which the crystals were obtained showed the presence of the two different metals in non-stoichiometric ratios that did not match the stoichiometry in the crystal. This indicated that there is always a possibility to obtain a mixture of homodinuclear complexes (*i.e.* [M_2TTHA] and [M'_2TTHA]) and/or homo- and hetero-dinuclear metal complexes (*i.e.* [M_2TTHA], [M'_2TTHA] and [MM′TTHA]), if a heterobimetallic complex is formed.

Hence, a true heterodinuclear complex is difficult to obtain in bulk by this method of preparation. The results of this work have been published.[3]

Despite this, from the discovery of a 1 : 1 Rh : Zn complex and a 3 : 1 Cr : Rh complex, the possibility of the formation of a true heterobimetallic complex clearly exists. This would be possible only if efforts can be made focusing on initial synthesis of inert, mononuclear TTHA complexes as there is strong possibility that the empty coordination sites of the ligand will tend to bind with the incoming ligand in the second metal coordination step. Nevertheless, the synthesis of mononuclear complex will require a more rigorous approach, for which careful selection of pH and separation of the mononuclear complex are the two main tasks that will be necessary.

Metal-TTHA complexes in true liquid crystal templating

The idea of using such aminopolycarboxylates metal complexes as a mixed-metal precursor suggested a possibility of a new route to synthesise heterobimetallic nanoparticles doped into a mesoporous support (silica). Therefore, despite the fact that the precursor complexes were of uncertain composition, they were evaluated as the metal source in true liquid crystal templating of silica using a neutral ethylene oxide surfactant and $Si(OMe)_4$ as the silica source. The silicas were characterised by a combination of low- and wide-angle X-ray diffraction, TEM and BET surface area analysis. The results of the analysis showed that hexagonal MCM-41 analogues were indeed formed, often with rather high surface areas (>950 $m^2\ g^{-1}$). Previous results from the group have inferred that such high surface areas often suggest that metal nanoparticles are not contained within the pores, for when they are,

they cause partial pore blocking that reduces the measured surface area. Results from TEM analysis were consistent with this view and often showed particles present on the surface or significantly larger than the pore diameter (and, by inference, not contained within them). Further, in some cases there was no evidence for nanoparticle formation in the pore structure at all, suggesting either that all the metal is on the surface or that some is contained within the silica framework. The metal particles were found either as a mixture of oxidised nanoparticles or as a mixture of reduced as well as oxidised particles and only on one occasion *i.e.* for Rh-Ni, were reduced nanoparticles observed. Thus, the final targets of well-dispersed, bimetallic nanoparticles remained unachieved. This major limitation of the particles being not always present within the pores can only be eliminated by the an alternative route which is yet to be discovered, by which, insertion of metal particles into the apolar region of the micelles in the mesophase would be possible. Such an approach has been demonstrated for monometallic precursors,[4] but remains to be deployed for bimetallic systems.

References

Chapter 1

1 C. E. Fairhurst, S. Fuller, J. Gray, M. C. Holmes and G. J. T. Tiddy, *The Handbook of Liquid Crystals*, Wiley-VCH, Series Editors: G. W. Gray, J. Goodby, D. Demus, H. W. Spies, V. Vill, Weinheim, 1998.

2 K. Lunkenheimer, A. Lind, and M. Jost, *J. Phys. Chem. B*, 2003, **107**, 7527.

3 L. L. Schramm, *Surfactants: Fundamentals and Applications in the Petroleum Industry*, Cambridge University Press, 2000.

4 D. F. Evans, and W. Wennerström, *The Colloidal Domain*, VCH, New York, 1994, 516 pp.

5 C. Tanford, *Hydrophobic Effect: Formation of Micelles and Biological Membranes*, Second Edition, Wiley: NewYork, 1980.

6 J. N. Ischalachvilli, *Intermolecular and Surface Forces*, Second Edition, Academic Press: London, 1992.

7 G. J. D. Soler-illia, C. Sanchez, B. Lebeau, and J. Patarin, *Chem. Rev.*, 2002, **102**, 4093.

8 F. Schüth, K. S. W. Sing, and J. Weitkamp, *Handbook of Porous Solids*, Wiley VCH, Vol. 3.

9 P. J. Colings and M. Hird, *An Introduction to Liquid Crystals: Chemistry and Physics*, Taylor and Francis, London, 1997.

10 J.-Feng, K. Aramaki, K. Yanagihara, and H. Kunieda, *J. Jpn. Oil Chem. Soc.*, 1998, **47**, 1233.

11 G. Burducea, *Rom. Rep. Phys.*, 2004, **56**, 66.

12 I. Muscutariu, *Cristale Lichide si Aplicatii*, Ed. Tehnica, Bucarest, 1981.

13 V. Luzzati, and F. Husson, *J. Cell Biol.*, 1962, **12**, 207.

14 V. Luzzati, A.Tardieu, T. G.-Krzywicki, E. Rivas, and F. R.-Husson, *Nature*, 1968, **220**, 485.

15 V. Luzzati and P. A. Spegt, *Nature*, 1967, **215**, 701.

16 J. Charvolin and J. F. Sadoc, *J. Phys.*, 1988, **49**, 521.

17 E. M. Landau and J. P. Rosenbush, *Proc. Natl. Acad. Sci.*, 1996, **93**, 14532.

18 B. Naik and N. N. Ghosh, *Recent Pat. Nanotechnol.*, 2009, **3**, 213.

19 L. B. McCusker, F. Liebau and G. Engelhardt, *Pure Appl. Chem.*, 2001, **73**, 381.

20 J. L. Schlenker, and G. H. Kuhl, *Proc. Ninth Intl. Zeolites Conf., ed.* R. von Ballmoos, J. B. Higgins and M. M. Treacy, Butterworth-Heinemann, Boston, MA, p 3. 1993.

21 M. M. Helmkamp and M. E. Davies, *Ann. Rev. Mater. Sci.*, 1995, **25**, 161.

22 M. Niwa, N. Katada, and K. Okumura, *Characterization and Design of Zeolite Catalysts: Solid Acidity, Shape Selectivity and Loading Properties*, Series: Springer Series in Materials Science, **141**, First Edition, 2010, X, p 184.

23 B. Yilmaz and U. Müller, *Top. Catal.*, 2009, **52**, 888.

24 A. Imhof and D. J. Pine, *Nature*, 1997, **389**, 948.

25 J. Rouquérol, D. Avnir, C. W. Fairbridge, D. H. Everett, J. H. Haynes, N. Pericone, J. D. F. Ramsay, K. S. W. Sing, and K. K. Unger, *Pure Appl. Chem.*, 1994, **66**, 1739.

26 *B. G. Trewyn*, I. I. Slowing, S. Giri, H.-T. Chen, and V. S.-Y. Lin, *Acc. Chem. Res., 2007, **40**, 846.*

27 J. S. Beck, J. C. Vartuli, W. J. Roth, M. E. Leonowicz, C. T. Kresge, K. D. Schmitt, C. T-W. Chu, D. H. Olsen, E. W. Sheppard, S. B. McCullen, J. B. Higgins, and J. L. Schlenker, *J. Am. Chem. Soc.*, 1992, **114**, 1083.

28 J. Y. Ying, C. P. Mehnert, and M. S. Wong, *Angew Chem. Int. Ed.*, 1999, **38**, 56.

29 F. Kleitz, in *Handbook of Heterogeneous Catalysis*, Second Edition, G. Ertl, H. Knötzinger, F. Schüth and J. Weitkamp, Eds., VCH-Wiley, Weinheim, 2008**,** Vol. 1, p. 168-219.

30 C. T. Kresge, M. E. Leonowicz, W. J. Roth, J. C. Vartuli, and J. S. Beck, *Nature*, 1992, **359**, 710.

31 C. T. Kresge, M. E. Leonowicz, W. J. Roth, and J. C. Vartuli, *Chem. Abstr.*, 1992, **117**, 72621.

32 J. C. Vartuli, K. D. Schmitt, C. T. Kresge, W. J. Roth, M. E. Leonowicz, S. B. McCullen, S. D. Hellring, J. S. Beck, J. L. Schlenker, D. H. Olsen, and E. W. Sheppard, *Chem. Mater.*, 1994, **6**, 2317.

33 C. T. Kresge, M. E. Leonowicz, W. J. Roth, and J. C. Vartuli: US5098684 (1992).

34 T. Yanagisawa, T. Shimizu, K. Kuroda, and C. Kato, *Bull. Chem. Soc. Jpn.*, 1990, **63**, 988.

35 N. Takashi, H. Tamura, D. Mochizuki, T. Kimura, and K. Kuroda, *Proceedings of International Symposium on EcoTopia*, 2007, ISETS07, 2007.

36 S. Vortmann, J. Rius, B. Marler and H. Gies, *Eur. J. Mineral.*, 1999, **11**, 125.

37 L. A. J. Garvie, B. Devouard, T. L. Groy, F. Camara and P. R. Buseck, *Am. Mineral*, 1999, **84**, 1170.

38 P. Piekarz, M. Derzsi, P. T. Jochym, J. Łażewski, M. Sternik, K. Parlinski, and E. M. Serwicka, *Phys. Rev. B: Condens. Matter*, 2009, **79**, 134105.

39 S. Inagaki, Y. Fukushima, and K. Kuroda, *J. Chem. Soc., Chem. Commun.*, 1993, 680.

40 S. Inagaki, A. Koiwai, N. Suzuki, Y. Fukushima, and K. Kuroda, *Bull. Chem. Soc. Jpn.*, 1996, **69**, 1449.

41 X. Ji, K. T. Lee, M. Monjauze, and L. F. Nazar, *Chem. Commun.*, 2008, 4288.

42 A. Steel, S. W. Carr, and M. W. Anderson, *J. Chem. Soc., Chem. Commun.*, 1994, 1571.

43 A. Monnier, F. Schüth, Q. Huo, D. Kumar, D. Margolese, R. S. Maxwell, G. D. Stucky, M. Krishnamurty, P. Petroff, A. Firouzi, M. Janicke, and B. F. Chmelka, *Science*, 1993, **261**, 1299.

44 A. Firouzi, D. Kumar, L. M. Bull, T. Besier, P. Sieger, Q. Huo, S. A. Walker, J. A. Zasadzinski, C. Glinka, J. Nicol, D. Margolese, G. D. Stucky, and B. F. Chmelka, *Science*, 1995, **267**, 1138.

45 O. Regev, *Langmuir*, 1996, **12**, 4940.

46 A. Hilonga, J.-K. Kim, P. B. Sarawade, D. V. Quang, G. N. Shao, G. Elineema, and H. T. Kim, *J. Ind. Eng. Chem.*, 2012, **15**, 1841.

47 P. Makowski, X. Deschanels, A. Grandjean, D. Meyer, G. Toquer, and F. Goettmann, *New J. Chem.*, 2012, **36**, 531.

48 J. Rathousky, A. Zukai, O. Franke, and G. J. Schulz-Ekloff, *J. Chem. Soc.*, Faraday Trans., 1995, **91**, 937.

49 A. Walcarius and J. Bessière, *Chem. Mater.*, 1999, **11**, 3009.

50 J. W. Lee, D. L. Cho, W. G. Shim and H. Moon, *Korean J. Chem. Eng*., 2004, **21**, 246.

51 K. Ghosh, S. Bashadi, H.-J. Lehmler, S. E. Rankin and B. L. Knutson, *Ind. Eng. Chem. Res.*, 2008, **113**, 106.

52 M. V. Regi, L. R. González, I. I.-Barba, and J. M. G.-Calbet, *J. Mater. Chem*., 2006, **16**, 26.

53 M. Hartmann, *Chem. Mater*., 2005, **18**, 4577.

54 T. J. Pinnavaia, *Science*, 1983, **220**, 365.

55 D. M. Moore, and Jr. R. C. Reynolds, *X-Ray Diffraction and the Identification and Analysis of Clay Minerals*, Second Edition, Oxford University Press; Oxford, 1997.

56 G. W. Brindley and R. E. Sempels, *Clay Miner*., 1977, **12**, 229.

57 S. Yamanaka and G. W. Brindley, *Clays Clay Miner*., 1978, **26**, 21.

58 P. Salerno, M. B Asenjo, and S. Mendioroz, *Thermochim. Acta*, 2001, **379**, 101.

59 R. J. Lussier, J. S. Magee, and D. E. W. Vaughan, preprints, *7th Canadian Symposium on Catalysis*, Edmonton, Alberta, 1980.

60 A. Corma, *Chem. Rev*., 1997, **97**, 2373.

61 F. Figueras, *Catal. Rev. Sci. Eng.*, 1988, **30**, 457.

62 C.-Y. Mou and H.-P. Lin, *Pure Appl. Chem*., 2000, **72**, 137.

63 C. J. Brinker and G. W. Scherer, *J. Sol-Gel Sci. Technol.*, 1990.

64 R. A. A. Melo, M. V. Giotto, J. Rocha, and E. A. U-González, *J. Mater. Res.*, 1999, **2**, 173.

65 G. S. Attard, J. C. Glyde, and C. G. Göltner, *Nature*, 1995, **378**, 366.

66 J. S. Beck, *US Patent No*.5, 1991, **296**, 057.

67 W. Guo, G.S. Luo, and Y.J. Wang, *J. Colloid and Interface Sci.*, 2004, **271**, 400.

68 Y. K. Hwang, K. R. Patil, S. H. Jhung, J.-S. Chang, Y. J. Ko, and S.-E. Park**,** *Microporous Mesoporous Mater.*, 2005, **78**, 245.

69 F. Zhang, Y. Yan, Y. Meng, Y. Xia, B. Tu, and D. Zhao, *Microporous Mesoporous Mater*., 2007, **98**, 6.

70 B.-G. Park, W. Guo, X. Cui, J. Park, and C.-S. Ha, *Microporous Mesoporous Mater*., 2003, **66**, 229.

71 T. Sano, Y. Kiyozumi, M. Kawamura, F. Mizukami, H. Takaya, T. Mouri, W. Inaoka, Y. Toida, M. Watanabe, and K. Toyoda, *Zeolites*, 1991, **11**, 842.

72 Q. Huo, D. I. Margolese, U. Ciesla, P. Feng, T. E. Gier, P. Sieger, R. Leon, P. M. Petroff, F. Schüth, and G. D. Stucky, *Nature*, 1994, **368**, 317.

73 G. D. Stucky, P. K. Hansma, G. Friedbacher, and E. Ramli, *Science*, 1991, **253**, 1261.

74 G. D. Stucky, D. E. Morse, M. A. Cariolou, and P. Hansma, *Mat. Res. Soc. Symp. Proc*., 1993, **292**, 59.

75 P. T. Tanev, and T. J. Pinnavaia, *Science*, 1995, **267**, 865.

76 C. H. Christensen and J. K. Nørskov, *J. Chem. Phys.*, 2008, **128**, 182503.

77 I. Maxwell, *Stud. Surf. Sci. Catal.*, 1996, **101**, 1.

78 P. L. J. Gunter, J. W. Niemantsverdriet, F. H. Ribeiro, and G. A. Somorjai, *Catal. Rev. Sci. Eng.*, 1997, **39**, 77.

79 D. S. Shepard, T. Maschmeyer, B. F. G. Johnson, J. M. Thomas, G. Sankar, D. Ozkaya, W. Zhou, and R.D. Oldroy, *Angew. Chem. Int. Ed. Eng.*, 1997, **36**, 2242.

80 D. S. Shephard, T. Maschmeyer, G. Sankar, J. M. Thomas, D. Ozkaya, B. F. G. Johnson, R. Raja, R. D. Oldroyd, and R. G. Bell, *Chem. Eur. J.*, 1998, **4**, 1214.

81 S. Hermans, R. Raja, J. M. Thomas, B. F. G. Johnson, G. Sankar, and D. Gleeson, *Angew. Chem. Int. Ed.*, 2001, **40**, 1211.

82 R. Raja, G. Sankar, S. Hermans, D. S. Shephard, S. Bromley, J. M. Thomas, and B. F. G. Johnson, *Chem. Commun.*, 1999, 1571.

83 J. Panpranot, J. G. Goodwin, Jr., and A. Sayari, *Catal. Today*, 2002, **77**, 269.

84 J. Panpranot, J. G. Goodwin, Jr., and A. Sayari, *J. Catal.*, 2002, **211**, 530.

85 Ö. Çelik and Ö. Dag, *Angew. Chem. Int. Ed.*, 2001, **40**, 3799.

86 Ö. Dag, O. Samarskaya, N. Coombs and G. A. Ozin, *J. Mater. Chem.*, 2003, **13**, 328.

87 D. W. Bruce, J. D. Holbrey, A. R. Tajbakhsh, and G. J. T. Tiddy, *J. Mater. Chem.*, 1993, **3**, 905.

88 K. E. Amos, N. Brooks, N. C. King, S. Xie, J. Canales-Vazquez, M. J. Danks, H. B. Jervis, W. Zhou, J. M. Seddon, and D. W. Bruce, *J. Mater. Chem.*, 2008, **18**, 5282.

89 M. J. Danks, H. B. Jervis, M. Nowotny, W. Zhou, T. A. Maschmeyer, and D. W. Bruce, *Catal. Lett.*, 2002, **82**, 95.

90 N. C. King, C. Dickson, W. Zhou, and D. W. Bruce, *Dalton Trans.*, 2005, 1047.

91 N. C. King, R. A. Blackley, W. Zhou, and D. W. Bruce, *Chem. Commun.*, 2006, 3411.

92 N. C. King, R. A. Blackley, M. L. Wears, D. M. Newman, W. Zhou, and D. W. Bruce, *Chem. Commun*., 2006, 3414.

93 B. I. Kharisov , P. E. Martínez , V. M. Jiménez-Pérez, O. V. Kharissova, B. N. Martínez and N. Pérez, *J. Coord. Chem.*, 2010, **63**, 1.

94 A. S. Potapov, E. A. Nudnova, V. D. Ogorodnikov, T. V. Petrenko, and A. I. Khlebnikov, *ScientificWorldJournal*, Volume 2012, Article ID 798271, 1.

95 S. Lanza, F. Nicoló, H. A. Rudbari, M. R. Plutino, and G. Bruno, *Inorg. Chem.* 2011, **50**, 11653.

96 Y. Mulyana, L. F. Lindoy, C. J. Kepert, J. McMurtrie, A. Parkin, P. Turner, G. Wei, and J. G. Wilson, *J. Incl. Phenom. Macrocycl. Chem.*, 2011, **71**, 455.

97 L. Yu, Z. Wang, J. Wu, S. Tu, and K. Ding, *Angew. Chem. Int. Ed*., 2010, **49**, 3627.

98 B. Chakraborty, P. Halder, S. Chakraborty, O. Das, and S. Paria, *Inorg. Chim. Acta*, **387**, 2012, 332.

99 Q.-T. Lin, L.-M. Pei, W.-C. Xu, H. Chao, and L.-N. Ji, *Inorg. Chem. Commun.*, 2012, **16**, 104.

100 A. Ray, G. Pilet, C. J. G.-García, and S. Mitra, *Polyhedron*, 2009, **28**, 511.

101 M. Ruben, J. Rojo, F. J. R.-Salguero, L. H. Uppadine, and J.-M. Lehn, *Angew. Chem. Int. Ed*., 2004, **43**, 3644.

102 S. Bullock, L. J. Gillie, L. P. Harding, C. R. Rice, T. R.-Johannessen, and M. Whitehead, *Chem. Commun.*, 2009, 4856.

103 P. A. Vigato, V. Peruzzo, and S. Tamburini, *Coord. Chem. Rev.*, 2012, **256**, 953.

104 H. S. Chow, E. C. Constable, C. E. Housecroft, M. Neuburger, S. Schaffner, *Polyhedron*, 2006, **25**, 1831.

105 G. A. Lawrance, *Introduction to Coordination Chemistry*, Wiley, Edition I, 2010.

106 M. S. Tremblay and D. Sames, *Chem. Commun.*, 2006, 4116.

107 C. R. Langrick, P. G. Pringle, and B. L. Shaw, *J. Chem. Soc. Dalton Trans.*, 1984, 1233.

108 C. R. Langrick, P. G. Pringle, and B. L. Shaw , *J. Chem. Soc. Dalton Trans.*, 1985, 1015.

109 N. W. Alcock, T. J. Kemp, P. G. Pringle, P. Bergamini and O. Traverso, *J. Chem. Soc., Dalton Trans.*, 1987, 1659.

110 P. G. Pringle and B. L. Shaw, *J. Chem. Soc., Chem. Commun.*, 1982, 1313.

111 C. R. Langrick, D. M. McEwan, P. G. Pringle, and B. L. Shaw, *J. Chem. Soc., Dalton Trans.*, 1983, 2487.

112 F. S. M. Hassan, D. P. Markham, P. G. Pringle, and B. L. Shaw, *J. Chem. Soc., Dalton Trans.*, 1985, 279.

113 P. G. Pringle and B. L. Shaw, *J. Chem. Soc., Dalton Trans.*, 1983, 889.

114 P. G. Pringle and B. L. Shaw, *J. Chem. Soc., Dalton Trans.*, 1984, 849.

115 A. T. Hutton, P. G. Pringle, and B. L. Shaw, *J. Chem. Soc., Dalton Trans.*, 1985, 1677.

116 P. G. Pringle and B. L. Shaw, *J. Chem. Soc., Chem. Commun.*, 1982, 81.

117 D. M. McEwan, P. G. Pringle, and B. L. Shaw, *J. Chem. Soc., Chem. Commun*., 1982, 1240.

118 P. G. Pringle and B. L. Shaw, *J. Chem. Soc., Chem. Commun.*, 1982, 956.

119 W. S. McDonald, P. G. Pringle, and B. L. Shaw, *J. Chem. Soc., Chem. Commun.*, 1982, 861.

120 G. R. Cooper, A. T. Hutton, C. R. Langrick, D. M. McEwan, P. G. Pringle, and B. L. Shaw, *J. Chem. Soc., Dalton. Trans.*, 1984, 855.

121 A. T. Hutton, C. R. Langrick, D. M. McEwan, P. G. Pringle, and B. L. Shaw, *J. Chem. Soc., Dalton Trans.*, 1985, 2121.

122 D. M. McEwan, P. G. Pringle, and B. L. Shaw, *J. Chem. Soc., Chem. Commun*., 1982, 859.

123 D. M. McEwan, D. P. Markham, P. G. Pringle, and B. L. Shaw, *J. Chem. Soc., Dalton Trans.*, 1986, 1809.

124 A. Blagg, P. G. Pringle, and B. L. Shaw, *J. Chem. Soc., Dalton Trans.*, 1987, 1495.

125 A. Blagg, A. T. Hutton, P. G. Pringle, and B. L. Shaw, *J. Chem. Soc.***,** *Dalton Trans.*, 1984, 1815.

126 K. M. C. Wong, S. C. F. Lam, C. C. Ko, N. Zhu, V. W. W. Yam, S. Roué, C. Lapinte, S. Fathallah, K. Costuas, S. Kahlal, and J. F. Halet, *Inorg. Chem.*, 2003, **42**, 7086.

127 K. L. Cheung, S. K. Yip, and V. W. W. Yam, *J. Organomet. Chem*., 2004, **689**, 4451.

128 E. C. Constable, P. Harverson, C. E. Housecroft, E. Nordlander, and J. Olsson, *Polyhedron*, 2006, **25**, 437.

129 A. Bencini and V. Lippolis, *Coord. Chem. Rev.*, 2010, **254**, 2096.

130 T. A. Kaden, *Top. Curr. Chem.* 1984, **121**, 157.

131 R. W. Hay, in: E. Kimura (Ed.), *Current Topics in Macrocyclic Chemistry in Japan*, Hiroshima University, 1987, p. 56.

132 T. Koullourou, L. S. Natrajan, H. Bhavsar, S. J. A. Pope, J. H. Feng, J. Narvainen, R. Shaw, E. Scales, R. Kauppinen, A. M. Kenwright, and S. Faulkner, *J. Am. Chem. Soc.*, 2008, **130**, 2178.

133 J. Paris, C. Gameiro, V. Humblet, P. K. Mohapatra, V. Jacques, and J. F. Desreux, *Inorg. Chem.*, 2006, **45**, 5092.

134 P. A. Vigato and S. Tamburini, *Coord. Chem. Rev.*, 2004, **248**, 1717.

135 H. Houjou, M. Ito, and K. Araki, *Inorg. Chem.*, 2009, **48**, 10703.

136 A. C. W. Leung, J. K.-H. Hui, J. H. Chong, and M. J. MacLachlan, *Dalton Trans.*, 2009, **26**, 5199.

137 A. Roth, E. T. Spielberg, and W. Plass, *Inorg. Chem.*, 2007, **46**, 4362.

138 U. S. Schubert, H. Hofmeier, and G. R. Newkome, *Modern Terpyridine Chemistry*, Wiley-VCH, Weinheim, 2006.

139 H. Hofmeier and U. S. Schubert, *Chem. Soc. Rev.*, 2004, **33**, 373.

140 W.-S. Li, J. Luo, and Z.-N. Chen, *Inorg. Chem. Comm*., 2011, **14**, 1898.

141 E. C. Constable, C. E. Housecroft, M. Neuburger, S. Schaffner, E. J. Shardlow, *Inorg. Chim. Acta*, 2007, **360**, 4069.

142 J. V. Ortega, B. Hong, S. Ghosal, J. C. Hemminger, B. Breedlove and C. P. Kubiak, *Inorg. Chem.*, 1999, **38**, 5102.

143 D. Xu, H. J. Murfee, W. E. van der Veer, and B. Hong, *J. Organomet. Chem.*, 2000, **596**, 53.

144 W.-Y. Wong, *Coord. Chem. Rev.*, 2005, **249**, 971.

145 N. Wheatley and P. Kalck, *Chem. Rev.*, 1999, **99**, 3379.

146 P. Braunstein, J. Durand, M. Knorr and C. Strohmann, *Chem. Commun.*, 2001, 211.

147 T. W. Graham, A. Llamazares, R. McDonald and M. Cowie, *Organometallics*, 1999, **18**, 3502.

148 R. Kempe, H. Noss, and T. Irrgang, *J. Organomet. Chem.*, 2002, **647**, 12.

149 N. Nakata, M. Sakashita, C. Komatsubara, and A. Ishii, *Eur. J. Inorg. Chem*., 2010, 447.

150 S. Leelasubcharoen, P. A. Zhizhko, L. G. Kuzmina, A.V. Churakov, J. A. K. Howard, and G. I. Nikonov, *Organometallics*, 2009, **28**, 4500.

151 Q. F. Mokuolu, A. G. Avent, P. B. Hitchcock, and J. B. Love, *J. Chem. Soc*., *Dalton Trans.*, 2001, 2551.

Chapter 2

1 N. C. King, *PhD thesis*, 2004, University of Exeter.

2 D. K. Seth and S. Bhattacharya, *Polyhedron*, 2011, **30**, 2438.

3 B. P. Andreini, D. B. Dell'Amico, F. Calderazzo and M. G. Venturi, *J. Organomet. Chem*., 1988, **354**, 357.

4 E. L. Dias and R. H. Grubbs, *Organometallics*, 1998, **17**, 2758.

5 A. A. H. van der Zeijden, G. van Koten, R. Luijk, K. Vrieze, C. Slob, H. Krabbendam and A. L. Spek, *Inorg. Chem.*, 1988, **27**, 1014.

6 J. R. Briggs, C. Crocker, W. S. McDonald and B. L. Shaw, *J. Chem. Soc.*, *Dalton*, 1980, 64.

7 R. Usón J. Fórnies, R. Navarro and M. P. García, *Inorg. Chim. Acta*, 1979, **33**, 69.

8 R. J. Goodfellow and L. M. Venanzi, *J. Chem. Soc.*, 1965, 7533.

9 P. L. Goggin, R. J. Goodfellow, and F. J. S. Reed, *J. Chem. Soc.*, *Dalton*, 1972, 1298.

10 P. L. Goggin, *J. Chem. Soc.*, *Dalton*, 1974, 1483.

11 D. C. Harris and H. B. Gray, *Inorg. Chem.*, 1974, **13**, 2250.

12 R. Usón, A. Lacuna, M. Lacuna and M. Abad, *J. Organomet. Chem.*, 1983, **249**, 437.

13 D. B. Dell'Amico, F. Calderazzo, F. Marchetti, S. Ramello and S. Samaritani, *Inorg. Chem.*, 2008, **47**, 1237.

14 J. Chatt, *J. Chem. Soc.*, 1950, 2301.

15 C. Masters and J. P. Visser, *J. Chem. Soc.*, *Chem. Comm.*, 1974, 932.

16 A. A. Kiffen, C. Masters and J. P. Visser, *J. Chem. Soc.*, *Dalton Trans.*, 1975, 1311.

17 H. C. Clark, G. Ferguson, V. K. Jain, and M. Parvez, *Inorg. Chem.*, 1985, **24**, 1477.

18 D. Steinborn, M. Tschoerner, A. Zweidorf, J. Sieler, and H. Bögel, *Inorg. Chim. Acta*, 1995, **234**, 47.

19 M. Gerisch, F. W. Heinemann, U. Markgraf and D. Steinborn, *Z. Anorg. Allg. Chem.*, 1997, **623**, 1651.

20 G. G. Talanova, K. B. Yatsimirskii and O. V. Kravchenko, *Ind. Eng. Chem. Res.*, 2000, **39**, 3611.

21 N. C. King, R. A. Blackley, M. L. Wears, D. M. Newman, W. Zhou, and D. W. Bruce, *Chem. Commun.*, 2006, 3414.

22 P. S. Pregosin and H. Rüegger, *Inorg. Chim. Acta*, 1984, **86**, 55.

23 F. Séby, M. Potin-Gautier, E. Giffaut, and O. F. X. Donard, *Geochimi. Cosmochim. Acta*, 2001, **65**, 3041.

24 A. L. Garay, A. Pichon and S. L. James, *Chem. Soc. Rev.*, 2007, **36**, 846.

25 M. N. Sokolov, A. L. Gushchin, D. Y. Naumov, O. A. Gerasko, and V. P. Fedin, *Inorg. Chem.*, 2005, **44**, 2431.

26 K. Fujii, A. G. Lazuen, J. Hill, E. Sbircea, Z. Pan, M. Xu, D. C. Apperley, S. L. James, and K. D. M. Harris, *Chem. Commun.*, 2010, 7572.

27 A. Nakamura, T. Sato and R. Kuroda, *Chem. Commun.*, 2004, 2858.

28 C. Jobbágy, T. Tunyogi, G. Pálinkás, and A. Deák, *Inorg. Chem.*, 2011, **50**, 7301.

29 A. Orita, L. Jiang, T. Nakano, N. Ma, and J. Otera, *Chem. Commun.*, 2002, 1362.

30 S. A. Mitchenko, E. V. Khomutov, V. V. Kovalenko, A. F. Popov, and I. P. Beletskaya, *Inorg. Chim. Acta*, 2001, **320**, 31.

31 C. Suryanarayana, *Prog. Mater. Sci.*, 2001, **46**, 1.

32 N. K. Sethi, A. C. Whitwood, and D. W. Bruce, *Eur. J. Inorg. Chem.*, 2013, 2078.

33 R. H. B. Mais, P. G. Owston, and A. M. Wood, *Acta Crystallogr., Sect. B*, 1972, **28**, 393.

34 W. Theilacker, *Z. Anorg. Allg. Chem.*, 1937, **234**, 161.

35 Y. Zhang and P. Coppens, private communication to Cambridge Crystallographic Database, 2002 (CCDC-185101).

36 CCDC-905392, -905393 and -905394 contain the supplementary crystallographic data for paper in reference 54. These data can be obtained free of charge from The Cambridge Crystallographic Data Centre *via* www.ccdc.cam.ac.uk/data_request/cif.

37 See, for example: P. S. Pregosin, *Coord. Chem. Rev.*, 1982, **44**, 247.

38 F. Basolo, and R. G. Pearson, *Mechanisms of Inorganic Reactions*, New York: Wiley, 1967, p. 359.

39 T. M. Buslaeva, D. S. Umreiko and G. G. Novitskii, *Khimiya i spektroskopiya galogenidov platinovykh metallov* (*Chemistry and Spectroscopy of Platinum Metal Halides*), Minsk: Universitetskoe, 1990.

40 I. A. Zakharova, *Issledovaniya po neorganicheskoi khimii i tekhnologii* (*Studies in Inorganic Chemistry and Technology*), Moscow: Nauka, 1988, p. 171.

41 RF Patent 202968, Byull. Izobret, 1994, no. 21.

42 RF Patent 2089186, Byull. Izobret, 1997, no. 25.

43 I. A. Efimenko, *Koord. Khim.*, (*Russ. J. Coord. Chem.*), 1998, **24**, 265.

44 A. K. Lyashchenko, D. V. Loginova, A. S. Lileev, N. A. Ivanova, and I. A. Efimenko, *Russ. J. Coord. Chem.*, 2009, **35**, 633.

45 R. M. Smith and A. E. Martell, *Critical Stability Constants*, New York: Plenum, 1976, **4**, p. 257.

46 Md. A. Hossain, D. R. Powell, and K. Bowman-James, *Acta Crystallogr.*, 2003, **E59**, m57.

47 B. N. Ivanov-Emin, L. D. Borzova, A. M. Egorov, and D. Subzhben, *Russ. J. Inorg. Chem.*, 1974, **19**, 855.

48 B. N. Ivanov-Emin, N. U. Venskovskii, I. N. Lin'ko, B. Zaitsev and L. D. Borzova, *Koord. Khim.*, 1980, **6**, 928.

49 A. F. Trotman-Dickenson, J. C. Bailar, H. J. Emeleus, and R. Nyholm, *Comprehensive Inorganic Chemistry*, vol. 4, Pergamon Press, Oxford, 1973.

50 R. Gilbert, M. Karabulut and P. E. Hoggard, *Inorg. Chim. Acta*, 2010, **363**, 146.

51 H. Hellot, '*Histoire de 1' academie royale des sciences*' 1737, 101.

52 A. Vogler and H. Kunkely, *Coord. Chem. Rev.*, 2001, **219–221**, 489.

53 A. M. Kini, J. P. Parakka, U. Geiser, H.-H. Wang, F. Rivas, E. DiNino, S. Thomas, J. D. Dudek and J. M. Williams, *J. Mater. Chem.*, 1999, **9**, 883.

54 K. Ortner, *PhD Thesis*, University of Tübingen, 1999.

55 S. J. Berners-Price, R. J. Bowen, T. W. Hambley, and P. C. Healy, *J. Chem. Soc*., *Dalton Trans*., 1999, 1337.

56 A. Venugopal, A. P. Shaw, K. W. Törnroos, R. H. Heyn, and M. Tilset, *Organometallics*, 2011, **30**, 3250.

57 L. Cao, M. C. Jennings, and R. J. Puddephatt, *Inorg. Chem.*, 2007, **46**, 1361.

58 M. Yamashita, H. Ohashi, Y. Kobayashi, Y. Okaue, T. Kurisaki, H. Wakita, and T. Yokoyama, *J. Colloid Interface Sci.*, 2008, **319**, 25.

59 B. V. Rao, *Anal. Chim. Acta*, 1992, **258**, 167.

60 O. Renn, B. Lippert, A. Albinati, and F. Lianza, *Inorg. Chim. Acta*, 1993, **211**, 177.

61 W. Micklitz, O. Renn, H. Schöllhorn, U. Thewalt and B. Lippert, *Inorg. Chem.*, 1990, **29**, 1836.

62 J. Kramer and K. R. Koch, *Inorg. Chem.*, 2007, **46**, 7466.

63 B. M. Still, P. G. A. Kumar, J. R. Aldrich-Wright, and W. S. Price, *Chem. Soc. Rev.*, 2007, **36**, 665.

64 P. Hollmann, and W. Z. Preetz, *Naturforsch. B*, 1991, **601**, 47.

65 P. M. Cook, L. F. Dahl, and D. W. Dickerhoof, *J. Am. Chem. Soc.*, 1972, **94**, 5511.

66 J. Kramer and K. R. Koch, *Inorg. Chem.*, 2006, **45**, 7843.

67 A. S. Gaballa, H. Schmidt, C. Wagner, and D. Steinborn, *Inorg. Chim. Acta*, 2008, **361**, 2070.

68 Ö. Gröning, T. Drakenberg, and L. I. Elding, *Inorg. Chem.*, 1982, **21**, 1820.

69 Chemical shifts are reported to high frequency of **Ξ** = 21.4617.

70 A. Gaballa, H. Schmidt, G. Hempel, D. Reichert, C. Wagner, E. Rusanov, and D. Steinborn, *J. Inorg. Biochem.*, 2004, **98**, 439.

71 J. J. Pesek and W. R. Mason, *J. Magn. Reson.*, 1977, **25**, 519.

72 T. M. Mitchell and B. Costisella, *NMR-From Spectra to Structures - An Experimental Approach*, Second Edition, Springer-Verlag Berlin Heidelberg, 2007.

73 D. C. Powers and T. Ritter, *Nat. Chem.*, 2009, **1**, 302.

74 D. C. Powers, M. A. L. Geibel, J. E. M. N. Klein, and T. Ritter, *J. Am. Chem. Soc.*, 2009, **131**, 17050.

75 A. Santoro, M. Wegrzyn, A. C. Whitwood, B. Donnio, and D. W. Bruce, *J. Am. Chem. Soc.*, 2010, **132**, 10689.

76 P. Murray and K. R. Koch, *J. Coord. Chem.*, 2010, **63**, 2561.

77 A. S. Gaballa, S. M. Teleb, and T. A. K. Al-Allaf, *Maced. J. Chem. Chem. Eng.*, 2005, **24**, 147.

78 D. Steinborn, O. Gravenhorst, C. Bruhn, D. Mikloš, M. Dunaj-Jurčo, and A. Kolbe, *Z. Anorg. Allg. Chem.*, 1997, **623**, 1954.

79 P. E. Slade and H. B. Jonassen, *J. Am. Chem. Soc.*, 1956, **79**, 1277.

80 P. J. Hendra and D. B. Powell, *Spectrochim. Acta*, 1962, **18**, 1195.

81 J. Chatt, *Inorg. Chem. Varenna, Accadamia Najionale dei Tircei*, 1961, **1959**, 161.

82 M. J. Grogan and K. Nakamoto, *Inorg. Chim. Acta*, 1967, **1**, 228.

83 G. Davidson, *Inorg. Chim. Acta*, 1969, 596.

84 M. J. Grogan and K. Nakamoto, *J. Am. Chem. Soc.*, 1966, **88**, 5454.

85 V. C. Adam, J. A. J. Jarvis, B. T. Kilbourn, and P. G. Owston, *Chem. Commun.*, 1971, 467.

86 H. C. Strauch, G. Erker, and R. Fröhlich, *Organometallics*, 1998, **17**, 5746.

87 J. Schottek and G. Erker, *J. Organomet. Chem.*, 1998, **569**, 217.

88 Akira Nakamura, Kazushi Mashima, *J. Organomet. Chem.*, 2004, **689**, 4552.

89 J. R. Briggs, C. Crocker, W. S. McDonald, and B. L. Shaw, *J. Chem. Soc., Dalton. Trans.*, 1982, 457.

90 R. T. Hobgood, Jr., and J. H. Goldstein, Journal of Molecular Spectroscopy, 1964, **12**, 76.

91 K. Nakamoto, *Applications in Organometallic Chemistry*, Fifth Edition, part B.

92 R. K. Sharma and J. L. Fry, *J. Org. Chem.*, 1983, **48**, 2112.

93 D. W. Bruce, Year 3 undergraduate lecture notes on NMR spectroscopy, University of York, UK.

94 R. N. Nair, J. A. Golen, A. L. Rheingold, and D. B. Grotjahn, *Inorg. Chim. Acta*, 2010, **364**, 272.

95 A. E. Shilov and G. B. Shul'pin, *Chem. Rev.*, 1997, **97**, 2879.

96 A. E. Shilov, *Activation of Saturated Hydrocarbons By Transition Metal Complexes*, D. Reidel: Dordrecht, 1984.

97 J. R. Sanders, D. E. Webster, and P. B. Wells, *J. Chem. Soc., Dalton. Trans.*, 1975, 1191.

98 J. H. Clark, *Chem. Rev.*, 1980, **80**, 429.

99 M. J. Heinsen and T. C. Pochapsky, *J. Labelled Compd. Rad.*, 2000, **43**, 473.

100 O. V. Dolomanov, L. J. Bourhis, R. J. Gildea, J. A. K. Howard, and H. Puschmann, OLEX2: A Complete Structure Solution, Refinement and Analysis Program. *J. Appl. Cryst.*, 2009, **42**, 339.

101 XS, G.M. Sheldrick, *Acta Crystallogr*., 2008, **A64**, 112.

102 XL, G.M. Sheldrick, *Acta Crystallogr.*, 2008, **A64**, 112.

103 B. G. Anex and N. Takeuchi, *J. Am. Chem. Soc.*, 1974, **96**, 4411.

Chapter 3

1 G. Schwarzenbach, *Helv. Chim. Acta*, 1952, **35**, 2344.

2 A. W. Adamson, *J. Am. Chem. Sec.*, 1954, **76**, 1578.

3 A. E. Martell, R. D. Hancock and R. J. Motekaitis, *Coord. Chem. Rev.*, 1994, **133**, 39.

4 A. W. Adamson, *J. Am. Chem. Soc.*, 1954, **76**, 1578.

5 R. D. Hancock and A. E. Martell, *Comments, Inorg. Chem.*, 1988, **6**, 237.

6 W. H. Zhang, S. J. Luo, F. Fang, Q. S. Chen, H. W. Hu, X. S. Jia and H. B. Zhai, *J. Am. Chem. Soc.*, 2005, **127**, 18.

7 O. Anderson, *Chem. Rev.*, 1999, **99**, 2683.

8 P. E. A. Andang'o, S. J. M. Osendarp, R. Ayah, C. E. West, D. L. Mwaniki, C. A. De Wolf, R. Kraaijenhagen, F. J. Kok and H. Verhoef, *Lancet*, 2007, **369**, 1799.

9 F. A. Dunand, A. Borel and L. Helm, *Inorg. Chem. Commun.*, 2002, **5**, 811.

10 R. K. Chatterjee, S. K. Das and S. K. Saha, *J. Radio Anal. Nucl. Chem.*, 2002, **251**, 171.

11 A. Asad, R.W. Bell, B. Dell and L. Huang, *Plant Soil*, 1997, **188**, 21.

12 M. V. Rossi, E. F. A. Neves and M. E. V. Suárez-Iha, *Analyst*, 1994, **119**, 1633.

13 G. Schwarzenbach and H. Flaschka, *Complexometric Titrations*, Methuen, London, 1969.

14 H. R. Maecke, A. Riesen and W. Ritter, *J. Nucl. Med.*, 1989, **30**, 1235.

15 A. Mondry and P. Starynowicz, *Inorg. Chem.*, 1997, **36**, 1176.

16 D. C. Finnen and A. Pinkerton, *Acta Crystallogr.*, 1997, C**53**, 1455.

17 J. Wang, Y. Wang, Z. Zhang, X. Zhang, X. Liu, X. Liu, Z. Liu, Y. Zhang, J. Tong, and P. Zhang, *J. Coord. Chem.*, 2006, **59**, 295.

18 P. Caravan, J. J. Ellison, T. J. McMurray and R. B. Lauffer, *Chem. Rev.*, 1999, **99**, 2293.

19 L.-J. Song, J. Zhang, Z.-R. Tang, W.-G. Wang and Z.-F. Ju, *Acta Crystallogr.*, 2003, **E59**, m867.

20 Y.-G. Chen and Z.-H. He, *Wuhan Daxue Xuebao*, 2005, **51**, 140.

21 D.-F. Li, Z.-R. Liao and Y. Xiong, *Acta Crystallogr.*, 1999, **C55**, IUC9900058.

22 T. Jin, C. Li, J. Li, G. Xu and S. Zhang, *Wuji Huaxue Xuebao*, 1994, **10**, 321.

23 P. Leverett, *J. Chem. Soc., Chem. Comm.*, 1974, 161.

24 R.-F. Song, Y.-G. Mao, F. Lei and S.-Y. Qin, *Chem. J. Chin. Univ.*, 1995, **16**, 1436.

25 G.-F. Xu, B. Liu, H.-B. Song, Q.-L. Wang, S.-P. Yang and D. Z. Liao, *Inorg. Chem. Commun.*, 2008, **11**, 714.

26 J. H. Grimes, A. J. Huogard and S. P. Wilford, *J. Inorg. Nucl. Chem.*, 1963, **25**, 1225.

27 T. A. Bohigian and A. E. Martell, *Inorg. Chem.*, 1965, **4**, 1264.

28 K. H. Schrøder, *Acta Chem. Scand.*, 1965, **19**, 1797.

29 K. H. Schrøder, *Acta Chem. Scand.*, 1966, **20**, 881.

30 T. A. Bohigian and A. E. Martell, *J. Inorg. Nucl. Chem.*, 1967, **29**, 453.

31 L. Harju and A. Ringbom, *Anal. Chim. Acta*, 1970, **49**, 221.

32 L. Harju and A. Ringbom, *Anal. Chim. Acta*, 1970, **49**, 205.

33 T**.** D. Smith and A. E. Martell, *J. Am. Chem. Soc.*, 1972, 4123.

34 J. F. Boas, R. H. Dunhill, J. R. Pilbrow, R. C. Srivastava, and T. D. Smith, *J. Chem. Soc. A*, 1969, 94.

35 J. F. Boas, J. R. Pilbrow, C. R. Hartzell, and T. D. Smith, *J. Chem. Soc. A*, 1969, 572.

36 J. F. Boas, J. R. Pilbrow, G. J. Group, C. Moore, and T. D. Smith, *J. Chem. Soc. A*, 1969, 965.

37 J. F. Boas, J. R. Pilbrow, and T. D. Smith, *J. Chem. Soc. A*, 1969, 721.

38 J. F. Boas, J. R. Pilbrow, and T. D. Smith, *J. Chem. Soc. A*, 1969, 723.

39 J. R. Pilbrow, A. D. Toy, and T. D. Smith, *J. Chem. Soc. A*, 1969, 1029.

40 S. Zhang, W. R. Dahl and R. E. Shepherd, *Transition Met. Chem.*, 1995, **20**, 280.

41 P. C. Kang, G. R. Eaton, and S. S. Eaton, *Inorg. Chem.*, 1994, **33**, 3660.

42 N. C. King, R. A. Blackley, M. Lesley Wears, D. M. Newman, W. Zhou and D. W. Bruce, *Chem. Commun.*, 2006, 3414.

43 A. Mondry and P. Starynowicz, *Eur. J. Inorg. Chem.*, 2006, 1859.

44 E. Z.-Bovins, R. N. Muller, S. Laurent, L. V. Elst, C. F. G. C. Geraldes, H. V. Bekkum, and J. A. Peters, *Helv. Chim. Acta*, 2005, **88**, 618.

45 H. R. Maecke, A. Riesen, and W. Ritter, *J. Nucl. Med.*, 1989, **30**, 1235.

46 S. Rubel and M. Wojciechowski, *Anal. Chim. Acta*, 1980, **115**, 69.

47 N. K. Sethi, A. C. Whitwood and D. W. Bruce, *Polyhedron*, 2012, **33**, 378.

48 A. L. Spek, *Acta Crystallogr., Sect. D*, 2009, **65**, 148.

49 F. Holtzberg, B. Post, and I Fankuchen, *Acta Crystallogr.*, 1953, **6**, 127.

50 A. G. Orpen, L. Brammer, F. H. Allen, O. Kennard, D. G. Watson, and R. Taylor, *J. Chem. Soc., Dalton Trans.*, 1989, S1.

51 G. M. Sheldrick, *Acta Crystallogr., Sect. A*, 2008, **64**, 112.

Chapter 4

1 G. S. Attard, J. C. Glyde, and C. G. Göltner, *Nature*, 1995, **378**, 366.

2 A. H. Whitehead, J. M. Elliott, J. R. Owen, and G. S. Attard, *Chem. Commun.*, 1999, 331.

3 G. S. Attard, C. G. Goltner, J. M. Corker, S. Henke, and R. H. Templer, *Angew. Chem. Inc. Ed.*, 1997, **36**, 1315.

4 G. S. Attard, S. A. A. Leclerc, S. Maniguet, A. E. Russell, I. Nandhakumar, and P. N. Bartlett, *Chem. Mater.*, 2001, **13**, 1444.

5 G. S. Attard, P. N. Bartlett, N. R. B. Coleman, J. M. Elliott, J. R. Owen, and J. H. Wang, *Science*, 1997, **278**, 838.

6 P. V. Braun, P. Osenar, V. Tohver, S. B. Kennedy, and S. I. Stupp, *J. Am. Chem. Soc.*, 1999, **121**, 7302.

7 S. Eftekharzadeh, and S. I. Stupp, *Chem. Mater.*, 1997, **9**, 2059.

8 Ö. Dag, A. Verma, G. A. Ozin, and C. T. Kresge, *J. Mater. Chem.*, 1999, **9**, 1475.

9 Ö. Çelik and Ö. Dag, *Angew. Chem. Int. Ed.*, 2001, **40**, 3800.

10 Ö. Dag, I. Soten, Ö. Çelik, S. Polarz, N. Coombs, and G. A. Ozin, *Adv. Funct. Mater.*, 2003, **13**, 30.

11 Ö. Dag, and S. Alayoğlu, Uysal, *J. Phys. Chem. B*, 2004, **108**, 8439.

12 F. Hofmeister, *Arch. Exp. Pathol. Pharmakol.*, 1888, **24**, 247.

13 T. Iwanaga, M. Suzuki, and H. Kunieda, *Langmuir*, 1998, **14**, 5775.

14 C. Rodriguez, and H. Kunieda, *Langmuir*, 2000, **16**, 8263.

15 Ö. Dag, O. Samarskaya, C. Tura, A. Günay, and Ö Çelik, *Langmuir* 2003, **19**, 3671.

16 Ö. Dag, O. Samarskaya, N. Coombs, and G. A. Ozin, *J. Mater. Chem.*, 2003, **13**, 328.

17 D. Zhao, Q. Huo, J. Feng, B. F. Chmelka, and G. D. Stucky, *J. Am. Chem. Soc.*, 1998, **120**, 6024.

18 N. C. King, *PhD Thesis*, University of Exeter, 2005.

19 N. C. King, R. A. Blackley, W. Zhou, and D. W. Bruce, *Chem. Commun.*, 2006, 3411.

20 N. C. King, R. A. Blackley, M. L. Wears, D. M. Newman, W. Zhou, and D. W. Bruce, *Chem. Commun.*, 2006, 3414.

21 http://www.microscopyu.com/articles/polarized/polarizedintro.html, 10/09/2010.

22 S. Brunauer, P. H. Emmett, and E. Teller, *J. Am. Chem. Soc.*, 1938, **60**, 309.

23 S. Brunauer, L. S. Deming, E. Deming and E. Teller, *J. Am. Chem. Soc.*, 1940, **62**, 1723.

24 IUPAC recommendations, *Pure Appl. Chem.*, 1985, **57**, 603.

25 S. J. Gregg and K. S. W. Sing, *Adsorption, Surface Area and Porosity*, Second Edition, Academic Press, London 1982.

26 J. Silvestre-Albero, A. Sepúlveda-Escribano, F. Rodríguez-Reinoso, *Microporous and Mesoporous Mater.*, 2008, **113**, 362.

27 J. M. Haynes, *Matériaux et constructions (Mater. Struct.)*, 1973, **33**, 209.

28 V. Meynen, P. Cool, and E. F. Vansant, *Microporous and Mesoporous Mater.*, 2009, **125**, 170.

29 P. Sherrer, *Nachr. Ges. Wiss. Göttingen, Math.-Physik. Klasse*, 1918, **2**, 98.

30 A. L. Patterson, *Phys. Rev.*, 1939, **56**, 978.

31 http://tem-modes-of-operation.blogspot.in/ , 26.01.2010.

32 S. Hudsonac, D. A. Tanner, W. Redington, E. Magner, K. Hodnettac and S. Nakaharaad, *Phys. Chem. Chem. Phys*., 2006, **8**, 3467.

33 A. Borgna, B. Moraweck, J. Massardier, and A. J. Renouprez, *J. Catal.*, 1991, **128**, 99.

34 L. Hu, G. Xia, L. Qu, M. Li, C. Li, Q. Xin, and D. Li, *J. Catal.*, 2001, **202**, 220.

35 M. Fernández-García, A. Martínez-Arias, A. Iglesias-Juez, A. B. Hungría, J. A. Anderson, J. C. Conesa, and J. Soria, *J. Catal.*, 2003, **214**, 220.

36 H. Saalfeld, *Z. Kristallogr.*, 1964, **120**, 342. 35.

37 J. Waser, H. A. Levy, and S. W. Peterson, *Acta Crystallogr.*, 1953, **6**, 661.

38 G. Bredig, and R. Allolio, *Z. Phys. Chem.*, 1927, **126**, 41.

39 M. Bañobre-López, C. Vázquez-Vázquez, J. Rivas and M. López-Quintela, *Nanotechnology*, 2003, **14**, 318.

40 B. Kucharczyk, W. Tylus, L. Kępiński, *Appl. Catal., B*, 2004, **49**, 27.

41 P. Araya and C. Weissmann, *Catal. Lett.*, 2000, **68**, 33.

42 B. Yoon, H.-B. Pan, and C. M. Wai, *J. Phys. Chem. C*, 2009, **113**, 1520.

43 R. S. Oosthuizen, and V. O. Nyamori, *Platinum Met. Rev.*, 2011, **55**, 154.

44 P. E. Araya, E. E. Miró and L. Cornaglia, *J. Chem. Res., Synop.*, 1997, 258.

45 K. J. Stanger, Y. Tang, J. Anderegg, and R. J. Angelici, *J. Mol. Catal. A: Chem.*, 2003, **202**, 147.

46 P. Araya and V. Díaz, *J. Chem. Soc., Faraday Trans.*, 1997, **93**, 3887.

47 K. J. Yoon, H. K. Kang and J. E. Yie, *Korean J. Chem. Eng.*, 1997, **14**, 399.

48 P. Araya, V. Díaz and J. Cortés, *J. Chem. Res., Synop.*, 1998, 194.

49 J. R. Renzas, W. Huang, Y. Zhang, M. E. Grass, D. T. Hoang, S. Alayoglu, D. R. Butcher, F. F. Tao, Z. Liu and G. A. Somorjai, *Phys. Chem. Chem. Phys.*, 2011, **13**, 2556.

50 E. A. Owen and E. L. Yates, *Philos. Mag.*, 1933, **15**, 472.

51 G. Bredig and R. Allolio, *Ber. Bunsen Ges. Phys. Chem.*, 1927, **126**, 41.

52 W. H. Zachariasen, *Skrifter utgitt av det Norske Videnskaps-Akademi i Oslo 1: Matematisk- Naturvidenskapelig Klasse* (*Norwegian Academy of Science and Letters in Oslo 1: Mathematics and Natural Scientific Class*, 1928, **1928**, 1-165.

53 G. R. Levi, and C. Fontana, *Gazz. Chim. Ital.*, 1926, **56**, 388.

54 W. K. Jóźwiak, M. Nowosielska, and J. Rynkowski, *Appl. Catal., A*, 2005, **280**, 233.

55 H. Arbag, S. Yasyerli, N. Yasyerli, and G. Dogu, *Int. J. Hydrogen Energy*, 2010, **35**, 2296.

56 T. Inui, *Stud. Surf. Sci. Catal.*, 1993, **77**, 17.

57 T. Inui, K. Saigo, Y. Fujii, and K. Fujioka, *Catal. Today*, 1995, **26**, 295.

58 S. Irusta, L.M. Cornaglia, and E.A. Lombardo, *J. Catal.*, 2002, **210**, 7.

59 S. Irusta, L.M. Cornaglia, and E.A. Lombardo, *J. Catal.*, 2002, **210**, 263.

60 M. Nowosielska, W.K. Jóźwiak, and J.M. Rynkowski, *Przem. Chem.*, 2003, **82**, 744.

61 G. Leclercq, S. Pietrzyk, L. Gengembre, and L. Leclercq, *Appl. Catal.*, 1986, **27**, 299.

62 Y. Li, X. Wang, C. Xie, and C. Song, *Appl. Catal., A*, 2009, **357**, 213.

63 J. Kugai, V. Subramani, C. Song, M. H. Engelhard, and Y.-H. Chin, *J. Catal.*, 2006, **238**, 430.

64 M. Nowosielska, W. K. Jozwiak, and J. Rynkowski, *Catal Lett.*, 2009, **128**, 83.

65 R. W. G. Wyckoff, Hexagonal closest packed, hcp, structure, Second Edition. Interscience Publishers, New York, *Crystal structures*, 1963, **1**, 7.

66 H. Weik, and P. Hemenger, *Bull. Am. Phys. Soc.*, 1965, **10**, 1140.

67 D. Liu, W. N. E. Cheo, Y. W. Y. Lim, A. Borgna, R. Lau, and Y. Yang, *Catal. today*, 2010, **154**, 229.

68 B. Gilbert, R. K. Ono, K. A. Ching, C. S. Kim, *J. Colloid Interface Sci.*, 2009, **339**, 285.

1 N. K. Sethi, A. C. Whitwood and D. W. Bruce, *Eur. J. Inorg. Chem.*, 2013, 2078.

2 A. E. Shilov and G. B. Shul'pin, *Chem. Rev.*, 1997, **97**, 2879.

3 N. K. Sethi, A. C. Whitwood and D. W. Bruce, *Polyhedron*, 2012, **33**, 378.

4 S. G. Wainwright, *PhD Thesis*, University of York, 2011.

Appendix

Appendix A

Chapter 2

Data for X-ray Crystal Structure Determinations

A.1 [K(18-crown-6)]$_2$[Cl$_2$Pt(μ-Cl)$_2$PdCl$_2$]

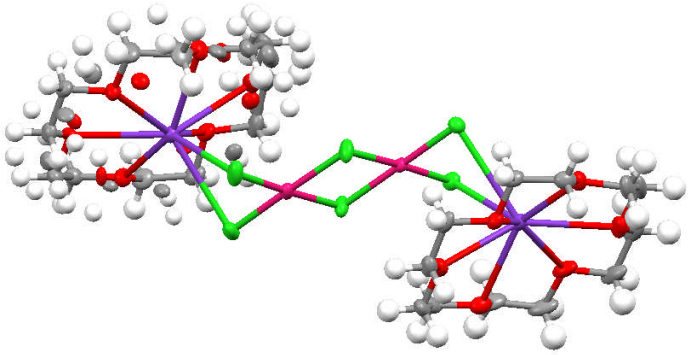

Fig. A.1 Structure of [K(18-crown-6)]$_2$[Cl$_2$Pt(μ-Cl)$_2$PdCl$_2$] showing disorder of one of the [18-crown-6)] units.

Table A.I Crystal data and structure refinement for [K(18-crown-6)]$_2$[Cl$_2$Pt(μ-Cl)$_2$PdCl$_2$].

Identification code	dwb1018m
Empirical formula	$C_{24}H_{48}Cl_6K_2O_{12}Pd_{1.42}Pt_{0.58}$
Formula weight	1083.76
Temperature/K	110(2)
Crystal system	Monoclinic
Space group	P2(1)/n
a/Å	21.9297(11)
b/Å	8.1463(4)
c/Å	22.1713(11)
α/°	90
β/°	98.4070(10)
γ/°	90
Volume/Å^3	3918.3(3)
Z	4
ρ_{calc}mg/mm^3	1.837
m/mm^{-1}	3.393
F(000)	2153.6
Crystal size/mm^3	0.16 × 0.15 × 0.08
2Θ range for data collection/°	1.22 to 28.30
Index ranges	-29<=h<=29, -10<=k<=10, -29<=l<=29
Reflections collected	39203
Independent reflections	9718 [R(int) = 0.0389]
Data/restraints/parameters	9718 / 108 / 580
Goodness-of-fit on F^2	1.130
Final R indexes [I>=2σ (I)]	R1 = 0.0380, wR2 = 0.0763
Final R indexes [all data]	R1 = 0.0526, wR2 = 0.0809
Largest diff. peak/hole / e Å^{-3}	1.495 and -0.999

A.2 [K(18-crown-6)]$_2$[Cl$_2$Pd(μ-Cl)$_2$PdCl$_2$]

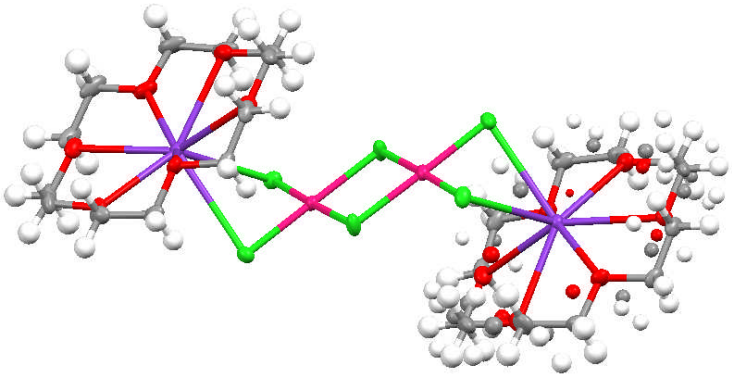

Fig. A.2 Structure of [K(18-crown-6)]$_2$[Cl$_2$Pd(μ-Cl)$_2$PdCl$_2$] showing disorder of one of the [18-crown-6] units.

Table A.II Crystal data and structure refinement for [K(18-crown-6)]$_2$[Cl$_2$Pd(μ-Cl)$_2$PdCl$_2$].

Identification code	dwb1137
Empirical formula	$C_{24}H_{48}Cl_6K_2O_{12}Pd_2$
Formula weight	1032.32
Temperature/K	109.9(2)
Crystal system	Monoclinic
Space group	$P2_1/c$
a/Å	22.0526(13)
b/Å	8.1185(2)
c/Å	28.8572(17)
α/°	90.00
β/°	130.685(10)
γ/°	90.00
Volume/Å^3	3917.7(7)
Z	4
ρ_{calc}mg/mm^3	1.750
m/mm^{-1}	1.591
F(000)	2080
Crystal size/mm^3	0.1993 × 0.1447 × 0.1088
2Θ range for data collection/°	5.76 to 58.2
Index ranges	-27<=h<=27, -10<=k<=10, -34<=l<=38
Reflections collected	15443
Independent reflections	8914[R(int) = 0.0234]
Data/restraints/parameters	8914/3/488
Goodness-of-fit on F^2	1.083
Final R indexes [I>=2σ (I)]	R1 = 0.0326, wR2 = 0.0568
Final R indexes [all data]	R1 = 0.0473, wR2 = 0.0645
Largest diff. peak/hole / e Å^{-3}	0.540 and -0.458

A.3 [K(18-crown-6)]$_2$[PtCl$_6$]·2DMSO

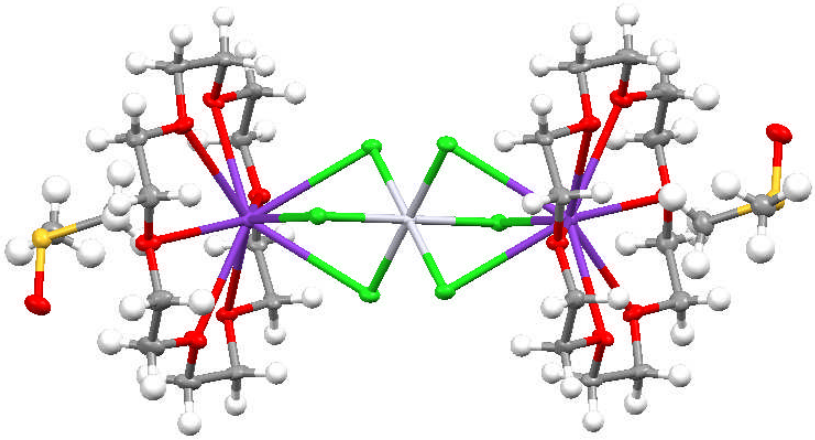

Fig. A.3 Structure of [K(18-crown-6)]$_2$[PtCl$_6$]·2DMSO.

Table A.III Crystal data and structure refinement for [K(18-crown-6)]$_2$[PtCl$_6$]·2DMSO.

Identification code	dwb1146
Empirical formula	$C_{28}H_{60}Cl_6K_2O_{14}PtS_2$
Formula weight	1170.87
Temperature/K	110.00(10)
Crystal system	Triclinic
Space group	P-1
a/Å	8.6843(5)
b/Å	8.8100(7)
c/Å	15.7083(11)
α/°	77.221(7)
β/°	82.663(6)
γ/°	73.980(6)
Volume/Å^3	1123.68(14)
Z	1
ρ_{calc}mg/mm^3	1.7390
m/mm^{-1}	3.813
F(000)	590
Crystal size/mm^3	0.1129 × 0.0779 × 0.0207
2Θ range for data collection/°	5.98 to 57.32
Index ranges	-11<=h<=11, -10<=k<=10, -21<=l<=16
Reflections collected	7163
Independent reflections	4827[R(int)=0.0310]
Data/restraints/parameters	4827/0/243
Goodness-of-fit on F^2	1.063
Final R indexes [I>=2σ (I)]	R1 = 0.0367, wR2 = 0.0828
Final R indexes [all data]	R1 = 0.0410, wR2 = 0.0853
Largest diff. peak/hole / e Å^{-3}	2.122 and -2.235

A.4 $[K(18\text{-crown-}6)]_2[PtCl_6]\cdot 2CH_3COOH$

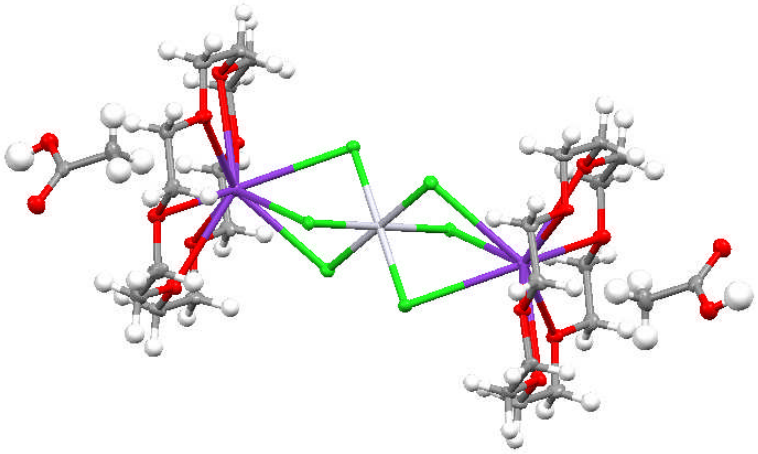

Fig. A.4 Structure of $[K(18\text{-crown-}6)]_2[PtCl_6]\cdot 2CH_3COOH$.

Table A.IV Crystal data and structure refinement for $[K(18\text{-crown-}6)]_2[PtCl_6]\cdot 2CH_3COOH$.

Identification code	dwb1145
Empirical formula	$C_{28}H_{56}Cl_6K_2O_{16}Pt$
Formula weight	1134.72
Temperature/K	110.00(10)
Crystal system	triclinic
Space group	P-1
a/Å	8.6176(5)
b/Å	8.7513(4)
c/Å	15.4487(9)
α/°	74.809(4)
β/°	83.397(4)
γ/°	74.351(4)
Volume/$Å^3$	1081.45(11)
Z	1
$\rho_{calc}mg/mm^3$	1.742
m/mm^{-1}	3.869
F(000)	570.0
Crystal size/mm^3	0.3296 × 0.0951 × 0.0464
2Θ range for data collection/°	5.74 to 65.08
Index ranges	$-12 \le h \le 10$, $-13 \le k \le 12$, $-22 \le l \le 13$
Reflections collected	11778
Independent reflections	7071[R(int) = 0.0254]
Data/restraints/parameters	7071/0/246
Goodness-of-fit on F^2	1.062
Final R indexes [I>=2σ (I)]	$R_1 = 0.0265$, $wR_2 = 0.0535$
Final R indexes [all data]	$R_1 = 0.0282$, $wR_2 = 0.0544$
Largest diff. peak/hole / e $Å^{-3}$	1.31 and -0.80

A.5 [K(18-crown-6)] [$AuCl_4$](start)

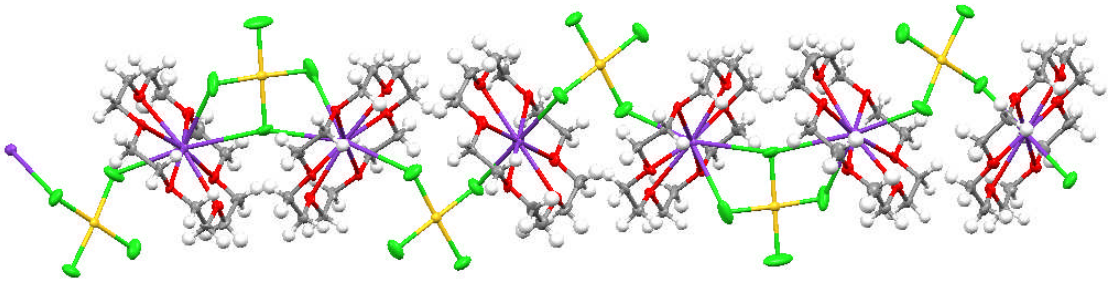

Fig. A.5 Crystal Structure of [K(18-crown-6)][$AuCl_4$] as present at the beginning of data set collection.

Table A.V Crystal data and structure refinement for [K(18-crown-6)][$AuCl_4$].

Identification code	dwb1109_Start
Empirical formula	$C_{12}H_{24}AuCl_4KO_6$
Formula weight	642.18
Temperature/K	110.0
Crystal system	triclinic
Space group	P-1
a/Å	9.0592(5)
b/Å	14.7606(8)
c/Å	24.6225(15)
α/°	98.815(5)
β/°	94.425(5)
γ/°	96.293(5)
Volume/$Å^3$	3219.2(3)
Z	6
$\rho_{calc}mg/mm^3$	1.988
m/mm^{-1}	7.569
F(000)	1860.0
Crystal size/mm^3	0.1682 × 0.1157 × 0.0525
2Θ range for data collection/°	6.06 to 61.2
Index ranges	$-5 \leq h \leq 12$, $-9 \leq k \leq 19$, $-32 \leq l \leq 10$
Reflections collected	6798
Independent reflections	6628[R(int) = 0.0101]
Data/restraints/parameters	6628/84/652
Goodness-of-fit on F^2	1.215
Final R indexes [I>=2σ (I)]	R_1 = 0.0598, wR_2 = 0.1291
Final R indexes [all data]	R_1 = 0.0679, wR_2 = 0.1345
Largest diff. peak/hole / e $Å^{-3}$	1.91 and -1.28

A.6 [K(18-crown-6)][AuCl$_4$](middle)

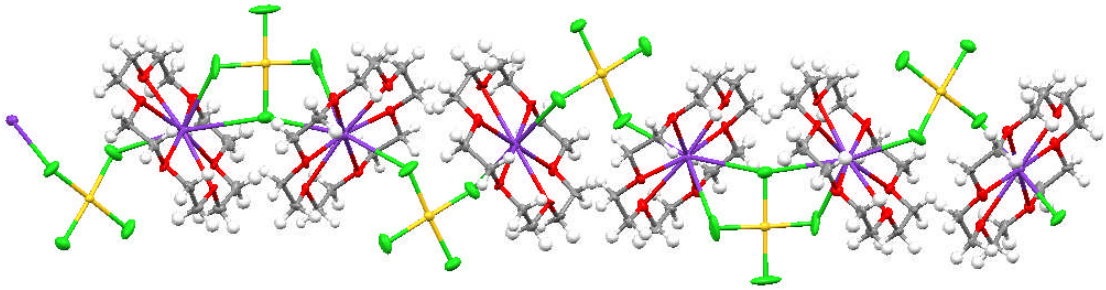

Fig. A.6 The arrangement of $[AuCl_4]^{1-}$ and [K(18-crown-6)] after exposure to X-ray radiation.

Table A.VI Crystal data and structure refinement for [K(18-crown-6)][AuCl$_4$].

Identification code	dwb1112
Empirical formula	$C_{12}H_{24}AuCl_4KO_6$
Formula weight	642.18
Temperature/K	110.00(10)
Crystal system	triclinic
Space group	P-1
a/Å	9.0720(14)
b/Å	14.7628(14)
c/Å	24.597(4)
α/°	98.807(12)
β/°	94.557(14)
γ/°	96.294(11)
Volume/Å^3	3220.2(8)
Z	6
ρ_{calc}mg/mm^3	1.987
m/mm^{-1}	7.567
F(000)	1860.0
Crystal size/mm^3	0.1354 × 0.0828 × 0.059
2Θ range for data collection/°	6.06 to 55.7
Index ranges	$-11 \leq h \leq 10$, $-15 \leq k \leq 19$, $-24 \leq l \leq 29$
Reflections collected	17338
Independent reflections	12417[R(int) = 0.0464]
Data/restraints/parameters	12417/108/652
Goodness-of-fit on F^2	1.072
Final R indexes [I>=2σ (I)]	R_1 = 0.0671, wR_2 = 0.1291
Final R indexes [all data]	R_1 = 0.0951, wR_2 = 0.1527
Largest diff. peak/hole / e Å^{-3}	4.02 and -2.46

A.7 [K(18-crown-6)][AuCl$_4$](end)

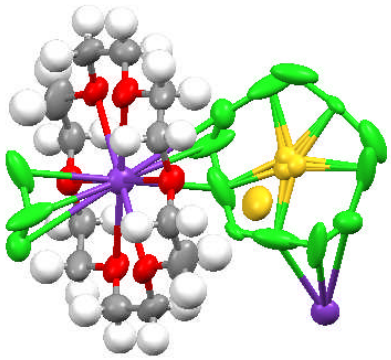

Fig. A.7 Showing disorder presence in the original structure of [K(18-crown-6)][AuCl$_4$].

Table A.VII Crystal data and structure refinement for [K(18-crown-6)][AuCl$_4$] (final structure).

Identification code	dwb1109_end
Empirical formula	$C_{12}H_{24}AuCl_3KO_6$
Formula weight	606.73
Temperature/K	109.95(10)
Crystal system	monoclinic
Space group	C2/c
a/Å	13.8702(18)
b/Å	11.5709(12)
c/Å	14.427(2)
α/°	90.00
β/°	109.396(18)
γ/°	90.00
Volume/Å^3	2184.1(5)
Z	4
ρ_{calc}mg/mm^3	1.845
m/mm^{-1}	7.313
F(000)	1172.0
Crystal size/mm^3	0.1682 × 0.1157 × 0.0525
2Θ range for data collection/°	6.22 to 60.76
Index ranges	-18 ≤ h ≤ 4, -14 ≤ k ≤ 8, -17 ≤ l ≤ 14
Reflections collected	2424
Independent reflections	1821[R(int) = 0.0266]
Data/restraints/parameters	1821/85/142
Goodness-of-fit on F^2	1.102
Final R indexes [I>=2σ (I)]	R_1 = 0.1054, wR_2 = 0.2842
Final R indexes [all data]	R_1 = 0.1275, wR_2 = 0.3063
Largest diff. peak/hole / e Å^{-3}	2.25 and -0.78

A.8 $(Bu_4N)_2[PtCl_3(\eta\text{-}CH_2\text{=}CH\text{-}CH\text{=}CH_2\text{-}\eta)PtCl_3]$

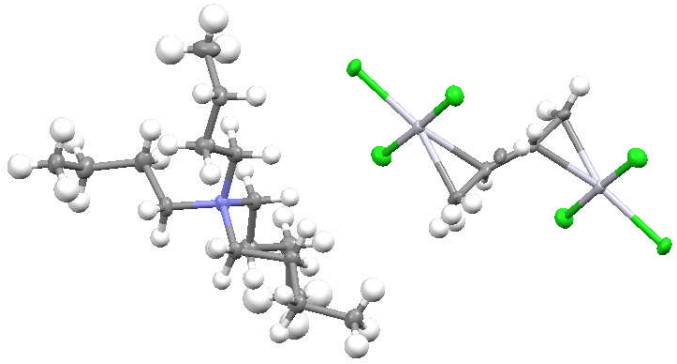

Fig. A.8 Structure of Pt^{II} butadiene complex showing two possibilities of C_4 fraction.

Table A.VIII Crystal data and structure refinement for $(Bu_4N)_2[PtCl_3(\eta\text{-}CH_2\text{=}CH\text{-}CH\text{=}CH_2\text{-}\eta)PtCl_3]$.

Identification code	dwb1140
Empirical formula	$C_{36}H_{78}Cl_6N_2Pt_2$
Formula weight	1141.88
Temperature/K	110.00(10)
Crystal system	monoclinic
Space group	$P2_1/n$
a/Å	13.2066(16)
b/Å	12.9014(10)
c/Å	13.3730(11)
α/°	90.00
β/°	98.265(11)
γ/°	90.00
Volume/$Å^3$	2254.9(4)
Z	2
$\rho_{calc}mg/mm^3$	1.682
m/mm^{-1}	6.579
F(000)	1132
Crystal size/mm^3	0.3169 × 0.1184 × 0.0508
2Θ range for data collection/°	5.64 to 64.4
Index ranges	$-19 \leq h \leq 16$, $-19 \leq k \leq 11$, $-19 \leq l \leq 19$
Reflections collected	12705
Independent reflections	7115[R(int) = 0.0317]
Data/restraints/parameters	7115/0/216
Goodness-of-fit on F^2	1.050
Final R indexes [I>=2σ (I)]	R_1 = 0.0358, wR_2 = 0.0726
Final R indexes [all data]	R_1 = 0.0454, wR_2 = 0.0785
Largest diff. peak/hole / e $Å^{-3}$	3.338 and -3.124

A.9 [K(18-crown-6)]$_2$[PdCl$_4$].4CH$_2$Cl$_2$

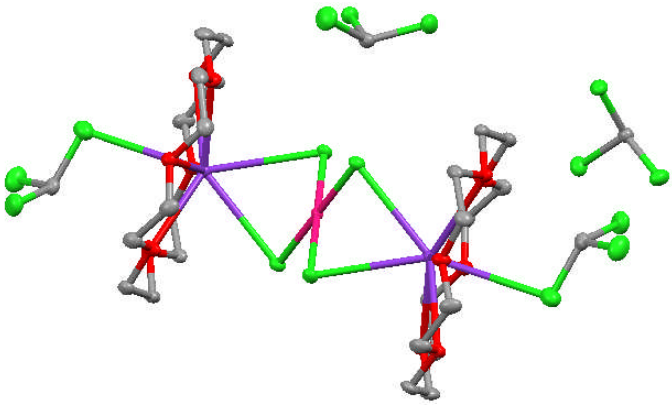

Fig. A.9 Structure of [K(18-crown-6)]$_2$[PdCl$_4$]·4CHCl$_3$.

Table A.IX Crystal data and structure refinement for [K(18-crown-6)]$_2$[PdCl$_4$]·4CHCl$_3$.

Identification code	dwb1122
Empirical formula	$C_{30}H_{54}Cl_{22}K_2O_{12}Pd$
Formula weight	1571.23
Temperature/K	110.0
Crystal system	triclinic
Space group	P-1
a/Å	10.5273(7)
b/Å	12.6415(10)
c/Å	13.4511(7)
α/°	63.530(7)
β/°	73.779(5)
γ/°	83.375(6)
Volume/Å^3	1538.6(2)
Z	1
ρ_{calc}mg/mm^3	1.696
m/mm^{-1}	1.439
F(000)	788
Crystal size/mm^3	0.274 × 0.1249 × 0.0555
2Θ range for data collection/°	6.12 to 64.48
Index ranges	-15 ≤ h ≤ 15, -18 ≤ k ≤ 14, -19 ≤ l ≤ 11
Reflections collected	14783
Independent reflections	9629[R(int) = 0.0223]
Data/restraints/parameters	9629/0/304
Goodness-of-fit on F^2	1.047
Final R indexes [I>=2σ (I)]	R_1 = 0.0324, wR_2 = 0.0582
Final R indexes [all data]	R_1 = 0.0421, wR_2 = 0.0631
Largest diff. peak/hole / e Å^{-3}	0.518 and -0.648

A.10 $(PPh_4)[AuCl_4]$

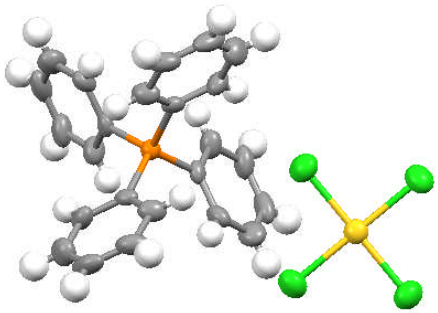

Fig. A.10 Structure of $(PPh_4)[AuCl_4]$.

Table A.X Crystal data and structure refinement for $(PPh_4)[AuCl_4]$.

Identification code	dwb1169
Empirical formula	$C_{24}H_{20}AuCl_4P$
Formula weight	678.14
Temperature/K	110.00(10)
Crystal system	tetragonal
Space group	P4/n
a/Å	12.3162(2)
b/Å	12.3162(2)
c/Å	7.84469(19)
α/°	90.00
β/°	90.00
γ/°	90.00
Volume/Å^3	1189.96(4)
Z	2
ρ_{calc}mg/mm^3	1.893
m/mm^{-1}	6.708
F(000)	652.0
Crystal size/mm^3	0.2073 × 0.0327 × 0.0231
2Θ range for data collection/°	6.16 to 58.92
Index ranges	$-16 \leq h \leq 15$, $-9 \leq k \leq 16$, $-10 \leq l \leq 10$
Reflections collected	5288
Independent reflections	1471[R(int) = 0.0340]
Data/restraints/parameters	1471/0/69
Goodness-of-fit on F^2	1.311
Final R indexes [I>=2σ (I)]	R_1 = 0.0450, wR_2 = 0.1133
Final R indexes [all data]	R_1 = 0.0490, wR_2 = 0.1151
Largest diff. peak/hole / e Å^{-3}	4.03/-2.37

A.11 $(Bu_4N)_2[PtCl_6]\cdot 3CH_2Cl_2$

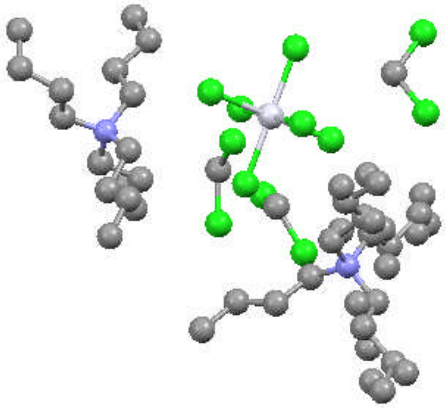

Fig. A.11 Structure of $(Bu_4N)_2[PtCl_6]\cdot 3CH_2Cl_2$.

Table A.XI Crystal data and structure refinement for $(Bu_4N)_2[PtCl_6]\cdot 3CH_2Cl_2$.

Identification code	dwb1211
Empirical formula	$C_{35}H_{78}Cl_{12}N_2Pt$
Formula weight	1147.48
Temperature/K	109.95(10)
Crystal system	orthorhombic
Space group	Pbca
a/Å	16.2280(4)
b/Å	19.5294(4)
c/Å	32.5682(6)
α/°	90.00
β/°	90.00
γ/°	90.00
Volume/Å3	10321.6(4)
Z	8
ρcalcmg/mm3	1.477
m/mm-1	3.366
F(000)	4672.0
Crystal size/mm3	0.2334 × 0.2041 × 0.1255
2Θ range for data collection/°	5.58 to 57.64
Index ranges	-20 ≤ h ≤ 19, -26 ≤ k ≤ 25, -44 ≤ l ≤ 38
Reflections collected	45718
Independent reflections	12069[R(int) = 0.0483]
Data/restraints/parameters	12069/36/511
Goodness-of-fit on F2	1.136
Final R indexes [I>=2σ (I)]	R1 = 0.0770, wR2 = 0.1486
Final R indexes [all data]	R1 = 0.1064, wR2 = 0.1611
Largest diff. peak/hole / e Å-3	4.56/-1.92

A.12 $(Bu_4N)_2[PtCl_6]$

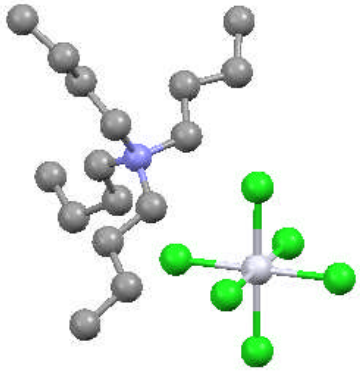

Fig. A.12 Structure of $(Bu_4N)_2[PtCl_6]$, unchanged as in cif file.

Table A.XII Crystal data and structure refinement for $(Bu_4N)_2[PtCl_6]$.

Identification code	dwb1141_twin1_hklf4
Empirical formula	$C_{32}H_{72}Cl_6N_2Pt$
Formula weight	678.14
Temperature/K	892.71
Crystal system	monoclinic
Space group	C2/c
a/Å	13.9750(5)
b/Å	18.0818(5)
c/Å	16.9978(5)
α/°	90.00
β/°	113.536(4)
γ/°	90.00
Volume/Å3	3937.9(2)
Z	4
ρcalcmg/mm3	1.506
m/mm-1	3.994
F(000)	1832.0
Crystal size/mm3	0.2275 × 0.1841 × 0.0804
2Θ range for data collection/°	6.36 to 64.52
Index ranges	$-20 \leq h \leq 20$, $-26 \leq k \leq 26$, $-24 \leq l \leq 25$
Reflections collected	8554
Independent reflections	8554[R(int) = 0.0000]
Data/restraints/parameters	8554/0/192
Goodness-of-fit on F2	1.042
Final R indexes [I>=2σ (I)]	$R_1 = 0.0555$, $wR_2 = 0.1574$
Final R indexes [all data]	$R_1 = 0.0692$, $wR_2 = 0.1648$
Largest diff. peak/hole / e Å-3	3.14/-4.54

A.13 $(PPh_4)_2[PtCl_4].H_2O$

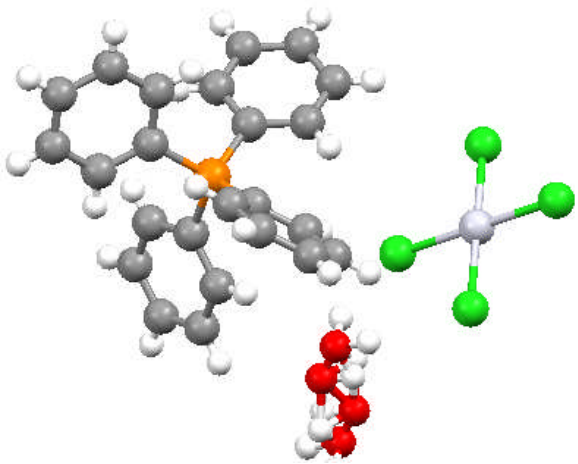

Fig. A.13 Structure of $(PPh_4)_2[PtCl_4]\cdot H_2O$.

Table A.XIII Crystal data and structure refinement for $(PPh_4)_2[PtCl_4]\cdot H_2O$.

Identification code	dwb1167
Empirical formula	$C_{48}H_{42}Cl_4OP_2Pt$
Formula weight	1033.65
Temperature/K	110.00(10)
Crystal system	monoclinic
Space group	$P2_1/n$
a/Å	10.3066(2)
b/Å	15.8633(3)
c/Å	12.9397(2)
α/°	90.00
β/°	95.3512(18)
γ/°	90.00
Volume/Å^3	2106.39(7)
Z	2
ρ_{calc}mg/mm^3	1.630
m/mm^{-1}	3.698
F(000)	1028.0
Crystal size/mm^3	0.2969 × 0.1869 × 0.125
2Θ range for data collection/°	5.9 to 58.46
Index ranges	$-13 \le h \le 12$, $-21 \le k \le 10$, $-17 \le l \le 17$
Reflections collected	9445
Independent reflections	4942[R(int) = 0.0251]
Data/restraints/parameters	4942/6/274
Goodness-of-fit on F^2	1.051
Final R indexes [I>=2σ (I)]	R_1 = 0.0288, wR_2 = 0.0592
Final R indexes [all data]	R_1 = 0.0388, wR_2 = 0.0655
Largest diff. peak/hole / e Å^{-3}	0.80/-0.67

A.14 $(PPh_4)_2[PtCl_6]\cdot 2CH_2Cl_2$

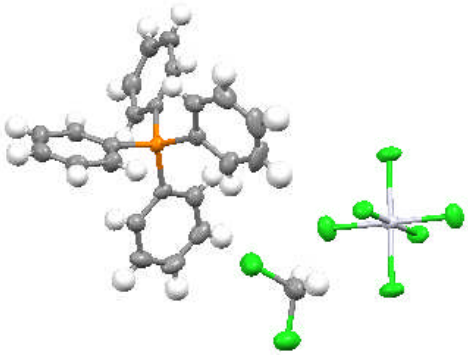

Fig. A.14 Structure of $(PPh_4)_2[PtCl_6]$.

Table A.XIV Crystal data and structure refinement for$(PPh_4)_2[PtCl_6]\cdot 2\ CH_2Cl_2$.

Identification code	dwb1168
Empirical formula	$C_{50}H_{44}Cl_{10}P_2Pt$
Formula weight	1256.38
Temperature/K	110.0
Crystal system	triclinic
Space group	P-1
a/Å	10.0801(6)
b/Å	11.0657(5)
c/Å	12.3409(6)
α/°	70.608(4)
β/°	80.132(4)
γ/°	80.085(4)
Volume/$Å^3$	1269.36(11)
Z	1
$\rho_{calc}mg/mm^3$	1.644
m/mm^{-1}	3.388
F(000)	622.0
Crystal size/mm^3	0.297 × 0.1795 × 0.1526
2Θ range for data collection/°	5.76 to 58.84
Index ranges	$-13 \leq h \leq 13, -14 \leq k \leq 13, -15 \leq l \leq 17$
Reflections collected	9469
Independent reflections	5917[R(int) = 0.0276]
Data/restraints/parameters	5917/0/286
Goodness-of-fit on F^2	1.019
Final R indexes [I>=2σ (I)]	R_1 = 0.0322, wR_2 = 0.0640
Final R indexes [all data]	R_1 = 0.0344, wR_2 = 0.0655
Largest diff. peak/hole / e $Å^{-3}$	1.59/-0.59

Chapter 3

Data for X-ray Crystal Structure Determinations

A.15 Na[RhZnCl(TTHA)(H$_2$O)$_4$]·xH$_2$O

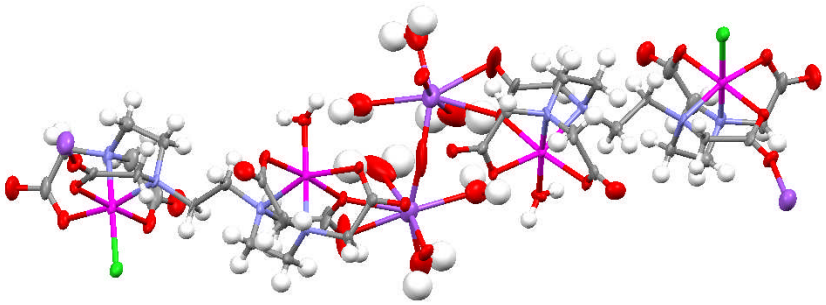

Fig. A.15 Structure of Na[RhZnCl(TTHA)(H$_2$O)$_4$]·*x*H$_2$O.

Table A.XV Crystal data and structure refinement for Na[RhZnCl(TTHA)(H$_2$O)$_4$]·*x*H$_2$O.

Identification code	dwb0912m
Empirical formula	$C_{18}H_{32}ClN_4NaO_{16}RhZn$
Formula weight	787.20
Temperature/K	110(2)
Crystal system	Monoclinic
Space group	P2/n
a/Å	11.459(3)
b/Å	14.181(4)
c/Å	22.384(6)
α/°	90
β/°	93.923(6)
γ/°	90
Volume/Å^3	3629.0(17)
Z	4
ρ_{calc}mg/mm^3	1.441
m/mm^{-1}	1.264
F(000)	1596
Crystal size/mm^3	0.09 × 0.08 × 0.02
2Θ range for data collection/°	1.44 to 25.05
Index ranges	-13<=h<=13, -16<=k<=16, -26<=l<=26
Reflections collected	28594
Independent reflections	6422 [R(int) = 0.0981]
Data/restraints/parameters	6422 / 17 / 409
Goodness-of-fit on F^2	0.914
Final R indexes [I>=2σ (I)]	R1 = 0.0557, wR2 = 0.1340
Final R indexes [all data]	R1 = 0.0910, wR2 = 0.1454
Largest diff. peak/hole / e Å^{-3}	1.200 and -0.921

A.16 $[Cr_{1.50}Rh_{0.50}(TTHA)(OH_2)_2]\cdot 3H_2O$

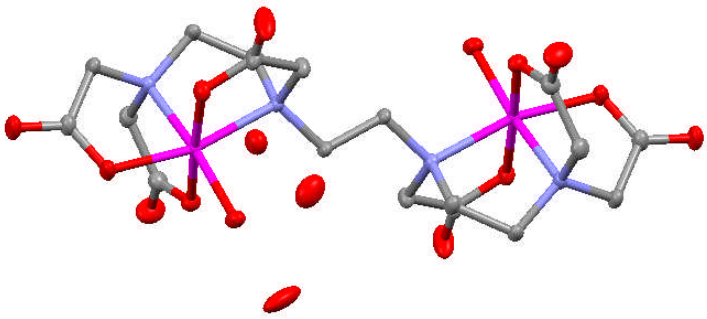

Fig. A.16 Structure of $[Cr_{1.50}Rh_{0.50}(TTHA)(OH_2)_2]\cdot 6H_2O$.

Table A.XVI Crystal data and structure refinement for $[Cr_{1.50}Rh_{0.50}(TTHA)(OH_2)_2]\cdot 6H_2O$.

Identification code	dwb0901m
Empirical formula	$C_{36}H_{80}Cr_3N_8O_{40}Rh$
Formula weight	762.00
Temperature/K	110(2)
Crystal system	Monoclinic
Space group	P2(1)/c
a/Å	8.6080(4)
b/Å	12.5555(6)
c/Å	13.7444(6)
α/°	90
β/°	99.3640(10)
γ/°	90
Volume/Å^3	1465.67(12)
Z	2
ρ_{calc}mg/mm^3	1.727
m/mm^{-1}	0.931
F(000)	789
Crystal size/mm^3	0.33 × 0.06 × 0.06
2Θ range for data collection/°	2.21 to 30.00
Index ranges	-12<=h<=12, -17<=k<=17, -18<=l<=18
Reflections collected	16350
Independent reflections	4228 [R(int) = 0.0199]
Data/restraints/parameters	4228 / 0 / 225
Goodness-of-fit on F^2	1.034
Final R indexes [I>=2σ (I)]	R1 = 0.0270, wR2 = 0.0662
Final R indexes [all data]	R1 = 0.0309, wR2 = 0.0685
Largest diff. peak/hole / e Å^{-3}	0.599 and -0.536

A.17 $[PPh_4]_2[Rh_2Cl_2(TTHA)]\cdot 11H_2O$

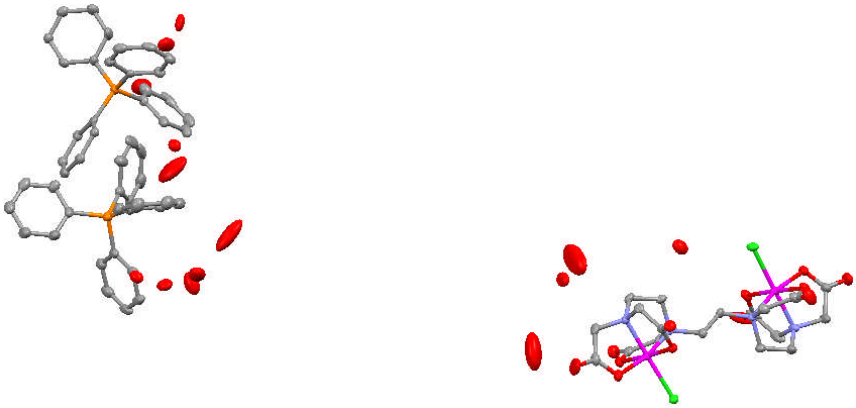

Fig. A.17 Structure of $[PPh_4]_2[Rh_2Cl_2(TTHA)]\cdot 11H_2O$

Table A.XVII Crystal data and structure refinement for $[PPh_4]_2[Rh_2Cl_2(TTHA)]\cdot 11H_2O$.

Identification code	dwb0905m
Empirical formula	$C_{66}H_{64}Cl_2N_4O_{23}P_2Rh_2$
Formula weight	1619.87
Temperature/K	110(2)
Crystal system	Monoclinic
Space group	C2/c
a/Å	35.403(4)
b/Å	13.1045(14)
c/Å	31.727(3)
α/°	90
β/°	106.180(2)
γ/°	90
Volume/$Å^3$	14136(3)
Z	8
ρ_{calc}mg/mm^3	1.522
m/mm^{-1}	0.667
F(000)	6608
Crystal size/mm^3	0.34 × 0.04 × 0.02
2Θ range for data collection/°	1.20 to 25.04
Index ranges	-42<=h<=42, -15<=k<=15, -37<=l<=37
Reflections collected	53307
Independent reflections	12465 [R(int) = 0.0897]
Data/restraints/parameters	12465 / 0 / 932
Goodness-of-fit on F^2	1.024
Final R indexes [I>=2σ (I)]	R1 = 0.0456, wR2 = 0.1093
Final R indexes [all data]	R1 = 0.0978, wR2 = 0.1302
Largest diff. peak/hole / e $Å^{-3}$	0.869 and -0.898

A.18 $Na_2[Rh_2Cl_2(TTHA)]\cdot 8H_2O$

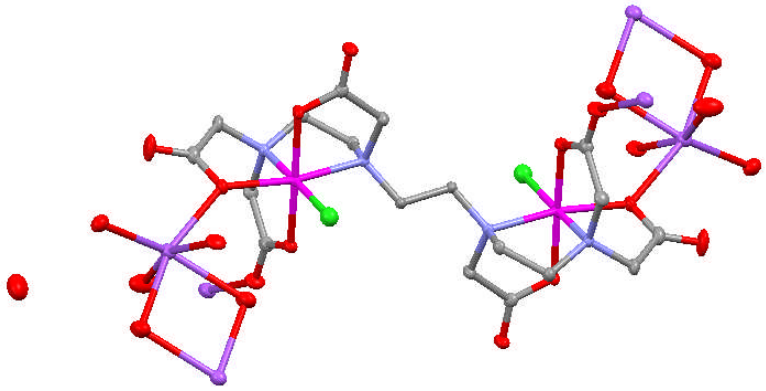

Fig. A.18 Structure of $Na_2[Rh_2Cl_2(TTHA)]\cdot 8H_2O$.

Table A.XVIII Crystal data and structure refinement for $Na_2[Rh_2Cl_2(TTHA)]\cdot 8H_2O$.

Identification code	dwb0933m
Empirical formula	$C_{18}H_{40}Cl_2N_4Na_2O_{20}Rh_2$
Formula weight	955.24
Temperature/K	110(2)
Crystal system	Monoclinic
Space group	P2(1)/n
a/Å	6.5140(6)
b/Å	13.6039(13)
c/Å	18.5105(17)
α/°	90
β/°	94.777(2)
γ/°	90
Volume/Å^3	1634.6(3)
Z	2
ρ_{calc}mg/mm^3	1.941
m/mm^{-1}	1.288
F(000)	964
Crystal size/mm^3	0.08 × 0.08 × 0.08
2Θ range for data collection	1.86 to 28.31
Index ranges	-8<=h<=8, -18<=k<=18, -24<=l<=24
Reflections collected	16696
Independent reflections	4073 [R(int) = 0.0404]
Data/restraints/parameters	4073 / 12 / 241
Goodness-of-fit on F^2	1.046
Final R indexes [I>=2σ (I)]	R1 = 0.0346, wR2 = 0.0833
Final R indexes [all data]	R1 = 0.0454, wR2 = 0.0882
Largest diff. peak/hole / e Å^{-3}	1.043 and -1.081

A.19 $[Cr_2(TTHA)(OH_2)_2]\cdot 6H_2O$

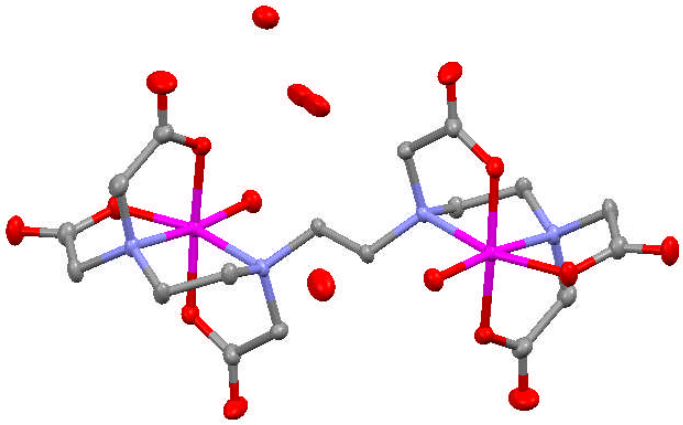

Fig. A.19 Structure of $[Cr_2(TTHA)(OH_2)_2]\cdot 6H_2O$.

Table A.XIX Crystal data and structure refinement for $[Cr_2(TTHA)(OH_2)_2]\cdot 6H_2O$.

Identification code	dwb0926a
Empirical formula	$C_{18}H_{40}Cr_2N_4O_{20}$
Formula weight	736.54
Temperature/K	110(2)
Crystal system	Monoclinic
Space group	P2(1)/c
a/Å	8.5913(9)
b/Å	12.5518(13)
c/Å	13.7513(15)
α/°	90
β/°	99.425(2)
γ/°	90
Volume/$Å^3$	1462.9(3)
Z	2
ρ_{calc}mg/mm^3	1.672
m/mm^{-1}	0.837
F(000)	768
Crystal size/mm^3	0.25 × 0.04 × 0.02
2Θ range for data collection	2.21 to 28.37
Index ranges	-11<=h<=11, -16<=k<=16, -18<=l<=18
Reflections collected	14718
Independent reflections	3651 [R(int) = 0.0427]
Data/restraints/parameters	3651 / 0 / 235
Goodness-of-fit on F^2	1.026
Final R indexes [I>=2σ (I)]	R1 = 0.0372, wR2 = 0.0838
Final R indexes [all data]	R1 = 0.0537, wR2 = 0.0912
Largest diff. peak/hole / e $Å^{-3}$	0.573 and -0.269

A.20 $C_{18}H_{34}KN_4NaNi_2O_{21.27}$

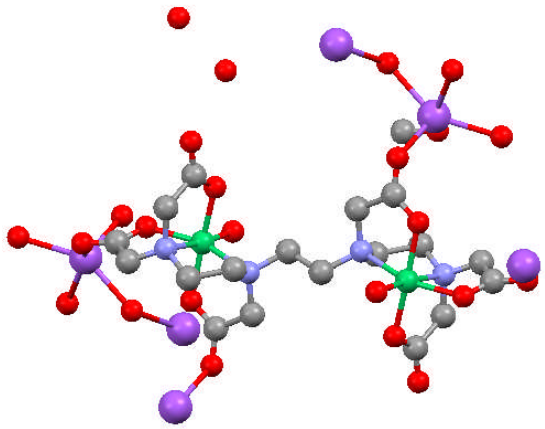

Fig. A.20 Structure of $C_{18}H_{34}KN_4NaNi_2O_{21.27}$.

Table A.XX Crystal data and structure refinement for $C_{18}H_{34}KN_4NaNi_2O_{21.27}$.

Identification code	ssi1068
Empirical formula	$C_9H_{12}N_2NaNiO_{11}$
Formula weight	405.89
Temperature/K	120(2)
Crystal system	Rhombohedral
Space group	R-3
a/Å	43.027(17)
b/Å	43.027(17)
c/Å	7.024(6)
α/°	90
β/°	90
γ/°	120
Volume/Å^3	11262(11)
Z	18
ρ_{calc}mg/mm^3	1.077
m/mm^{-1}	0.549
F(000)	3912
Crystal size/mm^3	0.10 × 0.01 × 0.01
2Θ range for data collection/°	0.92 to 21.26
Index ranges	-45<=h<=45, -45<=k<=45, -7<=l<=7
Reflections collected	21743
Independent reflections	3071 [R(int) = 0.1368]
Data/restraints/parameters	3071 / 0 / 217
Goodness-of-fit on F^2	0.986
Final R indexes [I>=2σ (I)]	R1 = 0.0955, wR2 = 0.2461
Final R indexes [all data]	R1 = 0.1350, wR2 = 0.2656
Largest diff. peak/hole / e Å^{-3}	0.702 and -0.790

A.21 $Na_2[Ni_2(TTHA)(OH_2)_2]\cdot 6H_2O$

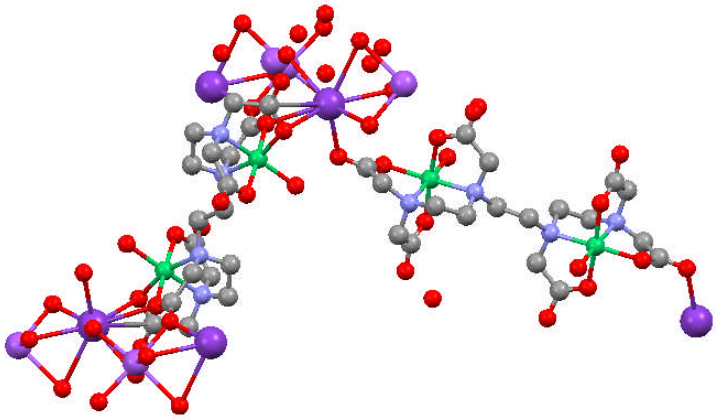

Fig. A.21 Structure of $Na_2[Ni_2(TTHA)(OH_2)_2]\cdot 6H_2O$.

Table A.XXI Crystal data and structure refinement for $Na_2[Ni_2(TTHA)(OH_2)_2]\cdot 6H_2O$.

Identification code	dwb0935m
Empirical formula	$C_{18}H_{34}KN_4NaNi_2O_{21.27}$
Formula weight	826.25
Temperature/K	110(2)
Crystal system	Triclinic
Space group	P-1
a/Å	6.9372(3)
b/Å	13.0782(7)
c/Å	18.3534(9)
α/°	105.4540(10)
β/°	96.5660(10)
γ/°	99.4420(10)
Volume/Å^3	1561.15(13)
Z	2
ρ_{calc}mg/mm^3	1.758
m/mm^{-1}	1.448
F(000)	852
Crystal size/mm^3	0.45 × 0.07 × 0.03
2Θ range for data collection/°	1.17 to 29.99
Index ranges	-9<=h<=9, -18<=k<=18, -25<=l<=25
Reflections collected	23671
Independent reflections	8927 [R(int) = 0.0267]
Data/restraints/parameters	8927 / 2 / 485
Goodness-of-fit on F^2	1.042
Final R indexes [I>=2σ (I)]	R1 = 0.0472, wR2 = 0.1229
Final R indexes [all data]	R1 = 0.0544, wR2 = 0.1281
Largest diff. peak/hole / e Å^{-3}	1.308 and -1.140

Appendix B

Chapter 2

Experimental

Attempted preparations of heterobimetallic Pt-Pd complexes

B.1 Attempted preparation of $(Bu_4N)_2[Cl_2Pt(\mu\text{-}Cl)_2PdCl_2]$ in the presence of solvent

$(Bu_4N)_2[PtCl_4]$ (**4**) (0.304 mmol, 0.250 g) was dissolved in CH_2Cl_2 (30 cm^3) to which solid $[PdCl_2]$ (0.304 mmol, 0.0539 g) was added. The mixture was then left to stir at room temperature for 24 h. No change was observed by UV-visible spectroscopy or by mass spectrometry.

Repeating the reaction under reflux (24 h) also showed no change.

Analysis: MS[ESI^-], found (expected): m/z: 300.9 $[PtCl_2(OH_2)_2]$, m/z: 177.8 $[H_2PdCl_2]$ (m/z: 513.68 $[PtPdCl_6]^{2-}$). No peak attributable to the product was obtained.

B.2 Attempted preparation of $(Bu_4N)_2[Cl_2Pt(\mu\text{-}Cl)_2PdCl_2]$ in absence of solvent

$(Bu_4N)_2[PtCl_4]$ (**4**) (0.122 mmol, 0.100 g) and $[PdCl_2]$ (0.128 mmol 0.023 g, 5% excess) were added to a flask, and were heated in the absence of solvent at 140 °C for 15 min. The paste that resulted was cooled to room temperature and acetone was added to it along with a pinch of charcoal. The mixture was boiled for a few minutes and was then filtered. The solvent was removed under vacuum from the resulted filtrate. Attempts of crystallisation in acetone at -5 °C were unsuccessful.

MS[ESI], found (expected): m/z: 265.9 $[HPtCl_2]^{1+}$, m/z: 300.9 $[PtCl_2(OH_2)(OH)H]^{1+}$, m/z: 328.9 unidentified (m/z: 510.68 $[PtPdCl_6]^{2-}$ remained unassigned).

B.3 Attempted preparation of $K_2[Cl_2Pt(\mu\text{-}Cl)_2PdCl_2]$ in water using silver salts

A solution of $K_2[PtCl_4]$ (0.24 mmol, 0.100 g) was prepared by stirring in water (30 cm^3) at room temperature. To the resulting red solution was added solid $K_2[PdCl_4]$ (0.24 mmol, 0.0786 g) followed by stirring of the contents for 30 min. Then, solid $AgNO_3$ (0.48 mmol, 0.0819 g) was added to the orange solution and the contents were stirred again at room temperature, overnight in the dark. The precipitate of AgCl was centrifuged to separate a brown filtrate, which was concentrated to recuperate a dark brown precipitate which was dried under vacuum. Attempts to crystallise the precipitate from $EtOH/H_2O$ and $MeOH/H_2O$ mixtures were unsuccessful and the coloured solutions showed signs of decomposition after a few days, observed as a black solid settled at the bottom of the flasks.

The same reaction was carried out with AgOTf showed similar results.

Analysis: MS[ESI^-]: only a peak of $[PtCl_3]^{1-}$ (m/z: 300.9) was observed; $[PtPdCl_6]$ (m/z: 425.62): unassigned. No signal attributable the target product was observed.

Attempted preparation of heterobimetallic Au-Pd complexes

B.4 Attempted preparations of $(Bu_4N)_2[Cl_2Pd(\mu\text{-}Cl)_2AuCl_2]$

To a solution of $(Bu_4N)[AuCl_4]$ (**5**) (0.430 mmol, 0.250 g) in CH_2Cl_2 (30 cm^3) was added solid $[PdCl_2]$ (0.430 mmol, 0.0763 g) and the mixture was stirred at room temperature for 24 h. The progress of the reaction was monitored by UV-visible spectroscopy. The reaction was continued up to 48 h but the results obtained were no different from that of 24 h reaction.

MS[ESI], found (expected): m/z: 242.3 $(Bu_4N)^+$, m/z: 266.9 $[AuCl_2]$, m/z: 388.8 $[H_2AuCl_4]^{1+}$. m/z: 751.5 $((Bu_4N)_2[AuCl_2])^{3+}$, 823.4 has close correspondence to $(Bu_4N)[Au_2Cl_5]$) λ_{max}: 327.09 nm (closely to correspond to $[AuCl_4]^-$, λ_{max} 323 nm).

The above reaction was also carried out in 1,4-dioxane and was analysed in by mass spectrometry. MS[ESI$^-$], found (expected): m/z: 242.3 $(Bu_4N)^+$, m/z: 266.9 $[AuCl_2]^{1+}$, m/z: 338.8 $[H_2AuCl_4]^{1+}$, m/z: 312.9 $[(Bu_4N)Cl(OH_2)(OH)]^{1-}$; no peaks attributable to the product was observed. λ_{max}: 327.69 nm (closely to correspond to $[AuCl_4]^-$, λ_{max} 323 nm).

B.5 Attempted preparation of $(Bu_4N)[Cl_2Pd(\mu\text{-}Cl)_2AuCl_2]$ in 1,4-dioxane

$(Bu_4N)[AuCl_4]$ (**5**) (0.344 mmol, 0.200 g) was dissolved in 1,4-dioxane (60 cm^3) and to this solution, solid $[PdCl_2(NCPh)_2]$ (0.344 mmol, 0.1319 g) was added. The mixture was heated under reflux for 18 h, under N_2 atmosphere. The reaction was monitored by UV-visible spectroscopy and was analysed after completion, indicating λ_{max} : 329 nm $[Pd_2Cl_6]^{2-}$. The resulted mixture was

analysed by mass spectrometry. The mixture was filtered to remove unreacted solid, and the solution was then analysed by mass spectrometry. MS[ESI], found (expected): m/z: 242.3 $(Bu_4N)^+$, m/z: 266.9 $[AuCl_2]^{1-}$, m/z: 338.8 $[H_2AuCl_4]^{1+}$ (m/z: 512.7 $[AuPdCl_6]^{1-}$). No peak attributable to the product was observed.

The solution obtained was then evaporated to dryness which resulted into an oily mass, which could not be solidified with any solvent. However, the solution obtained after filtration was dried to obtain an oily mass which was triturated with petroleum ether (40 - 60 °C) and Et_2O to remove excess of benzonitrile and give a solid. This was then redissolved in CH_2Cl_2, and precipitated with Et_2O resulting in a solid which was filtered and analysed by mass spectrometry. *Analysis*: ^{1}H NMR, $CDCl_3$: δ 1.12 (t, -CH_3, 24 H, *J* 7.6 Hz), 1.6-1.7 (m, -CH_2-, 16 H *J* 12.4 and 7.2 Hz), 1.82-1.93 (m, -CH_2-, 16 H, *J* 16 and 8.4 Hz), 3.51-3.56 (m, -NCH_2-, 16 H, *J* 8.4 and 5.6 Hz). MS[ESI], found expected: m/z: 266.9 $[AuCl_2]^{1-}$, m/z: $[AuCl(OH)]^{1+}$, m/z: 426.6 $[Pd_2Cl_6]^{2-}$, m/z: 318.7 $[H_2Pd_2Cl_3]^{3+}$, m/z: 646.9 ($(Bu_4N)[Pd_2Cl_5(OH_2)]$). The filtrate resulted from after filtration of the solid from CH_2Cl_2, formed yellow crystals and brown crystalline solid which were inseparable.

B.6 Attempted preparation of $(Bu_4N)_2[Cl_2Pd(\mu\text{-}Cl)_2AuCl_2]$ in CH_2Cl_2

A solution of $(Bu_4N)[AuCl_4]$ (**5**) (0.345 mmol, 0.200 g) was prepared in CH_2Cl_2 (60 cm^3) to which was added solid $[PdCl_2[(NCPh)_2]$ (0.345 mmol, 0.132 g) and the mixture was heated under reflux, under N_2 atmosphere for 48 h. The progress of the reaction was monitored by UV-visible spectroscopy. The resulted mixture was analysed by mass spectrometry. MS[ESI], found

(expected): m/z: 242.3 $(Bu_4N)^+$, m/z: 266.9 $[AuCl_2]^{1-}$, m/z: 338.8 $[AuCl_4]^{1-}$. After reflux, the mixture was filtered to obtain a deep-pink coloured precipitate.

^{1}H NMR, 400 MHz, $CDCl_3$: δ 1.01 (t, -CH_3, 12 H), 1.56 (q, -CH_2-, 8 H), 2.12 (m, -CH_2-, 8 H), 3.53 (m, -NCH_2-, 8 H). MS[ESI], found (expected): m/z: 312.2 $[Bu_4N(Cl)(OH_2)(OH)]^{1-}[M^-]$. $[C_{16}H_{36}AuCl_6NPd]$ (m/z: 754.97) was unassigned.

B.7 Attempted preparation of $K[Cl_2Pd(\mu\text{-}Cl)_2AuCl_2]$ in water using Ag^I

An aqueous solution (30 cm^3) of $K[AuCl_4]$ (0.265 mmol, 0.100 g) was prepared and to that solution was added $K_2[PdCl_4]$ (0.265 mmol, 0.0864 g) and the mixture was stirred for 30 min. Thereafter, solid $AgNO_3$ (0.530 mmol, 0.899 g) was added and the mixture was stirred at room temperature overnight (16 h) in the dark. The off-white precipitate of AgCl was then centrifuged to separate the brown coloured filtrate. This clear brown solution was concentrated to recuperate a brown coloured precipitate, which was dried under vacuum and was analysed as it was not possible to grow suitable crystal.

MS[ESI$^-$]: peaks of m/z: 318.9 $[AuCl_3HO]^{1-}$ $[M^-]$, m/z: 338.8 $[AuCl_4]^{1-}$, m/z: 266.9 $[AuCl_2]^{1+}$ and 300.9 $[AuCl_2(OH)_2]^{1-}$ were observed; m/z: 512.68 $[AuPdCl_6]$: unassigned. No signal attributable the target product was observed.

B.8 Attempted preparation of $K_2[Cl_2Pd(\mu\text{-}Cl)_2AuCl_2]$ in benzonitrile

$K[AuCl_4]$ (0.794 mmol, 0.300 g), $[PdCl_2(NCPh)_2]$ (0.794 mmol, 0.303 g) were added to benzonitrile (50 cm^3), and heated under reflux overnight. The progress of the reaction was monitored by UV-visible spectroscopy. The reaction mixture was then analysed by mass spectrometry. MS[ESI], found (expected): m/z: 282.9 $[H_2PdCl_5]^{1-}$, m/z: 268.8 $(K[PdCl_3(OH_3))^{1-}$. λ_{max}: 332 nm closely corresponds to $K_2[Pd_2Cl_6]$ (324.5, 430 nm, H_2O), and $[K(18\text{-crown-}6)]_2[Pd_2Cl_6]$ (339.5 nm, CH_2Cl_2).

Attempted preparation of heterobimetallic Au-Pt complexes

B.9 Attempted preparation of $(Bu_4N)[Cl_2Pt(\mu\text{-}Cl)_2AuCl_2]$

$(Bu_4N)_2[PtCl_4]$ (**4**) (0.054 mmol, 0.044 g) and $(Bu_4N)[AuCl_4]$ (**5**) (0.054 mmol, 0.031 g) were dissolved in CH_2Cl_2 (10 cm^3), with stirring. To this solution was added solid AgOTf and the mixture was stirred for 18 h. From the resulting mixture, the solvent was removed under vacuum. The yellow precipitate formed was re-dissolved in acetone, filtered, washed with Et_2O and dried under vacuum for a few hours.

MS[ESI], found (expected): m/z: 320.9 (unidentified) m/z: 406.8 $[AuCl_5(OH_2)(OH)]^{3-}$, m/z: 540.2 $[(Bu_4N)_2(OH_2)(Cl)H_2]$.

B.10 Attempted preparation of $(Bu_4N)[Cl_2Pt(\mu\text{-}Cl)_2AuCl_2]$

To a solution of $(Bu_4N)[AuCl_4]$ (**5**) (0.430 mmol, 0.250 g) in CH_2Cl_2 (30 cm^3) was added $[PtCl_2]$ (0.430 mmol, 0.114 g) followed by stirring at room

temperature for 22 h. The mixture solution was filtered to remove unreacted [$PtCl_2$] followed by analysis by mass spectrometry. MS[ESI^-], found (expected): m/z: 242.3 $(Bu_4N)^+$, m/z: 751.5 $((Bu_4N)_2[AuCl_2])^{3+}$, m/z: 823.4 $((Bu_4N)[Pt_2Cl_4(OH)_3])^{2-}$). The yellow solution was then crystallised at low temperature (-5 °C) which resulted into yellow-coloured crystals of $(Bu_4N)[AuCl_4]$.

Analysis (crystals): Elemental, found (expected): C 33.41, H 6.69, N 2.46 % (C 33.06, H 6.24, N 2.41 % corresponds to $(Bu_4N)[AuCl_4]$). ^{1}H NMR, 400 MHz, $CDCl_3$: δ 1.04 (t, $-CH_3$, 12 H), 1.41-1.53 (m, $-CH_2$, 8 H), 1.61-1.73 (m, $-CH_2$, 8 H), 3.14-3.29 (m, $-NCH_2$, 8 H). MS[ESI], found (expected), crystals: 266.9 [$AuCl_2$] (m/z: 266.90 $[AuCl_2]^+$); m/z: 338.8 $[H_2AuCl_4]^+$ (m/z: 338.86 $[H_2AuCl_4]^{1+}$).

B.11 Attempted preparation of $(Bu_4N)[Cl_2Pt(\mu\text{-}Cl)_2AuCl_2$

$(Bu_4N)[AuCl_4]$ (**5**) (0.128 mmol, 0.074 g, 5% excess) and $(Bu_4N)_2[PtCl_4]$ (**4**) (0.122 mmol, 0.100 g) were added to a flask and the mixture was heated at 140 °C in the absence of solvent. This resulted into a paste which was cooled to room temperature. To this paste, acetone (12 cm^3) and a pinch of charcoal were added, and the mixture was boiled for a few minutes. This mixture was then filtered off and the solution obtained was analysed.

MS[ESI], found (expected): m/z: 266.9 $[AuCl_2]^{1+}$, m/z: 300.9 $[H_2PtCl_2O_2]^{2+}$, m/z: 335.8 $[PtCl_3(OH_2)_2]^{1-}$ (m/z: 601.7 $[PtAuCl_6]^{1-}$ was unassigned).

An attempt was made to crystallise the mixture in acetone (-5 °C) and in acetone/Et_2O but no crystals were obtained, rather an oily mass resulted which could not be solidified.

The above reaction was also carried out with a 1 : 1 ratio of Pt : Au, but the results obtained were no different to the above.

B.12 Attempted preparation of [K(18-crown-6)][$Cl_2Pt(\mu$-$Cl)_2AuCl_2$] in water

$K_2[PtCl_4]$ (0.25 mmol, 0.1037 g) was dissolved in water (6 cm^3) *via* stirring for a few minutes until a red solution was obtained. To this solution was added solid [18-crown-6] (0.814 mmol, 0.2152 g) followed by stirring the contents for 1 h at room temperature. Then, to this red solution was added solid $K[AuCl_4]$ (0.25 mmol, 0.0945 g), and the mixture was left to stir for 48 h in the dark. This resulted in a slight pink-coloured precipitate with accompanying gold mirror which was difficult to separate. Yield: 0.1612 g.

Analysis (precipitate mixed with Au^0): ^{195}Pt NMR, 107.5 MHz, DMSO: δ -823 (corresponds to $[PtCl_5(dmso)]^{1-}$), -2953 ($[PtCl_3(dmso)]^{1-}$). ^{1}H NMR, 400 MHz, $CDCl_3$: δ 3.66 (s). MS[ESI$^-$] found (expected), m/z: 203.88 (unidentified), m/z: 248.97 $[AuCl(OH)]^{1+}$, m/z: 300.97 $[PtCl_2(OH_2)_2]$, m/z: 338.84 $[H_2AuCl_4]^{1+}$, m/z: 372.80 $[H_3PtCl_5]$, m/z: 430.76 $[H_8PtCl_6(OH_2)]^{4+}$, m/z: 897.57 ($[K(18\text{-crown-6})]_2[AuCl_2(OH_2)H_6]$)$^{6+}$, m/z: 908.5 ($[K(18\text{-crown-6})]_2[AuCl_2(OH_2)_2]$)$^{3+}$, m/z: 916 ($[K(18\text{-crown-6})]_2[AuCl(OH_2)_4H_6]$). IR ($\nu_{Pt\text{-}Cl}$): 325 cm^{-1} corresponds to $[PtCl_6]^{2-}$. AAS metal ratio, found (expected): 1 : 2.13 (Au : Pt). The filtrate

resulted into pale yellow crystals on standing. Yield: 2 mg. The crystals were not suitable for X-ray diffraction yet they were analysed.

Analysis (crystals from filtrate): Elemental, found (expected): C 23.75, H 3.99 % (C 23.83, H 4.00 % corresponds to $[K(18\text{-crown-}6)]_2[Pt_2Cl_6]$).

B.13 Attempted preparation of $[K(18\text{-crown-}6)][Cl_2Pt(\mu\text{-}Cl)_2AuCl_2]$ in acetic acid : water (1 : 1 v/v) with Pt : Au (1 : 1)

$K_2[PtCl_4]$ (0.25 mmol, 0.1038 g) was dissolved in water with stirring. To this red solution was added [18-crown-6] (0.78 mmol, 0.208 g) with continuous stirring and the mixture was left to stir at room temperature for an hour. Then, to this mixture was added solid $K[AuCl_4]$ (0.25 mmol, 0.0945 g) and the contents of the flask were stirred at room temperature for 48 h in the dark. This resulted in a beige-coloured precipitate, which was filtered, washed with water (2 cm^3), EtOH (4 cm^3), Et_2O (4 cm^3) and then dried under vacuum for 48 h. Yield: 0.2652 g. *Analysis (precipitate)*: Elemental, found: C 23.77, H 4.02 %, overall calculated concentration value is 4.19 ppm for Pt^{IV} and 6.55 ppm for Au^{I}. ^{195}Pt NMR, 107.49 MHz, DMSO (dry): δ -823 corresponds to $[PtCl_5(dmso)]^{1-}$. ^{1}H NMR, 400 MHz, $CDCl_3$: δ 3.72 (s), ^{1}H NMR, 400 MHz, d_6-DMSO: δ 3.54 (s). MS[ESI], found (expected): m/z: 568.79 $[Au_2Cl_5]^{1+}$, m/z: 641.21 $([K(18\text{-crown-}6)]_2Cl)^{1+}$, m/z: 719.22 $([K(18\text{-crown-}6)]_2Cl(OH_2)_4H_6)$. IR ($\nu_{M\text{-}X}$ str.): 325 cm^{-1} correspond to $[PtCl_6]^{2-}$; 350 cm^{-1} correspond to $[AuCl_2]^{1-}$. AAS metal ratio, found (expected): 3.4 : 6.6 (Au : Pt) (1 : 1 (Au : Pt) with respect to ratio used).Crystals suitable for X-ray diffraction were obtained from concentrated solution of the precipitate in

DMSO (dry) in an NMR tube by slow cooling process. They corresponded to $[K(18\text{-crown-6})]_2[PtCl_6]\cdot 2DMSO$ (yellow crystals).

Analysis (filtrate): ^{195}Pt NMR, 107.49 MHz, $CH_3COOH : H_2O$(1 : 1): +533.92 $[PtCl_5(OH_2)]^{1-}$, -1512.138 $[PtCl_4]^{2-}$ and -2412.56 (Pt^{II} species). The filtrate obtained resulted into orange-coloured plates which were also analysed by X-ray diffraction as $[K(18\text{-crown-6})][PtCl_5(OH_2)]$.

B.14 Attempted preparation of $[K(18\text{-crown-6})][PtAuCl_6]$ in $H_2O:CH_3COONa$ (1 : 3) with Pt : Au (1 : 1)

The salt CH_3COONa (solid, 0.0524 mol, 4.30 g) was dissolved in water (9 cm^3), until a clear solution was obtained (pH 9). Then, [18-crown-6] (0.814 mmol, 0.2152 g), was added and the mixture was heated until a clear solution was obtained. The mixture was then cooled and $K_2[PtCl_4]$ (0.25 mmol, 0.104 g) was added, and the contents were left to stir until the salt was completely dissolved. The colour of solution was yellowish red after dissolution was complete. To this solution was added $K[AuCl_4]$ (0.25 mmol, 0.0945 g), contents were stirred under same conditions for 48 h in the dark. The colour of final mixture was yellowish grey. From the mixture, a pinkish grey precipitate was filtered off, washed with water, EtOH and Et_2O followed by drying under vacuum for 24 h. Yield: 0.082 g. *Analysis (precipitate)*: Elemental, found (expected): C 24.70, H 4.03 % (C, 25.23; H, 4.23 % corresponds to $[K(18\text{-crown-6})][AuCl_2]$, expected product). ^1H NMR, 400 MHz, $(CD_3)_2CO$: δ 3.66 (s). Colourless crystals were obtained from sample used for ^1H NMR spectroscopy. XRD (single crystals), $(CH_3)_2CO$: colourless crystals correspond with $[K(18\text{-crown-6})][AuCl_2]$. IR: 350 cm^{-1} ($\nu_{Au\text{-}Cl}$) corresponds to $[AuCl_2]^-$.

To the yellow solution obtained after filtration was added $(Bu_4N)Cl$ (3 eq., 0.748 mmol 0.208 g) followed by stirring for 3 h at room temperature but no precipitate resulted. *Analysis (filtrate)*: ^{195}Pt NMR, 107.49 MHz, CH_3COONa : H_2O (1 : 3): no peak was observed.

The above filtrate was then placed in the fridge for a few days which resulted into needle-shaped colourless crystals. Yield: 0.395 g. *Analysis (crystals from filtrate)*: Elemental, found (expected): C 24.77, H 4.05 % (C 25.23, H 4.23 % corresponds to $[K(18\text{-crown-6})][AuCl_2]$). MS[ESI], found (expected): m/z: 446.9 $[AuCl_2(OH_2)]^{1-}$, rest of the peaks were unidentifiable. XRD (single crystals), CH_3COONa : H_2O (1 : 3): colourless crystals, $[K(18\text{-crown-6})][AuCl_2]$.

B.15 Attempted preparation of $[K(18\text{-crown-6})][Cl_2Pt(\mu\text{-}Cl)_2AuCl_2]$ in HCl (dil.) with Pt : Au (1 : 1)

To a solution of HCl (conc., 1.62 cm^3) in water (3 cm^3) was added $K_2[PtCl_4]$ (0.25 mmol, 0.104 g), and [18-crown-6] (0.814 mmol, 0.2152 g); the contents were left to stir for 1 h until dissolved to form a red-coloured solution. Solid $K[AuCl_4]$ (0.25 mmol, 0.0945 g) was added and after a few minutes of stirring the mixture solidified, therefore, water (3 cm^3) was added to it, followed by stirring the contents for 48 h at room temperature in the dark. This resulted in a peach-coloured precipitate, which was filtered followed by washing with H_2O (2 cm^3), EtOH (4 cm^3), and Et_2O (4 cm^3). It was then dried under vacuum for a few days. Yield: 0.1978 g. *Analysis (precipitate)*: Elemental, found: C 24.93, H 4.08 %. ^{195}Pt NMR, 107.49, DMSO (dry): δ +424 corresponds to [K(18-

crown-6)]$_2$[PtCl$_6$]. ^{1}H NMR, 400 MHz, d_6-DMSO: δ 3.54 (s). IR (ν_{M-X}): 325 cm^{-1} (ν_{Pt-Cl}) [PtCl$_6$]$^{2-}$, 350 cm^{-1} (ν_{Au-Cl})[AuCl$_2$]$^{1-}$.

The filtrate obtained was analysed. *Analysis (filtrate)*: ^{195}Pt NMR, 107.49 MHz, HCl (dil): δ -2.6 corresponds to [PtCl$_6$]$^{2-}$. The filtrate resulted into very fine creamy yellow coloured crystals in the fridge after a few days. *Analysis (crystals from filtrate)*: Elemental (crystals), found (expected): C 22.86, H 3.42 % (C 22.44, H 3.77 % corresponds to [K(18-crown-6)][AuCl$_4$]).

B.16 Attempted preparation of [K(18-crown-6)][Cl$_2$Pt(μ-Cl)$_2$AuCl$_2$] in water with Pt : Au (1 : 1) 3 h reaction appendix

K$_2$[PtCl$_4$] (0.25 mmol, 0.104 g) was dissolved in water with stirring. To this red solution was added [18-crown-6] (0.78 mmol, 0.208 g) with continuous stirring and the mixture was left to stir at room temperature for an hour. Then, to this mixture was added solid K[AuCl$_4$] (0.25 mmol, 0.0945 g) and the contents of the flask were stirred at room temperature for 3 h in the dark. This resulted in a pale yellow precipitate, which was filtered followed by washing with H$_2$O, EtOH and Et$_2$O. The precipitate was then dried under vacuum for 18 h. Yield: 0.1723 g.

Analysis (precipitate): Elemental found: C 22.91, H 3.87 %. ^{195}Pt NMR, δ 107.49, DMSO (dry): +815. closely corresponds to [K(18-crown-6)]$_2$[PtCl$_6$]. IR (ν_{M-X}): 350 cm^{-1} (ν_{Au-Cl}) [AuCl$_2$]$^{1-}$, 370 cm^{-1} (ν_{Pt-Cl}) [PtCl$_6$]$^{2-}$.

Analysis (filtrate): ^{195}Pt NMR, δ 107.49, H$_2$O: -1602 close to [Pt$_2$Cl$_6$]$^{2-}$; -2360 close to [PtCl$_2$(OH$_2$)$_4$]$^{2-}$.

The approximate ratio of peaks of Pt^{II} : Pt^{IV} was 3 : 1.

B.17 Attempted preparation of [K(18-crown-6)][$Cl_2Pt(\mu\text{-}Cl)_2AuCl_2$] in water with Pt : Au (3 : 2)

$K_2[PtCl_4]$ (0.25 mmol, 0.104 g) was dissolved in water (6 cm^3). To this solution [18-crown-6] (0.814 mmol, 0.215 g) was added and it was stirred for an hour. To this red solution was added solid $K[AuCl_4]$ (0.167 mmol, 0.063 g), and the contents were stirred at room temperature for 48 h in the dark. A beige-coloured precipitate resulted along with gold metal which was carefully filtered, washed with water (2 cm^3), EtOH (4 cm^3) and Et_2O (4 cm^3). The precipitate was then dried under vacuum for a few days. Yield: 0.1461 g. *Analysis (precipitate)*: Elemental, found: C 26.93, H 4.45 %, calculated overall ratio of Pt^{IV} : Pt^{II} is 2.3 : 1. ^{195}Pt NMR, 107.5 MHz, DMSO (dry): δ -2953 corresponds to $[PtCl_3(dmso)]^{1-}$ was the only peak obtained as the sample produced crystals on standing in NMR tube of $[K(18\text{-crown-6})]_2[PtCl_6]$. ^{1}H NMR, 400 MHz, d_6-dmso: δ 3.54 (s). IR (M-X str.): 325 cm^{-1} corresponds to ($\nu_{Pt\text{-}Cl}$) $[PtCl_6]^{2-}$. *Analysis (crystals from precipitate)*: Elemental (crystals), found (expected): C 28.25, H 4.77 % (C 28.41, H 4.77 % corresponds to $[K(18\text{-crown-6})]_2[PtCl_6]$).

To the light yellow filtrate was then added $(Bu_4N)Cl$ which was stirred for 2 h. This could not result into any precipitate. ^{195}Pt NMR, 107.5 MHz, H_2O: no peak was observed.

B.18 Attempted preparation of Pt^{II} butadiene type complex from PPh_4^+ complexes

General Preparation of $(PPh_4)[MCl_x]$ x = 4 or 6 mononuclear metal complexes of Pt^{II}, Au^{III} and Pt^{IV}

$K_2[MCl_x]$ (0.482 mmol, ′a′ g) was stirred to dissolve in water (5 cm^3). To this coloured solution was added another solution of $(PPh_4)Cl$ (0.964 mmol, ′b′ g, amount equivalent to K^+ ion concentration) in water (5 cm^3) followed by stirring the contents for 10 min. This resulted into a precipitate which was filtered and washed with water in excess followed by drying it under vacuum for 48 h (for Pt^{IV}). In Pt^{II} and Au^{III} complexes, the resulted solid was pasty hence it was redissolved in CH_2Cl_2, dried over Mg_2SO_4 followed removal of solvent and then drying the resulted crystalline solid under vacuum for 18 h (Pt^{II} and Au^{III}).

*$(PPh_4)_2[PtCl_4]$ (**9**)*

Yield: 92% (0.442 mmol, 0.449 g). *Analysis*: Elemental, found (expected): C 56.51, H 3.97 % (C 56.76, H 3.97 %). ^{1}H NMR, 400 MHz, CD_2Cl_2: δ 7.63-7.68 (m, 8 H), 7.79-7.84 (m, 8 H), 7.93-7.97 (m, 4 H). ^{13}C NMR, 100 MHz, CD_2Cl_2: δ 131.04 (d, Ph_{meta}), 134.84 (d, Ph_{ortho}), 136.05 (d, Ph_{para}). ^{195}Pt NMR, 107.5 MHz, CD_2Cl_2: δ -1446 (s).

*$(PPh_4)[AuCl_4]$ (**10**)*

Yield: 94% (0.497 mmol, 0.3372 g). *Analysis*: Elemental, found (expected): C 42.24, H 3.02 % (C 42.51, H 2.97 %). ^{1}H NMR, 400 MHz, CD_2Cl_2: δ 7.59-7.65 (m, =CH, 8 H), 7.74-7.78 (m, =CH, 8 H), 7.91-7.95 (m, =CH,

4 H). ^{13}C NMR, 400 MHz, CD_2Cl_2: δ 131.1 (d, Ph_{meta}) 134.8 (d, Ph_{ortho}), 136.2 (d, Ph_{para}).

*$(PPh_4)_2[PtCl_6]$ (**11**)*

Yield: 65% (0.1445 mmol, 0.1571 g). *Analysis*: Elemental, found (expected): C 52.94, H 3.74 % (C 53.06, H 3.71 %). ^{1}H NMR, 400 MHz, d_6-dmso: δ 7.72-7.77 (m, =CH, 16 H), 7.79-7.84 (m, =CH, 16 H), 7.95-7.98 (m, =CH, 8 H). ^{13}C NMR, 100 MHz, d_6-dmso: δ 130.45 (d, Ph_{meta}), 134.54 (d, Ph_{ortho}), 135.34 (Ph_{para}). ^{195}Pt NMR, 400 MHz, DMSO (dry): δ +430 (s).

a. By using mono-nuclear metal complexes of tetraphenylphosphonium cation i.e. Pt^{II} and Au^{III}

To $(PPh_4)_2[PtCl_4]$ (**9**) (0.098 mmol, 0.100 g) in CH_2Cl_2 (2.5 cm^3) was added $(PPh_4)[AuCl_4]$ (**10**) (0.098 mmol, 0.067 g) in CH_2Cl_2 (2.5 cm^3) mixture was stirred at room temperature for 48 h in the dark. This resulted into an orange-yellow coloured precipitate which was dried under vacuum for a few days. Yield: 7.5% (0.0074 mmol, 0.008 g). *Analysis (precipitate)*, Elemental, found (expected): C 47.02, H 3.40 % (C 53.06, H 3.71 % corresponds to $(PPh_4)_2[PtCl_6]$). ^{195}Pt NMR, 107.5 MHz, DMSO (dry): δ +430 (s) corresponds to $(PPh_4)_2[PtCl_6]$. ^{1}H NMR, 400 MHz, d_6-DMSO: δ 7.72-7.76 (m, =CH, 8 H), 7.79-7.84 (m, =CH, 8 H), 7.92-7.98 (m, 4 H). ^{13}C NMR, 100 MHz, d_6-DMSO: δ 130.44 (d, Ph_{meta}), 134.58 (d, Ph_{ortho}), 135.36 (d, Ph_{para}).

The orange filtrate was then recuperated and was analysed *via* ^{195}Pt NMR. The filtrate produced orange-yellow coloured crystals which were analysed

via XRD hence corresponds to $(PPh_4)_2[PtCl_6]\cdot 2CH_2Cl_2$. Yield: 6.9% (0.016 mmol, 0.014 g). Also, from the mixture of CH_2Cl_2/hexane two different types of crystals were produced as yellow and pale yellow crystals *i.e.* $(PPh_4)_2[PtCl_4]$ and $(PPh_4)[AuCl_4]$ respectively. *Analysis (filtrate),* ^{195}Pt NMR, 107.5 MHz, CH_2Cl_2: δ -1445 (s) correspond with $(PPh_4)_2[PtCl_4]$. XRD (single crystals), CH_2Cl_2/hexane: pale yellow crystals and yellow crystals correspond with $(PPh_4)[AuCl_4]$ and $(PPh_4)_2[PtCl_4]$ respectively. XRD (single crystals), CH_2Cl_2: orange-yellow crystals correspond with $(PPh_4)_2[PtCl_6]\cdot 2CH_2Cl_2$.

b. By using mono-nuclear metal complexes of tetraphenylphosphonium cation i.e. Pt^{II} and Au^{III} with hex-1-ene

To the solution of $(PPh_4)_2[PtCl_4]$ (**9**) (0.0985 mmol, 0.100 g) in CH_2Cl_2 (2.5 cm^3) was added another solution of $(PPh_4)[AuCl_4]$ (**10**) (0.0985 mmol, 0.067 g), in CH_2Cl_2 (2.5 cm^3) followed by stirring at RT in the dark for 48 h after the addition of hex-1-ene (0.0986 mmol, 0.0083 g or 0.0123 ml). This resulted into a yellow precipitate which was filtered off, dried under vacuum for 18 h. $(PPh_4)_2[PtCl_6]$, Yield: 1.9% (0.0018 mmol, 2 mg). *Analysis (precipitate),* Elemental, found (expected): C 48.395, H 3.283 % did not corresponds to the expected product (C 53.06, H 3.71 % corresponds to $(PPh_4)_2[PtCl_6]$). ^{195}Pt NMR, 107.5 MHz, $(CD_3)_2CO$: δ +374 (s) corresponds to $[PtCl_6]^{2-}$; +97 (s) (unidentified peak). ^{1}H NMR, 400 MHz, CD_2Cl_2: δ 7.61-7.66 (m, 16 H), 7.75-7.80 (m, 16 H), 7.91-7.95 (m, 8 H). ^{13}C NMR, 400 MHz, CD_2Cl_2: δ 131.1 (d, Ph_{meta}), 134.9 (d, Ph_{ortho}), 136.15 (d, Ph_{para}).

To the resulted yellowish-orange filtrate was added hexane is excess which produced an orange coloured precipitate which was recuperated by filtrate

and was dried under vacuum for 18 h. Yield: 0.034 g. *Analysis (precipitate from filtrate),* ^{195}Pt NMR, 107.5 MHz, CH_2Cl_2: no peak was observed. The resulted filtrate was also placed at room temperature for crystallisation. The precipitate obtained was recrystallised from CH_2Cl_2. XRD (single crystal), CH_2Cl_2: yellow crystals, correspond with $(PPh_4)_2[PtCl_6]\cdot 2CH_2Cl_2$.

c. By using mono-nuclear metal complexes of tetraphenylphosphonium cation i.e. Pt^{II} and Pt^{IV} with hex-1-ene

To the solution of $(PPh_4)_2[PtCl_4]$ (**9**) (0.0985 mmol, 0.100 g), in CH_2Cl_2 (2.5 cm^3) was added another solution of $(PPh_4)_2[PtCl_6]$ (**11**) (0.0985 mmol, 0.107 g) in CH_2Cl_2 (2.5 cm^3) which resulted into a suspension to which hex-1-ene (0.0986 mmol, 0.0083 g or 0.0123 ml) was added and was stirred at room temperature for 48 h in the dark. From the resulted mixture unreacted $(PPh_4)_2[PtCl_6]$ which was removed *via* filtration. Elemental, found (expected): C 52.16, H 3.64 % (C 53.06, H 3.71 % corresponds to $(PPh_4)_2[PtCl_6]$). To the resulted filtrate was added hexane in excess this resulted into precipitate which was then filtered off and was dried under vacuum for a few days. Yield: 0.0661 g. *Analysis (precipitate from filtrate),* Elemental, found (expected): ^{1}H NMR, 400 MHz, CD_2Cl_2: δ 7.63-7.69 (m, 8 H), 7.78-7.83 (m, 16 H), 7.93-7.97 (m, 16 H), 1.7913 (s, broad, 24H), ^{13}C NMR, 400 MHz, CD_2Cl_2: δ 131.07 (d, Ph_{meta}), 134.9 (d, Ph_{ortho}), 136.11 (d, Ph_{para}), 117.5 (s, unidentified), 118.4 (s, unidentified). XRD (single crystal), CD_2Cl_2: yellow coloured and colourless crystals corresponds to $(PPh_4)_2[PtCl_4]$) and $(PPh_4)Cl\cdot 2CH_2Cl_2$ respectively. XRD (single crystal), CH_2Cl_2/hexane: $(PPh_4)_2[PtCl_4]$.

Chapter 3

Experimental

B.19 Attempted preparation of sodium triethyltetraamine-N,N',N'',N'''-hexaacetatoiridate(III)palladate(II)

H_6TTHA (0.5 mmol, 0.2473 g), $IrCl_3.3H_2O$ (0.5 mmol, 0.158 g), $K_2[PdCl_4]$ (0.5 mmol, 0.1633 g) and NaOH (3 cm^3, 1 mol dm^{-3}) were used.

To the brownish solution was added ethanol (*ca* 200 cm^3), leading to a brownish-yellow coloured precipitate, which was filtered and dried under vacuum. A portion was dissolved in an ethanol/water mixture but no single crystals were obtained.

Analysis: Elemental: found, C 20.61, H 3.11, N 5.15% corresponds to a calculated overall ratio of Ir : Pd as 2.08 : 1. MS[ESI^-], found (expected): m/z: 787.0 [$C_{18}H_{24}IrN_4O_{12}Pd$]; m/z: 822.98 [$C_{18}H_{24}ClIrN_4O_{12}Pd$] (m/z: 788.01 [$C_{18}H_{24}IrN_4O_{12}Pd$]; m/z: 822.98 $C_{18}H_{24}ClIrN_4O_{12}Pd$). IR ($\nu$ = cm^{-1}) 1744 (C=O str.).

B.20 Attempted preparation of tetraphenylphosphonium triethytetraamine-N,N',N'',N'''-hexaacetatocobaltate(II)rhodate(III) $(PPh_4)_x[Co_yRh_z(TTHA)]$

H_6TTHA (0.5 mmol, 0.2472 g), $RhCl_3.3H_2O$ (0.5 mmol, 0.1318 g,), NaOH (3 cm^3, 1 mol dm^{-3}), $(PPh_4)Cl$ (3.0 mmol, 1.123 g,) and $Co(NO_3)_2.6H_2O$ (0.5 mmol, 0.1455 g).

The dark pink solution was precipitated with ethanol (*ca* 200 cm^3). This resulted into a deep pink coloured precipitate which was filtered and dried

under vacuum. Yield: 0.29 g). The precipitate was re-dissolved in water to crystallise the product but no crystals were obtained.

Analysis: AAS metal concentration (ppm), found: Rh 1.95, Co 5.56. Elemental: found, C 26.13, H 4.62, N 6.84 % corresponds to a calculated overall ratio of Rh : Co of 1.9 : 1. MS[ESI$^-$], found (expected), (mixture): m/z: 668.0 $[C_{18}H_{26}N_4O_{13}RhCo]^{1-}$ (m/z: 667.99 $[C_{18}H_{26}N_4O_{13}RhCo]^{1-}$). IR ($\nu$ cm^{-1}): 1636 (C=O str.).

B.21 Attempted preparation of tetraphenylphosphonium triethylenetetraamine-N,N′,N″,N‴-heaxacetatonickelate(II)rhodate(III), $(PPh_4)_x[Ni_yRh_z(TTHA)]$

H_6TTHA (0.5 mmol, 0.247 g), $RhCl_3.3H_2O$ (0.5 mmol, 0.1317 g), NaOH (3 cm^3, 1 mol dm^{-3}), $(PPh_4)Cl$ (3.0 mmol, 1.123 g,) and $Ni(NO_3)_2.6H_2O$ (0.5 mmol, 0.1454 g) were used. The solution obtained was precipitated with ethanol (*ca* 200 cm^3). Yield: 0.32 g. The precipitate was re-dissolved with water but no crystals were obtained.

Analysis: AAS metal concentration (ppm), found: Rh 2.01, Ni 4.67. MS[ESI$^-$], found (expected): m/z: 667.0 $[C_{18}H_{26}N_4NiO_{13}Rh]$ (m/z: 666.99 $[C_{18}H_{26}N_4NiO_{13}Rh]$). IR ($\nu$ cm^{-1}): 1636 (C=O str.).

B.22 Attempted preparation of tetraphenylphosphonium triethytetraamine-N,N',N'',N'''-hexaacetatochromate(III)nickelate(II), $(PPh_4)_x[Ni_yCr_z(TTHA)]$

H_6TTHA (0.5 mmol, 0.247 g), $Cr(NO_3)_3.9H_2O$ (0.5 mmol, 0.200 g), NaOH (3 cm^3, 1 mol dm^{-3}), $(PPh_4)Cl$ (3.0 mmol, 1.123 g) and $Ni(NO_3)_2.6H_2O$ (0.5 mmol, 0.1454 g) were used.

The solution obtained was precipitated with ethanol (*ca* 200 cm^3) resulting violet-coloured precipitate. The precipitate was re-dissolved with water but no crystals were obtained.

Analysis: AAS metal concentration (ppm), found: Ni 2.0, Cr 1.2. MS[ESI$^-$], found (expected): m/z: 616.0 $[C_{18}H_{26}CrN_4NiO_{13}]$ (m/z: 616.03 $[C_{18}H_{26}CrN_4NiO_{13}]$). IR ($\nu$ cm^{-1}): 1636 (C=O str.).

B.23 Attempted preparation of tetraphenylphosphonium triethytetraamine-N,N',N'',N'''-hexaacetatochromate(III)cobaltate(II), $(PPh_4)_x[Co_yCr_z(TTHA)]$

H_6TTHA (0.5 mmol, 0.247 g), $Cr(NO_3)_3.9H_2O$ (0.5 mmol, 0.200 g), NaOH (3 cm^3, 1 mol dm^{-3}), $(PPh_4)Cl$ (3.0 mmol, 1.123 g) and $Co(NO_3)_2.6H_2O$ (0.5 mmol, 0.1455 g) were used.

The violet solution was precipitated by ethanol (*ca* 200 cm^3). Yield: 0.36 g. The precipitate was re-dissolved with water but no crystals were obtained.

Analysis: AAS metal ratio (ppm), found: Cr 1.2 and Co 2.2. MS[ESI$^-$], found (expected): m/z: 599.0 $[C_{18}H_{24}N_4O_{12}CrCo]^{-1}$ (m/z: 599.01 $[C_{18}H_{24}N_4O_{12}CrCo]^-$

^{1}), m/z: 617.0 $[C_{18}H_{26}N_4O_{13}CrCo]^{-1}$ (m/z: 617.02 $[C_{18}H_{26}N_4O_{13}CrCo]^{-1}$). IR ($\nu$ cm^{-1}): 1636 (C=O str.).

B.24 Attempted preparation of tetraphenylphosphonium triethytetraamine-N,N',N'',N'''-hexaacetatocuprate(II)rhodate(II), $(PPh_4)_x[Cu_yRh_z(TTHA)]$

H_6TTHA (0.5 mmol, 0.2472 g), $RhCl_3.3H_2O$ (0.5 mmol, 0.13175 g), $Cu(NO_3)_2.2.5H_2O$ (0.5 mmol, 0.1163 g) and NaOH (3 cm^3, 1 mol dm^{-3}) were used.

The green solution obtained was concentrated to 15 cm^3 followed by precipitation with ethanol (*ca.* 200 cm^3) and was placed at low temperature (5 °C) for crystallisation. This resulted into yellow-coloured, needle-shaped crystals which corresponds to $(PPh_4)_2[Rh_2(TTHA)(Cl_2)]$ *via* unit cell X-ray analysis.

Analysis: AAS metal concentration (ppm), found: Rh 2.7, Cu 12.8. MS [ESΙ], found (expected): m/z: 672.0 $[C_{18}H_{26}N_4O_{13}RhCu]$ (m/z: 671.99 $[C_{18}H_{26}N_4O_{13}RhCu]$). IR ($\nu$ cm^{-1}): 1636 C=O (str).

B.25 Attempted preparation of tetraphenylphosphonium triethytetraamine-N,N',N'',N'''-hexaacetatoferrate(III)platinate(II), $(PPh_4)[FePt(TTHA)]$

$K_2[PtCl_4]$ (0.125 mmol, 0.051875 g), H_6TTHA (0.125 mmol, 0.0618 g), $Fe(NO_3)_3.9H_2O$ (0.125 mmol, 0.05048 g), NaOH (0.75 cm^3, 0.25 mol dm^{-3}), PPh_4Cl (0.75 mmol, 0.28086 g) were used.

H_6TTHA (0.125 mmol, 0.0618 g) was dissolved in water (3 cm^3) at 100 °C *via* stirring. To it was added another solution of $K_2[PtCl_4]$ (0.125 mmol, 0.0519 g)

in water (1 cm^3), followed by heating the contents of the flask at 60 °C (reduced from 100 °C) to avoid decomposition of Pt salt. The reaction was carried out under N_2 atmosphere. After 4 h of stirring at 60 °C, NaOH (0.75 mmol, 0.030 g) solution in water (1 cm^3) was added. The contents were again stirred for 10 min. Then, to these contents was added $Fe(NO_3)_3.9H_2O$ (0.125 mmol, 0.0505 g) in water (1 cm^3), and the mixture was refluxed for 1 h. To the resulting solution was added an aqueous solution (1 cm^3) of PPh_4Cl (0.75 mmol, 0.281 g) and the contents were stirred for 10 min. An orange-coloured precipitate resulted which was filtered and dried under vacuum. The precipitate was re-dissolved in water and was placed at room temperature for crystallisation. The crystals obtained were feathery and were not suitable for single crystal X-ray diffraction.

Analysis: MS[ESI^-], found (expected): m/z: 776.0 [$C_{18}H_{25}N_4O_{12}FePtCl$] (m/z: 776.0 [$C_{18}H_{25}N_4O_{12}FePtCl$]).